NCAT Report 09-06

# MECHANISTIC CHARACTERIZATION OF RESILIENT MODULI FOR UNBOUND PAVEMENT LAYER MATERIALS

By
Adam J. Taylor
Dr. David H. Timm, P.E.

October 2009

National Center for Asphalt Technology
NCAT
at AUBURN UNIVERSITY

277 Technology Parkway ■ Auburn, AL 36830

# MECHANISTIC CHARACTERIZATION OF RESILIENT MODULI FOR UNBOUND PAVEMENT LAYER MATERIALS

**by**

**Adam J. Taylor**
**and**
**David H. Timm, PhD, P.E., Gottlieb Associate Professor of Civil Engineering**
**National Center for Asphalt Technology**
**Auburn University, Alabama**

**NCAT Report 09-06**

**October 2009**

## ACKNOWLEDGEMENTS

On behalf of the entire NCAT Test Track team, the authors wish to thank the Alabama, Florida, Missouri and Oklahoma state departments of transportation for their support and cooperation in this study. The Federal Highway Administration was also an integral part of this study and deserves special recognition. Finally, special recognition is given to Burns, Cooley, Dennis, Inc., for providing the laboratory test results integral to this research.

## ABSTRACT

In recent years, there has been an industry shift in pavement design methodology from purely empirically based methods (e.g. The AASHTO Guide for the Design of Pavement Structures) to design methods that combine both mechanistic and empirical elements (e.g. the new Mechanistic-Empirical Pavement Design Guide). One of the critical inputs for accurate mechanistic-empirical (M-E) pavement design is accurate characterization of the stiffness of the unbound pavement material layers. This stiffness is quantified as resilient modulus, and this value can be determined either through laboratory testing with the triaxial apparatus or though non-destructive testing in the field with the falling weight deflectometer (FWD). Resilient modulus is typically expressed as a function of unbound material stress-state using a non-linear stress-sensitivity model.

For this project, five unbound materials utilized in the construction of eleven instrumented pavement test sections at the NCAT Test Track were characterized through both triaxial and FWD testing. Additionally, multiple non-linear stress-sensitivity models were evaluated for both testing methods with each material to determine which model provided the best fit to the respective data sets.

For the materials tested in the laboratory, stress-sensitivity models that account for both the effects of shear and confining pressure provided a better fit to the triaxial data than models that only accounted for the effects of only one of these variables. The same held true for base layer materials tested with the FWD at the Test Track. Generally, poor agreement was seen between the stress-sensitivity models and moduli generated by different methods for the base layer materials. Reasonable agreement between the data sets was seen for the subgrade material utilized at the Test Track.

As a result of this study, the models generated in the laboratory for the various unbound materials were deemed suitable for Level 1 MEPDG pavement design. FWD testing provided a good measure of pavement material variability in the field. The field-calibrated constitutive equations were shown to reasonably predict the backcalculated unbound material moduli at the Test Track. However, it is recommended that these models be made more robust through the addition of additional deflection data and validation at other testing sites containing the specified unbound materials.

## TABLE OF CONTENTS

## LIST OF TABLES

## LIST OF FIGURES

# CHAPTER 1 - INTRODUCTION

## BACKGROUND

A fundamental requirement for a successfully constructed structure is a solid foundation. Asphalt pavements are no exception to this requirement. Flexible pavements are constructed in layers with higher quality materials at the surface of the pavements where the loading stresses are highest and lower quality materials deeper in the pavement structure where the loading stresses diminish with depth. The lowermost layers of a flexible pavement structure are often layers of unbound materials (e.g., granular bases or compacted fill) above the existing soil material. These materials are employed to protect the subgrade from stresses capable of causing rutting or pumping of fines (Huang, 2004). Unbound materials are a critical component of the pavement structure, and as such it is important to understand how these materials behave for design.

Specifically, accurate stiffness (modulus) characterization of the unbound layers is critical for accurate pavement layer thickness design. For any mechanistically based pavement design, an accurate knowledge of the strains at critical locations in the pavement structure (such as the bottom of the HMA or surface of the subgrade) are necessary to give a quality prediction of the design life of that pavement. Given the fundamental relationship between stress and the multiple of modulus and strain (Hooke's Law), it is evident that accurate modulus characterization of the unbound pavement layers is necessary to accurately determine the critical strains in the structure based upon the stresses imparted by a design traffic loading. As such, accurate resilient modulus characterization is necessary to model the performance and life span of a given pavement structure.

Often, the stiffness of the unbound materials is quantified as the resilient modulus. Equation 1-1 provides the general definition of resilient modulus, which is the ratio of deviatoric stress (from a triaxial compression test) to recoverable strain. This term is utilized since unbound material behavior is not completely elastic; these materials usually experience some permanent deformation after each load application. However, if the load is small compared to the strength of the material and is repeated often, the deformation under the subsequent load repetitions is almost completely recoverable (Huang, 2004). This results in the material behaving in a pseudo-elastic manner under repetitive traffic loads. Figure 1.1 illustrates the concept of recoverable strain under repetitive loading following a small amount of permanent deformation.

$$M_r = \frac{\sigma_d}{\varepsilon_r} \tag{1-1}$$

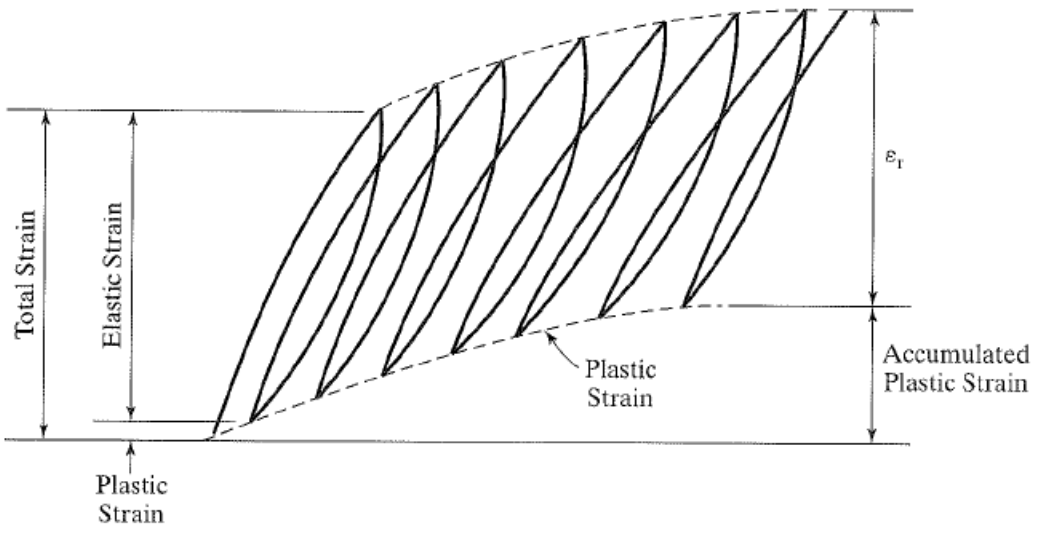


**Figure 1.1 Unbound Material Strains under Repeated Traffic Loading (Huang, 2004).**

Unbound material resilient moduli can be determined either in the laboratory using the triaxial testing apparatus or in the field using a variety of non-destructive testing methods. The laboratory resilient modulus test calculates resilient modulus by directly measuring the load and deformation of the test specimen under repeated loadings that simulate the quick loads imparted on the pavement structure by moving traffic. One of the most common field tests for resilient modulus is done with a falling weight deflectometer (or FWD). This apparatus drops a large loading on the pavement structure that is representative of a heavy vehicle load. After this loading, an array of deflection sensors near the loading measures the resulting deflections of the pavement surface. From these deflection and loading data, the moduli of the pavement layers can be 'backcalculated' by using layered-elastic analyses that relate pavement layer modulus to deformation and loading. Both of these tests determine the resilient moduli of unbound paving material, but achieve that value by very different means. As such, multiple studies have shown poor agreement between laboratory and field-measured resilient moduli (these studies will be discussed in greater detail in Chapter 2).

The resilient moduli of unbound paving materials often exhibit non-linear stress-dependent behavior with varying stress-states within the material (Irwin, 2002). This behavior can either be stress-hardening (increasing stiffness with increasing stress) or stress-softening (decreasing stiffness with increasing stress) (Irwin, 2002). Research into unbound material performance through laboratory and field testing has yielded several constitutive relationships relating resilient modulus to stress-state. However, no one relationship is universally used to model resilient modulus data. These models contain a wide range of terms that quantify the stress-state of the unbound materials, such as: bulk stress ($\theta$), deviatoric stress ($\sigma_d$), and octahedral shear stress ($\tau_{oct}$). Equations 1-2, 1-3, and 1-4, respectively, define the bulk stress, deviatoric stress, and octahedral shear stress

terms as a function of the axial and confining stresses inducted during resilient modulus testing.

Many of these models require non-linear regression analysis techniques to model the behavior of the material resilient modulus as a function of one or more terms that represent the material state of stress. Equations 1-5 and 1-6 are single-variable stress-sensitivity models that relate resilient modulus to bulk stress and deviatoric stress, respectively. These models are commonly specified based on whether the material is a coarse-grained (Equation 1-5) or fine-grained soil (Equation 1-6). Equations 1-7 and 1-8 are multi-variable stress-sensitivity models that model resilient modulus as a function of two stress terms. These models are more universal given they are not constrained to use on a particular soil type. In each model, the first term (the bulk stress) models stress-sensitivity as a function of confining pressure while the second term (either deviatoric or octahedral shear stress) models stress-sensitivity due to shearing stresses.

$$\theta = \sigma_1 + \sigma_2 + \sigma_3 \tag{1-2}$$

$$\sigma_d = \sigma_1 - \sigma_3 \tag{1-3}$$

$$\tau_{oct} = \frac{1}{3}\sqrt{(\sigma_1 - \sigma_2)^2 + (\sigma_2 - \sigma_3)^2 + (\sigma_3 - \sigma_1)^2} \tag{1-4}$$

$$M_r = k_1 * \left(\frac{\theta}{p_a}\right)^{k_2} \tag{1-5}$$

$$M_r = k_1 * \left(\frac{\sigma_d}{p_a}\right)^{k_2} \tag{1-6}$$

$$M_r = k_1 p_a * \left(\frac{\theta}{p_a}\right)^{k_2} * \left[\left(\frac{\tau_{oct}}{p_a}\right) + 1\right]^{k_3} \tag{1-7}$$

$$M_r = k_1 p_a * \left(\frac{\theta}{p_a}\right)^{k_2} * \left(\frac{\sigma_d}{p_a}\right)^{k_3} \tag{1-8}$$

where: $M_r$ = Resilient Modulus
$P_a$ = Atmospheric Pressure (14.7 psi)
$\theta$ = Bulk Stress
$\sigma_d$ = Deviatoric Stress

$\tau_{oct}$ = Octahedral Shear Stress
$\sigma_1$ = Axial Stress
$\sigma_2$,$\sigma_3$ = Confining Stress
$k_1$, $k_2$, $k_3$ = Regression Coefficients

Recent trends in the pavement design industry have facilitated a need for better understanding of unbound material behavior and its use in pavement design and construction. The pavement industry is currently undergoing a shift from more empirically based design methods (such as that used in the AASHTO Guide for the Design of Pavement Structures (1993)) to mechanistic-empirical pavement design (such as that used by the new mechanistic-empirical pavement design guide (MEPDG) (2004)). These design philosophies utilize very different methods of unbound materials characterization.

The current AASHTO design methodology (1993) reduces the resilient modulus value of the unbound paving layers to a single value, the structural coefficient. The structural coefficient was intended to represent the relative strength of the various construction materials used throughout the pavement structure. The AASHTO design methodology uses the resilient modulus to calculate a structural coefficient for a given unbound material. This coefficient is a point estimate that is supposedly representative of the overall layer behavior (under various loading, environmental conditions, etc.).

The AASHTO design guide (1993) offers multiple options for obtaining the structural coefficient for unbound materials. The guide emphasizes that the most reliable value will come from laboratory or non-destructive resilient modulus testing in the field. However, the guide also offers multiple correlations to other, less expensive laboratory tests (i.e. California bearing ratio, R-value) that will result in the calculation of a structural coefficient that is given equal weight to one obtained through more precise testing. Figure 1.2 illustrates this concept with a correlation chart from the AASHTO design guide that is used to generate a structural coefficient for granular base materials based on correlations to multiple laboratory unbound material tests.

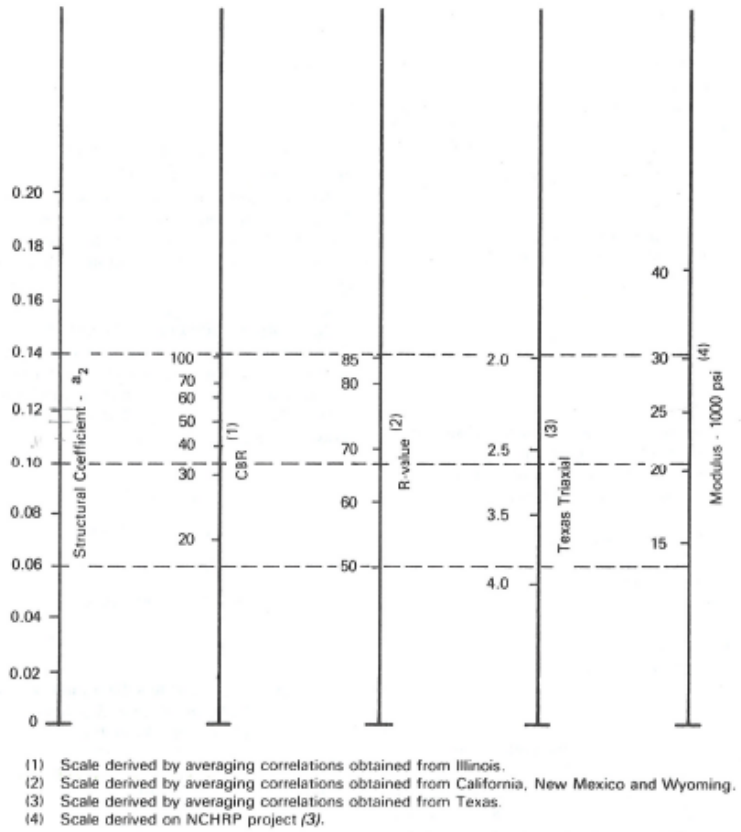


**Figure 1.2 AASHTO Structural Coefficient Correlation Nomograph (AASHTO, 1993).**

The new MEPDG offers a hierarchical approach to the quality of pavement design inputs, with different 'levels' of design input accuracy available based on the needs of a given project. There are three levels of accuracy available for unbound material resilient modulus characterization. The lowest level of accuracy (Level 3) consists merely of a designer estimate or tabulated default value of the material modulus based upon its AASHTO or USCS soil classification. The next highest level of design (Level 2) consists of correlations to other laboratory tests (similar to those found in the AASHTO design guide). The most accurate design level (Level 1) involves comprehensive resilient modulus testing (either in the laboratory or in the field) that result in the generation of a suitable constitutive relationship that models the non-linear stress-sensitivity of those materials. Equation 1-7 is the model recommended by the new MEPDG, but it also allows for the use of other constitutive models to achieve the best possible prediction of resilient modulus behavior. Therefore, this design methodology will take into account material–specific variations of modulus with stress at its most accurate design level.

In order to effectively characterize the stiffness behavior of unbound materials, several factors must be considered. First of all, does laboratory or field resilient modulus testing provide a better representation of material behavior? Secondly, is the material stress-sensitive and, if so, which stress-sensitivity model best quantifies the behavior of that

material? Answering these questions allow for the most accurate quantification of resilient modulus for pavement design and more accurate modeling of pavement design life.

For many agencies, these questions can be resolved through full-scale accelerated pavement testing (APT). One such facility is the National Center for Asphalt Technology (NCAT) Test Track. The Test Track is a 1.7 mile accelerated testing facility containing 46 pavement test sections, each 200 foot long, designed to test the performance of a wide variety of asphalt mixes and structural designs. Each of these test sections are subjected to live traffic loading under a fleet of triple-trailer trucks that are operated by human drivers (a more detailed description of the Test Track is given in Chapter 3). Part of the testing program at the Test Track involves characterization of the various paving layer materials in both the laboratory and the field, making this facility ideal for a study of this nature.

## OBJECTIVES OF STUDY

The overall goal of this study was to mechanistically characterize the unbound paving materials at the NCAT Test Track for effective use in pavement design. Specific objectives included:

- A comparison of laboratory and field derived resilient moduli.
- An evaluation of common non-linear stress-sensitivity models with respect to laboratory and field moduli.
- Developing a recommendation as to the effective use of unbound material moduli in pavement design and analysis.

## SCOPE OF REPORT

Several resources were used to perform this study. First, a review of relevant literature was performed to assess the state of the practice with regards to unbound material characterization. Topics reviewed include: laboratory triaxial resilient modulus testing, non-destructive pavement testing with the FWD, non-linear constitutive relationships relating resilient modulus to unbound material stress state, and agreement between resilient modulus data for a given unbound material collected in both the laboratory and the field.

The NCAT Test Track provided an ideal setting for a study of this nature. The five unbound materials utilized for this study were constructed in various capacities within the eleven full-depth instrumented pavement test sections (or structural sections) located at the Test Track. Laboratory triaxial resilient modulus testing on each of these unbound materials was performed by Burns, Cooley, Dennis Inc using test specification NCHRP 1-28A. For in-situ pavement characterization, NCAT operates a falling weight deflectometer (FWD) as part of a regular testing program at the Test Track on each of the eleven structural sections. Four dates worth of deflection data from this testing program were used in the development of field-calibrated stress-sensitivity models for the five unbound materials. An additional four dates worth of deflection data were then used for the model validation process. Additional FWD testing was performed above the

embedded pressure and strain instrumentation to assess the measured pavement responses versus the responses predicted with the backcalculation software.

EVERCALC v5.0 was the backcalculation software utilized to generate the unbound layer moduli from the FWD data. Microsoft Access was used for managing the database of deflection data and querying the data into a usable format. AUDEF is a file conversion program that was used to convert the deflection files from an Access database format to a deflection file that could be used by EVERCALC. This software also converted the backcalculation output files into usable EXCEL spreadsheets. Finally, DATAFIT non-linear regression modeling software was used to generate non-linear stress-sensitivity models for the various resilient modulus data.

The availability of multiple data sets regarding the unbound material behavior was especially useful in performing a complete study regarding unbound material characterization. Equations 1-5 through 1-8 were then evaluated to determine which stress-sensitivity model provided the best fit to both the laboratory and backcalculated resilient moduli. Finally, comparisons were made between the laboratory and the field-measured resilient moduli.

**ORGANIZATION OF REPORT**

A review of relevant literature concerning unbound material characterization is presented in Chapter 2. Chapter 3 gives an overview of the NCAT Test Track, as well as information regarding the in-situ unbound material properties and construction of the eleven instrumented pavement test sections. This chapter also outlines the FWD testing program utilized at the Test Track and provides details concerning the FWD testing performed atop the embedded pavement response instrumentation.

A detailed look at the laboratory resilient modulus testing procedure is given in Chapter 4, along with the results of this testing on the unbound materials utilized in the structural sections at the Test Track. Chapter 5 outlines the procedure utilized to select the optimum cross-section for backcalculation for each of the eleven structural sections, as well as the results of this investigation.

Chapter 6 presents the results of the field modulus characterization using the FWD on the structural sections at the Test Track. This chapter includes the calibration and validation process used to develop constitutive relationships for the various unbound materials based on field testing. Chapter 7 gives a comparison between the unbound material behavior in the lab and in the field, along with an assessment on the degree of agreement. Chapter 8 is the final chapter in which the conclusions and recommendations of this study are presented.

# CHAPTER 2 - LITERATURE REVIEW

## INTRODUCTION

The mechanistic-empirical (M-E) pavement design process is based on the mechanics of materials that relates an input, such as a wheel load, to a particular pavement response, such as a stress or a strain at a structurally critical location within the pavement structure (Huang, 2004). The M-E design process utilizes detailed knowledge of a trial pavement structure regarding the material composition, expected traffic loading, and environmental conditions to more accurately model the pavement structure and project its design life (Priest and Timm "Fatigue," 2006). Monismith (1992) states that "the intent of the analysis and design process is to simulate, in advance, the expected performance of the asphalt pavement so that the optimum thicknesses of the various components can be selected and the available materials used effectively."

Given accurate knowledge of the materials to be used in the pavement structure and the environmental and traffic conditions, the pavement responses at critical locations in the pavement structure (bottom of the HMA for fatigue cracking, surface of the subgrade for rutting, etc.) can be simulated using various methods, such as layered-elastic analysis (Huang, 2004). With these calculated critical responses, the cycles to failure for the pavement under loading of a critical design vehicle can be calculated by utilizing calibrated transfer functions. These equations typically take the form of Equation 2-1 for fatigue and Equation 2-2 for rutting (Priest and Timm "Fatigue," 2006). Therefore, this method of pavement design can generate reliable optimal thicknesses that have basis in mechanistic theory and are not based purely on empirical methods. Figure 2.1 shows a flow chart outlining the conceptual framework of M-E design and analysis.

$$N_f = k_1 * \left(\frac{1}{\varepsilon_t}\right)^{k_2} \tag{2-1}$$

$$N_r = k_3 * \left(\frac{1}{\varepsilon_v}\right)^{k_4} \tag{2-2}$$

where: $N_f$ = Number of cycles to failure via fatigue cracking
$\varepsilon_t$ = Critical horizontal tensile strain at the bottom of the HMA layer
$N_r$ = Number of cycles to failure via structural rutting
$\varepsilon_v$ = Critical vertical compressive strain at the surface of the subgrade soil
$k_n$ = empirical constants

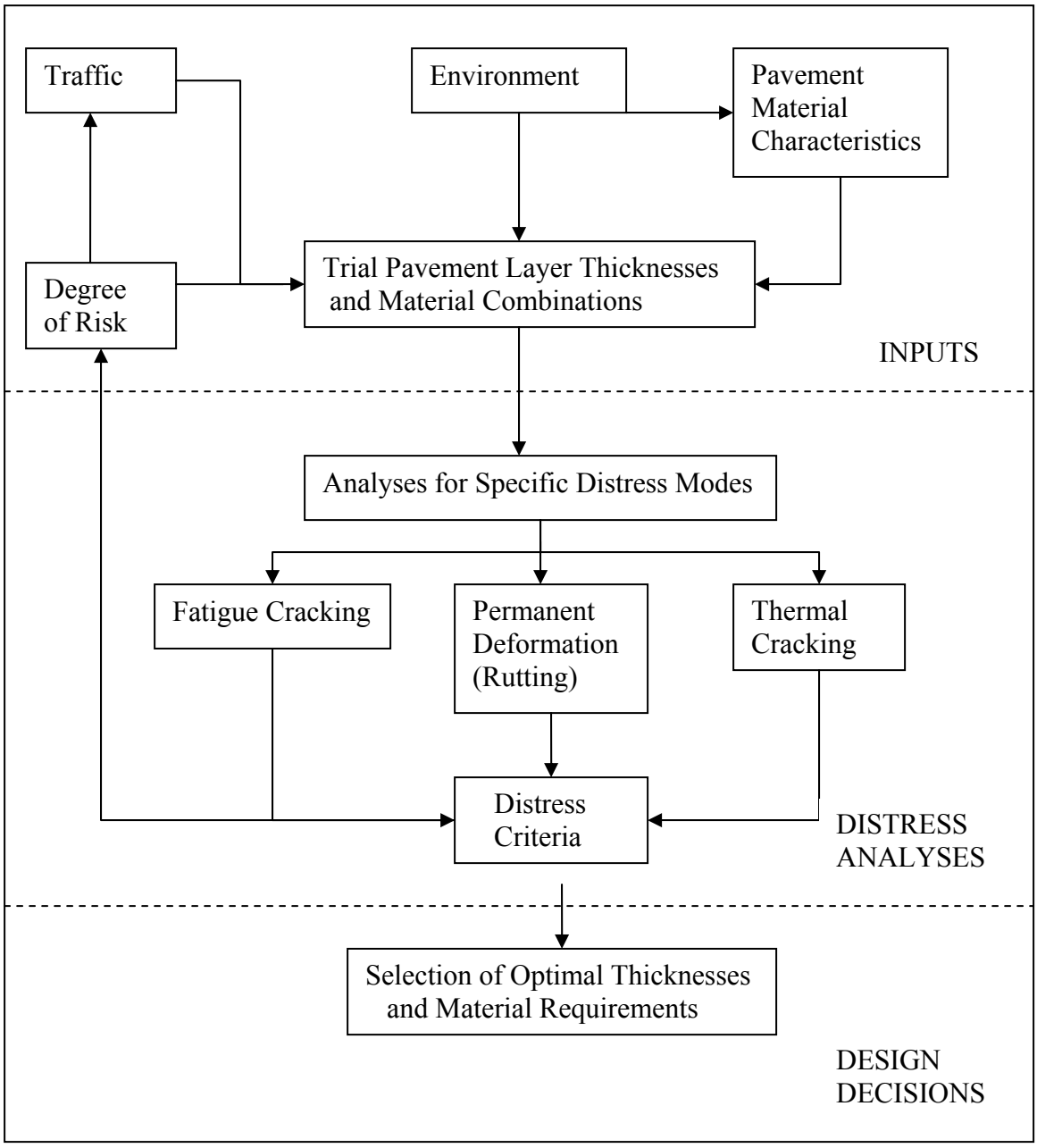


**Figure 2.1 M-E Design Flowchart (after Monismith 1992).**

One of the critical inputs for M-E pavement design is accurate knowledge of the stiffness characteristics of the unbound materials to be used in the pavement structure, specifically the resilient modulus of these layers. The new MEPDG (2004) offers three different levels of accuracy in determining the resilient modulus of the unbound layer materials. A level 3 design value is the least accurate and consists of a designer estimate or typical values of the resilient modulus at the optimum moisture content for various AASHTO and USCS soil classification. A level 2 design value consists of correlations between resilient modulus and other material properties (such as California bearing ratio and dynamic cone penetrometer penetration data). These correlations are very similar to

those found in the AASHTO Guide for the Design of Pavement Structures (1993). Level 1 design is the most accurate design value and involves using either laboratory triaxial testing or field non-destructive testing to generate a constitutive relationship between material stress-state and resilient modulus. Characterization of resilient modulus in this manner is the focus of this study and of this literature review.

The focus of this literature review is to assess the state of the practice with regards to resilient modulus testing and data analysis methods. First of all, resilient modulus testing in the laboratory using a triaxial chamber and in the field using a falling weight deflectometer (FWD) will be discussed. Next, the various constitutive relationships that relate unbound material stresses to resilient modulus will be discussed, along with examples of their use in practice. Finally, studies that have compared the results of laboratory and field resilient modulus (using the triaxial chamber and FWD, respectively) will be presented and discussed.

## LABORATORY TESTING

The most common laboratory test utilized to determine the resilient modulus of granular base materials and subgrade soils for flexible pavement construction is the triaxial resilient modulus test. According to the specification outlined by NCHRP 1-28A (2004), "The resilient modulus test simulates the conditions in a pavement due to the application of moving wheel loadings. As a result, the test provides an excellent means for comparing the behavior of pavement construction materials under a variety of conditions and stress-states." The primary advantage of the triaxial test is that it allows the unbound material to be tested in a controlled environment over a variety of stresses, making it ideal for the development of the stress-sensitivity model relating stress-state to resilient modulus (Nazarian et al., 1998).

Though testing is conducted in a controlled environment, there are several disadvantages to this mode of testing as well. First, the laboratory resilient modulus is not completely representative of in-situ conditions due to several factors: sample disturbance, differences in aggregate orientation, differences in water content, and differences in level of compaction (Seeds et al., 2000; Nazarian et al., 1998). Imperfect instrumentation in the triaxial apparatus creates difficulties in reproducing the in-situ state of stress and accurately measuring axial deformation in laboratory samples (Seeds et al., 2000). Additionally, multiple test specifications and variable equipment calibration and verification procedures tend to make triaxial results variable both within and between laboratories (Seeds et al. 2000). The laboratory specimens represent the properties of a material from a very small location and not necessarily the larger mass of material that would respond to the pass of a typical truck axle (Seeds et al., 2000). Finally, laboratory resilient modulus testing tends to be very time consuming and expensive to perform in order to generate accurate results (Nazarian et al., 1998).

Throughout the literature concerning laboratory resilient modulus testing, multiple specifications by which this test was conducted were encountered. Zhou (2000) utilized AASHTO T274-82 for their testing. Ping et al. (2001) utilized AASHTO T292-91 for

their triaxial testing. Yau and Von Quintus (2002) performed a synthesis on resilient modulus data generated within the LTPP database that had been tested according to LTPP Protocol P46. The MEPDG (2004) recommends using one of two specifications for laboratory resilient modulus testing, either NCHRP 1-28A or AASHTO T307. According to Andrei et al. (2004), the NCHRP 1-28A procedure was developed to harmonize the existing resilient modulus test protocols and develop a single test method utilizing the best features of the existing specifications. This particular testing specification will be discussed in greater detail in Chapter 4 (laboratory testing).

**Sampling of Materials for Laboratory Resilient Modulus Testing**

As previously noted, one of the primary disadvantages of laboratory resilient modulus testing has to do with preparing samples that are representative of the unbound samples that are compacted in the field. NCHRP 1-28A (2004) recommends compacting samples to the in-situ density and moisture content, but allows samples to be compacted to 95 percent of maximum laboratory dry density and the optimum moisture content in the absence of these data. To generate accurate laboratory modulus values, the material must be sampled and then recompacted in such a manner that yields representative results.

Nazarian et al. (1998) conducted a study in which the laboratory determined moduli of unbound materials utilized in various pavement structures were compared for the materials obtained from the quarry and for materials excavated from the existing pavement structure. The authors concluded that there is a large difference in material properties based on the location from which these materials were obtained. The quarry and in-situ unbound materials were found to have varying gradation curves, Atterberg limits, and optimum moisture contents of the quarry materials were found to vary from the in-situ moisture content by an average of 2 percent. The authors also concluded that that quarry materials compacted to Proctor maximum dry densities and moisture contents yielded notably different constitutive model regression coefficients than the in-situ samples compacted to the field densities and moisture contents.

Yau and Von Quintus (2002) conducted a study in which the LTPP resilient modulus database was analyzed to determine the effect of sampling technique on testing results. The authors concluded that sampling technique (boring with an auger versus trenching in the pavement structure) had an effect on the resilient modulus test results for the uncrushed gravel and crushed stone base and subbase materials. This is logical given the ability of a boring to alter the gradation of a coarse-grained material. For the subgrade soils in the database, whether the sample was obtained through disturbed or undisturbed sample proved to impact at least one of the regression coefficients in the constitutive model for each of the soil types.

Ping et al. (2001) conducted a study in which disturbed samples of soils taken from various excavated pavement sites throughout Florida were tested at both the in-situ moisture content and the optimum moisture content. The results of this comparison showed that the average laboratory resilient modulus at optimum compacted conditions was about 1.1 times higher than the average laboratory resilient modulus at in-situ

conditions. The data for this comparison are shown in Figure 2.2. It was also noted that the average dry density at optimum compacted conditions was higher than the field-measured in-situ dry density. Therefore, sample preparation did have an impact on the results of resilient modulus testing.

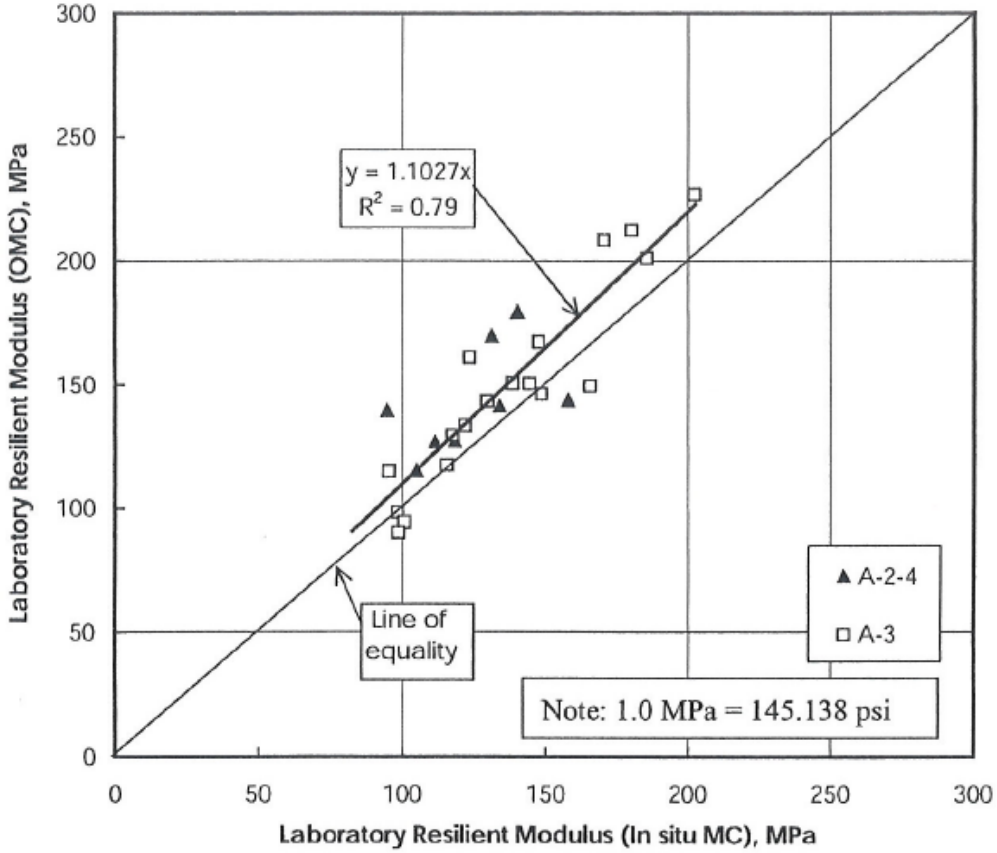


**Figure 2.2 Comparison of Resilient Modulus values for Laboratory Samples with Different Moisture Contents (Ping et al., 2001).**

**Target Moisture Contents and Densities for Laboratory Samples**

Several authors make various recommendations about whether the triaxial samples should be compacted to optimum or in-situ conditions. Based on the results of the study outlined above, Ping et al. (2001) recommended the use of the laboratory determined optimal conditions as a standard representation of unbound material conditions for design. Parker and Elton (1990) also utilized the optimum moisture content and maximum laboratory dry density for testing, citing that these conditions would reasonably approximate field conditions. Zhou (2000) utilized data from two field FWD testing sites, and the data from one site was compacted to the maximum dry density and optimum moisture content, while the other was compacted to field conditions. Buchanan (2007) states that samples for laboratory resilient modulus testing should be compacted as close as possible to in-situ conditions for testing. Hence, there is no general consensus in literature as to whether triaxial resilient modulus samples should be compacted to optimum laboratory or in-situ measured conditions.

**Stress-States Utilized in Laboratory Testing**

According to the MEPDG (2004), the stress-states at which the laboratory triaxial samples are tested should be representative of the stress-states that are to be expected in the field. Both NCHRP 1-28A (2004) and AASHTO T307 (2003) define a range of stresses to be tested based on whether the material tested is located in the base or the subgrade (since varying depths in the pavement structure correspond to different stresses under loading). The resilient modulus test is designed to characterize the unbound layer moduli under loading conditions that will not result in the failure of the material (Buchanan, 2007). These testing methods have varying treatments of the stress-sequences that the material endures. The original NCHRP 1-28 laboratory specification procedure holds the confining pressure constant while increasing the deviatoric stress, causing the material to rapidly approach the Mohr-Coulomb failure envelope on a plot of shear stress versus normal stress (Andrei et al., 2004). A similar method of load application is applied in the AASHTO T307 (2003) procedure. The NCHRP 1-28A procedure takes a different approach by holding the principal stress ratio constant ($\sigma_1/\sigma_3$) and simultaneously increasing the deviatoric and confining stresses, minimizing the probability of premature sample failure (Andrei et al., 2004). This contrast in loading philosophies is illustrated in Figure 2.3.

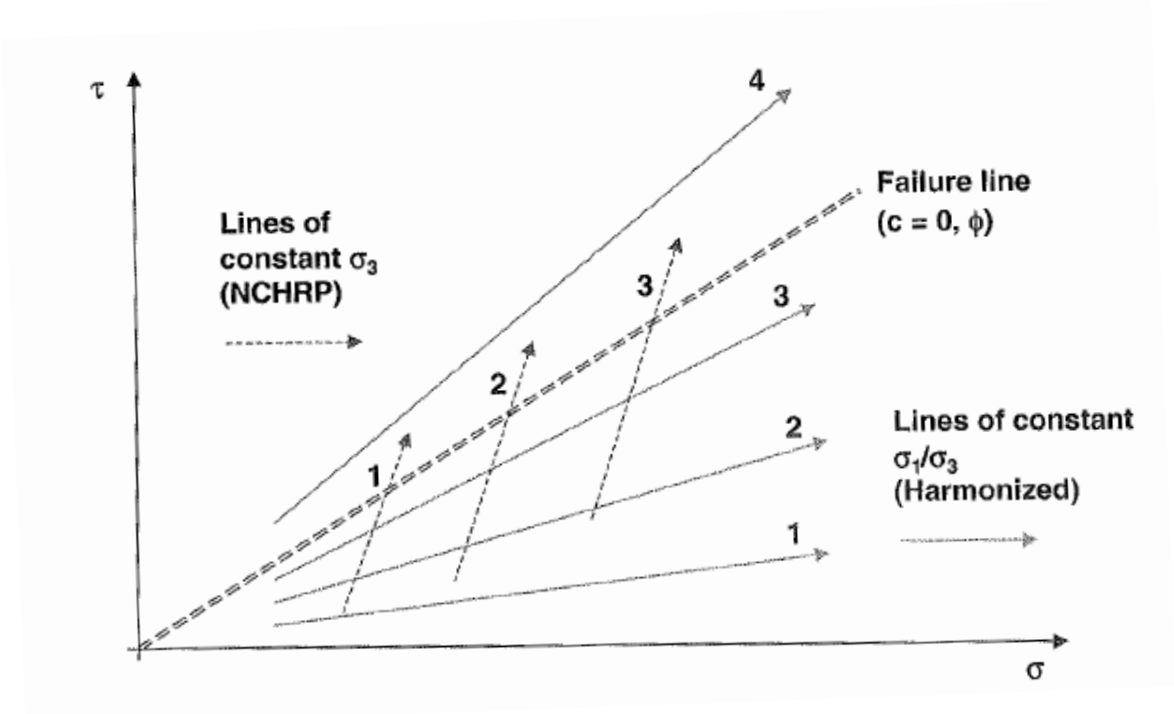


**Figure 2.3 Comparison of Loading Stress Sequences for Granular Materials (Andrei et al. 2004).**

**FIELD MODULUS CHARACTERIZATION**

An alternative method of determining pavement material moduli comes from the use of non-destructive pavement testing equipment on the existing pavement structure. Non-destructive testing (NDT) typically applies some form of loading to the in-situ pavement structure so that pavement deflections can be measured at various distances from the

loading point. This form of testing is necessary to perform the process of backcalculation to determine the respective pavement layer moduli at a particular testing location. Irwin (2002) provided the following definition of backcalculation: "The procedure to determine Young's modulus of elasticity for pavement materials using measured surface deflections by working elastic layer theory 'backwards' is generally called backcalculation."

Perhaps the earliest form of NDT was called the Benkelman Beam. This apparatus is used to measure the pavement deflection basin between two rear truck tires. Other forms of NDT testing include seismic pavement analyzers and falling weight deflectometers. Seismic pavement analyzers utilize a small seismic source and can determine pavement layer moduli by measuring and analyzing the generated seismic waves (Nazarian et al., 1998). Falling weight deflectometers (FWD) are commonly used NDT equipment that apply a pulse loading to the pavement. The pavement deflection basin resulting from this load is measured by a series of velocity transducers at various distances from the loading apparatus (Irwin, 2002). This equipment uses a pulse loading to more closely simulate the pavement loading applied by a moving wheel load (Irwin, 2002). A Dynatest 8000 Model FWD is shown in Figure 2.4. The focus of this literature review will be FWD testing, since this form of NDT was available for this research.

**Figure 2.4 Dynatest 8000 Falling Weight Deflectometer.**

FWD testing has multiple advantages. First, it allows testing the in-situ condition of the pavement without damaging the pavement structure by trenching or coring. Secondly, it allows for the determination of the structural capacity of a pavement. This is critical for

determining optimum overlay thicknesses and potentially identifying structural weaknesses in a given pavement (Von Quintus and Killingsworth, 1998). Typically, the overall expense associated with non-destructive testing is less than with laboratory testing (Seeds et al., 2000). The FWD loadings can typically be adjusted to approximate the critical wheel loadings experienced by the pavement structure (Nazarian et al., 1998). Finally, the sampling frequency with non-destructive testing can be increased much more economically than with laboratory testing. Therefore, a better representation of the natural and random variability within the pavement properties can be obtained (Seeds et al., 2000).

Despite the appeal of being able to accurately characterize paving materials in the field, there are multiple disadvantages to FWD testing as well. One disadvantage of the FWD is that generating accurate pavement layer moduli is not an exact science, and accurate modulus determination requires good quality control of raw data and precision in analysis (Von Quintus and Killingsworth, 1998; Nazarian et al., 1998). It is possible for backcalculation software to produce multiple combinations of pavement layer moduli from the same deflection basin. This non-unique solution dilemma therefore requires some interpretation of the most logical combination of layer moduli (Seeds et al., 2000). Most backcalculation programs assume pavements are loaded in a static manner, when in reality wheel loads are dynamic in nature (Seeds et al., 2000). Additionally, most backcalculation programs assume purely linear-elastic behavior, when HMA typically behaves as an elastic visco-plastic material and unbound materials behave in a non-linear elastic fashion (Seeds et al., 2000). Finally, extremely accurate pavement cross-section information (thicknesses and layer composition) is required to generate reasonable backcalculated results (Seeds et al., 2000).

**Field FWD Testing Programs**

To accurately assess the in-situ pavement conditions, an FWD testing program must be able to accurately quantify the variability inherent to the pavement structure. FWD moduli represent both the pavement conditions at the time of measurement and the stress conditions induced by the applied loading (Parker, 1991). Therefore, multiple tests are useful to quickly gain a quality data representation of the overall pavement structure. There are several types of variability inherent to most pavements: loading variability, spatial and construction variability, and seasonal variability. These sources of variability can readily be accounted for with a quality FWD testing program.

**Load Levels Used for FWD Testing**

A common practice in FWD testing is to test the pavement at load levels that are representative of the load magnitudes to be placed on the pavement structure by live traffic (Parker, 1991; Nazarian et al., 1998). Timm and Priest ("Material Properties," 2006) utilized 2 repetitions of a 9,000 lb load at each testing location. The 9,000 lb load is useful because it represents the loading placed on the pavement structure by one-half of a standard 18,000 lb axle load (Parker and Elton, 1990). Sometimes multiple loadings can be used at each testing location to account for varying traffic levels and to measure the stress-sensitivity of the underlying pavement layers (Parker and Elton, 1990; Von

Quintus and Killingsworth, 1998). Von Quintus and Killingsworth (1998) performed analysis on Long Term Pavement Performance (LTPP) database deflection data that contained 6 kip, 9 kip, 12 kip, and 16 kip loadings. Parker and Elton (1990) utilized 9 kip, 12 kip, and 15 kip loadings in their FWD testing program. Zhou (2000) utilized FWD loadings between 13 kN and 67 kN (approximately 3 kip and 15 kip). Sebally et al. (2000) state that the state of Nevada uses 3 to 4 drops of the FWD at each testing location with increasing load levels. These load levels range between 27 kN and 67 kN (approximately 6 kip to 15 kip) for standard pavements and loads between 45 kN and 90 kN (approximately 10 kip to 20 kip) for thicker pavement structures. Seeds et al. (2000) used increasing load levels of 27, 40, 53, and 71 kN (6, 9, 12, and 16 kip) at the WESTRACK accelerated testing facility.

**Spatial Variability**

As mentioned previously, one of the primary advantages of FWD testing is the ability to test multiple pavement locations in a short period of time. This is important because pavements are generally not homogenously constructed structures, and contain several possible sources of spatial variability. Some of these sources of variability include: layer thickness variability throughout the longitudinal profile of the pavement, density variation due to construction and traffic, varying depth to bedrock or the water table, and varying density and moisture content of the unbound materials (Irwin, 2002). Irwin (2002) recommends testing at various points across the transverse profile, due to variations in deflection testing results within and between the wheelpaths. Priest and Timm (2006) performed testing at multiple longitudinal locations throughout the pavement structure in both the inside and outside wheelpath to quantify spatial variability. Nazarian et al. (1998) utilized 11 longitudinal FWD drop locations at their sites to be tested. Parker (1991) utilized testing at 10 longitudinal locations spaced 200 feet apart at the FWD testing sites used for seasonal materials characterization. The state of Nevada tests at 0.15 km (0.09 mile) intervals for highway projects in each direction of travel (Sebally et al., 2000). Testing was performed at 10 meter (33 foot) intervals within each of the pavement test sections at WESTRACK (Seeds et al. 2000). Therefore, spatial variability can be quantified by FWD testing at multiple longitudinal and transverse pavement locations.

**FWD Deflection Sensor Spacing**

Another critical component of the FWD is the configuration of the deflection sensors used to measure the deflection of the pavement surface immediately after loading. A sufficient number of these sensors must be present to yield an accurate deflection basin for backcalculation. Zhou (2000) utilized a KUAB model FWD with 6 deflection sensors, three of which were adjustable depending on the project requirements. Rwebangira et al. (1987) utilized a KUAB FWD with four sensors spaced 11.8 inches apart with one sensor beneath the loading plate. Timm and Priest ("Material Properties," 2006) utilized an FWD with 7 sensors spaced 12 inches apart with one sensor beneath the loading plate. Nevada utilizes an FWD using 7 sensors that have variable spacing depending on the thickness of pavement for a given project. The sensors are spaced at 0, 203, 305, 457, 915, 1219, and 1524 mm (approximately 0, 8, 12, 18, 36, 48, and 60

inches) away from the loading plate for standard projects. The sensors are spaced at 0, 305, 610, 864, 1219, 1524, and 1829 mm (approximately 0, 12, 24, 34, 48, 60, and 72 inches) away from the loading plate for Interstate Highway projects with thicker pavements. The logic behind the variable sensor spacing is that closely spaced sensors near the load are useful for the accurate delineation of pavement surface conditions while the sensors farther from the load are useful for the accurate determination of subgrade layer moduli (Sebally et al., 2000). The FWD at WESTRACK utilized a similar sensor setup, with seven sensors spaced at 0, 305, 457, 610, 914, 1219, and 1524 mm (approximately 0, 12, 18, 24, 36, 48, and 60 inches) away from the load plate.

The sensor configuration is critical in determining how accurately the moduli of the layers can be determined. The presence of sensors far away from the loading is critical to accurately determining the moduli of the deeper subgrade layers. This is because at larger distances from the loading, only the deeper pavement layers are influenced by the loading and thereby deflecting (Irwin, 2002). This concept is illustrated graphically in Figure 2.5 below.

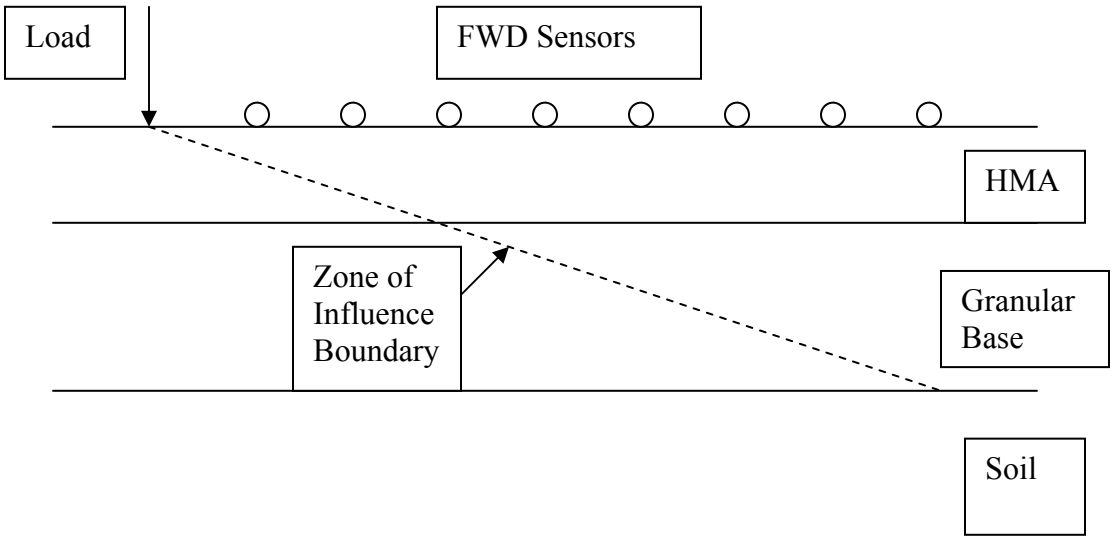


**Figure 2.5 Impact of Zone of Influence on Pavement Deflections.**

The presence of outer sensors can also be useful in determining whether a rigid layer exists at a given testing site. By plotting the deflections of the outer sensors against the normalized radial distance of these sensors from the loading (dividing the load plate radius by the radial distance), this curve can be extrapolated to ascertain an approximate depth to the stiff layer. This is based on the assumption that the depth to the stiff layer is approximately where the deflections will be equal to zero. If the curve intersects the x-axis at a positive value, this value gives a good approximation of the depth to the stiff layer (Irwin, 2002). This concept is illustrated in Figure 2.6.

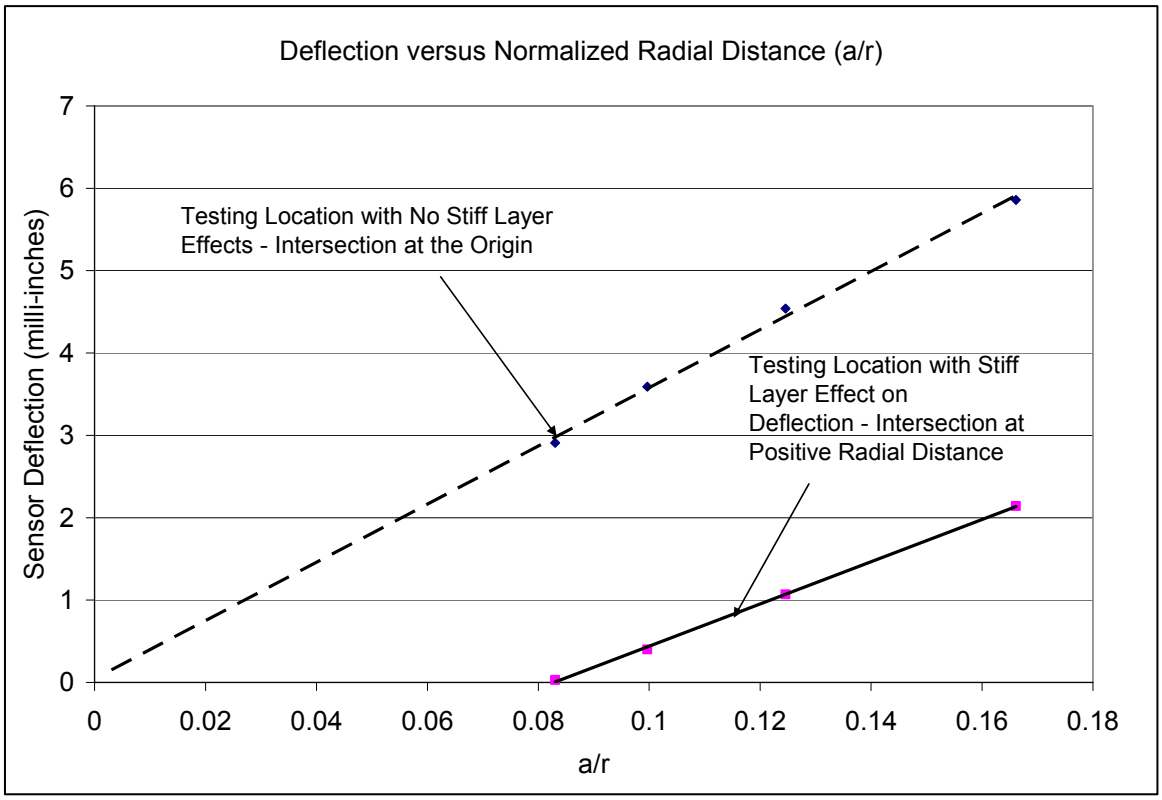


**Figure 2.6 Determination of Bedrock Depth with Deflection Measurements.**

**Seasonal Variation**

A critical component of any FWD testing program is ensuring that it captures the performance variability associated with the changing seasonal conditions at the test site. Several studies have been performed that document the effects of seasonal changes on the various pavement layers.

Parker and Elton (1990) conducted a study in which FWD testing was performed at several seasonal sites throughout the state of Alabama at approximately 2 month intervals over the course of three years to quantify the seasonal modulus variability. Figure 2.7 shows the behavior of the backcalculated base layer moduli with time as well as the variations in temperature in rainfall as percentages of their respective maximum monthly averages. In the absence of frost action, temperature and moisture were the major seasonal factors to consider in the state of Alabama. The figure shows the general trend that an increase in temperatures combined with low rainfall levels corresponded to an increase in base moduli. A decrease in temperature combined with increased rainfall levels would serve to decrease the base layer moduli. This was believed to occur since high moisture levels in the absence of higher temperatures would lead to a moisture build-up in the unbound layers, and a subsequent reduction in strength.

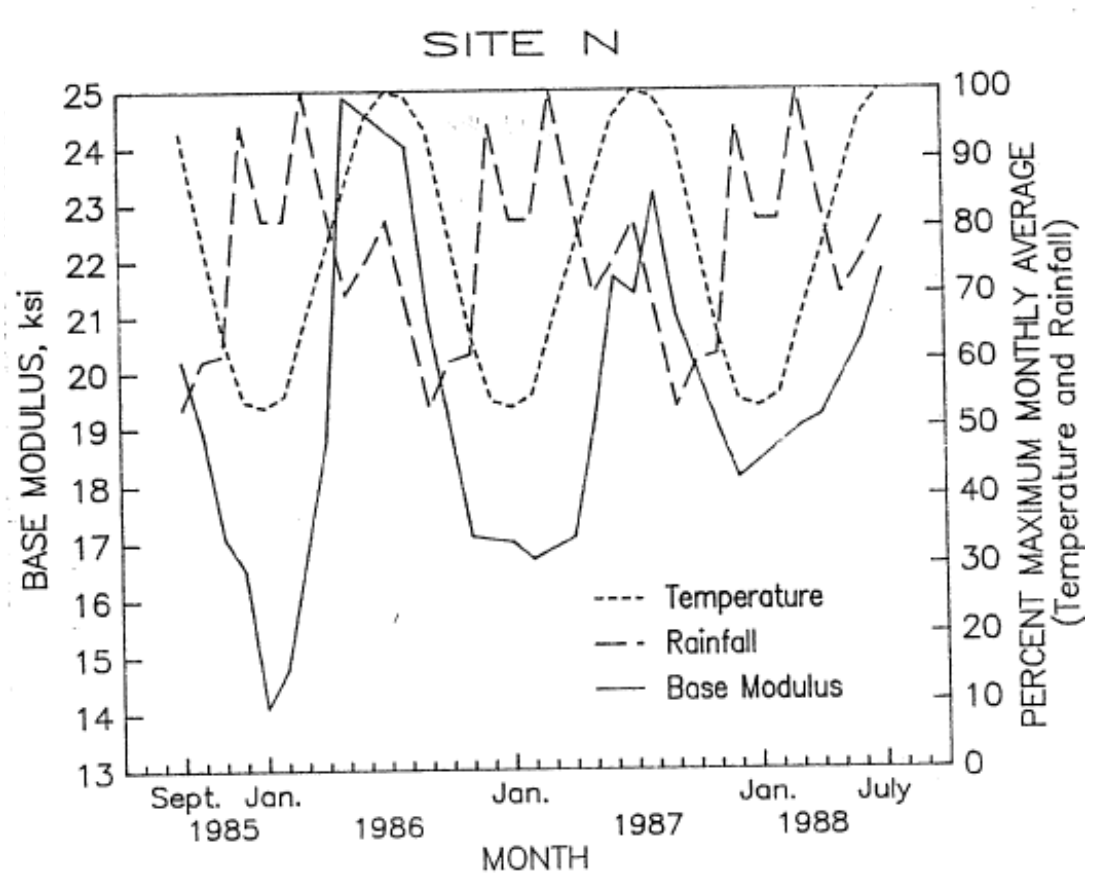


**Figure 2.7 Seasonal Base Moduli Behavior in Alabama (Parker and Elton 1990).**

Timm and Priest ("Material Properties," 2006) conducted a study at the NCAT Test Track in which FWD testing was performed at approximately one month intervals as a means of quantifying the seasonal behavior of the pavement layer moduli. The findings from this study were that the HMA modulus was greatly affected by seasonal changes and those seasonal effects seemed to decline lower in the pavement structure. Both the backcalculated base moduli and subgrade moduli seemed to experience a slight reduction in modulus with increasing temperature. This was opposite of the expected result since hotter pavement temperatures reduce asphalt modulus and allow for higher stresses to be imparted on the unbound layers, causing an increase in modulus for a stress-hardening material. The authors concluded that this seasonal effect might be an artifact of the backcalculation process, and that an annual average unbound layer modulus would be most representative of those materials.

Briggs and Lukanen (2000) conducted a study in which the seasonal pavement layer moduli for 25 different LTPP seasonal monitoring sites across North America were analyzed to quantify seasonal effects. The data for this study were collected between the fall of 1993 and the spring of 1995 on a monthly basis. The authors concluded that seasonal temperature variation affects the modulus of all the pavement layers, not just the surface layer. The study showed that the temperature-induced modulus variations of the

surface layer induce changes in the moduli of the underlying unbound layers. Figure 2.8 illustrates this concept by showing the base modulus variation for a seasonal site near Estillene, Texas, a location that subject to warmer summer temperatures and not subject to frost action. The authors noted that this temperature influence was more notable on thicker asphalt pavements as opposed to thinner ones. It was also evident that the moduli of the unbound layers were most affected by a freezing cycle, and that precipitation had relatively little impact on the unbound layer moduli.

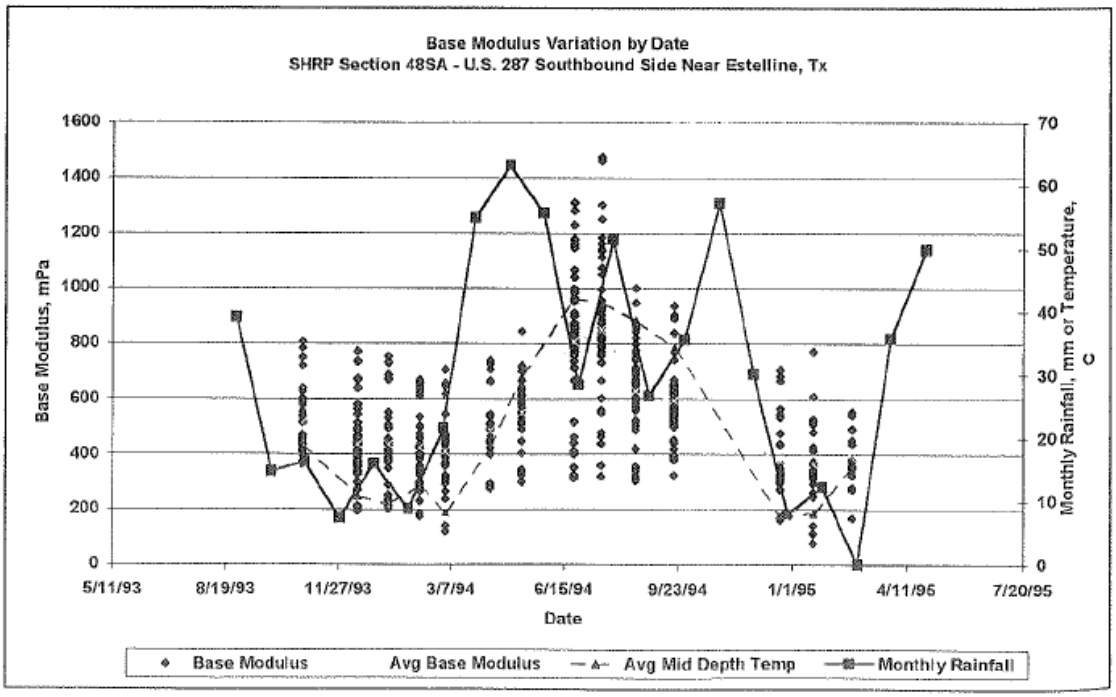


**Figure 2.8 Seasonal Base Moduli Variation at Estillene, Texas LTPP Seasonal Monitoring Site (Briggs and Lukanen 2000).**

The general consensus of the literature on seasonal variation of backcalculated moduli is that there can be a significant fluctuation in modulus values with changing conditions over time. Therefore, a quality FWD testing program should take this into account and test the pavement structure at regular intervals across multiple seasons to best quantify seasonal pavement layer moduli..

**Quality Control of Backcalculated Data**

To get accurate backcalculated modulus values from FWD testing, it is necessary to regularly calibrate the FWD deflection sensors to run good quality control (QC) of the output deflection basins (Von Quintus and Killingsworth, 1998; Irwin 2002). Irwin (2002) states "It is a basic principle that a mismatch between the theoretical assumptions and the actual data will almost inevitably result in an error, sometimes large and sometimes small, in the calculated modulus." Rwebangira et al. (1987) performed a study in which they compared the sensitivity of multiple backcalculation programs to various

inputs. The authors concluded that every backcalculation program they experimented with was very sensitive to the deflection measurements.

Von Quintus and Killingsworth (1998) point out that layered-elastic analysis methods are not necessarily applicable to all deflection basins, and moduli backcalculated from these basins may not be representative of the layer moduli. In their analysis of the LTPP deflection basins, Von Quintus and Killingsworth eliminated several types of deflection basins as being unsuitable for analysis. Typically, these basins exhibited an increase in deflection farther away from the loading point or a large magnitude of deflection increase or decrease between sensors. Figure 2.9 below shows an example of quality deflection basins that exhibit a reasonable decrease in deflection as distance from the load increases, while Figure 2.10 illustrates 'problem' deflection basins where there is an increase in deflection farther away from the load.

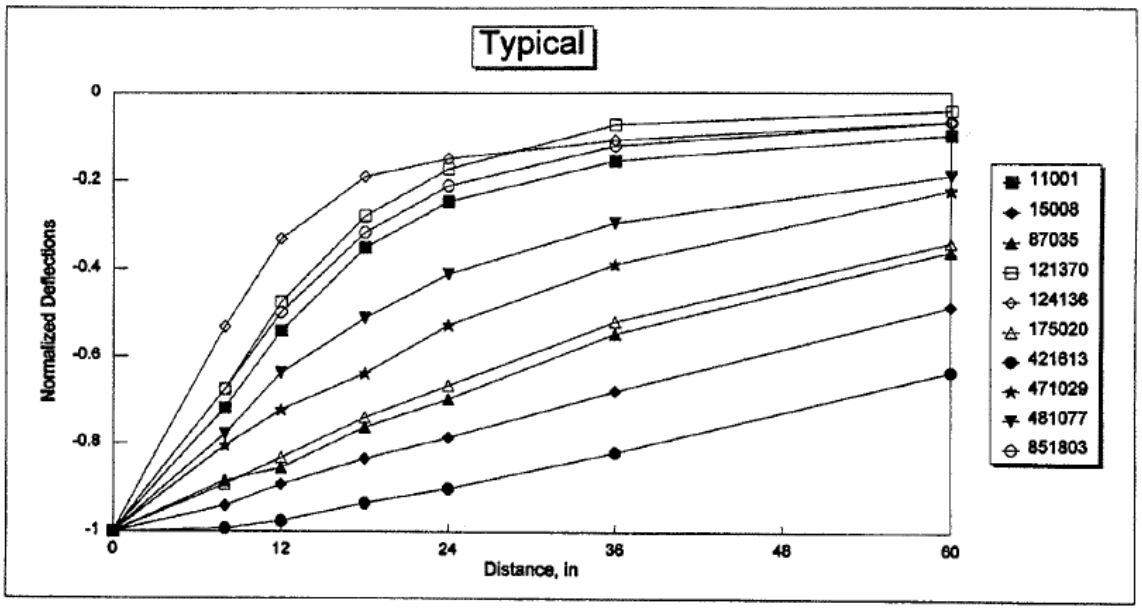


**Figure 2.9 Examples of Quality Deflection Basins (Von Quintus and Killingsworth, 1998).**

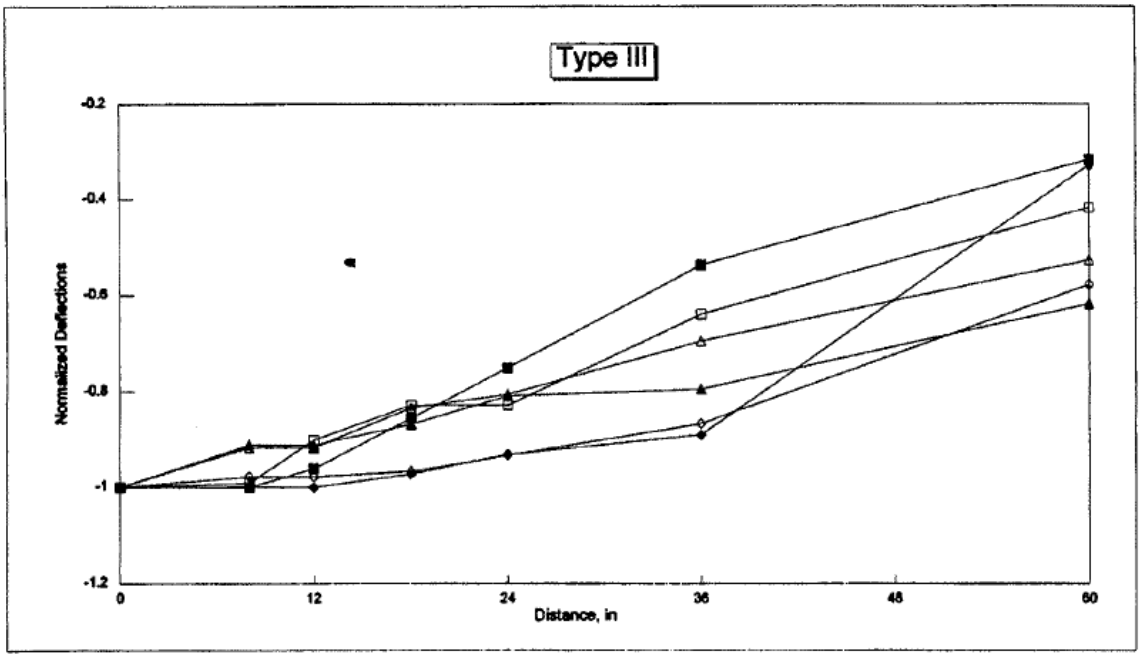


**Figure 2.10 Examples of Problematic Deflection Basins (Von Quintus and Killingsworth, 1998).**

.

A common representation of the overall difference between the measured deflection basin and the layered-elastic predicted deflections is the root mean squared (RMS) error. This term, shown as equation (2-3) below, represents the overall percentage error between the calculated and measured deflections (Sivaneswaran et al., 2001). Commonly, minimization of this error term is desirable to ensure reasonable backcalculated moduli. Von Quintus and Killingsworth (1998) utilized the practice of eliminating deflection basins with an RMS error term above a specific cut-off value. For their data set, this value was set at 2.5 percent. Nevada also uses a cut-off value of 2.5 percent RMS error for their deflection basins (Sebally et al., 2000). For the FWD testing at the WESTRACK experiment, RMS error values were ranked on a relative scale, with RMS error less than 1 being considered 'excellent', values between 1 and 4 percent RMS error being 'very good', and values between 5 and 7 percent RMS error being 'good' (Seeds et al., 2000).

$$RMS\ Error\ (\%) = 100 * \sqrt{\frac{\sum_{i=1}^{N}\left(\frac{d_m - d_c}{d_m}\right)^2}{N}} \qquad (2\text{-}3)$$

where: N = Number of Sensors
$d_m$ = measured deflections
$d_c$ = calculated deflections

**Software Used in Backcalculation**

Several different types of backcalculation software were encountered through various literature involving FWD testing. Some of the more commonly used programs include ELMOD (developed by Dynatest), EVERCALC (developed by the Washington State DOT), MODCOMP (developed by Cornell University), PADAL (developed by the University of Nottingham), and WESDEF (developed by the U.S. Army Waterways Experiment Station) (Irwin, 2002). These different backcalculation programs are equipped with a wide range of features to assist in analysis.

Most backcalculation programs treat all the layers as linear-elastic, and ignore the stress-dependency of the unbound materials. However, both BOUSDEF (Zhou, 2000) and EVERCALC (Sivaneswaran et al., 2001) are capable of modeling the non-linear behavior of the base and subgrade material if multiple FWD loadings are utilized. These programs are able to perform this analysis due to having built-in layered-elastic analysis software to compute comprehensive stress-states at critical locations within the pavement structure after any FWD loading. For programs not containing this feature, a separate layered-elastic analysis would have to be performed to generate these critical stresses. ELMOD is the software designed to be compatible with Dynatest FWD data and is capable of adjusting the HMA modulus based on temperature and adjusting the base and subgrade moduli for seasonal variations (Parker, 1991). Some FWD programs are capable of utilizing the outer deflections to calculate the depth to any existing stiff layer within the pavement structure, while other programs require the entry of a fixed stiff layer depth. Both ELMOD and EVERCALC can utilize the outer deflection sensors to predict the depth to bedrock if indicated to do so by the user, while CHEVDEF and ELSDEF require the location of the stiff layer to be specified by the user (Parker and Elton, 1990; Sivaneswaran et al., 2001).

Though many different backcalculation programs exist, studies have shown that these programs can often yield varying results. Von Quintus and Killingsworth (1998) state that layer moduli generated with different backcalculation programs should not be used interchangeably due to differences in the calculation schemes within these programs. Parker and Elton (1990) evaluated the serviceability of four different backcalculation programs for use in their study. They concluded that while there were differences between the output values generated by each program on identical deflection basins, no one program provided obviously superior results. Rwebangira et al. (1987) also concluded that even with identical input values, the three backcalculation programs evaluated (BISDEF, MODCOMP2, and SEARCH) would generate very different layer moduli. The authors attribute these differences to MODCOMP2 not having the option of including a stiff layer for analysis and SEARCH treating stress distribution differently than the other two linear-elastic based programs. Therefore, it is necessary to be consistent with a given backcalculation procedure and ensure that those results are reasonable for any given project.

**Determining the Optimal Pavement Cross-Section for Backcalculation**

A critical component in generating accurate backcalculated data is the determination of the backcalculation cross-section (or pavement model). This cross-section defines the pavement layers within the backcalculation software. Prior to developing this cross-section, accurate knowledge of the pavement structure to be tested must be obtained. Accurate layer thicknesses are critical for backcalculation to ensure accuracy in material characterization. Von Quintus and Killingsworth (1998) report that a 10% change in layer thickness can easily result in more than a 20% change in layer modulus. Rwebangira et al. (1987) state that the predicted moduli are very sensitive to changes in thickness for both the base and surface layers. The authors reported that a one inch change in surface layer thickness could alter both the base and surface layer moduli by over 60% each. As a result, coring, trenching, or surveyed construction thicknesses are recommended to obtain the site-specific layer thicknesses.

A critical decision involving the cross-section selection involves how many layers to use in the model and whether or not to include a stiff layer for analysis. Rarely is the as-built pavement cross-section used as the pavement model for backcalculation. It is often necessary to combine and subdivide various pavement layers to achieve reasonable results.

In their study regarding the evaluation of pavement layer moduli in Alabama, Parker and Elton (1990) were required to develop a suitable pavement model for backcalculation at each of the testing sites. For this model, all the lifts of hot mix asphalt were combined for the surface layer. For the second layer, the granular base and subbase layers were combined for each site. Additionally, several of the sites included the processed subgrade layer (fill) in the second layer. The authors concluded that the in-situ moisture and density measurements were excellent indicators as to whether to include this fill layer with the base/subbase layer or with the deep subgrade. The results of their analysis showed that this layer should be included with the base/subbase layer if it has moisture and density values similar to those measured in the base/subbase (and vice versa should the moisture and density values be more similar to the deep subgrade). The inclusion of the processed subgrade in the base/subbase layer typically had little effect on the HMA layer modulus, minor impact on the deep subgrade modulus, and significant impact on the base/subgrade layer modulus. In cases where the moisture and density values of the processed subgrade and base/subbase were similar, the composite base layer including the processed subgrade exhibited more consistent and reasonable base layer modulus values than a base layer not including the processed subgrade for backcalculation.

Beneath the composite base layer, the deep subgrade was modeled as the third layer in the pavement model. Below this subgrade, a rigid layer was set at 20 feet beneath the pavement surface. The authors utilized a stiff layer in the pavement model for several reasons: due to the existence of bedrock at a finite depth at many testing locations, due to the natural stiffening of most soils with depth due to increasing confinement leading to an over-prediction of subgrade moduli in the pavement model, and to avoid the calculation of infinitely large subgrade moduli for soils with non-linear stress-strain behavior.

Therefore, the stiff layer was utilized to generate more reasonable pavement moduli at each of the test locations. Figure 2.11 shows the final pavement model used by Parker and Elton for their study.

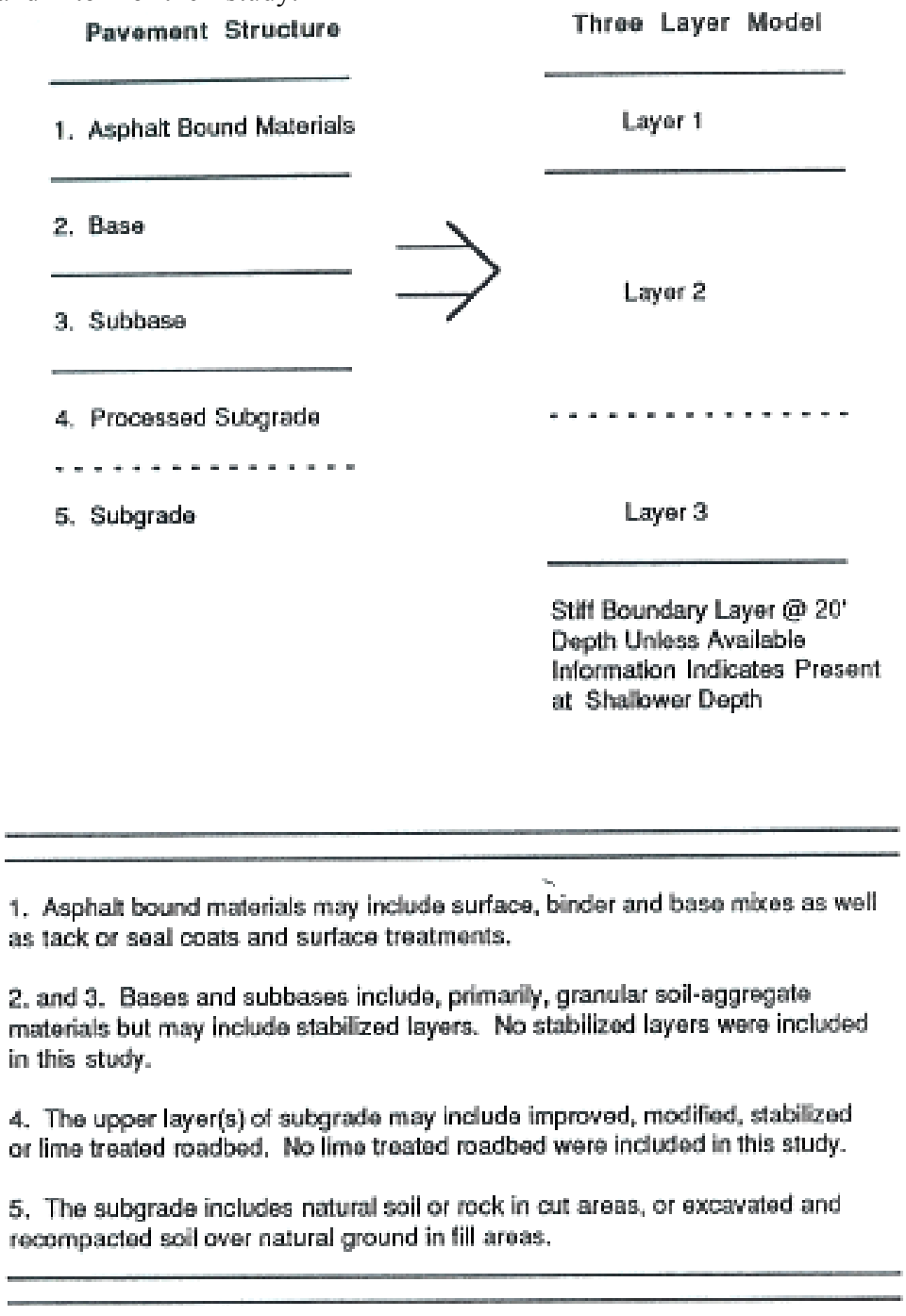


**Figure 2.11 Pavement Model used by Parker and Elton in Alabama (Parker and Elton, 1990).**

Seeds et al. (2000) proposed a three-layer backcalculation cross-section for analysis of the deflection data at the WESTRACK experiment. The contrast between the actual

pavement section and the cross-section for backcalculation are shown in Figure 2.12 below. For these sections, the total thickness of HMA, granular base, and fill material were placed in multiple lifts (two lifts each for both the HMA and granular base, three for the engineered fill). In the final backcalculation cross-section, the top two layers were grouped by material type, using one layer each for combined HMA and granular base thickness. The engineered fill was also combined with the natural subgrade soil due to the backcalculation software (EVERCALC) producing similar results for these two layers. Additionally, a rigid layer was added to the program to account for the stiff layer effects imposed by the water table (typically 3 to 4 meters below the pavement surface).

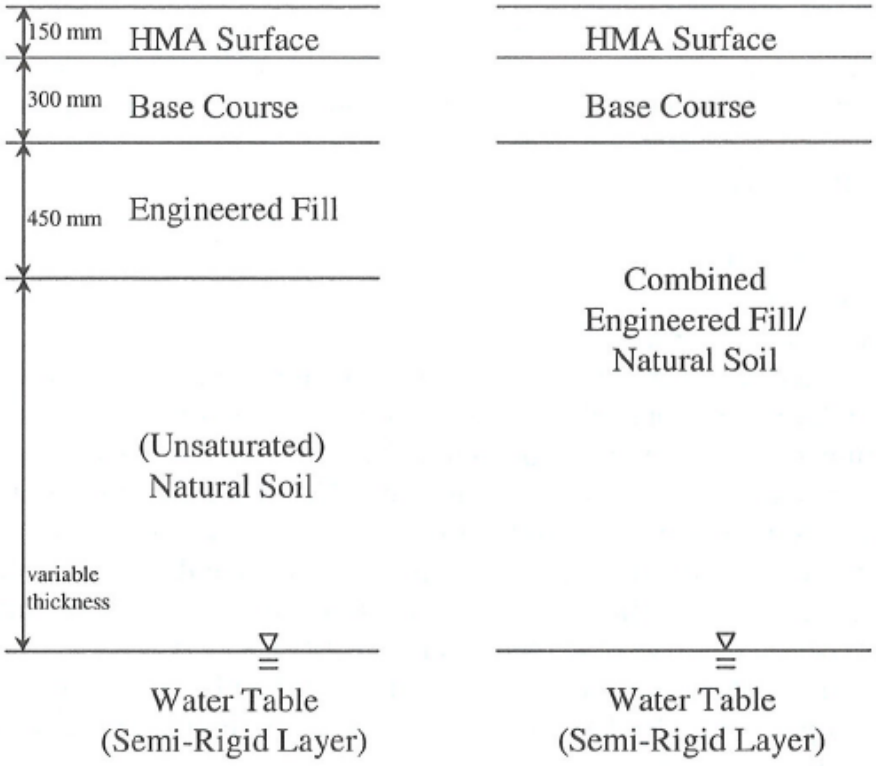


**Figure 2.12 Pavement Model used by Seeds et al. at WESTRACK (Seeds et al., 2000).**

Timm and Priest ("Material Properties," 2006) utilized a three-layer cross-section for analysis of the deflection data from the instrumented sections at the NCAT Test Track. In that study, four trial cross-sections were evaluated on the basis of RMS Error, reasonableness of backcalculated moduli for the different layer materials, and measured (with embedded instrumentation) versus predicted (with layered-elastic analysis) pavement response from FWD testing directly above embedded instrumentation. In their analysis, a stiff layer was deemed inappropriate for use in analysis because the trial cross-section using a stiff layer generated unreasonably high RMS error values and unreasonably low HMA stiffnesses. For the final backcalculation cross-section, a combined HMA layer was used above a composite base layer (consisting of the granular

base material combined with the improved subgrade material) above the deep subgrade layer.

A common theme in the literature is to ensure that the site conditions are well known for the purposes of backcalculation. Von Quintus and Killingsworth (1998) indicated that a layer with different conditions (material type, moisture content, density, etc.) should most often be modeled as a separate layer. Irwin (2002) also suggests that water content and density be used as a differentiating factor between two layers for backcalculation, even if these layers consist of the same material type. Both Ping et al. (2001) and Nazarian et al. (1998) recommend that test pits be excavated near the testing site to accurately measure the pavement layer thicknesses as well as to determine the moisture contents and densities of the pavement layers in-situ. Nevada recommends coring near the testing site to determine HMA thicknesses while utilizing construction information to acquire the base and fill layer properties (Sebally et al., 2000).

The literature points out several pavement conditions that could prove potentially problematic in establishing a viable cross-section for backcalculation. Typically, layers with relatively small thickness within the pavement structure are combined with similar layers for the purposes of backcalculation. If this layer is too thin to have much impact on the surface deflections, then these deflections cannot be used to determine the modulus of that layer (Irwin 2002). Additionally, unbound layers with significantly lower moduli than their supporting layers tend to present problems for the backcalculation process. These issues should be taken into account when deciding upon a backcalculation cross-section for analysis.

When evaluating trial cross-sections, several factors should be considered. First, the match between measured and predicted deflections should be reasonably low (i.e. low RMS error for the solution) (Irwin, 2002). Secondly, good deflection matches does not necessarily mean that the backcalculated moduli are reasonable (Seeds et al., 2000). The modulus values for the individual layers should be compared to ensure that there are no fluctuating moduli or compensating layer effects present (Timm and Priest "Material Properties," 2006). Additionally, the solution should be checked to ensure that the variability within the backcalculated solution can be attributed to variability within the pavement structure (spatial or seasonal) and is not an artifact of the backcalculated solution (Irwin, 2002).

**Typical Inputs for Backcalculation**

Most backcalculation programs require multiple inputs in order to accurately determine pavement layer moduli. In addition to the deflection measurements, some of these inputs include: the pavement layer thicknesses (site-specific), the FWD sensor spacing and load plate radius (FWD specific), a modulus range for solution iterations in each layer, a seed (or initial) modulus value for each layer, the number of allowable solution iterations, Poisson ratios for each layer, and RMS error and modulus tolerances for each pavement layer. These inputs must be carefully selected to generate a viable backcalculation solution.

An iteration range and seed moduli are typically required for each pavement layer in backcalculation to create a boundary for a reasonable solution. Rwebangira et al. (1987) conducted a sensitivity analysis on various backcalculation programs to their required inputs. The authors concluded that the range of moduli used in BISDEF could impact the accuracy of the backcalculated solution. The best results were achieved when the modulus ranges were on the same order of magnitude as the typical modulus values of the layer materials and that narrow modulus ranges could cause the solution to rest on the upper and lower modulus boundaries. The seed moduli selected within the modulus iteration range seemed to have little effect on the backcalculated moduli (provided reasonable seed moduli were used). The authors used a range of 250 to 850 ksi with a seed value of 375 ksi for HMA, a range of 10 to 50 ksi with a seed value of 30 ksi for base layer materials, and a range of 3 to 23 ksi with a seed value of 14.5 ksi for subgrade materials. Both Zhou (2000) and Parker and Elton (1990) recommend using seed moduli that are close to the typical estimated moduli for that layer material. Parker and Elton (1990) also suggest that wide iteration boundaries be set to minimize the constraint on solution iterations. Sebally et al. (2000) recommend that reasonable modulus boundaries be set for each layer with the seed moduli being set mid-range.

Considerable variance was found in literature concerning the number of iterations the program should use along with the RMS error and modulus tolerance used to determine when the measured and backcalculated deflection basins have sufficiently converged. Parker and Elton (1990) used 30 iterations with ELMOD to get deflection and modulus tolerances within 10 percent. This contrasts with the findings of Bush and Alexander (1985) who determined that 3 iterations were most often sufficient to get deflection matching within 3 percent. Rwebangira et al. (1987) determined that a number of iterations greater than 2 typically don't have much effect on the backcalculated moduli, though 10 iterations were used for their study. The authors also determined that using a modulus tolerance below 0.2 percent did not improve the results, while modulus tolerances above 5 percent generate erratic solution behavior. The EVERCALC software (Sivaneswaran et al., 2001) recommends using 5 iterations with a 1 percent tolerance for both RMS error and backcalculated layer moduli.

For each pavement layer to be backcalculated, a Poisson ratio must be specified as a general input. Parker and Elton (1990) noted that ELMOD uses a Poisson Ratio of 0.35 for all materials. For the layered-elastic computation of stresses beneath the FWD load, Parker and Elton (1990) used Poisson ratios of 0.35, 0.40, and 0.45 for the HMA, granular base, and subgrade materials, respectively. Zhou (2000) used Poisson Ratios of 0.35, 0.40, and 0.45 for the HMA, granular base, and subgrade materials, respectively. The MEPDG (2004) does not recommend testing of pavement materials for Poisson's ratio and contains a table of standard values for use with various unbound material types. Irwin (2002) claims that a quality estimate of Poisson's ratio is important, but "the consequences of being slightly incorrect are not very significant."
Typically, the stiffness of the rigid layer is fixed within the program and the bedrock modulus is required as a program input if a stiff layer is to be used. Parker and Elton (1990) noted that ELMOD automatically locates a stiff layer with fixed properties using

the measurements from the outer deflection sensors. In their analysis of other backcalculation software (CHEVDEF and ELSDEF) the authors used a bedrock stiffness of 1,000 ksi and a Poisson Ratio of 0.5. The MEPDG (2004) recommends using bedrock stiffness between 750 and 2000 ksi and a Poisson's ratio between 0.1 and 0.25. Rwebangira et al. (1987) concluded that both the HMA and base layer moduli were very sensitive to the depth to the stiff layer, making an accurate determination of this depth very important.

## COMMONLY USED STRESS-SENSITIVITY MODELS

Given its definition as the ratio of deviatoric stress to recoverable strain, it stands to reason that the state of stress is the primary factor that affects the resilient modulus of a given unbound material. A common issue in resilient modulus testing is the selection of the most appropriate constitutive model relating material stress-state to resilient modulus. There are multiple constitutive equations in literature that relate resilient modulus to a combination of a variety of different stress-states. Some of these stress-states include: the confining pressure ($\sigma_3$), the difference in principal stresses (or deviatoric stress) ($\sigma_d$), the sum of the principal stresses (or bulk stress) ($\theta$), and the octahedral shear stress ($\tau_{oct}$).

### Single Variable Non-Linear Stress Sensitivity Models

The most basic non-linear stress-sensitivity models found in literature relate resilient modulus to a single stress term. All of these models are typically recommended for use with either a coarse-grained (typically non-cohesive) or fine-grained (typically cohesive) soil based on the stress-states used for the regression analysis. Therein exists a fundamental drawback with the use of these models: no one model is suitable for use with all soil types.

One of the most common models in practice relates the resilient modulus to the sum of the principal stresses (or bulk stress). This model accounts for the stress-dependency of coarse-grained soils, which is typically seen with an increase in resilient modulus at increasing confining pressures (Andrei et al., 2004). This model is shown as Equation 2-4, and will be referred to as the 'bulk' model throughout this report. The atmospheric pressure term ($p_a$) is typically used to eliminate the influence of units of pressure on the calculated resilient modulus (Papagiannakis and Masad, 2008). A form of this model that utilizes only the confining stress term instead of the sum of the principal stresses is shown as Equation 2-5 (Papagiannakis and Masad, 2008).

$$M_r = k_1 * \left( \frac{\theta}{p_a} \right)^{k_2} \tag{2-4}$$

$$M_r = k_1 * \left( \frac{\sigma_3}{p_a} \right)^{k_2} \tag{2-5}$$

The model form shown in Equation 2-4 has been widely employed for modeling the stress-dependency of coarse-grained granular materials (Parker and Elton, 1990; Zhou, 2000; Ping et al., 2001; Irwin, 2004; AASHTO, 1993). This model is the recommended constitutive relationship for triaxial testing in the AASHTO Guide for the Design of Pavement Structures (1993). The AASHTO guide states that for base materials the value of the $k_1$ coefficient should be between 3,000 and 8,000 psi and the value of $k_2$ should be between 0.5 and 0.7. Table 2.1 shows the typical coefficients recommended for the bulk model in the AASHTO guide for varying material properties and moisture contents.

**Table 2.1 Typical Values for Bulk Model Coefficients from AASHTO Design Guide (AASHTO, 1993)**

| Moisture Condition | $k_1$* | $k_2$* |
|---|---|---|
| | (a) Base | |
| Dry | 6,000–10,000 | 0.5–0.7 |
| Damp | 4,000–6,000 | 0.5–0.7 |
| Wet | 2,000–4,000 | 0.5–0.7 |
| | (b) Subbase | |
| Dry | 6,000–8,000 | 0.4–0.6 |
| Damp | 4,000–6,000 | 0.4–0.6 |
| Wet | 1,500–4,000 | 0.4–0.6 |

*Range in $k_1$ and $k_2$ is a function of the material quality.

Parker and Elton (1990) conducted triaxial testing on soils collected from various FWD testing sites throughout Alabama and reported the results using the bulk model. The authors reported that the average $k_1$ value for dampened base materials in Alabama was 6.09 ksi, and the average $k_2$ value was 0.43. These coefficients were in reasonable agreement with those presented in the AASHTO guide concerning damp base materials (4 to 6 ksi for $k_1$ and 0.5 to 0.7 for $k_2$). The authors attribute the higher $k_1$ values to the significant cohesion exhibited by natural aggregate materials in Alabama. These materials also tend to have lower frictional resistance between the aggregate particles, resulting in a lower $k_2$ value compared to the AASHTO recommendations.

Zhou (2000) conducted a study in which FWD testing was performed on two different pavement structures at multiple load levels. The use of multiple load levels, combined with utilizing backcalculation program with built in layered-elastic analysis software, allowed the author to use the bulk model to model the stress-sensitivity of the base layer materials in-situ. For each FWD loading, the stress-state at the mid-depth of the base layer was simulated using LEA and regressed against the backcalculated modulus. The $k_1$ coefficients generated from the data set at each job site fall between approximately 9

and 40 MPa (approximately 1.3 and 5.8 ksi). The $k_2$ coefficients range between 0.29 and 0.72 (calibrated to metric units). These coefficients are in reasonable agreement with those presented in the AASHTO guide, especially considering the considerable variability inherent to field testing.

Typically, the resilient modulus of the fine-grained or cohesive soils is modeled as a function of the deviatoric stress, or the octahedral shear stress. The octahedral shear stress is a scalar invariant of the principal stresses which represents the state of shear within the material, shown in Equation 2-6 (Irwin, 2002). When the confining pressures are assumed to be equal on all sides of the test specimen (as with a typical triaxial test), this term can be expressed as a coefficient multiple of the deviatoric stress (shown in Equation 2-7) (Papagiannakis and Masad, 2008). The most common single-term model using the octahedral shear follows the same form as the bulk model, and is shown in Equation 2-8.

$$\tau_{oct} = \frac{1}{3}\sqrt{(\sigma_1 - \sigma_2)^2 + (\sigma_2 - \sigma_3)^2 + (\sigma_3 - \sigma_1)^2} \tag{2-6}$$

$$\tau_{oct} = \frac{\sqrt{2}}{3} * \sigma_d \tag{2-7}$$

$$M_r = k_1 * \left(\frac{\tau_{oct}}{p_a}\right)^{k_2} \tag{2-8}$$

The more commonly used model for the stress-sensitivity of fine-grained soil moduli is a power model using the deviatoric stress, shown as Equation 2-9. This model form is recommended by several authors for use in modeling cohesive soils (Ping et al., 2001; Parker and Elton, 1990). A bi-linear variation of this model (shown in Equations 2-10 and 2-11) is utilized by the ILLI-PAVE and KENLAYER layered-elastic analysis programs (Andrei et al., 2004; Seeds et al., 2000). The power-law form of the model shown in Equation 2-9 will be referred to as the 'deviatoric' model for the purposes of this report.

$$M_r = k_1 * \left(\frac{\sigma_d}{p_a}\right)^{k_2} \tag{2-9}$$

$$M_r = k_2 + k_3(k_1 - \sigma_d) \quad where\ k_1 \geq \sigma_d \tag{2-10}$$

$$M_r = k_2 + k_4(\sigma_d - k_1) \quad where\ k_1 < \sigma_d \tag{2-11}$$

**Multi-Variable Non-Linear Stress Sensitivity Models**

More complicated resilient modulus stress-sensitivity models exist that utilize more than one stress term to describe the stress-state of the material. These models describe the behavior of the material both with changes in confinement pressure and shearing stresses. These models are more complete in that they calculated modulus based on a more

complete state of stress and they are applicable to all soil types regardless of gradation or cohesion.

Uzan (1985) performed a study to ascertain the most suitable equation for modeling the stress-sensitivity of granular materials. The results of his study showed that the single-variable bulk model showed poor agreement with a control set of laboratory data. This poor agreement was mostly due to poor modulus prediction at low levels of axial deformation due to the bulk model not including the effect of shearing strains. The author proposed another model form that included the effect of shearing strains as well as the effect of confinement. This model, commonly referred to as the 'universal' model, is shown as Equation 2-12 (with the addition of the atmospheric pressure terms for unit normalization). Figure 2.13 illustrates the predicted model behavior for both the bulk model and the universal model for their control set of lab data. The figure clearly shows the universal model does a much better job of predicting the resilient modulus at smaller vertical strain values.

$$M_r = k_1 p_a * \left( \frac{\theta}{p_a} \right)^{k_2} * \left( \frac{\sigma_d}{p_a} \right)^{k_3} \tag{2-12}$$

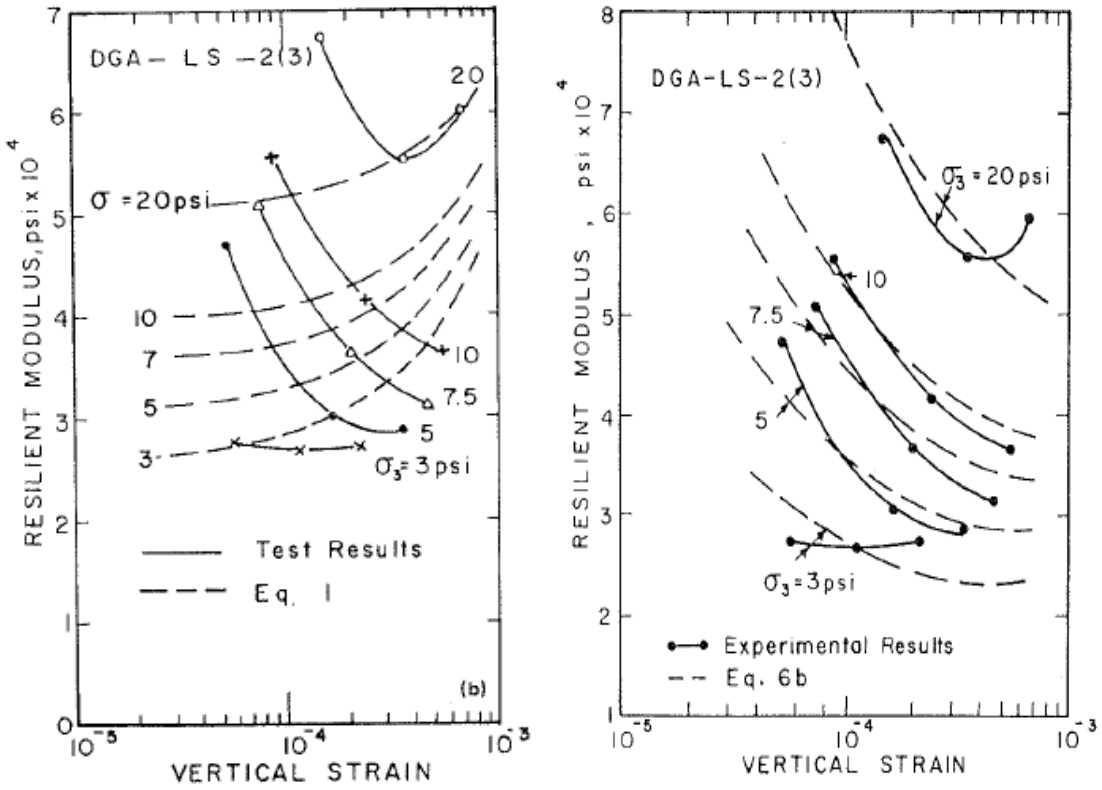


**Figure 2.13 Comparison the Bulk (left) and Universal (right) Model Modulus Predictions for a Given Set of Laboratory Data (Uzan, 1985).**

Equation 2-12 is only valid for a data set in which the confining pressure is assumed to be equal on all sides of the test specimen (typically the case for laboratory triaxial testing). As demonstrated in Equations 2-6 and 2-7, the deviatoric stress can represent the effects of shear when all confining pressures are assumed to be equal. If this assumption is not valid (i.e. in a pavement structure) then the deviatoric term within the universal model should be replaced with the octahedral shear stress term (Papagiannakis and Masad, 2008). This revised equation is shown as Equation 2-13.

$$M_r = k_1 p_a * \left(\frac{\theta}{p_a}\right)^{k_2} * \left(\frac{\tau_{oct}}{p_a}\right)^{k_3} \quad (2\text{-}13)$$

Von Quintus and Killingsworth (1998) performed a study in which the universal model (Equation 2-12) was utilized to represent the stress-sensitivity of the laboratory determined resilient moduli within the LTPP database. The authors evaluated this model, as well as a variant of this model shown as Equation 2-14. The authors concluded that both models provided an excellent fit to the data present in the LTPP laboratory resilient modulus database. The average values for the coefficients to be used with the universal model and the modified model (Equation 2-14) are shown in Table 2.2 and are distinguishable by generic unbound material type (e.g. silt, gravel, clay, etc.) For the universal model, the authors reported testing values ranging from 0 to 3000 MPa for $k_1$, -0.3 to 1 for $k_2$, and -0.5 to 0.9 for $k_3$.

$$M_r = k_1 * (\sigma_d)^{k_2} * (1 + \sigma_3)^{k_3} \quad (2\text{-}14)$$

**Table 2.2 Average Regression Coefficients Using Equation 2-12 and Equation 2-14 for Various Soil Types within the LTPP Laboratory Resilient Modulus Database (after Von Quintus and Killingsworth, 1998)**

| Material/Soil Type | Equation 2-12 | | | Equation 2-14 | | |
|---|---|---|---|---|---|---|
| | $k_1$ | $k_2$ | $k_3$ | $k_1$ | $k_2$ | $k_3$ |
| Clay | 594 | 0.44 | -0.19 | 8300 | -0.08 | 0.26 |
| Silts | 426 | 0.42 | -0.23 | 5800 | 0.08 | 0.48 |
| Sands | 598 | 0.44 | -0.12 | 5400 | 0.14 | 0.45 |
| Gravels | 836 | 0.23 | -0.08 | 8100 | -0.02 | 0.46 |
| Base | 869 | 0.65 | -0.04 | 5500 | 0.21 | 0.59 |

A modified version of the universal model that utilizes the effects of confining pressure (in terms of bulk stress) and the effects of shear (in terms of the octahedral shear stress) is recommended for use to model laboratory resilient modulus data by the NCHRP 1-28A procedure (2004). This general form of this model is shown as Equation 2-15. The coefficient $k_6$ was meant to quantify the effects of capillary suction in unbound materials while the coefficient $k_7$ was meant to mitigate numerical problems with regression analysis when the octahedral shear term approached zero. NCHRP 1-28A stipulates that coefficients $k_1$ and $k_2$ should be greater than or equal to zero, $k_3$ and $k_6$ should be less

than or equal to zero, and $k_7$ should be greater than or equal to one for laboratory data. NCHRP 1-28A recommends that the coefficients $k_6$ and $k_7$ be set to initial estimates of zero and one, respectively, for purposes of analysis. This version of the equation, shown as Equation 2-16, is recommended for unbound material characterization in the new MEPDG (2004). This model will be referred to as the 'MEPDG' model for the purposes of this report.

$$M_r = k_1 p_a * \left( \frac{\theta - 3k_6}{p_a} \right)^{k_2} * \left[ \left( \frac{\tau_{oct}}{p_a} \right) + k_7 \right]^{k_3} \quad (2\text{-}15)$$

$$M_r = k_1 p_a * \left( \frac{\theta}{p_a} \right)^{k_2} * \left[ \left( \frac{\tau_{oct}}{p_a} \right) + 1 \right]^{k_3} \quad (2\text{-}16)$$

Yau and Von Quintus (2002) performed a study in which the entire LTPP laboratory resilient modulus database was analyzed using the model shown as Equation 2-15. For their study, $k_7$ was assumed to be one. First of all, the regression indicated that the coefficient $k_6$ was equal to zero for over half of the resilient modulus tests. The authors subsequently set this coefficient equal to zero for further analysis. The results of the analysis on the LTPP database showed that coefficient $k_1$ ranged from 0 to 3 MPa, $k_2$ varied between 0 and 1.5, and $k_3$ varied between 0 and -7. This analysis was also performed on three different soil groupings: unbound base-subbase materials, coarse-grained soils, and fine-grained soils. The results of this analysis are shown in Table 2.3.

**Table 2.3 Statistical Summary of MEPDG Models Calibrated to the LTPP Database (after Yau and Von Quintus, 2002)**

| Coefficient | Type | Unbound Base-Subbase Materials | Coarse-Grained Soils | Fine-Grained Soils |
|---|---|---|---|---|
| $k_1$ | Median | 0.853 | 0.764 | 0.804 |
| $k_1$ | Mean | 0.873 | 0.802 | 0.896 |
| $k_1$ | Standard Deviation | 0.2726 | 0.2661 | 0.3133 |
| $k_2$ | Median | 0.628 | 0.446 | 0.243 |
| $k_2$ | Mean | 0.626 | 0.452 | 0.282 |
| $k_2$ | Standard Deviation | 0.1330 | 0.1927 | 0.1552 |
| $k_3$ | Median | -0.129 | -1.052 | -1.399 |
| $k_3$ | Mean | -0.170 | -1.140 | -1.576 |
| $k_3$ | Standard Deviation | 0.2148 | 0.7365 | 1.1014 |
| | Number of Tests | 423 | 257 | 105 |

Andrei et al. (2004) performed an evaluation of multiple constitutive models with a control set of 25 laboratory resilient model tests to determine the most appropriate model form. The authors concluded that the single-variable constitutive models (using bulk or octahedral shear stresses) provided the lowest accuracy of resilient modulus prediction and the poorest goodness-of-fit statistics. The model form of Equation 2-15, placing no restrictions on any of the five regression coefficients, provided the best goodness-of-fit statistics. However, the authors believed that the form of the model given as Equation 2-16 (the MEPDG model) gave the best compromise between accuracy, ease of implementation, and computational stability (in the case of low shear stresses).

## COMPARISON OF LABORATORY AND FIELD MODULUS VALUES FOR UNBOUND MATERIALS

Multiple studies have been performed to compare laboratory measured resilient modulus and backcalculated modulus values for the same unbound materials. The majority of the studies show a significant disconnect between the lab and field measured values, with the backcalculated moduli being higher than the laboratory measured moduli for the same material in most cases. Additionally, the general consensus from these studies is that most materials exhibit the same stress-sensitivity behavior (either stress-hardening or stress-softening) in both the laboratory and in the field.

Von Quintus and Killingsworth (1998) performed a study in which they compared backcalculated and laboratory moduli of the same material type within the LTPP database. The authors compared the material moduli at equivalent stress-states, and the stress-states that were simulated under the FWD load were adjusted to include the effect of overburden pressures. These stresses for comparison were simulated at the quarter-depth of the base/subbase materials and 18 inches into the subgrade. The analysis showed that backcalculated moduli were usually considerably higher than lab determined moduli at equivalent stress-states. The average ratios of field moduli to laboratory moduli were 1.61 and 2.86 for base materials and subgrade materials in a typical flexible pavement, respectively. Also, considerably more variability was determined in the ratio of lab to field moduli for base materials than with subgrade materials. Finally, unbound materials that exhibited stress-hardening or stress-softening behavior in the laboratory were found to have similar stress-sensitivity in the field.

Von Quintus and Killingsworth (1998) concluded that a good reason for the documented poor agreement between laboratory and field determined moduli is that lab samples are typically intact, homogeneous samples and the field modulus represents the effective modulus of a much larger, less homogeneous in-place structure. The authors recommend that the backcalculated moduli be adjusted to represent or equal lab values since most pavement design procedures were developed on the basis of using laboratory determined moduli (e.g. The AASHTO Design Guide).

Parker and Elton (1990) offered a comparison between laboratory and backcalculated unbound material moduli in their study on evaluating pavement layer moduli in the state of Alabama. To generate data for this comparison, the authors compared the field

generated moduli (using the FWD) to laboratory moduli generated by entering simulated layered-elastic stresses into the laboratory determined constitutive equation (the bulk stress model). The results showed generally poor agreement between the laboratory and field determined moduli. The average ratio of FWD moduli to lab moduli was determined to be 2.78 with a standard deviation of 1.79 for base and subbase materials in Alabama. The average ratio of FWD moduli to lab moduli was determined to be 1.31 with a standard deviation of 0.29 for subgrade materials in Alabama. These results indicate better agreement and less variability between the lab and field determined moduli for the subgrade materials as opposed to the base materials. Some of these differences were attributed to the differences in lab and field testing and the laboratory samples being disturbed and non-representative of the field materials.

Nazarian et al. (1998) conducted a study in which field modulus testing was performed with an FWD and a Seismic Pavement Analyzer (SPA) at various test sites throughout the state of Texas. These values were then compared to laboratory modulus values from testing conducted both on samples obtained from the source quarry and samples excavated from the site. To compare the moduli generated by the FWD and the laboratory testing on the in-situ samples, representative stresses were generated by simulating stresses beneath a standard dual tandem truck load using the backcalculated layer moduli. These stresses were then input into the laboratory determined constitutive equation for the various unbound materials to generate moduli for comparison. Figure 2.14 shows the comparison between the laboratory and FWD determined moduli at the various test sites throughout Texas. The results of analysis showed that the laboratory and FWD moduli are typically different by anywhere between 40 and 90 percent, with the laboratory moduli usually being smaller than the field moduli (albeit with a few exceptions). The authors concluded that the laboratory and field tests generated completely different results, and no relationship could be determined between the two. Suggested reasons for this poor agreement include: sampling disturbance, non-representative sampling, and long-term effects on the in-situ materials (such as changes in moisture, degradation, cementation of particles, etc.).

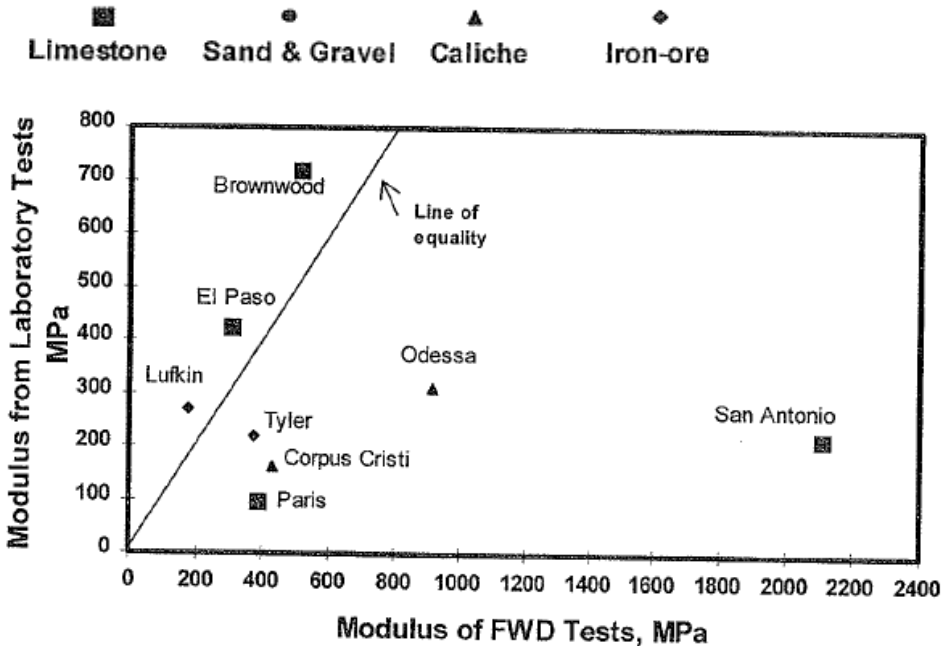


**Figure 2.14 Comparison of Laboratory and FWD Moduli in Texas (Nazarian et al., 1998).**

Seeds et al. (2000) compared the moduli generated from resilient modulus testing and FWD testing on the unbound materials at the WESTRACK experiment. For this comparison, the laboratory moduli were calculated with the material specific constitutive equation using typical stresses under a 40 kN (9 kip) FWD load. Figure 2.15 shows the comparison between the laboratory and FWD moduli for the base layer materials (note an average and standard deviation are present to encompass the variability within each section for FWD testing). Figure 2.16 illustrates the same comparison for the combined fill and natural soil layer. Figure 2.15 clearly shows that the backcalculated base layer moduli are typically 2-3 times higher than the laboratory moduli computed at the same state of stress. Figure 2.16 shows that there is much better agreement between the laboratory and FWD moduli for the unbound materials that are deeper in the structure. The results of this study illustrated that laboratory and FWD measured moduli were not in agreement and no relationship between the two data sets were suggested.

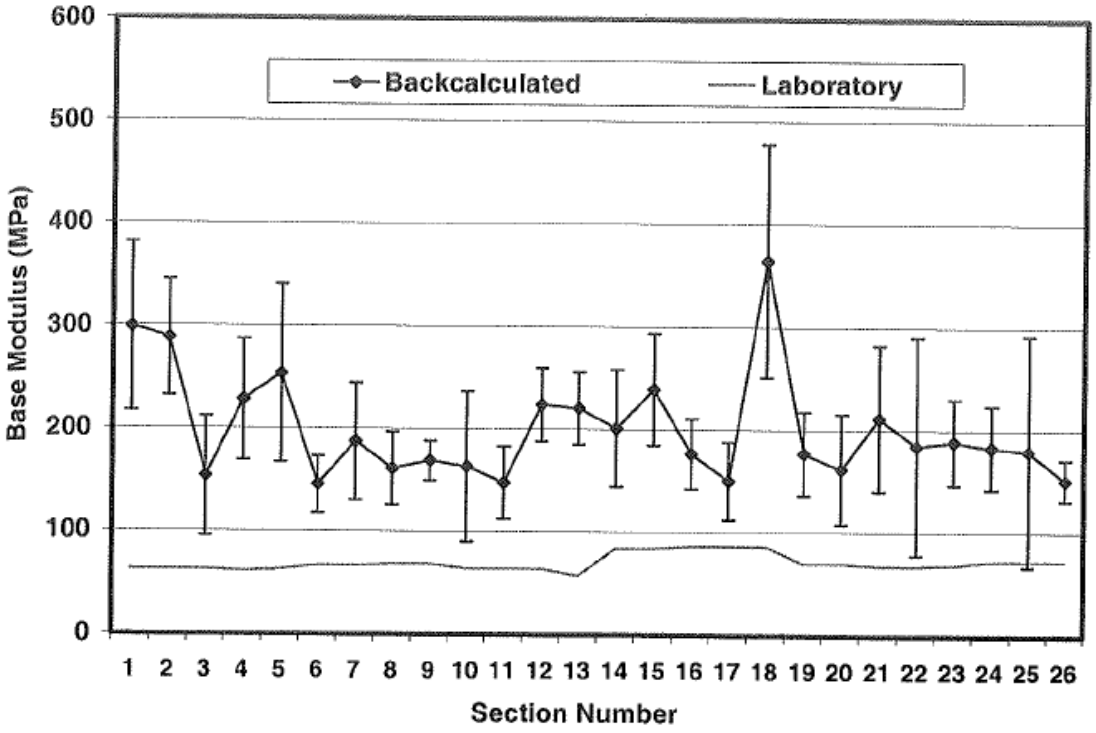


**Figure 2.15 Comparison of Laboratory and FWD Moduli for Base Layer Materials at WESTRACK (Seeds et al., 2000).**

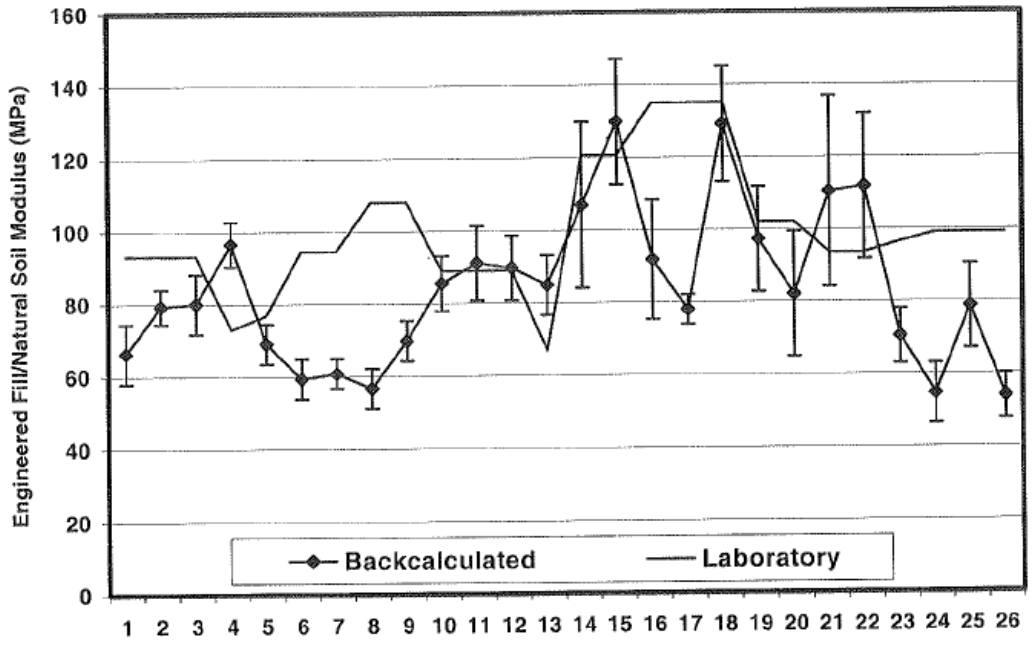


**Figure 2.16 Comparison of Laboratory and FWD Moduli for Fill and Subgrade Layer Materials at WESTRACK (Seeds et al. 2000).**

Zhou (2000) performed a comparison between the laboratory and backcalculated modulus values for granular base materials at two FWD testing sites in the state of Oregon. For comparisons between the laboratory and field modulus values, the resilient modulus was plotted against the bulk stress for each testing site. For the backcalculation, the trendlines represent the constitutive equations (bulk stress model) developed through field testing. Figure 2.17 shows the comparison between the laboratory tested and backcalculated moduli and multiple stress states for the Rufus project, while Figure 2.18 shows the same data for the Centennial Project. The data show that for both projects, the lab and field data both exhibit the same stress-sensitivity behavior (stress-hardening, in this case). The analyses showed that the field calculated moduli were generally higher than the laboratory moduli. The authors concluded that the data showed reasonable agreement in the range of bulk stresses most commonly experienced in pavement base layers, between 40 and 140 kPa (5.8 and 20.3 psi).

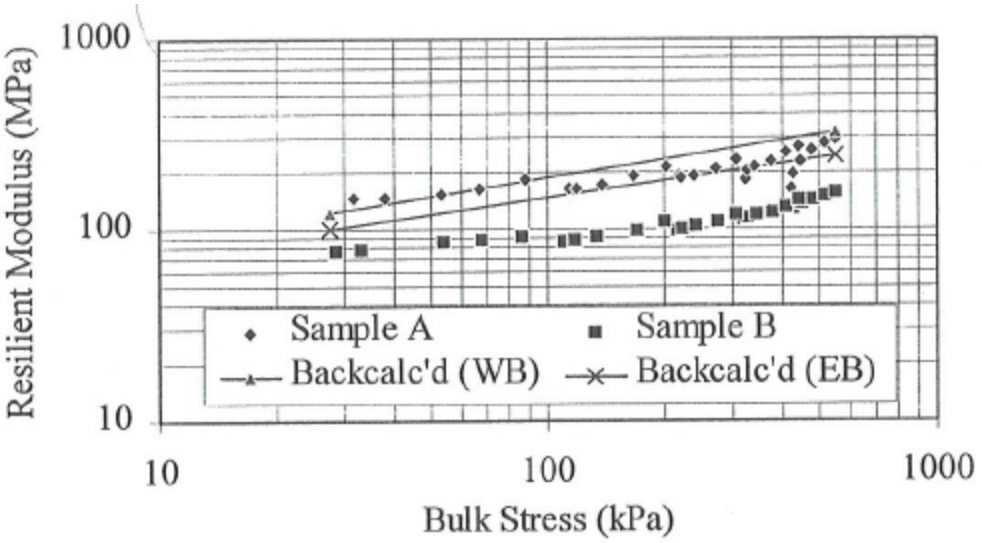


**Figure 2.17 Comparison of Laboratory and FWD Moduli for Base Layer Materials for the Rufus, Oregon Project (Zhou 2000).**

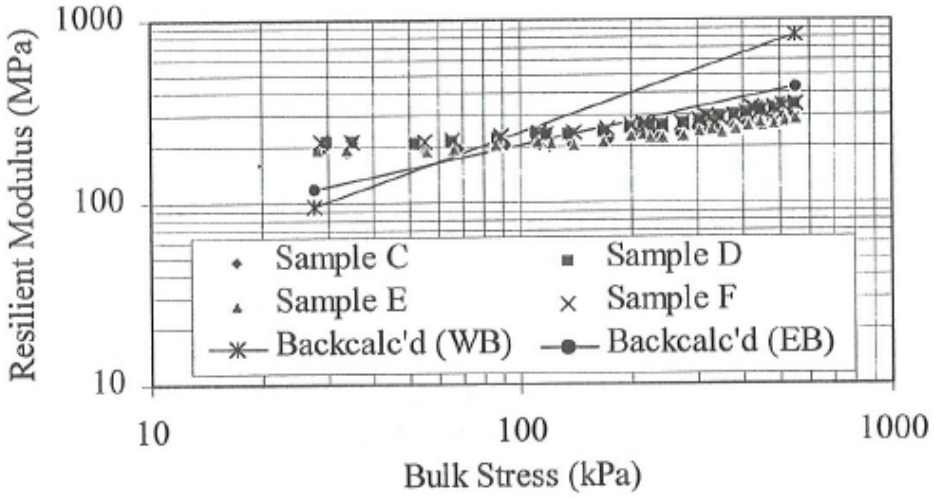


**Figure 2.18 Comparison of Laboratory and FWD Moduli for Base Layer Materials for the Rufus, Oregon Project (Zhou 2000).**

Ping et al. (2001) conducted a study comparing the laboratory and FWD measured moduli for granular materials in Florida. The results of their study concluded that the backcalculated moduli were about 1.8 times higher than the laboratory resilient moduli for the granular materials compacted to in-situ moisture contents and densities. The authors noted that this finding was in general agreement with the AASHTO design guide, which states that FWD moduli are typically between 2 and 3 times higher than laboratory moduli. For this comparison, the 9,000 lb FWD loadings were used for the backcalculated moduli, and the layered-elastic simulated stress-states beneath this loading were entered into the laboratory generated constitutive equation (Equation 2-4 and 2-9). Figure 2.19 below illustrates the comparison between laboratory and field moduli used for this study.

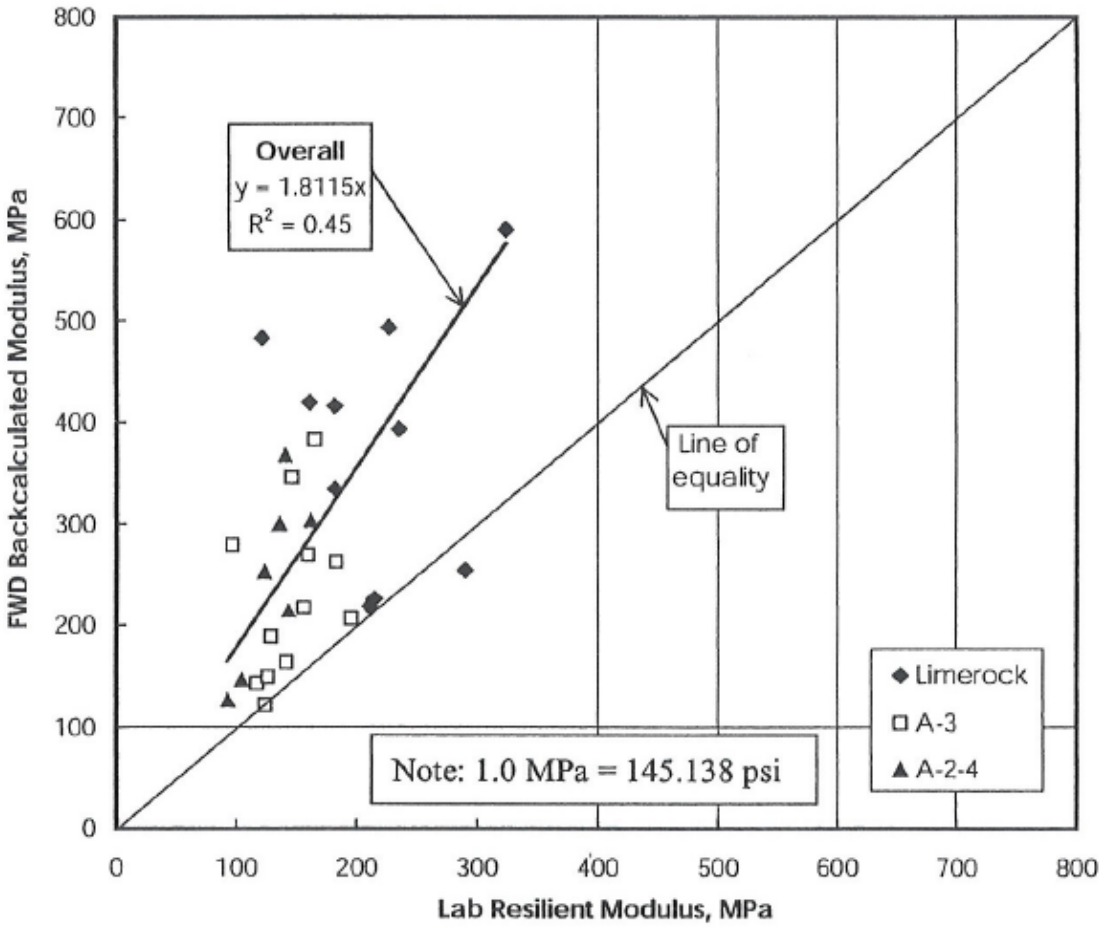


**Figure 2.19 Comparison of Laboratory and FWD Moduli for Unbound Materials used in Florida (Ping et al. 2001).**

**SUMMARY OF KEY FINDINGS IN LITERATURE**

Multiple specifications are currently in practice regarding triaxial resilient modulus testing in the laboratory. However, the new MEPDG (2004) recommends the use of NCHRP 1-28A (2004) or AASHTO T307 (2003) for testing unbound pavement materials to be used in mechanistic design. For this testing, the samples tested in the laboratory should attempt to represent the in-situ condition of the unbound pavement layers (e.g. compaction effort, density, water content) to get the most accurate representation of material stiffness.

Non-destructive testing with the falling weight deflectometer (FWD) can also be used to determine the unbound pavement layer moduli in-situ. However, this method of testing requires careful analysis to get practical results. A very accurate knowledge of the pavement conditions in the field is necessary to generate reasonable backcalculated moduli. Also, the FWD testing program should attempt to capture the many forms of variability experienced by the pavement structure (e.g. seasonal, spatial, and loading variability). Care must also be taken in generating the cross-section for backcalculation.

The cross-section used must provide reasonable deflection matching (low RMS error) and reasonable pavement layer moduli to be considered viable.

Multiple non-linear constitutive models exist in practice that are used to quantify the stress-sensitivity of resilient moduli both in the lab and in the field. The models that contain only one term relating to stress-state (e.g. bulk or deviatoric stress) are only useful for either coarse-grained or fine-grained soils. The multi-variable stress-sensitivity models (e.g. the MEPDG or universal models) are applicable to all soil types regardless of gradation. While the single-variable stress-sensitivity models are still commonly used, other studies have shown that the multi-variable models more accurately predict resilient moduli with changing stress in the laboratory (Uzan, 1985; Andrei et al., 2004).

Several studies have attempted to compare the resilient moduli of laboratory triaxial and field FWD testing for the same material. The results of these studies have shown generally poor agreement between the laboratory and field-measured resilient moduli for granular materials used in the base layer of a flexible pavement. However, the agreement was shown to improve for materials deeper in the pavement structure. Usually, the backcalculated moduli were larger than the laboratory moduli for the same material and the materials exhibited the same stress-sensitivity behavior (either stress-hardening or stress-softening) both in the lab and in the field.

# CHAPTER 3 - TESTING FACILITY AND PROGRAM

## INTRODUCTION

The NCAT Test Track is a 1.7 mile Accelerated Pavement Testing (APT) Facility located in Opelika, Alabama. This facility contains forty-six 200-foot pavement sections that are sponsored by various state DOTs and the Federal Highway Administration for accelerated testing of various pavement performance properties. An aerial view of the NCAT Test Track is shown in Figure 3.1. The Test Track was opened to traffic for the first research cycle in 2000. The first research cycle, for which trafficking was completed in 2002, was designed to investigate pavement rutting and surface distress in various mixes. The second research cycle, which underwent trafficking from October 2003 through December 2005, continued to test mixture-related distress but was also expanded to include eight sections featuring pavement response instrumentation (known as structural sections in this report). The third research cycle commenced trafficking in November of 2006 and features pavement sections with a wider variety of mix types and unbound materials as well as a structural study that was expanded to include 11 instrumented test sections.

**Figure 3.1 Aerial Photo of NCAT Test Track.**

**Trafficking**

The NCAT Test Track employs a fleet of five triple-trailer trucks to apply approximately 10 million equivalent single axle loads (ESALs) to the pavement over a two year research cycle. The trucks are operated by human drivers at a target speed of 45 miles per hour. Trucks are operated approximately 16 hours per day, 5 days per week during the two-year research cycle. Loading the pavement in this manner allows testing the pavement with approximately 10 years worth of traffic in a two year research cycle. Table 3.1 summarizes the axle weights for each of the triple trailer trucks. Table 3.2 summarizes the axle spacing (using the steer axle as a reference point) for the trucking fleet.

**Table 3.1 Axle Weights for Trucking Fleet at NCAT Test Track**

| Truck # | Steer | Front Drive Tandem | Rear Drive Tandem | Single # 1 | Single # 2 | Single # 3 | Single # 4 | Single # 5 |
|---|---|---|---|---|---|---|---|---|
| 1 | 9,400 | 20,850 | 20,200 | 20,500 | 20,850 | 20,950 | 21,000 | 20,200 |
| 2 | 11,200 | 20,100 | 19,700 | 20,650 | 20,800 | 20,650 | 20,750 | 21,250 |
| 3 | 11,300 | 20,500 | 19,900 | 20,500 | 20,500 | 21,000 | 20,650 | 21,100 |
| 4 | 11,550 | 21,200 | 19,300 | 21,000 | 21,050 | 21,000 | 20,750 | 20,800 |
| 5 | 11,450 | 20,900 | 19,400 | 20,100 | 20,450 | 21,000 | 20,050 | 20,650 |

**Table 3.2 Axle Spacings (from Center of Steer Configuration (ft)) for Trucking Fleet at NCAT Test Track**

| Truck # | Steer | Front Drive Tandem | Rear Drive Tandem | Single # 1 | Single # 2 | Single # 3 | Single # 4 | Single # 5 |
|---|---|---|---|---|---|---|---|---|
| 1 | 0.0 | 13.6 | 17.9 | 36.6 | 47.8 | 67.8 | 79.0 | 99.0 |
| 2 | 0.0 | 13.6 | 17.9 | 35.0 | 52.0 | 69.0 | 86.0 | 103.0 |
| 3 | 0.0 | 13.6 | 17.9 | 35.0 | 52.0 | 69.0 | 86.0 | 103.0 |
| 4 | 0.0 | 13.6 | 17.9 | 35.0 | 52.0 | 69.0 | 86.0 | 103.0 |
| 5 | 0.0 | 13.6 | 17.9 | 32.7 | 45.1 | 62.3 | 73.3 | 90.5 |

**THE STRUCTURAL EXPERIMENT**

The 2006 research cycle at the Test Track featured 11 test sections with embedded pavement response instrumentation (known as structural sections). These sections feature a wide variety of hot mix asphalt (HMA) materials, as well as varying unbound materials utilized as the granular base, compacted fill, and subgrade layers. Each section features pressure plates at the surface of the base and compacted fill layers, a strain gauge array at the bottom of the HMA layer, and thermistors at various depths throughout the pavement structure. Further details regarding the instrumentation layout will be given later in this chapter. Figure 3.2 shows a layout of the different structural sections, along with the sponsoring agency, HMA lift composition and construction, and unbound material composition. Sections N1, N2, N8, N9, N10, and S11 were newly constructed for the 2006 research cycle while sections N3, N4, N6, and N7 were left in-place from the 2003 research cycle. Section N5 was rehabilitated with a two-inch mill-and-inlay of the uppermost HMA lift, but the remainder of the pavement construction was left intact.

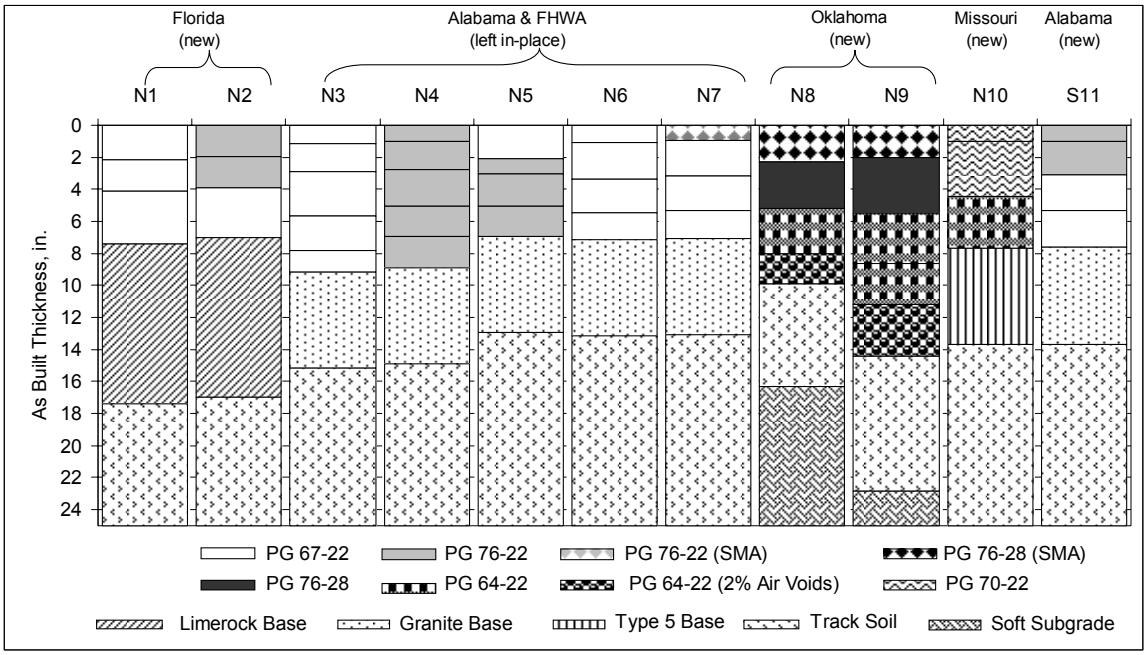


**Figure 3.2 As-Built Cross-Sections for the Structural Sections at the Test Track.**

As shown in Figure 3.2, each of the 11 structural sections features a unique combination of paving layer materials. Each of these sections was constructed as a typical flexible pavement, with HMA materials supported by a base layer supported by compacted fill material and the subgrade soil. Each of the structural sections constructed for the 2003 and 2006 research cycle were constructed by milling the pavement down into the subgrade material, and then building it from the ground up. Table 3.3 shows the milled depth into the pavement structure for each of the structural sections.

**Table 3.3 Milled Depth for the Structural Sections**

| Section | Year of Milling | Milled Depth (in) |
|---|---|---|
| N1 | 2006 | 18.5 |
| N2 | 2006 | 18.5 |
| N3 | 2003 | 30 |
| N4 | 2003 | 30 |
| N5 | 2003 | 30 |
| N6 | 2003 | 30 |
| N7 | 2003 | 30 |
| N8 | 2006 | 58 |
| N9 | 2006 | 62 |
| N10 | 2006 | 34 |
| S11 | 2006 | 30 |

Above the milled depth, a layer of compacted fill material was utilized for every structural section (except N8 and N9, which used the Seale subgrade material). This fill material was the same soil that exists as the deep subgrade material at the Test Track.

Typically, the track fill was compacted to two different density requirements. The six inches of fill directly below the granular base was compacted to a target density that was 100 percent of the laboratory maximum dry density (123.8 pcf, accepting no less than 119 pcf). The remainder of the fill above the milled depth was compacted to 95 percent of the laboratory maximum dry density (118 pcf, accepting no less than 113 pcf). In this way, the subgrade materials at the track were engineered to provide a stable pavement foundation.

**Unbound Materials used in the Structural Study**

There are five different types of unbound materials that are utilized for the structural study at the Test Track. A Florida limerock base was utilized as the base layer material in sections N1 and N2. This material was quarried in Newberry, Florida, and is commonly utilized by the Florida DOT. The granite graded aggregate base material supplied by Vulcan Materials, Inc. was utilized as the base layer material in section N3, N4, N5, N6, N7, and S11. This material is commonly used by ALDOT and was quarried in Columbus, GA. The Type 5 material supplied by the Missouri DOT was used as the base material in section N10. This material is a dolomitic limestone that was quarried in Maryland Heights, Missouri, and is commonly used by the Missouri DOT. The Seale subgrade material was employed by the Oklahoma DOT as the subgrade layer in sections N8 and N9. This material is high clay content borrow material imported from Seale, Alabama. This soil is classified as an A-7-6 material by AASHTO soil classification. Finally, the metamorphic quartzite soil material quarried from the Test Track was utilized as the fill material in every section except N8 and N9. This material was used as the base layer material for N8 and N9 and formed the deep subgrade material for each structural section. This material is classified as an A-4(0) soil by AASHTO classification, and is referred to as either the Track soil, Track fill, or Track subgrade material in this report (depending on its utilization).

Table 3.4 shows the material gradations for each of the unbound materials. Note that the three base layer materials (the limerock, granite, and Type 5) have reasonably well-graded particle distributions, with relatively small percentages of material retained above the ¾" sieve. These materials also exhibit lower amounts of material passing the #200 sieve than the two materials that are predominantly used as subgrade materials (the Seale and Track soil). The Seale material is by far the most fine-graded of the materials, with almost 58 percent of the material passing a #200 sieve. The Track soil appears to be gap-graded, with 17 percent of the material retained on the 1" sieve and 48 percent of the material passing the #200 sieve.

**Table 3.4 Unbound Material Gradations**

| Material | Limerock | Seale | Type 5 | Track Soil | Granite |
|---|---|---|---|---|---|
| Layers | Base | Subgrade | Base | Subgrade | Base |
| Sections | N1, N2 | N8, N9 | N10 | All (N8, N9 Base) | S11 |
| Sieve | Percent Passing Control Sieve | | | | |
| 1 1/2" | 100 | 100 | 100 | 100 | 100 |
| 1" | 100 | 100 | 99 | 83 | 95 |
| 3/4" | 100 | 100 | 97 | 81 | 88 |
| 1/2" | 88 | 100 | 92 | 78 | 83 |
| 3/8" | 81 | 100 | 88 | 75 | 78 |
| #4 | 61 | 100 | 79 | 71 | 57 |
| #8 | 44 | 100 | 71 | 68 | 47 |
| #16 | 32 | 99 | 64 | 66 | 39 |
| #30 | 26 | 98 | 58 | 64 | 31 |
| #50 | 23 | 92 | 49 | 61 | 23 |
| #100 | 21 | 82 | 36 | 56 | 15 |
| #200 | 18.8 | 57.7 | 25.1 | 48.0 | 10.2 |

Tables 3.5 and 3.6 show the in-situ densities and moisture contents, respectively, that were utilized for this study. It should be noted that the densities and moisture contents for the 2003 structural sections were taken from testing near the gauge location and not across the entire section. However, for the purposes of this study these values were deemed to reasonably approximate the in-situ densities required for the calculation of overburden stresses within the pavement layers. Table 3.5 shows that the granite material is compacted to the highest density of the unbound materials layers while the limerock base appears to have the lowest in-situ wet density. All of the material wet densities fall in a range between 127 and 147 pcf. Table 3.6 shows that the Seale material has the highest in-place moisture content, followed by the limerock and Track soil materials. In-situ moisture contents for the structural study range anywhere from 3.7 percent to 18.9 percent.

**Table 3.5 In-Situ Unbound Material Wet Densities for the Structural Study**

| Section | Granular Base-Wet Density (pcf) | Material Type | High Density Fill-Wet Density (pcf) | Material Type | Low Density Fill-Wet Density (pcf) | Material Type |
|---|---|---|---|---|---|---|
| N1 | 127.0 | Limerock | 132.2 | Track Soil | 131.0 | Track Soil |
| N2 | 129.6 | Limerock | 132.6 | Track Soil | 130.9 | Track Soil |
| N3 | 146.5 | Granite | 128.0 | Track Soil | 129.1 | Track Soil |
| N4 | 145.9 | Granite | 127.2 | Track Soil | 128.8 | Track Soil |
| N5 | 146.1 | Granite | 131.7 | Track Soil | 130.2 | Track Soil |
| N6 | 146.5 | Granite | 135.9 | Track Soil | 132.5 | Track Soil |
| N7 | 146.8 | Granite | 132.3 | Track Soil | 129.6 | Track Soil |
| N8 | 133.9 | Track Soil | 126.9 | Seale | N/A | N/A |
| N9 | 133.8 | Track Soil | 127.4 | Seale | N/A | N/A |
| N10 | 137.4 | Type 5 | 133.0 | Track Soil | N/A | Track Soil |
| S11 | 145.5 | Granite | 136.6 | Track Soil | 130.4 | Track Soil |

**Table 3.6 In-Situ Unbound Material Moisture Contents for the Structural Study**

| Section | Granular Base – Moisture Content (%) | Material Type | High Density Fill – Moisture Content (%) | Material Type | Low Density Fill – Moisture Content (%) | Material Type |
|---|---|---|---|---|---|---|
| N1 | 11.9 | Limerock | 9.8 | Track Soil | 12.1 | Track Soil |
| N2 | 13.0 | Limerock | 8.3 | Track Soil | 10.5 | Track Soil |
| N3 | 6.2 | Granite | 7.8 | Track Soil | 12.8 | Track Soil |
| N4 | 5.8 | Granite | 7.2 | Track Soil | 11.8 | Track Soil |
| N5 | 6.2 | Granite | 10.4 | Track Soil | 12.4 | Track Soil |
| N6 | 6.5 | Granite | 9.7 | Track Soil | 11.4 | Track Soil |
| N7 | 6.6 | Granite | 8.7 | Track Soil | 11.7 | Track Soil |
| N8 | 10.4 | Track Soil | 18.9 | Seale | N/A | N/A |
| N9 | 10.7 | Track Soil | 17.7 | Seale | N/A | N/A |
| N10 | 4.5 | Type 5 | 6.2 | Track Soil | N/A | Track Soil |
| S11 | 3.7 | Granite | 10.5 | Track Soil | 12.5 | Track Soil |

**Section Construction**

For the purposes of developing a suitable backcalculation cross-section, it is necessary to have a good understanding of the layer composition and construction for a given pavement section. Therefore, for each of the structural sections, it was useful to generate a detailed diagram showing how each section was constructed. These diagrams show the composition of each section both before and after construction.

Sections N1 and N2 were both sponsored by the Florida DOT and are constructed very similarly. Both sections had approximately 7 inches of HMA atop 10 inches of limerock base over compacted Track fill and subgrade. Both sections were milled to a depth of 18.5 inches for the 2006 research cycle, and only 1.5 inches of additional Track fill was compacted (to 100% of maximum laboratory dry density) in each section above the existing Track fill. Approximately 11.5 inches of Track fill remained in-place below the milled depth from the 2003 research cycle above 12 inches of Track fill compacted for the 2000 research cycle. The only difference in these sections was that all the HMA in N1 used unmodified binder (PG 67-22) while the top two HMA lifts in N2 contained modified binder (PG 76-22). Figures 3.3 and 3.4 show how each section was constructed by comparing the section cross-section in 2003 versus the cross-section in 2006 for section N1 and N2, respectively.

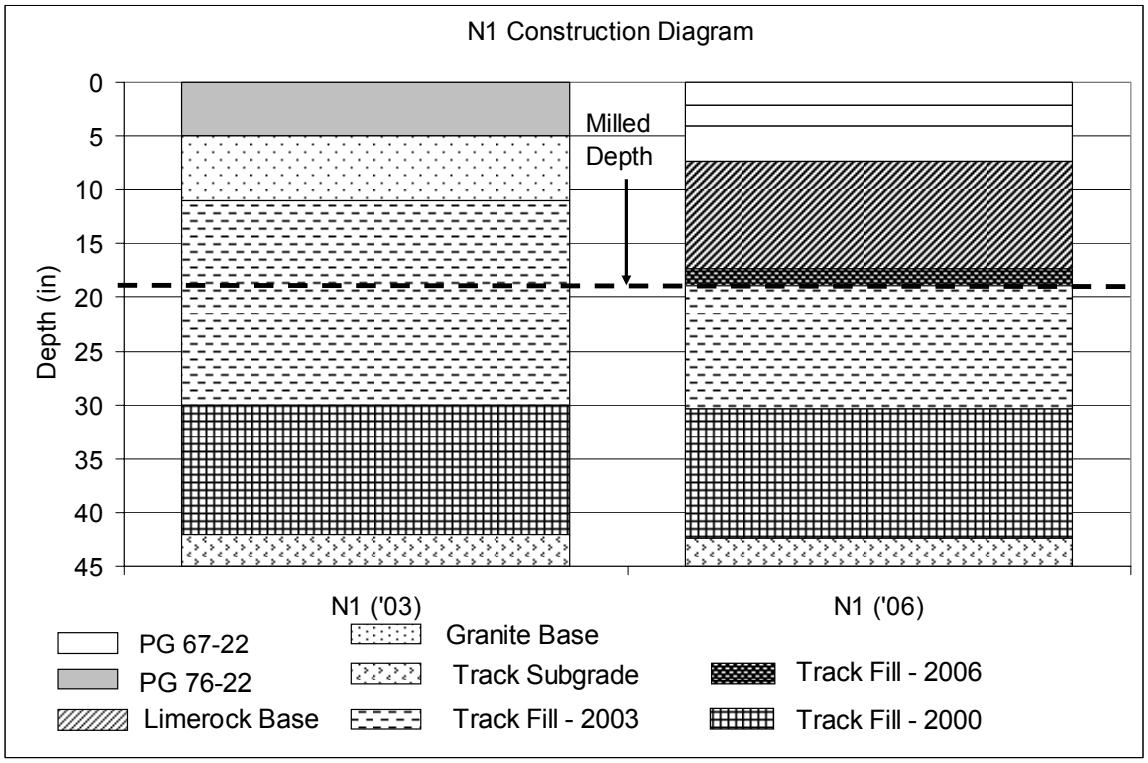


**Figure 3.3 Construction Diagram for Section N1.**

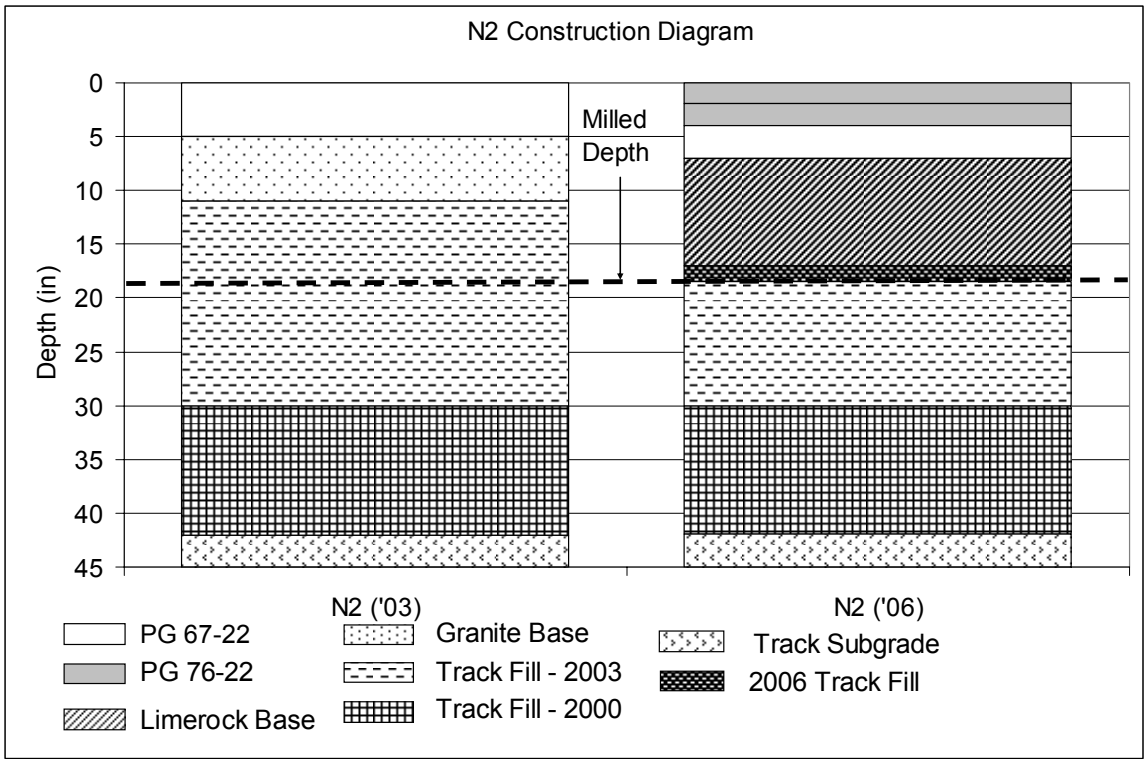


**Figure 3.4 Construction Diagram for Section N2.**

Sections N3 through N7 were constructed as part of the original structural study for the 2003 research cycle and were left in-place for the 2006 research cycle. The only rehabilitation performed was a mill-and-inlay of the upper lift on N5. These sections were sponsored by the Alabama DOT and the Federal Highway Administration (FHWA). Sections N3 and N4 were constructed very similarly, with 9 inches of HMA over 6 inches of granite base above compacted fill to a milled depth of 30 inches. The Track fill above the milled depth was compacted for the 2003 research cycle. The only difference in these sections was that N3 consisted of unmodified HMA (PG 67-22) and N4 contains modified HMA (PG 76-22). Sections N5, N6, and N7 were also constructed very similarly, with 7 inches of HMA above 6 inches of granite base above various layers of compacted Track fill and deep Track soil subgrade. The difference in these sections again was within the HMA composition. Section N5 utilized unmodified binder for its uppermost lift, but modified binder through the rest of the HMA depth. Section N6 was comprised entirely of unmodified HMA. Section N7 had unmodified HMA for its lower three lifts but a surface lift of a modified (PG 76-22) Stone Matrix Asphalt (SMA). Figure 3.5 shows the composition of each of the structural sections constructed in 2003 versus the structural cross-section for the original construction in 2000.

Section N8 was sponsored by the Oklahoma DOT. This section was milled to a depth of 58 inches, and contained approximately 40 inches of the clay-like Seale subgrade above the milled depth. Above the Seale subgrade, approximately 6 inches of the Track soil material was compacted as a base layer and 10 inches of HMA was placed above this. The HMA consisted of a PG 76-28 SMA upper lift above lifts containing PG 76-28

HMA, PG 64-22 HMA, and PG 64-22 HMA compacted to 2 percent air voids, from top to bottom. Figure 3.6 outlines the construction and material composition of this section.

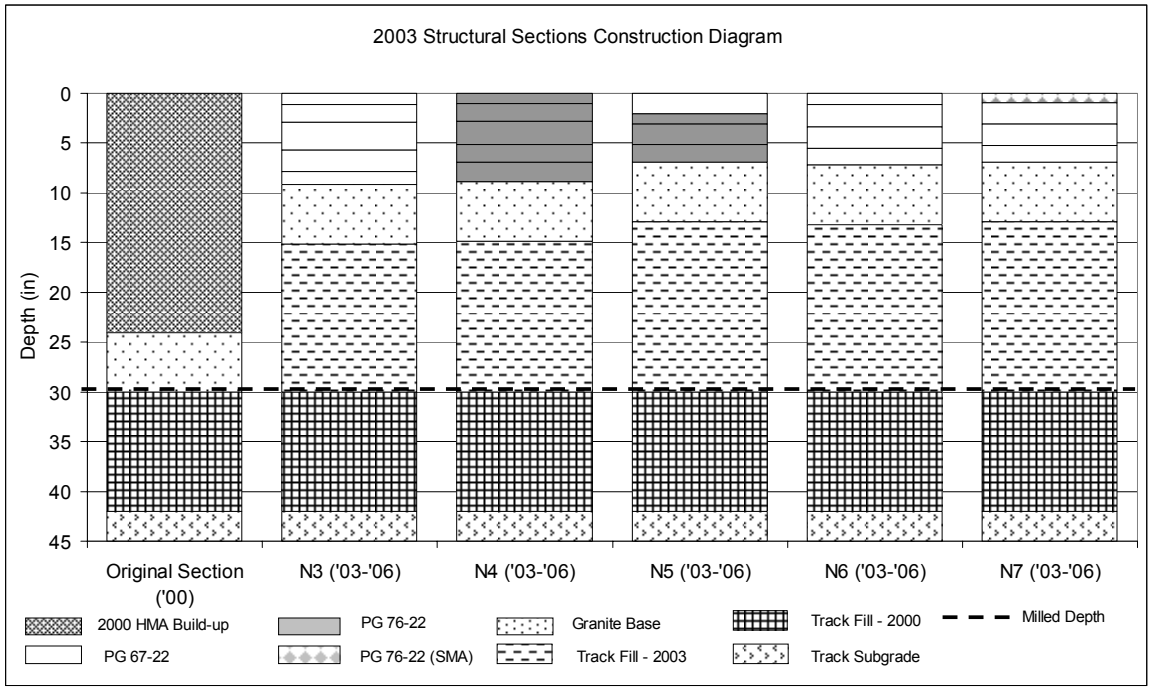


**Figure 3.5 Construction Diagram for 2003 Structural Sections.**

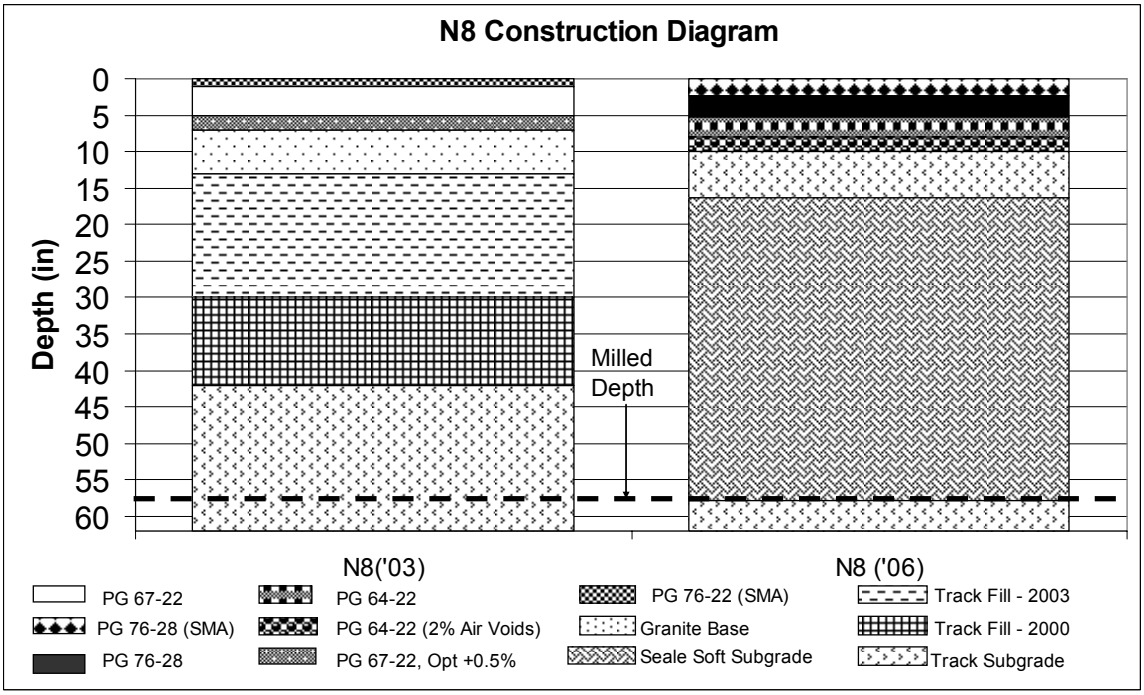


**Figure 3.6 Construction Diagram for Section N8.**

Section N9 was also sponsored by the Oklahoma DOT. This section was milled to a depth of 62 inches, and contained approximately 40 inches of the clay-like Seale subgrade above the milled depth. Above the Seale subgrade, approximately 8 inches of the Track soil material was compacted as a base layer and 14 inches of HMA was placed above this. This section was designed to perform as a perpetual pavement. The HMA also consisted of a PG 76-28 SMA upper lift above lifts containing PG 76-28 HMA, two lifts of PG 64-22 HMA, and PG 64-22 HMA compacted to 2 percent air voids, from top to bottom. Figure 3.7 outlines the construction and material composition of this section.

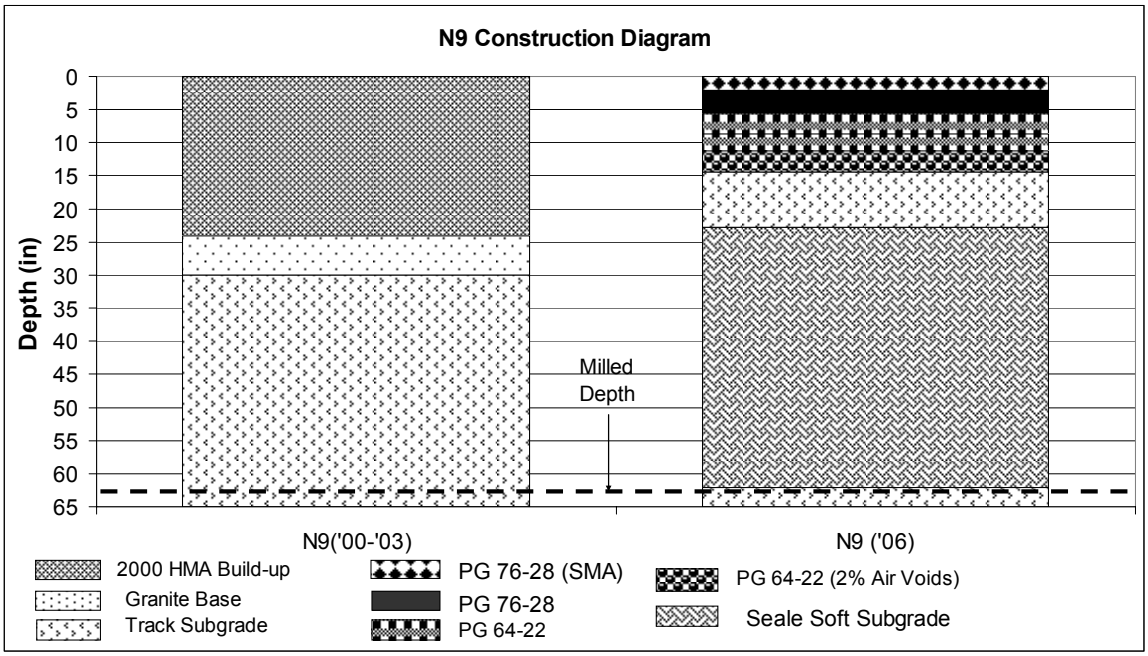


**Figure 3.7 Construction Diagram for Section N9.**

Section N10 was sponsored by the Missouri DOT and consisted of approximately 8 inches of HMA above 4 inches of Type 5 base material above Track fill and subgrade. The section was milled to a depth of 34 inches. Below the milled depth lies 8 inches of Track fill compacted for the 2000 research cycle above the deep Track subgrade. Above the milled depth was approximately 16 inches of the Track fill compacted to 95 percent of laboratory maximum dry density below 6 inches of Track fill compacted to 100 percent of laboratory maximum dry density. The HMA consisted of two upper lifts of PG 70-22 HMA over one lift of PG 64-22 HMA. Figure 3.8 shows the constructed cross-section for section N10 in detail.

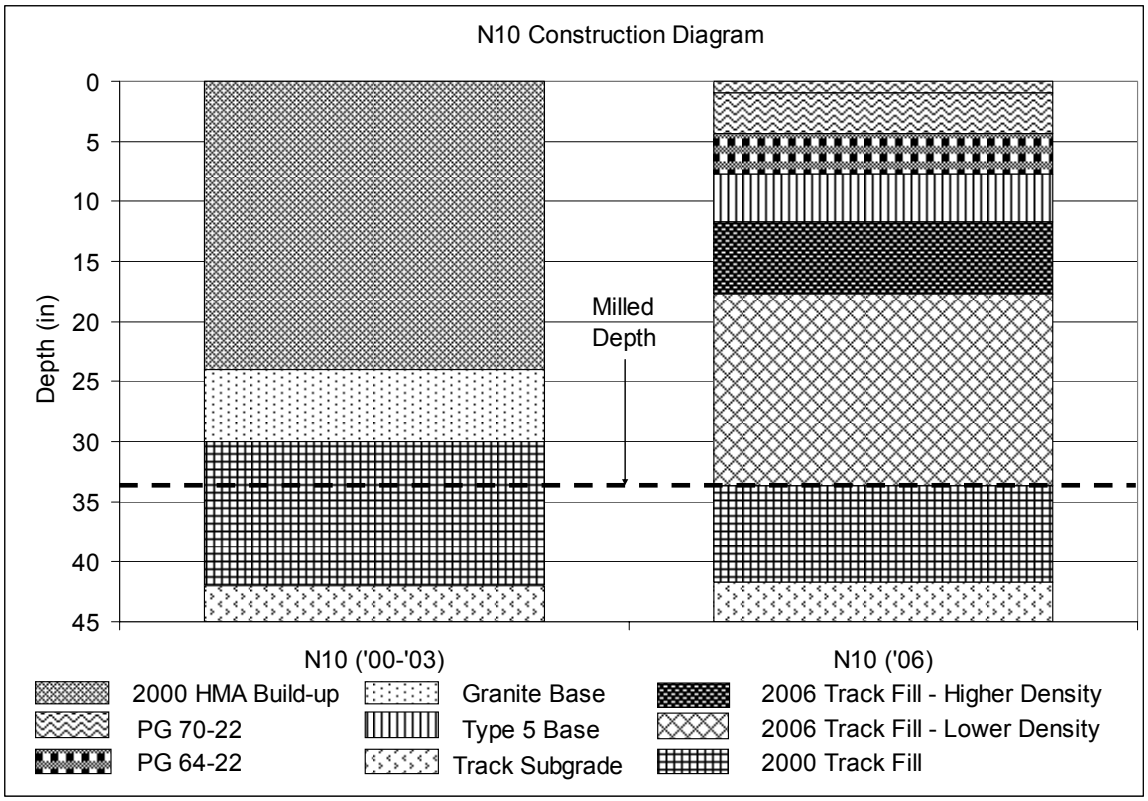


**Figure 3.8 Construction Diagram for Section N10.**

Section S11 was sponsored by the Alabama DOT and was constructed very similarly to the structural sections left in-place from the 2003 research cycle. The section was milled to a depth of 30 inches above 12 inches of Track fill compacted for the 2000 research cycle and the deep Track subgrade. Above the milled depth, approximately 11 inches of Track fill compacted to 95 percent of maximum laboratory dry density was added. Above this, another 6 inch lift of Track fill compacted to 100 percent of maximum laboratory dry density was added. Above the fill layer, 6 inches of granite base was compacted beneath 8 inches of HMA. The upper two lifts of the HMA utilized a modified binder (PG 76-22) while the lower lifts utilized unmodified binder (PG 67-22). Figure 3.9 shows the full constructed cross-section for section S11.

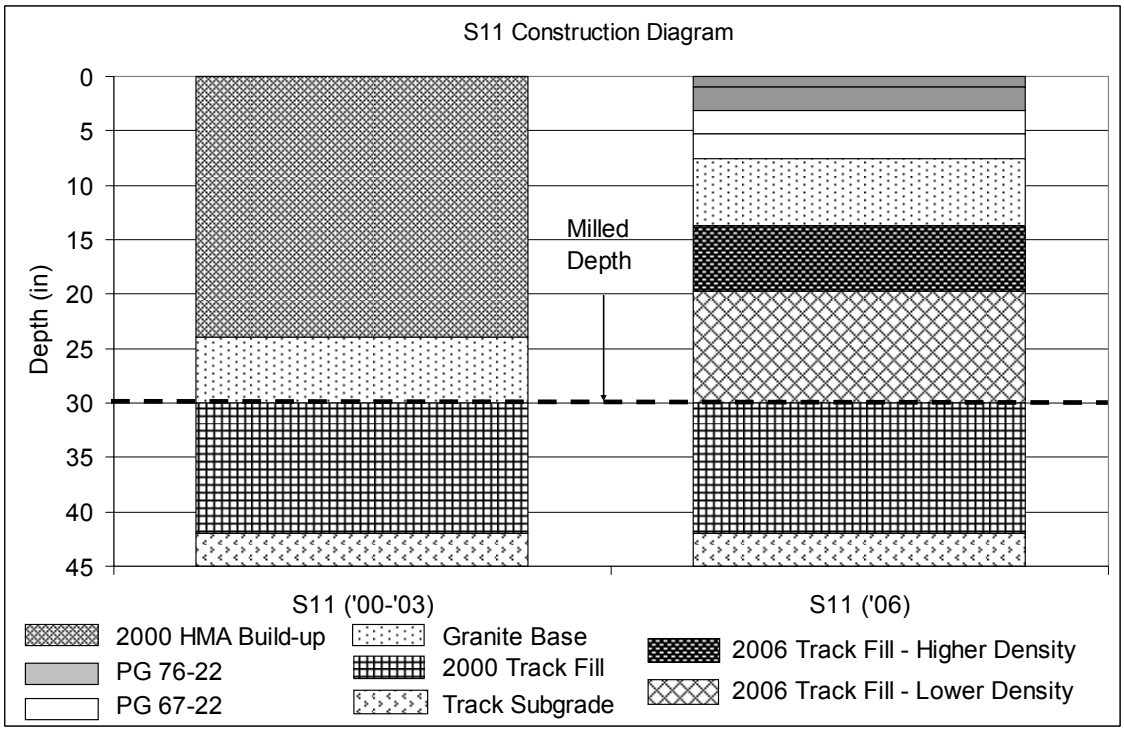


**Figure 3.9 Construction Diagram for Section S11.**

For the purposes of backcalculation and predicting accurate stress-states within the pavement structure, it is necessary to have accurate as-built information regarding pavement layer thicknesses and densities. Figure 3.10 shows the average as-built thicknesses for both the HMA and granular base layers for each of the 11 structural sections. These values constitute an average of the surveyed thicknesses acquired at various random locations across each structural section (random locations will be discussed in detail later in this chapter). Table 3.7 shows the average HMA densities for each structural section. Again, the density values for the 2003 structural sections were specific to the gauge array location, but were considered to be representative of the test section and sufficient for overburden calculation.

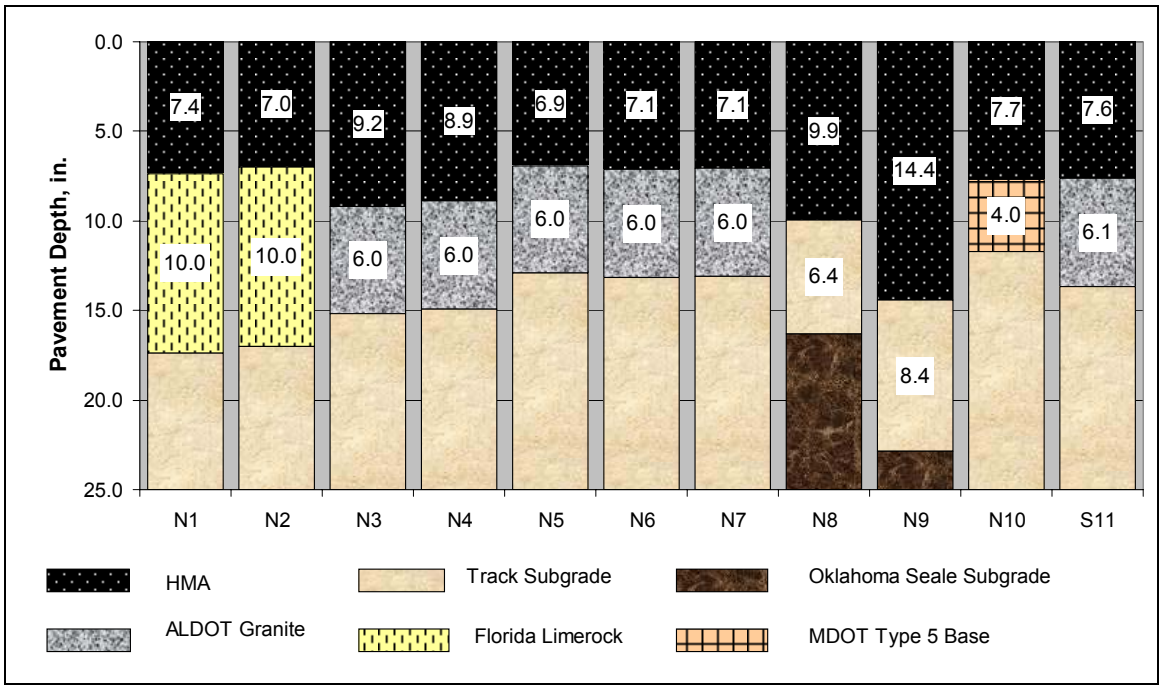


**Figure 3.10 Average HMA and Base As-Built Thicknesses for All Structural Sections.**

**Table 3.7 HMA Densities for Overburden Calculation**

| Section | HMA Density (pcf) |
|---|---|
| N1 | 145.6 |
| N2 | 148.0 |
| N3 | 148.0 |
| N4 | 147.6 |
| N5 | 146.6 |
| N6 | 148.9 |
| N7 | 148.1 |
| N8 | 143.3 |
| N9 | 144.0 |
| N10 | 142.4 |
| S11 | 146.9 |

**Structural Instrumentation**

Each of the sections used for the structural study were equipped with a standard array of subsurface pavement response instrumentation. Each section contained 12 asphalt strain gauges, 2 earth pressure cells, and a bundle of 4 thermistors at various depths throughout the pavement structure. Some sections were equipped with additional instrumentation for other studies, but this instrumentation is beyond the scope of this report. Figure 3.11 shows the general layout of the gauges used in a typical structural section. Figure 3.12 shows a photograph of the gauge layout prior to installation.

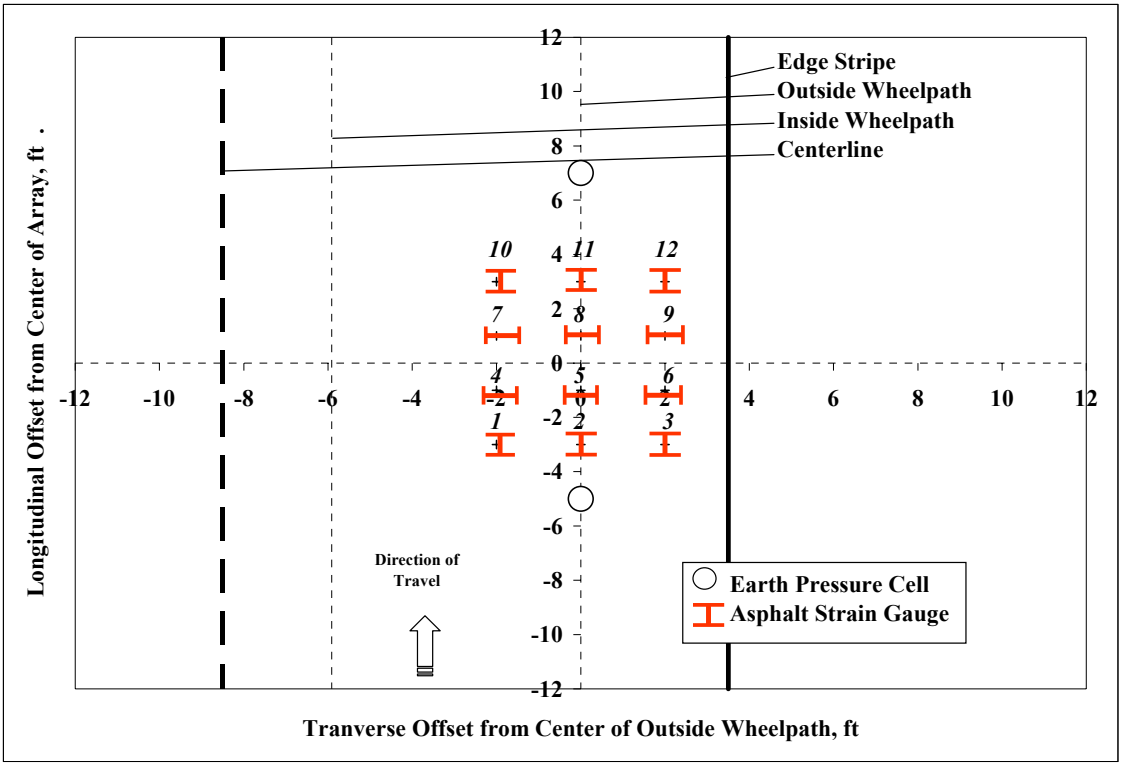


**Figure 3.11 Layout of Gauge Array for a Typical Structural Section (after Willis and Timm 2008).**

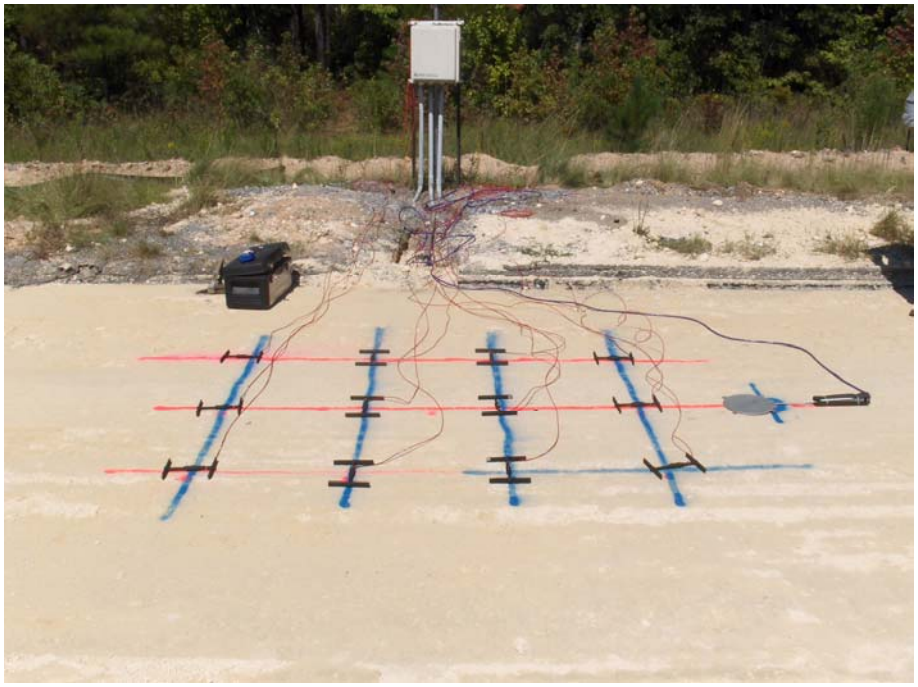

**Figure 3.12 Gauge Array Prior to Construction.**

Each gauge array contained 12 CTL Model ASG-152 asphalt strain gauges located at the bottom of the HMA layer. A typical strain gauge is shown as Figure 3.13. The gauge array for each section was centered on the outside wheelpath in the trucking lane. Each array consisted of 6 longitudinally oriented (parallel to traffic) gauges on either side of six transversely oriented (perpendicular to traffic) gauges. One gauge in each of the four rows was centered on the outside wheelpath, while the others were offset two feet to the left and the right to capture wheel-wander strain effects. For data collection, three longitudinal and three transverse gauges were sufficient to capture the full range of strain variability under loading. However, duplicate gauges were employed so that strain repeatability can be validated and gauge redundancy allows a full range of strain data to be collected in the event of gauge failure.

**Figure 3.13 CTL ASG-152 Asphalt Strain Gauge Employed at the NCAT Test Track.**

Two Geokon Model 3500 Pressure Plates were installed in each structural section. These gauges were centered on the outside wheelpath in the trucking lane. One gauge was placed at the surface of the base layer and one was placed at the surface of the fill layer to measure these critical stresses within the pavement structure. A typical pressure plate is shown as Figure 3.14.


**Figure 3.14 Geokon Model 3500 Earth Pressure Cell at the Test Track.**

Thermistor bundles were installed in each section to capture pavement temperature with depth. The thermistors were installed at different depths for the structural sections constructed for the 2003 and 2006 research cycles. For the 2003 structural sections, the thermistor bundle was installed to capture pavement temperatures at the pavement surface, 2 inches below the pavement surface (within the HMA layer), 4 inches below the pavement surface (within the HMA layer), and 3 inches below the HMA layer (in the aggregate base). For the 2006 structural study, different installation depths were selected to acquire a measured (rather than interpolated) mid-depth HMA temperature. These probes were installed at the surface of the pavement, mid-depth of the HMA layer, bottom of the HMA layer, and 3 inches below the HMA layer. Figure 3.15 shows a typical thermistor bundle used at the Test Track and Table 3.8 summarizes the thermistor installation depths for the structural study.


**Figure 3.15 Typical Sub-Surface Thermistor Bundle Employed at the NCAT Test Track (after Priest and Timm "Fatigue," 2006).**

**Table 3.8 Thermistor Depths for the Structural Sections**

| Sections | T1 Depth (in.) | T2 Depth (in.) | T3 Depth (in.) | T4 Depth (in.) |
|---|---|---|---|---|
| N1,N2 | 0 | 3.5 | 7 | 10 |
| N3,N4,N5,N6,N7 | 0 | 2 | 4 | 10 |
| N8 | 0 | 5 | 10 | 13 |
| N9 | 0 | 7 | 14 | 17 |
| N10 | 0 | 4 | 8 | 11 |
| S11 | 0 | 3.5 | 7 | 10 |

## LABORATORY TESTING

For this study, each of the unbound materials utilized in the structural study were tested to determine laboratory stress-sensitivity and resilient modulus using the triaxial apparatus. For this project, the laboratory testing was subcontracted to Burns, Cooley, Dennis, Inc of Jackson, Mississippi. The testing was performed in accordance with NCHRP 1-28A. The laboratory testing is discussed in greater detail in Chapter 4.

## FWD TESTING PROGRAM

NCAT operates a Dynatest 8000 model falling weight deflectometer (FWD) and conducted regular testing on the eleven structural sections at the NCAT Test Track. Testing was typically performed three times per month with relative calibration being

performed on the deflection sensors once per month. This method of testing generated a database of deflection measurements that captured the seasonal variation of the materials the Test Track.

To quantify the spatial variability within each section, testing was performed at multiple random locations throughout the length of each section. Within each random location, there were three testing locations: in the inside wheelpath, between the wheelpaths, and in the outside wheelpath. Most sections contained four longitudinal random locations, with sections N8 and N10 containing an additional random location due to one of the other random locations experiencing pavement distress or falling within the section of pavement containing the gauge array. Table 3.9 lists the locations of all the longitudinal random locations where FWD testing was performed at the Test Track. For these locations, the reference point is the far end of each section (in the direction of traffic), and 'begin' represents the total length of each test section. Figure 3.16 illustrates the layout of the random locations within the trucking lane for section N1.

**Table 3.9 Longitudinal Random Locations used for FWD Testing (from end of test section, ft)**

| Section | RL 1 | RL 2 | RL 3 | RL 4 | RL 5 | Begin |
|---|---|---|---|---|---|---|
| N1 | 128 | 101 | 51 | 71 | N/A | 201 |
| N2 | 159 | 103 | 39 | 77 | N/A | 206 |
| N3 | 143 | 107 | 56 | 75 | N/A | 198 |
| N4 | 171 | 90 | 25 | 74 | N/A | 199 |
| N5 | 154 | 86 | 44 | 76 | N/A | 202 |
| N6 | 164 | 95 | 37 | 75 | N/A | 199 |
| N7 | 173 | 124 | 59 | 74 | N/A | 199 |
| N8 | 175 | 146 | 60 | 98 | 200 | 225 |
| N9 | 134 | 122 | 62 | 184 | N/A | 227 |
| N10 | 144 | 118 | 74 | 127 | 168 | 204 |
| S11 | 123 | 98 | 44 | 156 | N/A | 216 |

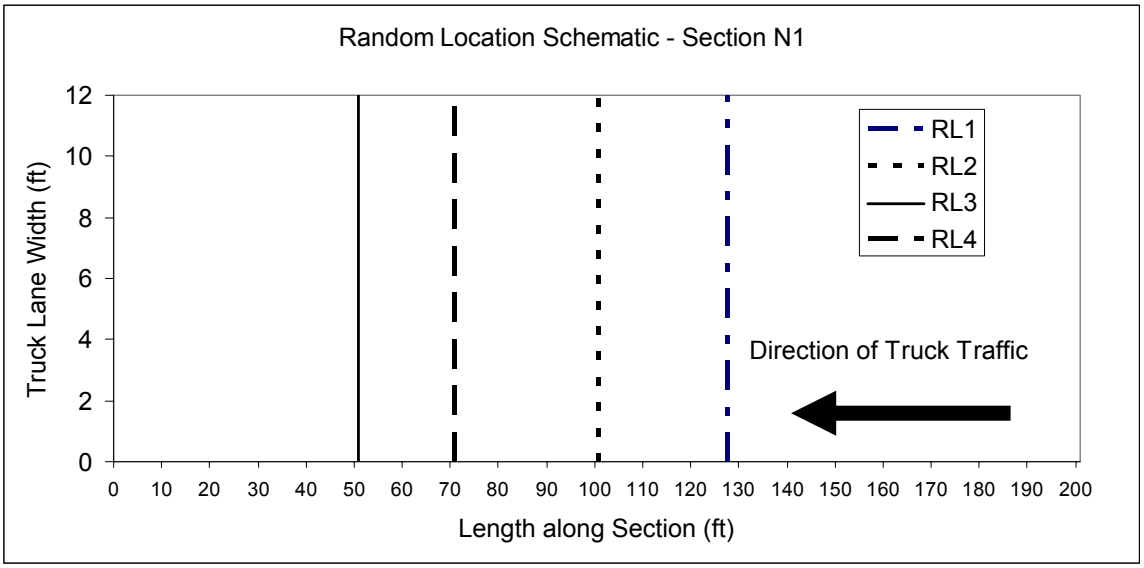


**Figure 3.16 Random Location Layout for Section N1.**

The Dynatest FWD used at the Test Track was configured with 9 sensors arranged with the sensor spacing in Table 3.10. The sensors were arranged with the five sensors closest to the load all being spaced within two feet of the loading plate. This was done to ensure accurate characterization of the moduli of the surface layers. The outer four sensors were spaced at one foot intervals, with the outermost sensor at six feet from the loading plate. This was done to ensure accurate characterization of the deeper unbound layers.

**Table 3.10 FWD Sensor Spacings (Sensor 1 is beneath the load plate)**

| **Sensor #** | 1 | 2 | 3 | 4 | 5 | 6 | 7 | 8 | 9 |
|---|---|---|---|---|---|---|---|---|---|
| **Distance from Load Plate (in.)** | 0 | 8 | 12 | 18 | 24 | 36 | 48 | 60 | 72 |

At each testing location, a total of twelve FWD drops were conducted at varying load levels. Three repetitions were performed at four different drop heights. The loadings corresponding to these drop heights are listed in Table 3.11. This loading variation was performed to impart different stress states on the pavement structure so that the effects of load variation could be assessed in the different pavement layers. The loadings were transmitted to the pavement through a split loading plate with a radius of 5.91 inches. The split loading plate of the Dynatest FWD allows for better contact of the load plate with the pavement and more efficient transfer of the load onto the pavement structure.

**Table 3.11 FWD Drop Heights and Corresponding Loadings**

| Height | Load (lb) |
|---|---|
| 1 | 6,000 |
| 2 | 9,000 |
| 3 | 12,000 |
| 4 | 16,000 |

## FWD ON GAUGE TESTING

On July 17, 2007 a special study was conducted utilizing the FWD and the existing pavement instrumentation. For this study, the FWD testing locations were directly above every functioning pressure plate and strain gauge at the Test Track (testing was not performed on the gauges that were off-scale or non-functioning). This testing was performed in every structural section except N5, due to the absence of surveyed gauge locations. Table 3.12 lists the gauges where the testing was performed. Gauges 1-12 refer to strain gauges, and correspond to the numbering shown in the standard instrumentation layout diagram in Figure 3.11. Gauge 13 corresponds to the pressure plate above the base layer and gauge 14 corresponds to the pressure plate above the fill layer.

**Table 3.12 Matrix of Gauges Tested for FWD on Gauge Testing.**

| | Gauges Tested | | | | | | | | | | | | | |
|---|---|---|---|---|---|---|---|---|---|---|---|---|---|---|
| Section | 1 | 2 | 3 | 4 | 5 | 6 | 7 | 8 | 9 | 10 | 11 | 12 | 13 | 14 |
| N1 | x | | | x | | x | | x | | x | x | | x | x |
| N2 | x | x | x | x | x | x | x | x | x | x | x | x | x | x |
| N3 | | | | | | | | x | | | | | x | x |
| N4 | | x | x | x | | x | x | | | | | | | x |
| N5 | | | | | | | | | | | | | | |
| N6 | x | | | x | x | | | x | x | | | x | | x |
| N7 | | | | | | | x | | | x | | | x | |
| N8 | x | x | | x | | x | x | | x | | x | x | x | x |
| N9 | | x | x | x | x | x | x | x | x | x | x | | x | x |
| N10 | | x | | x | | x | x | x | x | x | x | | x | x |
| S11 | x | x | | x | x | | x | x | x | x | x | x | x | |

This testing generated two data sets for comparison. First, deflection basins were generated at each testing location allowing for the backcalculation of layer moduli as well as the generation of theoretical pavement responses though layered-elastic analysis. Secondly, data were obtained from the pressure and strain instrumentation beneath the pavement surface. Comparison of these data sets was useful to validate the quality of the layered-elastic outputs generated by the backcalculation process by comparing the measured versus theoretical pavement responses.

## SUMMARY REGARDING THE TESTING FACILITY AND TESTING PROGRAM

The NCAT Test Track is an Accelerated Pavement Testing facility that is well-suited to an in-depth unbound materials characterization study. At the Test Track, eleven instrumented pavement sections containing a variety of unbound materials provide an excellent environment for field modulus characterization using the FWD. Laboratory testing of the unbound materials plus performing FWD testing above the embedded pavement response instrumentation served to generate a valuable data set for unbound material characterization.

# CHAPTER 4 - LABORATORY TESTING

## INTRODUCTION

As part of the materials characterization study for the unbound materials at the NCAT Test Track, laboratory resilient modulus testing was performed to assess the behavior of the unbound materials in a laboratory environment. Both the AASHTO and MEPDG pavement design methods recommend laboratory resilient modulus testing to accurately characterize the stiffness of the unbound layers (AASHTO 1993, MEPDG 2004). According to testing specification outlined in NCHRP 1-28A (2004), "The resilient modulus test simulates the conditions in a pavement due to the application of a moving wheel loading. As a result, the test provides an excellent means for comparing the behavior of pavement construction materials under a variety of conditions and stress states." This testing allowed for analyses to be conducted regarding the stress-sensitivity of these materials. It also allows for the determination of modulus values at varying stress-states and for comparisons to be drawn between the relative stiffnesses of these materials.

For this study, triaxial resilient modulus testing was performed in accordance with NCHRP 1-28A "Laboratory Determination of Resilient Modulus for Flexible Pavement Design." A schematic of the triaxial testing apparatus used for testing in NCHRP 1-28A is shown in Figure 4.1. This testing was performed on each of the five unbound materials present in the eleven structural sections at the NCAT Test Track. This testing was subcontracted to Burns, Cooley, Dennis, Inc.

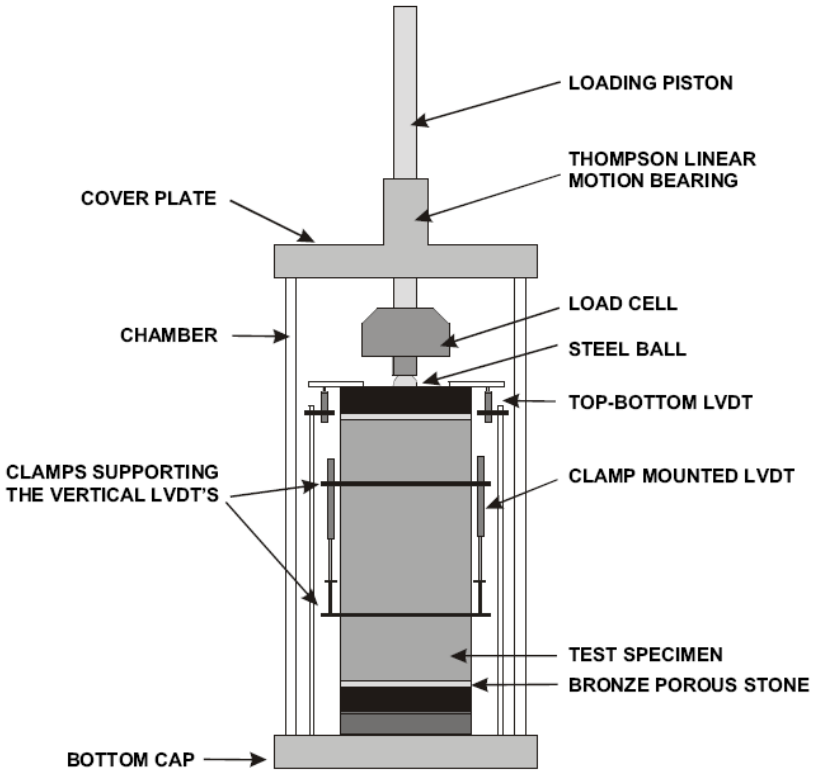


a) Triaxial Cell

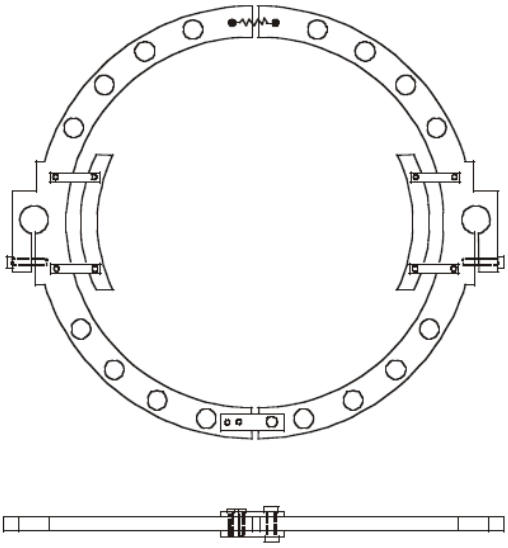

b) Typical Clamps Used To Measure Axial Deformation

*Figure A-3. Triaxial Cell Set-up*

**Figure 4.1 Triaxial Testing Apparatus (NCHRP, 2004).**

**Testing Procedure**

The first step in the laboratory testing process was the preparation of samples for triaxial testing. Sample size and compaction method for a given material are recommended in NCHRP 1-28A based on the gradation of the given material. The mold size used is determined by the maximum particle size. If the maximum particle size is greater than ¾", then a 6 inch mold should be used for the testing sample. For these samples, all particles retained on the 1" sieve should be scalped off prior to testing. If the maximum particle size is less than ¾", then a 4 inch mold is specified. However, the specification allows the use of 6 inch molds if 4 inch molds are not available for use. Undisturbed soil specimens are thin-walled tube specimens of untreated subgrade soils that are 2.8 inches in diameter.

For NCHRP 1-28A, disturbed soil specimens can be classified as three different material types (1, 2, or 3) based on gradation and are compacted differently based on this classification. For these samples, either impact, vibratory, or kneading compaction may be deemed appropriate. Samples with a maximum particle size of 3/8" or greater are classified as type 1 material and compacted using either impact or vibratory compaction. Samples with a maximum particle size less than 3/8" but with $P_{200}$ (percent passing the #200 sieve) greater than 10 percent are considered type 2 material. These specimens are compacted with vibratory methods. Samples with a maximum particle size less than 3/8" but with $P_{200}$ less than 10 percent are considered type 3 material. These specimens are compacted with either impact or kneading compaction. Undisturbed specimens are not compacted further prior to testing and are classified as a type 4 material. Figure 4.2 shows a flowchart of the typical specimen preparation decision process.

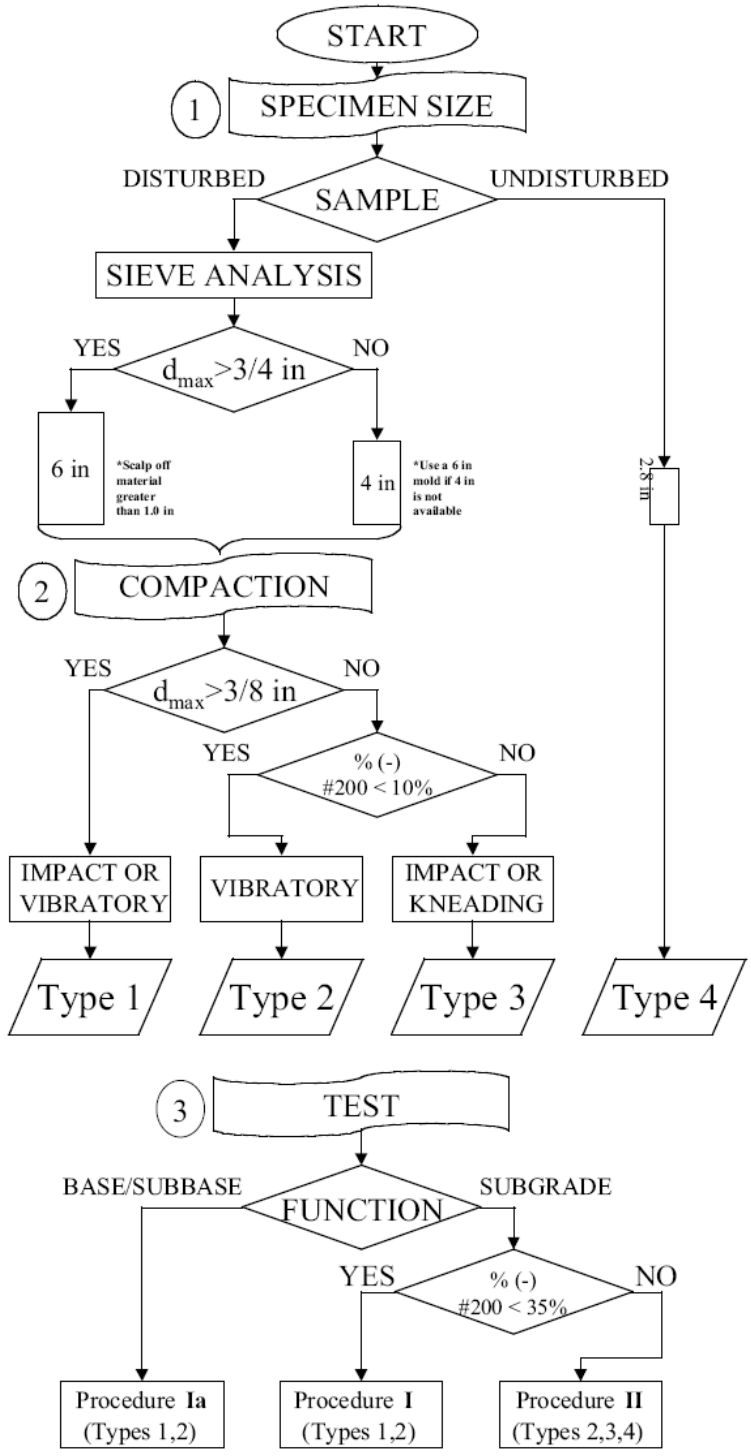


*Figure A-2. Test Method Flowchart*

**Figure 4.2 NCHRP 1-28A Specimen Preparation Flowchart (NCHRP, 2004).**

NCHRP 1-28A (2004) specifies that reconstituted specimens of all types shall be prepared to the specified or in-situ dry density and moisture content. However, the specification allows the samples to be compacted to the optimum moisture content and 95 percent of the maximum dry density obtained through standard Proctor compaction (AASHTO T180 for base/subbase materials and AASHTO T99 for subgrade soils).

The sample testing is performed in a triaxial chamber (see Figure 4.1) for which the drainage lines are held open and air is the fluid used to achieve confining pressure within the chamber. The chamber must apply a haversine load form and sufficient measure of axial deformation (e.g. optical extensometers, non-contact sensors, clamp-mounted LVDT's). In this way, the load (or stress) and axial deformation can be measured so that an accurate resilient modulus can be determined (see definition of resilient modulus, Chapter 1).

The haversine loading device is employed with this testing method so that the triaxial chamber can simulate the rapid nature of a moving wheel load. For all materials tested, the complete loading cycle (loading plus resting period) is one second. During this loading cycle, the sample will receive a cyclic load pulse over the course of 0.1 second for base materials and 0.2 seconds for subgrade materials. The remainder of the loading cycle is a resting period between loadings. Figure 4.3 illustrates the wave form typical of the haversine load pulse by plotting load versus load duration.

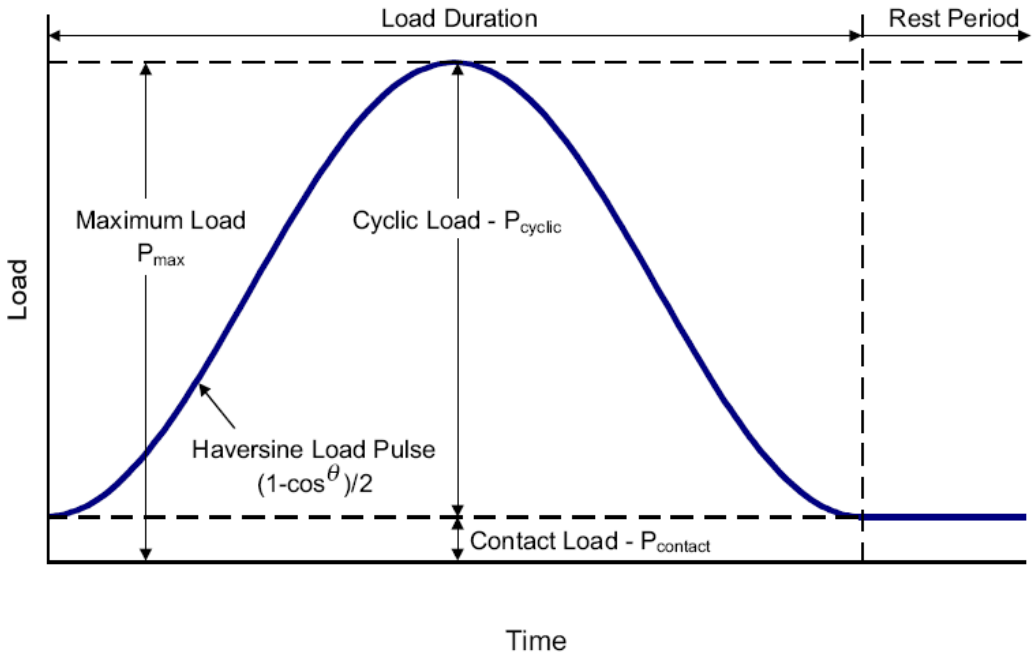


*Figure A-1. Definition of Resilient Modulus Terms*

**Figure 4.3 Diagram of Haversine Load Pulse Used in NCHRP 1-28A (NCHRP, 2004).**

The stresses under which the material is to be tested is specified based on material type and whether or not that material is used primarily as a base/subbase or a subgrade material. According to NCHRP 1-28A (2004), "the stress conditions used in the test represent the range of stresses likely to be developed beneath flexible pavements undergoing moving wheel loads." The lower portion of Figure 4.2 illustrates how the material usage and gradation is used to recommend stress-states (or procedures) for testing.

Procedure Ia is the stress-state sequence utilized for base and subbase material testing. The test begins with a conditioning cycle that utilizes 1000 cycles of a load at a maximum stress of 33 psi (See Figure 4.3) and a confining pressure of 15 psi. This cycle is followed by 5 testing sequences that utilizes 100 loading cycles at confining pressures increasing from 3 to 20 psi and maximum applied stresses ranging between 2.1 and 14.0 psi. These 5 sequences are followed by another 5 sequences at identical confining pressures, but with increased maximum stresses. The maximum stresses tested for Procedure Ia can range between 2.1 and 144 psi. For each set of 100 load cycles, the axial deformation is recorded for the last 5 cycles of each set. In this way, the deviatoric stress can be divided by the recoverable axial strain to generate a resilient modulus for each stress condition. The testing is terminated when either all the recommended loading cycles have been performed or the sample reaches a cut-off value of 5 percent vertical strain.

Procedure II is the stress-state sequence utilized for fine-grained subgrade material testing. The test begins with a conditioning cycle that utilizes 1000 cycles of a load at a maximum stress of 7.8 psi and a confining pressure of 4.0 psi. Following conditioning, 4 testing sequences are performed that utilize 100 loading cycles at confining pressures that reduce incrementally between 8 and 2 psi with maximum stresses decreasing between 5.6 and 4.4 psi. These 4 sequences are followed by another 4 sequences at identical confining pressures, but with increased maximum stresses that reduce incrementally between cycles. The maximum stresses used for this test range between 4.4 and 15.6 psi. The resilient modulus is determined for each stress condition in the same way as with the base/subbase procedure.

It is notable that the stress-states used for subgrade testing are much smaller than those used for the base/subbase testing. This is practical since layers that are constructed deeper in the flexible pavement structure typically encounter lower stresses than layers constructed above them. It is also notable that the base/subbase testing procedure increases the confining pressures and maximum stresses between cycles while the subgrade testing procedure decreases these stresses in subsequent cycles. This is most likely done because most coarse-grained granular materials are assumed to be stress-hardening (increasing stiffness under increasing load) while most fine-grained subgrade materials are assumed to be stress-softening (decreasing stiffness under increasing load).

**Sample Preparation**

For each of the five unbound materials tested, three samples were prepared and then tested in accordance with NCHRP 1-28A. All of the unbound materials were specified as type 1 for this project. The Track soil material was compacted to target the in-situ dry density and moisture content while the other samples were compacted to 95 percent of laboratory maximum dry density and optimum moisture content. The Track soil samples were tested at the request of NCAT while the other samples were made available for this study through testing performed through another project, owing to the difference in sample preparation. Table 4.1 summarizes the testing parameters for the unbound materials. The maximum dry density and moisture content for each material is listed along with the average compacted dry density and moisture content from each of the three prepared samples.

**Table 4.1 Testing Parameters for Unbound Materials**

| Material Type | NCHRP 1-28A Material Type | Maximum Dry Density (pcf) | Optimum Moisture Content (%) | Average Compacted Dry Density (pcf) | Average Compacted Sample Moisture Content (%) |
|---|---|---|---|---|---|
| Limerock Base | 1 | 116.1 | 12.5 | 110.1 | 13.2 |
| Granite Base | 1 | 138.1 | 5.0 | 130.3 | 4.8 |
| Seale Subgrade | 1 | 99.9 | 21.8 | 96.8 | 21.4 |
| Type 5 Base | 1 | 130.0 | 10.0 | 124.3 | 9.1 |
| Track Soil | 1 | 121.7 | 10.0 | 121.1 | 10.5 |

## MODELING NON-LINEAR STRESS-SENSITIVITY BEHAVIOR OF TRIAXIAL DATA

For each unbound material tested, stress and modulus data generated from testing the three samples were combined into one database for each material. For each 100 load testing sequence, the following data were generated: the total axial stress ($\sigma_1$), the confining pressure ($\sigma_2$ and $\sigma_3$), and the calculated resilient modulus. Given these stresses, the bulk stress ($\theta$), deviatoric stress ($\sigma$), and octahedral shear stress ($\tau_{oct}$) were calculated for each testing sequence using equations 4-1, 4-2, and 4-3, respectively.

$$\theta = \sigma_1 + \sigma_2 + \sigma_3 \quad (4\text{-}1)$$

$$\sigma_d = \sigma_1 - \sigma_3 \quad (4\text{-}2)$$

$$\tau_{oct} = \frac{1}{3}\sqrt{(\sigma_1 - \sigma_2)^2 + (\sigma_2 - \sigma_3)^2 + (\sigma_3 - \sigma_1)^2} \quad (4\text{-}3)$$

Therefore, for each sample, the resilient modulus was determined over a wide range of stress-states. Figure 4.4 illustrates the calculated resilient modulus values over the tested range of bulk stresses for one sample of the limerock base material. This plot shows the wide range of bulk stresses over which the sample was tested, ranging between approximately 10 and 165 psi. The calculated resilient modulus values also vary between approximately 15,000 and 75,000 psi over the tested stress range. The data appear to show a stress-hardening behavior of the material, albeit with considerable variability due to variations in deviatoric stress. Figures 4.5 and 4.6 show the data from the same limerock sample for resilient modulus versus deviatoric stress and octahedral shear stress, respectively. These plots show considerable variability in the data over a wide range of stress-states. Similar observations were made regarding the other materials tested.

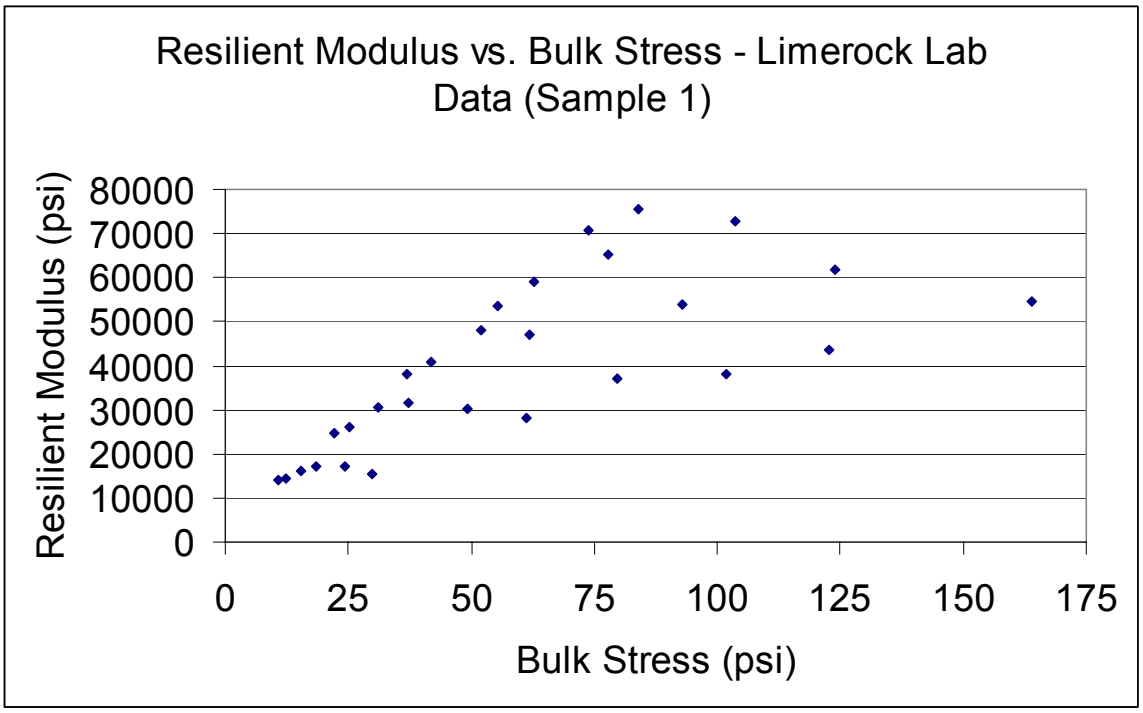


**Figure 4.4 Resilient Modulus versus Bulk Stress – Limerock Base – Sample 1.**

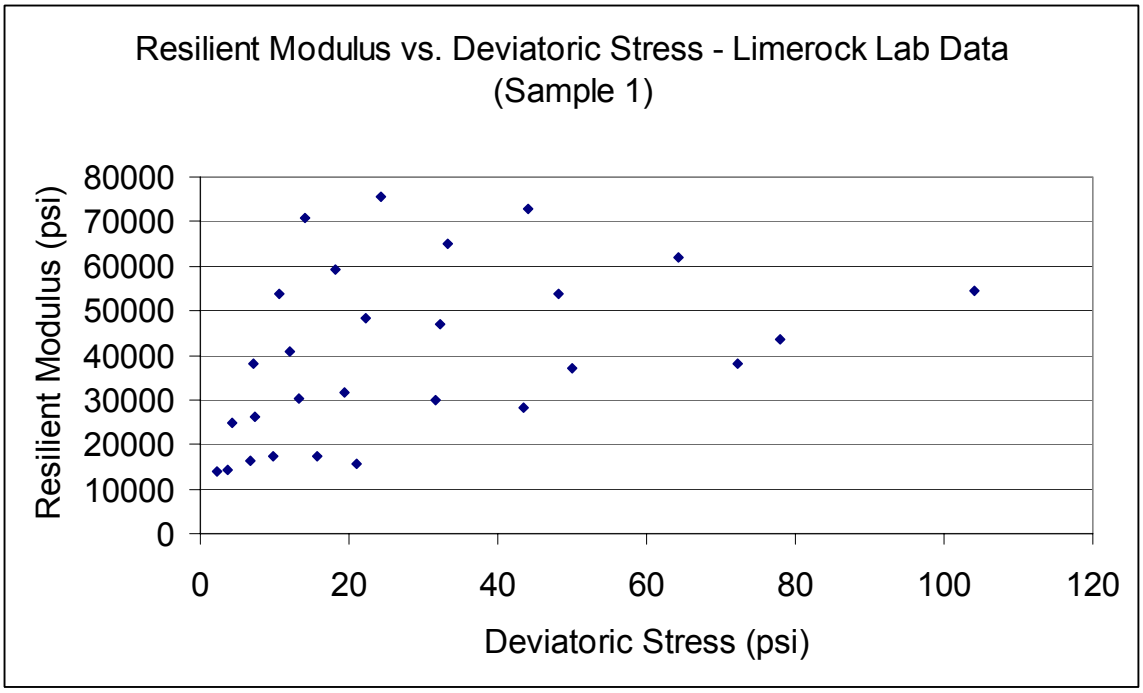


**Figure 4.5 Resilient Modulus vs. Deviatoric Stress – Limerock – Sample 1.**

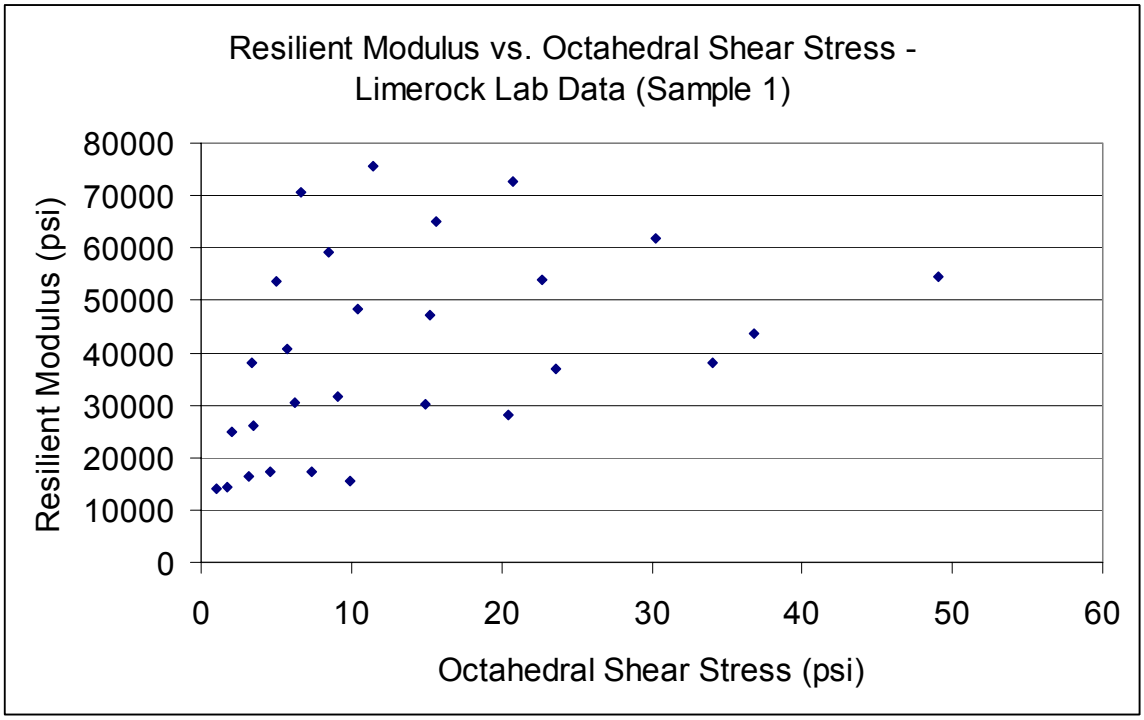


**Figure 4.6 Resilient Modulus versus Octahedral Shear Stress – Limerock – Sample 1.**

For this study, four common non-linear models relating the material stress-state to the resilient modulus were evaluated for each unbound material. The regression coefficients

for these models were generated for each unbound material by entering in the stress-state and resilient modulus data into DATAFIT, a non-linear regression modeling software package developed by Oakdale Engineering. This software is capable of generating multiple non-linear models from a given data set containing one or more independent variables and one dependent variable. This software also allows the user to define the model for which the software will calculate the regression coefficients ($k_1$, $k_2$, etc.) as well as pertinent statistics such as those regarding model fit ($R^2$) and statistical significance of the calculated regression coefficients (p-values).

The first model evaluated relates resilient modulus to the material bulk stress, as shown in Equation 4-4 (where $k_1$ and $k_2$ are regression coefficients). This model was suggested by the AASHTO design guide for the determination of resilient modulus in the laboratory and is widely used in literature. This model will be referred to as the 'bulk' model for the purposes of this report.

$$M_r = k_1 * \left( \frac{\theta}{p_a} \right)^{k_2} \tag{4-4}$$

Table 4.2 summarizes the results of the regression analysis conducted on the resilient modulus data for the different materials using the bulk model. The results of this analysis do not show excellent model fit for any of the unbound materials. No material exhibits a model $R^2$ above 0.9, which is a common benchmark for lab data (MEPDG, 2004). As expected, the granular base materials (limerock, granite, Type 5) tend to generate higher model $R^2$ values than the subgrade materials (Seale and Track soil). This is due to coarse-grained granular materials typically showing a higher bulk stress-dependency than fine-grained subgrade materials. Neither the Seale subgrade nor the Track soil seem to exhibit any stress-sensitivity with respect to bulk stress.

**Table 4.2 Summary of Bulk Stress-Sensitivity Models by Material Type**

| Material Type | $k_1$ | p-value ($k_1$) | $k_2$ | p-value ($k_2$) | $R^2$ |
|---|---|---|---|---|---|
| Limerock Base | 22966.66 | 0 | 0.4773 | 0 | 0.5618 |
| Granite Base | 10862.11 | 0 | 0.6267 | 0 | 0.886 |
| Seale Subgrade | 6009.80 | 0 | -0.1201 | 0 | 0.0288 |
| Type 5 Base | 14049.68 | 0 | 0.6710 | 0 | 0.8721 |
| Track Soil | 26833.28 | 0 | 0.0447 | 0.23123 | 0.0179 |

The next model evaluated relates resilient modulus to the material deviatoric stress, as shown in Equation 4-5 (where $k_1$ and $k_2$ are regression coefficients). This model is a variation of the bulk model that is more commonly used to model the stress-sensitivity of

cohesive subgrade materials (Irwin, 2002). This model will be referred to as the 'deviatoric' model for the purposes of this report.

$$M_r = k_1 * \left( \frac{\sigma_d}{p_a} \right)^{k_2} \tag{4-5}$$

Table 4.3 summarizes the results of the regression analysis conducted on the resilient modulus data for the different materials using the deviatoric model. The results of this analysis do not show excellent model fit for any of the unbound materials, with no material showing an $R^2$ value above 0.9. The best model fit was exhibited by the Seale subgrade material ($R^2 = 0.78$). This was expected since the Seale subgrade was a very fine-grained material, making it the material most applicable for use with the deviatoric model.

**Table 4.3 Summary of Deviatoric Stress-Sensitivity Models by Material Type**

| Material Type | $k_1$ | p-value ($k_1$) | $k_2$ | p-value ($k_2$) | $R^2$ |
|---|---|---|---|---|---|
| Limerock Base | 39001.39 | 0 | 0.2174 | 0.00004 | 0.2204 |
| Granite Base | 21349.99 | 0 | 0.3866 | 0 | 0.5765 |
| Seale Subgrade | 4305.81 | 0 | -0.5571 | 0 | 0.7834 |
| Type 5 Base | 29487.16 | 0 | 0.3876 | 0 | 0.5334 |
| Track Soil | 28878.92 | 0 | -0.0572 | 0.04653 | 0.0478 |

Equation 4-6 is a more comprehensive constitutive model originally suggested by Uzan (1985). This model accounts for the effects of shearing strains in the pavement structure by relating resilient modulus to both the bulk stress and deviatoric stress (Uzan, 1985). This model is applicable regardless of soil type tested. This model will be termed the 'universal' model for the purposes of this report.

$$M_r = k_1 p_a * \left( \frac{\theta}{p_a} \right)^{k_2} * \left( \frac{\sigma_d}{p_a} \right)^{k_3} \tag{4-6}$$

Table 4.4 summarizes the results of the regression analysis conducted on the resilient modulus data for the different materials using the universal model. The results of the analysis show that this model generates much higher model $R^2$ values than the previous simpler bulk and deviatoric models. The Granite base, Seale subgrade, and Type 5 base all exhibit model $R^2$ values above 0.9 with statistically significant regression coefficients (p-values below 0.05). The limerock base shows reasonably strong stress-sensitivity with an $R^2$ value of approximately 0.86. The Track soil material exhibits the worst stress-sensitivity with a model $R^2$ of approximately 0.66.

**Table 4.4 Summary of Universal Stress-Sensitivity Models by Material Type**

| Material Type | $k_1$ | p-value (k1) | $k_2$ | p-value ($k_2$) | $k_3$ | p-value ($k_3$) | $R^2$ |
|---|---|---|---|---|---|---|---|
| Limerock Base | 717.04 | 0 | 1.2338 | 0 | -0.5645 | 0 | 0.8562 |
| Granite Base | 581.08 | 0 | 0.8529 | 0 | -0.1870 | 0.00001 | 0.9172 |
| Seale Subgrade | 225.09 | 0 | 0.3598 | 0 | -0.7551 | 0 | 0.9786 |
| Type 5 Base | 643.69 | 0 | 1.0318 | 0 | -0.2833 | 0 | 0.9349 |
| Track Soil | 1095.43 | 0 | 0.5930 | 0 | -0.4727 | 0 | 0.6642 |

Equation 4-7 is the constitutive model recommended for use with laboratory testing in the new MEPDG (2004) and is recommended for use by NCHRP 1-28A. This model is an expanded version of the universal model which relates the bulk and octahedral shear stresses to the resilient modulus (where $k_1$, $k_2$, and $k_3$ are regression coefficients) (Yau and Von Quintus, 2002). This model will be referred to as the 'MEPDG' model for the purposes of this report.

$$M_r = k_1 p_a * \left( \frac{\theta}{p_a} \right)^{k_2} * \left[ \left( \frac{\tau_{oct}}{p_a} \right) + 1 \right]^{k_3} \tag{4-7}$$

Table 4.5 summarizes the results of the regression analysis conducted on the resilient modulus data for the different materials using the MEPDG model. The results of the analysis show that all the unbound materials except the Track soil material exhibit strong stress-sensitivity through the use of the MEPDG model ($R^2$ at or above 0.9 with statistically significant regression coefficients). Again, the Track soil material exhibits the poorest stress-sensitivity of the unbound materials ($R^2 = 0.42$).

**Table 4.5 Summary of MEPDG Stress-Sensitivity Models by Material Type**

| Material Type | $k_1$ | p-value (k1) | $k_2$ | p-value ($k_2$) | $k_3$ | p-value ($k_3$) | $R^2$ |
|---|---|---|---|---|---|---|---|
| Limerock Base | 1266.83 | 0 | 1.2081 | 0 | -1.2332 | 0 | 0.9326 |
| Granite Base | 716.28 | 0 | 0.8468 | 0 | -0.4632 | 0 | 0.9253 |
| Seale Subgrade | 817.63 | 0 | 0.3305 | 0 | -3.3946 | 0 | 0.957 |
| Type 5 Base | 883.54 | 0 | 1.0050 | 0 | -0.6575 | 0 | 0.9478 |
| Track Soil | 1878.97 | 0 | 0.4067 | 0 | -0.7897 | 0 | 0.4202 |

Figure 4.7 shows a summary of the model $R^2$ for each model type when applied to the test data generated by the five different unbound materials. This analysis clearly shows that the constitutive models with multiple stress terms are better predictors than the models that relate resilient modulus to only bulk or deviatoric stress. Both the MEPDG and universal constitutive models exhibit a good model fit for each of the unbound material except for the Track soil material. The Track soil material was clearly the least stress dependent material tested, with none of the four stress-sensitivity models generating an $R^2$ above 0.7 for this material. For the laboratory data, an average Track soil modulus of 28,335 psi with a standard deviation of 6,650 psi was calculated.

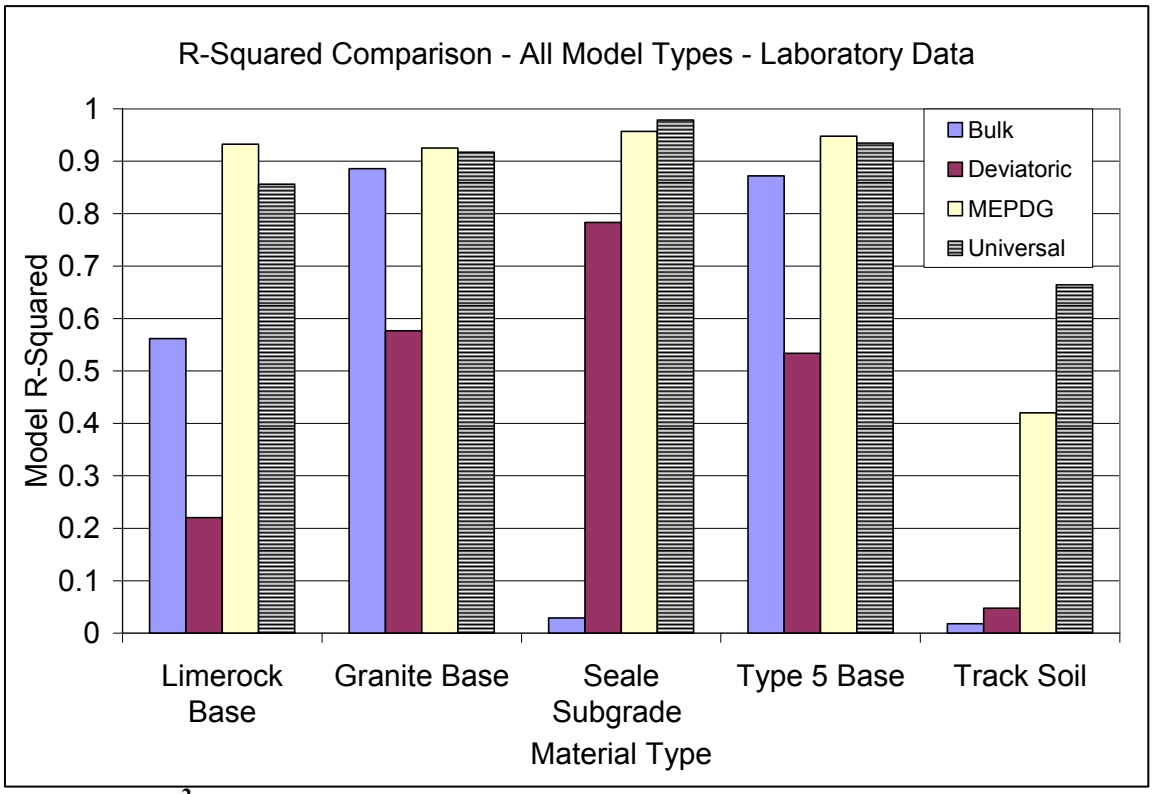


**Figure 4.7 $R^2$ Comparison for All Stress-Modulus Models by Material Type.**

**UNBOUND MATERIAL COMPARISON AND STRESS-SENSITIVITY**

In order to quantify the relative stiffness of the different unbound materials, three representative stress states for each material were entered into the laboratory generated constitutive equations (for the MEPDG and universal models). These stress-states were generated by analyzing the cumulative distribution functions (CDF) of the stress-states used for testing with each of the different unbound materials. These distributions were very similar for the limerock, Granite base, Type 5 base, and Track soil. This is because these samples were all tested under virtually the same stresses (Procedure Ia in NCHRP 1-28A). The Seale subgrade material was tested using Procedure II for fine-grained subgrade materials.

Table 4.6 lists the representative stress-states that were used to compare the various resilient moduli. Stress states 1 and 2 represent the lower and upper limit of the testing stresses for the Seale subgrade material. Stress states 1, 2, and 3 represent the $0^{th}$, $25^{th}$, and $50^{th}$ percentile stresses at which the granular materials were tested, respectively. For the granular materials, stress-states one, two, and three most closely approximate testing sequences 1, 7, and 13, respectively, from Procedure Ia. For the Seale subgrade, stress-states one, two, and three most closely approximate testing sequences 1, 6, and 13, respectively, from Procedure II. The increase between stress-states 1 and 3 represents a significant increase in the loading on the pavement. These stress-states were believed to encompass the full range of stresses that could realistically be expected in the field.

**Table 4.6 Representative Stress-States used for Modulus Normalization**

| Stress State | Bulk Stress (psi) | Deviatoric Stress (psi) | Octahedral Shear (psi) |
|---|---|---|---|
| State 1 | 10 | 2 | 1 |
| State 2 | 25 | 7 | 3.5 |
| State 3 | 50 | 15 | 8 |

The next step was to compare the modulus values generated by entering the three representative stress-states into the laboratory calibrated MEPDG and universal constitutive models for each unbound material. Figure 4.8 shows the calculated modulus values for each of the unbound materials at the various stress-states with the laboratory calibrated MEPDG models. The data show that the limerock base, Granite base, and Type 5 base material all exhibit stress-hardening behavior under increasing load. The limerock base exhibits the most dramatic stress-hardening, with moduli increasing between approximately 11 and 47 ksi with a 40 psi increase in bulk stress. The Track soil material also seems to exhibit stress-hardening behavior with this model despite the low model $R^2$ value of 0.42. The Seale subgrade exhibits stress-softening behavior, as expected for a cohesive subgrade material.

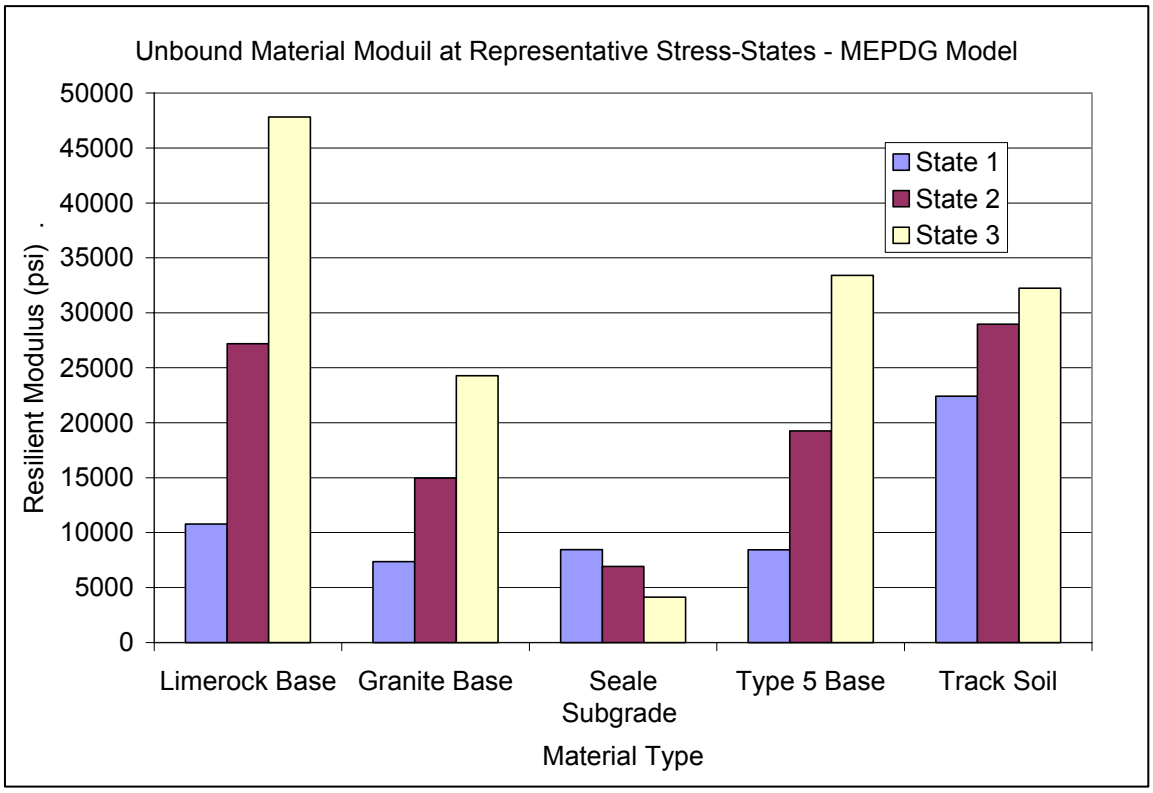


**Figure 4.8 Unbound Material Moduli at Representative Stress-States – MEPDG Model.**

Figure 4.9 shows the calculated modulus values for each of the unbound materials at the various stress-states with the laboratory calibrated universal models. The majority of the materials exhibit the same stress-sensitivity to changing load as with the MEPDG model, with the exception of the Track soil material. With the universal model, this material does not seem to exhibit any stress-sensitivity, with moduli varying between approximately 31 and 33 ksi regardless of stress-state. Again, this is not surprising given the low model $R^2$ of 0.66 reported for this material.

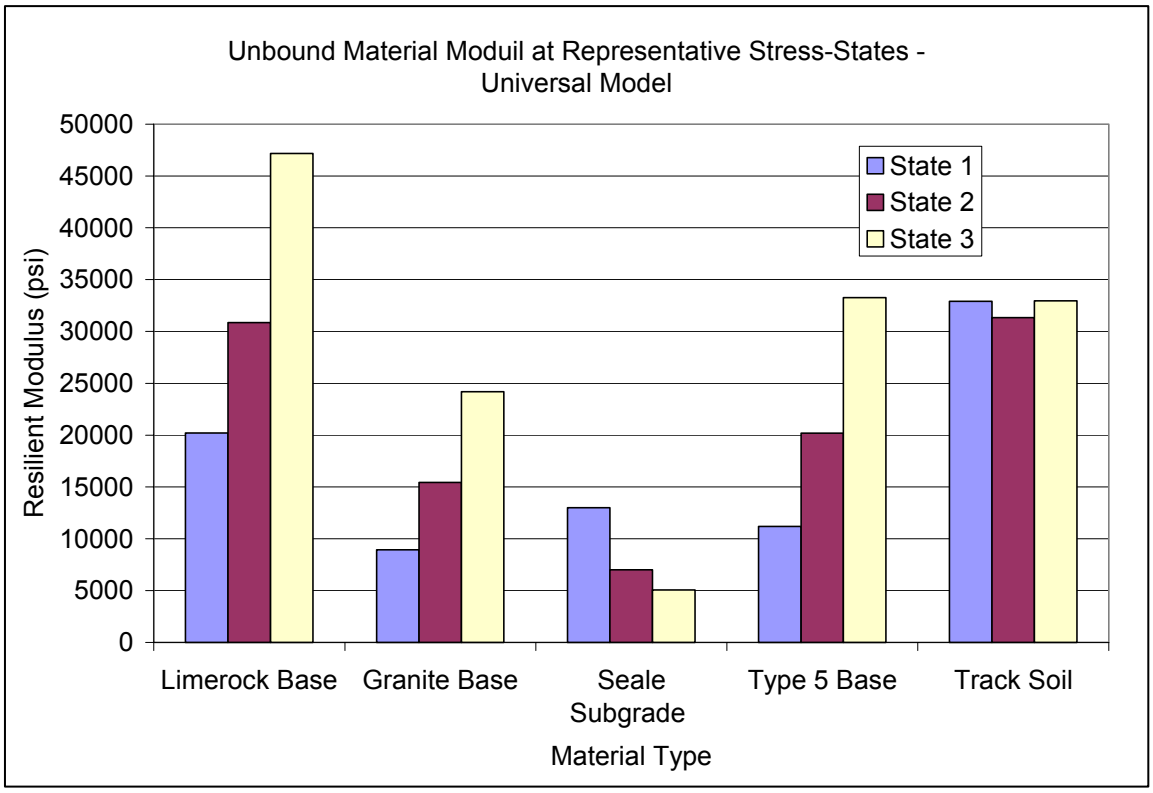


**Figure 4.9 Unbound Material Moduli at Representative Stress-States – Universal Model.**

The MEPDG and universal models seem to report almost identical moduli at stress-states 2 and 3 while reporting slightly different moduli at the lowest stress-state (state 1). This agreement between the two models gives reasonable confidence in their ability to accurately predict unbound material moduli at different stress-states.

Through analysis of the moduli at the varying stress-states, the limerock material seems to be the stiffest under the heaviest loading (stress-state 3), while the Seale subgrade appears to be the least stiff under this loading. Under moderate stresses (state 2), the Track soil material appears to have the greatest stiffness, followed closely by the limerock base material. Again, the Seale subgrade appears to be the softest material under this loading. At low stress levels, the Seale subgrade has stiffnesses that equal or surpass both the Granite base and Type 5 base materials. This is not surprising since the Seale material is stress-softening and the other granular base materials are stress-hardening. The Track soil exhibits the highest stiffness under the smaller stresses, primarily due to its relative lack of stress-sensitivity.

## SUMMARY OF KEY FINDINGS FROM LABORATORY TESTING

The triaxial resilient modulus testing on the unbound materials used in the NCAT Test Track structural study provided a good data set from which to assess the material behavior. For each material, multiple constitutive equations were modeled to fit the laboratory generated stress and modulus data. The results of this testing showed the

'MEPDG' and 'universal' models to most accurately represent the laboratory data sets. Additionally, multiple representative stress-states were input into these models for each material to assess general material behavior. This analysis showed general agreement between the two models for the same material at the same stress-state. From these data, the Florida limerock, Granite base, and Type 5 base materials were shown to exhibit stress-hardening behavior, with the Florida limerock exhibiting the highest overall stiffness of these materials at equivalent stresses. The Seale subgrade generally exhibited the lowest stiffness values and exhibited stress-softening behavior typical of cohesive soils. The Track soil material exhibited little stress-sensitivity with the various models (given its poor model $R^2$) and showed minimal modulus variation at multiple stress-states. It should also be noted that the Track soil material exhibited the highest modulus of all the materials at the lower stress states.

# CHAPTER 5 -
# BACKCALCULATION CROSS-SECTION DETERMINATION

## INTRODUCTION

The principle behind non-destructive falling-weight deflectometer (FWD) testing is relatively simple compared to the amount of analysis and judgment required to generate viable results from the actual testing. The testing typically consists of a large load being placed on a pavement structure so that pavement deflections at increasing distances from the loading can be measured and subsequently correlated to in-situ pavement moduli. This process generates moduli for the different layers using well-known engineering relationships (e.g. Boussinesq Theory) (Irwin, 2002). Such logic dictates that if one has detailed knowledge of the pavement construction (layer thicknesses, densities, moisture contents, etc.) they should be able to calculate the moduli for each of these layers independently. However, in practice this is rarely the case.

Typically, adjustments have to be made to the actual pavement cross-section in order to create a cross-section that is suitable for backcalculation of pavement layer moduli. For example, if there are layers within the pavement system that are relatively thin when compared with the surrounding layers, typically the backcalculation software will be unable to isolate the pavement deflections caused by that layer alone. Consequently, the small deflections cause the software to be unable to accurately determine the modulus of that pavement layer, creating a large amount of error in the final solution. Another prime example of adjusting the actual cross-section to suit backcalculation is combining layers that were constructed separately, but are of the same material or have similar densities or moisture contents (Parker and Elton, 1990). Even though these layers were constructed in separate lifts, the backcalculation software cannot isolate the differences in the deflections caused by these lifts due to their material similarities. Consequently, a compensating layer effect between these layers or erratic layer moduli behavior is often witnessed. Finally, a stiff layer (bedrock or shallow water table) may be present at the FWD testing site and have to be compensated for in the backcalculation cross-section (Irwin, 2002). The presence of this rigid layer within the pavement structure will have a dramatic effect on the pavement surface deflections, and must be compensated for when generating the optimum cross-section for backcalculation.

The objective of this portion of the study was to generate the optimal cross-section for backcalculation for each of the eleven structural sections at the NCAT Test Track. Optimizing the backcalculation cross-section will allow for the generation of accurate pavement layer moduli for each of the structural sections. Confidence in this data set is necessary for the calibration of viable stress-sensitivity models for the unbound pavement layer materials in the field.

## SOFTWARE UTILIZED

This project required multiple software tools for use in generating backcalculated data. First of all, the raw deflection data files were compiled in a Microsoft Access database. This database contained all the deflection basins generated on the various test dates from

the NCAT FWD Testing program as well as the surveyed pavement thickness information and pavement temperature data. Queries within this database were used to generate deflection files that could be interfaced with the backcalculation software. These queries were generated to show the FWD drop location (station), the force from the drop, the deflections from the various deflectometers, and the surveyed pavement thicknesses at each location. For these queries, only stations with twelve "good" deflection basins were utilized. For the purposes of this thesis, a "good" deflection basin is defined as a deflection basin where the measured deflections decrease as distance from the load increases. Additionally, the pavement thicknesses for the different layers could be combined or divided in these queries to generate deflection files that were conducive to different trial cross-sections (i.e. cross-sections with different layer configurations).

EVERCALC (version 5.0) was the backcalculation software utilized for this project. EVERCALC was developed by the Washington State DOT. This software was utilized for several reasons. First of all, the program is capable of providing a detailed output file which includes a complete state of stress at a user-specified point within each of the pavement layers. These stresses are generated through layered-elastic analysis within the software program and are generated for every deflection basin. These stresses due to the loading are a critical component in modeling the non-linear stress-sensitivity behavior of the unbound pavement layers. The program also reports a non-linear stress-modulus relationship for each set of deflection basins. The program reports the model coefficients and $R^2$ value for a bulk model (for coarse-grained soils) or deviatoric model (for fine-grained soils) for each drop location based on which stress term provides the better fit. Additionally, the software can provide a simple summary file which gives the layer moduli and RMS Error for each of the individual deflection basins.

The EVERCALC software requires several inputs to provide accurate backcalculation results. This was done by creating a general file which contained all the necessary inputs. This file contains: the FWD sensor spacings ( see Table 3-10, Chapter 3), the number of layers for the cross-section, the load plate radius, an indicator for whether or not a stiff layer exists within the structure, and an option to supply initial modulus values and an modulus range for each of the pavement layers, Poisson ratios for each of the pavement layers, an iteration limit for the software, modulus and RMS error iteration tolerances for the software, and the location within each layer that the program will compute generate stress and strain values within that layer.

For this project, the initial HMA modulus was set at 1,000 ksi and the program was allowed to iterate between the boundaries of 25 and 4,000 ksi. For the unbound materials, the initial modulus was set to 20 ksi and the program was allowed to iterate between 1 and 80 ksi. These boundaries were set to encompass the typical values exhibited by these layer types (Rwebangira et al., 1987). The Poisson ratios were set at 0.35 for the HMA materials, 0.40 for the base materials, and 0.45 for the subgrade materials, which were commonly reported in literature (Parker and Elton, 1990; Zhou, 2000). Ten iterations were allowed for the program to backcalculate the layer moduli within and RMS Error tolerance of one percent and a modulus tolerance of one percent

between iterations. Each of these values had been cited in literature (Rwebangira et al., 1987; Sivaneswaran et al., 2001).

Within EVERCALC, the program allows for the use of a stiff layer within the cross-section by selecting whether or not to include a stiff layer in the general file. In using a stiff layer, the program will utilize the outer deflections to calculate the depth to any subsurface stiff layer (if present) within the pavement structure. Additionally, the moduli and Poisson Ratio for this stiff layer must be set within the general file. For the trial cross-sections with bedrock, a stiff layer modulus of 2000 ksi and Poisson ratio of 0.15 were utilized for this project. These values were within the recommended ranges for modulus and Poisson's ratio for bedrock outlined in the MEPDG (2004).

The stress-strain critical location was always set at the bottom of the HMA layer and the surface of the deep subgrade layer directly beneath the FWD load (critical locations for fatigue cracking and rutting, respectively). The critical location at the bottom of the HMA layer was useful for calculating measured versus predicted (backcalculated) strains at the bottom of the HMA layer. The critical location was set at the mid-depth of the granular base and fill layers for typical FWD testing to generate representative stresses that were most suitable for stress-sensitivity characterization. For the FWD on gauge testing, this location was set at the surface of the base and surface of the fill to compare the measured pressures to the predicted (backcalculated) pressures at that location within the pavement structure.

The AUDEF software program was utilized to convert the Access deflection files to deflection files that could be used by the backcalculation software (EVERCALC v 5.0). This program was also used to convert the resultant summary and output files from EVERCALC to EXCEL files, which were more conducive to data analysis.

**CROSS-SECTION SELECTION METHODOLOGY**

To generate accurate in-situ moduli for each of the structural sections at the NCAT Test Track, an investigation was conducted on each of the structural sections to determine the optimum cross-section for backcalculation. For each structural section, multiple possible backcalculation cross-sections were generated based on how each section was constructed and the composition of the different pavement layers. These cross-sections included a number of 3-layer, 4-layer, and 5-layer pavement systems. Trial cross-sections including a stiff layer were also included to ensure that bedrock or a shallow water table were not influencing the results of the backcalculation. Given the topography of the Test Track, one would not expect bedrock to be present, but it was checked anyway since many researchers insist on checking for bedrock in any backcalculation (see Chapter 2). A summary diagram of the material composition of the structural sections along with surveyed thicknesses of the HMA and granular base layers are shown in Figure 5.1.

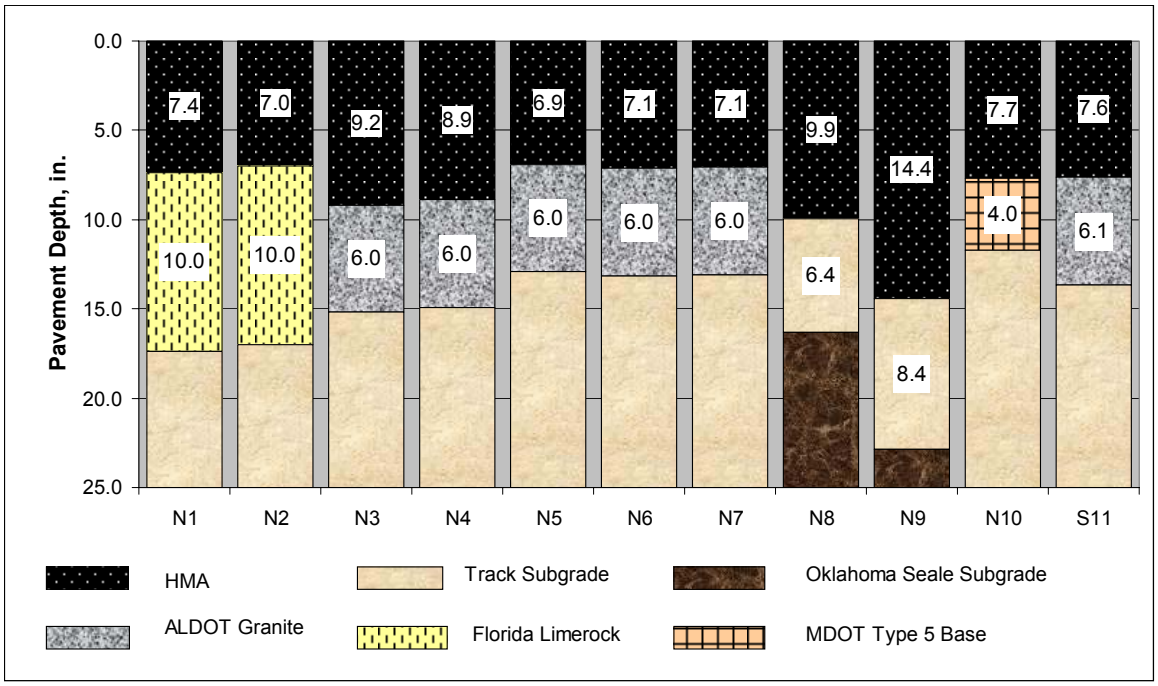


**Figure 5.1 Thickness and Material Summary of the Structural Sections at Test Track.**

To determine the optimal backcalculation cross-section for each structural section, several sources of information were utilized. First, FWD testing was performed on four different dates for each of the structural section at the Test Track (these data were collected as part of the regular NCAT FWD testing program). The dates used for this investigation were selected to encompass a wide variety of pavement temperatures. The pavement temperatures on these dates ranged from approximately 45°F to over 130°F. The only difference used in the dates for each section was that the 10/30/06 testing date was available for sections N1 and N2, but not for the remaining pavement sections. This date was preferable for use in N1 and N2 because this testing date was prior to the Track opening for truck traffic, thereby well representing the initial condition of the pavement structure. Therefore, a date with a similar temperature profile (4/23/07) was selected for use for the investigations regarding the other structural sections. Table 5.1 shows the testing dates utilized for this investigation as well as the structural sections in which the testing was performed.

**Table 5.1 FWD Testing Dates Used in Cross-Section Determination**

| FWD Testing Date | Sections N1 and N2 | Sections N3-N10 and S11 |
|---|---|---|
| 10/30/2006 | X | |
| 11/27/2006 | X | X |
| 1/29/2007 | X | X |
| 4/23/2007 | | X |
| 8/20/2007 | X | X |

The data from these four testing dates were crucial to determining the optimum backcalculation cross-section. For each structural section, the deflection data from these four dates were backcalculated using each of the trial backcalculation cross-sections. From this, a database of summary files detailing the layer moduli and RMS error for each drop was compiled. These individual databases were then analyzed to determine the quality of the solution. First, the results from each cross-section were analyzed to determine the percentage of drops exhibiting a reasonable match between measured and calculated deflections (RMS Error). For the purposes of this investigation, the percentage of drops that exhibited an RMS error below 4% was used to determine whether a trial cross-section presented a reasonable solution. The concept of using a cut-off RMS error value between acceptable and unacceptable deflection basins is present in literature (Von Quintus and Killingsworth, 1998). Seeds et al. (2000) label any deflection basin with an RMS error below 4 percent as being 'very good' for the purposes of backcalculation. This threshold was deemed acceptable for research at the track in order to generate a sufficiently large data set for analysis.

Secondly, the summary files were analyzed to ensure that the solution for a particular cross-section was stable and presented consistent modulus values between drops at the same load levels. A quality backcalculation solution will generate consistent pavement layer moduli under similar loading conditions. Erratic layer moduli on subsequent drops at identical load levels serve as an excellent indicator of solution instability. Additionally, these files were analyzed to ensure that the modulus values for two adjoining layers were not compensating for one another on consecutive drops. An example of this behavior will be given later in this chapter. Finally, the individual solutions were analyzed to ensure that the modulus values were reasonable for that particular material. The process outlined above typically eliminated several of the trial cross-sections from consideration, leaving only two or three viable solutions.

The second data set used in determining the optimum backcalculation cross-section was the data from the FWD on gauge testing conducted on 7/17/07 (See Chapter 3 for full details on testing). For each structural section, the deflection files from this testing were backcalculated using the trial cross-sections that were deemed viable after analyzing the data from the multiple FWD testing dates. These files were backcalculated to determine the pavement responses at the locations in which instrumentation was embedded within the pavement structure (e.g. the bottom of the HMA layer, the surface of the base layer, and the surface of the fill layer). These predicted pavement responses generated through backcalculation were then paired with the corresponding measured pavement response from the instrumentation for that particular FWD loading (drop). Comparing the measured versus predicted strain behavior for the remaining trial cross-sections were used as a deciding factor in determining the best cross-section for analysis. Measured versus predicted pressures at the surface of the base and fill layers were also calculated and analyzed to validate the use of the selected backcalculation cross-section. Figure 5.2 shows a flowchart which summarizes the decision making process used in determining the optimum backcalculation cross-sections for each of the structural sections. The

following sub-sections present sections grouped into their respective sub-experiments, where applicable.

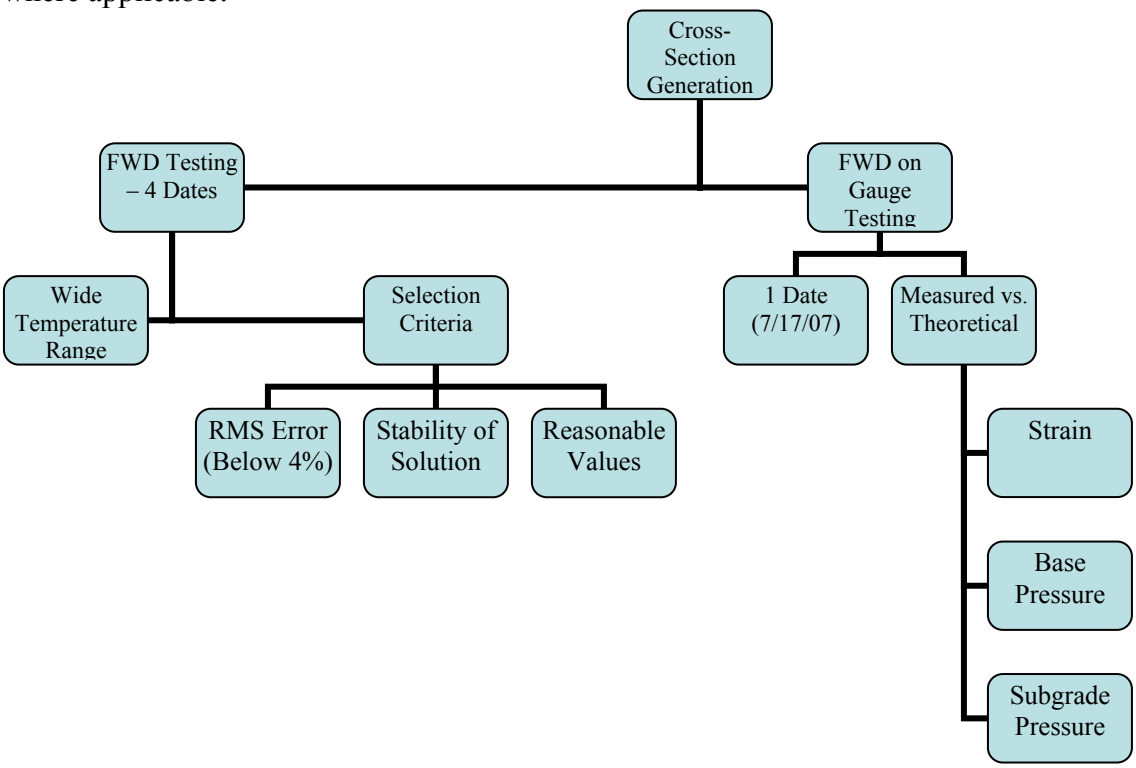


**Figure 5.2 Cross-Section Trials Investigation Flowchart**.

**N1-N2 CROSS-SECTION INVESTIGATION**

Sections N1 and N2 were analyzed together for the purposes of determining their optimum backcalculation cross-section. These sections are constructed in almost an identical manner, as can be seen from Figure 5.1. Each have approximately 7 inches of HMA over approximately 10 inches of Florida limerock granular base material over approximately 1.5 inches of compacted Track fill. Each section was milled to 18.5 inches for the 2006 construction, and the fill composition from the previous research cycles is identical below that depth. The only major difference in these sections is that the top two lifts of HMA in Section N2 contain a modified binder (PG 76-22) (See the construction notes on N1 and N2 in Chapter 3 for complete details).

Through analyzing the construction information and combining layers which might be indistinguishable from one another for the purposes of backcalculation, multiple trial cross-sections were developed for Sections N1 and N2. These cross-sections are illustrated in Figure 5.3. The numbering scheme for each of the cross-sections contains a trial number in parentheses followed by the number of layers used in that trial cross-section. For example, (2)-3layer is the second trial 3-layer cross-section. A capital B in parenthesis indicates that the trial cross-section included a rigid layer (or bedrock). HMA represents all the combined lifts of hot mix asphalt. GB represents the compacted granular base layer (in this case, Florida Limerock). New Fill represents the Track fill compacted in both the 2003 and 2006 research cycles (the 1.5 inches of fill added for

2006 was too thin to constitute a separate layer). Old Fill represents the 12 inches of Track fill compacted for the 2000 research cycle. Finally, Subgrade represents the infinitely deep Track soil embankment and Bedrock represents the trial rigid layer entered into the backcalculation software.

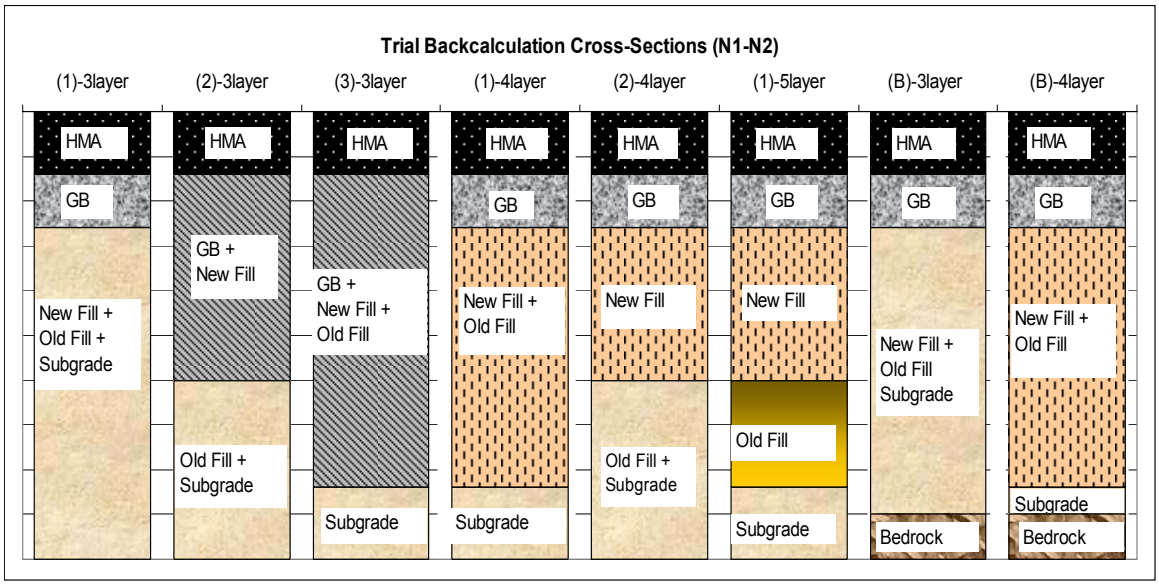


**Figure 5.3 Trial Backcalculation Cross-Sections (Sections N1 and N2).**

The first step in the analysis procedure was to run the designated four FWD testing dates worth of deflection basins through EVERCALC for each of the trial cross-sections. For each cross-section, a database of backcalculated layer moduli and RMS error values were developed for each FWD loading. First, the error values for each cross-section were analyzed by generating a cumulative distribution function (CDF) of RMS error for all the backcalculated FWD loadings for that cross-section. Figure 5.4 shows the CDF of RMS error for each of the trial cross-sections for N1 and N2. Two things are evident from this plot. First, two of the cross-sections show a CDF with a large percentage of high RMS error drops. These cross-sections are (B)-3layer and (B)-4layer, the two cross-sections using a stiff layer in the backcalculation. Given the high error values from this cross-section, it is evident there are no stiff layers factoring the deflection behavior of the pavement in N1 and N2. Aside from the cross-sections with bedrock, the remainder of the cross-sections appear to have very similar CDFs.

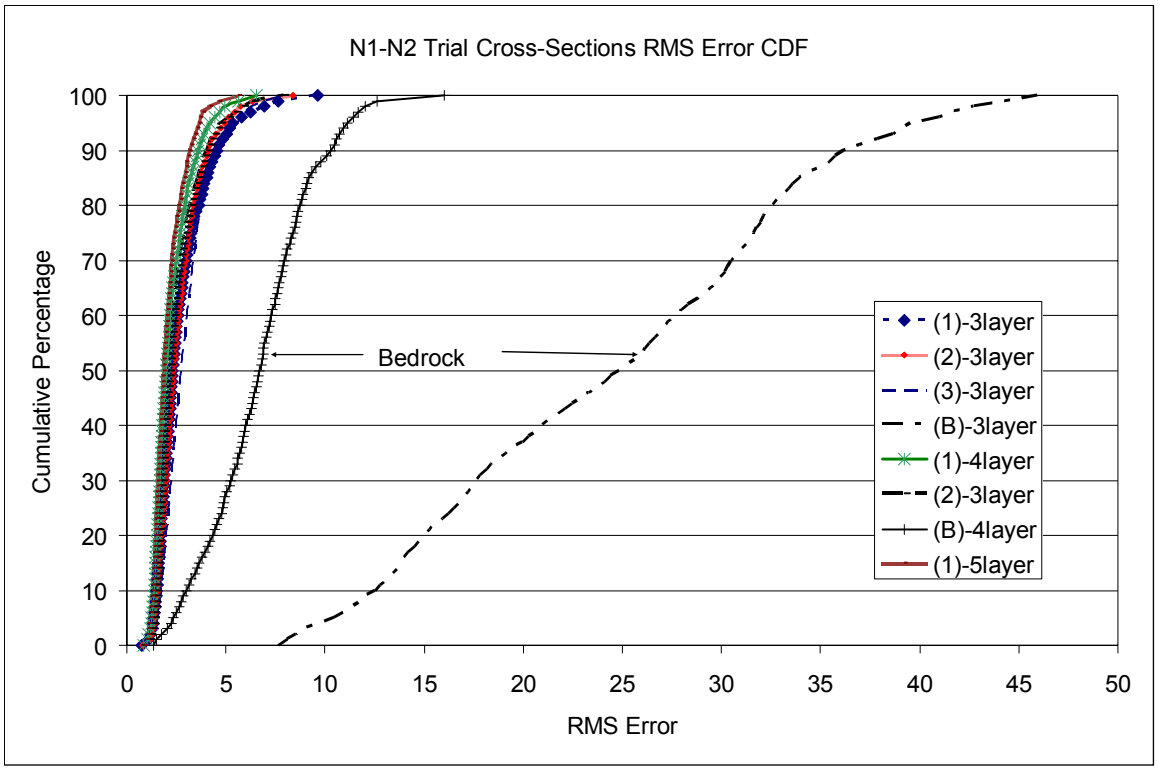


**Figure 5.4 RMS Error Cumulative Distribution Functions (CDF) for the Trial Backcalculation Cross-Sections in Sections N1 and N2.**

The next step in the cross-section elimination process was to analyze the backcalculated modulus values and determine whether these values were reasonable and whether the solution was stable. Table 5.2 shows an example of an output summary file from the backcalculation software for the FWD testing at one station on one day using the (1)-5layer cross-section. This table clearly illustrates both unreasonable modulus behavior and layer compensation effects. It should first be noted that the moduli of the HMA, granular base, and deep subgrade all seem to behave consistently and reasonably (E1, E2, and E5). However, the modulus of the new fill material (2003 and 2006 Track fill) almost always approaches the upper limit of 100 ksi. These modulus values are far too high to be reasonable for any unstabilized unbound material. Also, the behavior of the old fill material (2000 Track fill) seems to behave erratically between drops. For the first three drops at the 6,000 lb load level, the backcalculated soil moduli range from 43.2 to 66.8 ksi. Typically, the modulus values from a stable backcalculation solution would be much more consistent than that at the same load level. Although the RMS error values are very good for this cross-section, the modulus values do not seem to behave in a reasonable manner. Therefore, the (1)-5layer cross-section was eliminated from further consideration.

**Table 5.2 (1)-5layer Cross-Section Modulus Behavior (Station N1-12, 10/30/06)**

| LOAD(LB) | E1(KSI) | E2(KSI) | E3(KSI) | E4(KSI) | E5(KSI) | Error (%) |
|---|---|---|---|---|---|---|
| 5454 | 334.8 | 13.6 | 100 | 43.2 | 43.3 | 3.51 |
| 5454 | 329.2 | 16.3 | 38.8 | 66.8 | 42.7 | 3.97 |
| 5457 | 331.8 | 13.3 | 100 | 52 | 42.5 | 3.56 |
| 8651 | 314.1 | 13.1 | 100 | 18.1 | 44.4 | 2.13 |
| 8659 | 312.4 | 13.2 | 100 | 17.8 | 44.3 | 2.11 |
| 8659 | 311 | 12.9 | 100 | 22.3 | 42.4 | 1.83 |
| 11781 | 325.6 | 10.7 | 95.6 | 23.1 | 41.7 | 2.16 |
| 11785 | 322.2 | 10.7 | 100 | 21.7 | 41.7 | 2.19 |
| 11793 | 315.4 | 11.3 | 100 | 18 | 41.5 | 1.96 |
| 15559 | 328.5 | 9.3 | 100 | 22.1 | 40.3 | 1.82 |
| 15566 | 328.7 | 9.5 | 100 | 19.9 | 40.8 | 1.59 |
| 15570 | 322.1 | 9.8 | 100 | 19.7 | 40.7 | 1.7 |

Similar erratic modulus behavior was also witnessed when the 4-layer trial cross-sections were analyzed. Figure 5.5 shows the modulus behavior of the fill layer (layer 3) for the (1)-4layer cross-section for Section N1. This graph summarizes only the 9 kip FWD loadings and shows the backcalculated moduli for all the FWD testing locations within N1 for four different dates. Again, there are several stations where the modulus values spike on an upper boundary. Additionally, one would expect the modulus values on a given day to be relatively consistent (barring small changes for spatial variability) if they were normalized to the same load level. Figure 5.5 shows that this is not the case, as the modulus behavior on 11/27/06 and 1/29/07 are shown to be incredibly erratic. Additionally, the standard deviations for some of the drop locations are quite sizable, indicating an unstable solution where the backcalculated moduli vary greatly from loading to loading. Similar behavior was also witnessed on the (2)-4layer cross-section. Therefore, the 4-layer trial solutions were eliminated from further consideration.

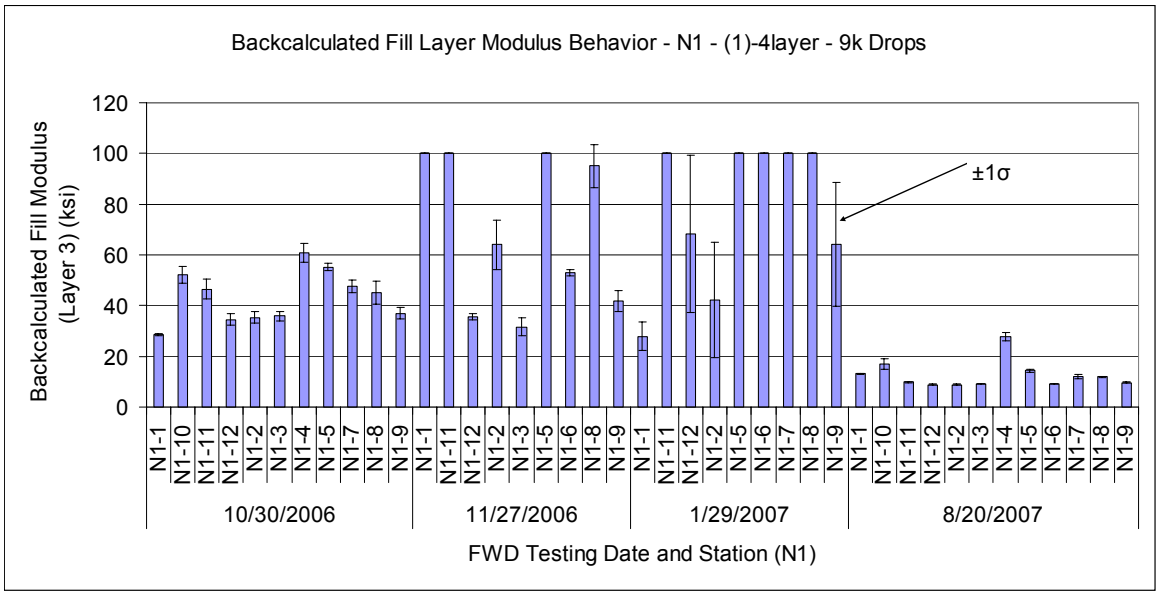


**Figure 5.5 Fill Layer Modulus Behavior (Layer 3) (Section N1, All Testing Stations and Dates, 9 kip drops).**

With the 4-layer and 5-layer cross-sections being eliminated due to unreasonable modulus behavior, a closer look was then taken at the RMS error cumulative distribution functions for the 3-layer systems. These CDFs are shown in Figure 5.6. It can be seen from this figure that all three trial cross-sections have at least 85% of the FWD loadings for the four dates with an RMS error below the 4% cutoff limit. The (2)-3layer cross-section (granular base combined with 2003 and 2006 Track fill above 2000 Track fill combined with deep subgrade) exhibits the best RMS error behavior, having 89% of the FWD loadings below 4% RMS error. Both the (1)-3layer (isolated granular base with all fill combined with subgrade) and the (3)-3layer (granular base combined with all fill above deep subgrade) have the same percentage of drops below 4% RMS Error (approximately 85% of drops). However, the (1)-3layer CDF is to the left of the (3)-3layer CDF below the cut-off of 4%, indicating generally lower RMS error values.

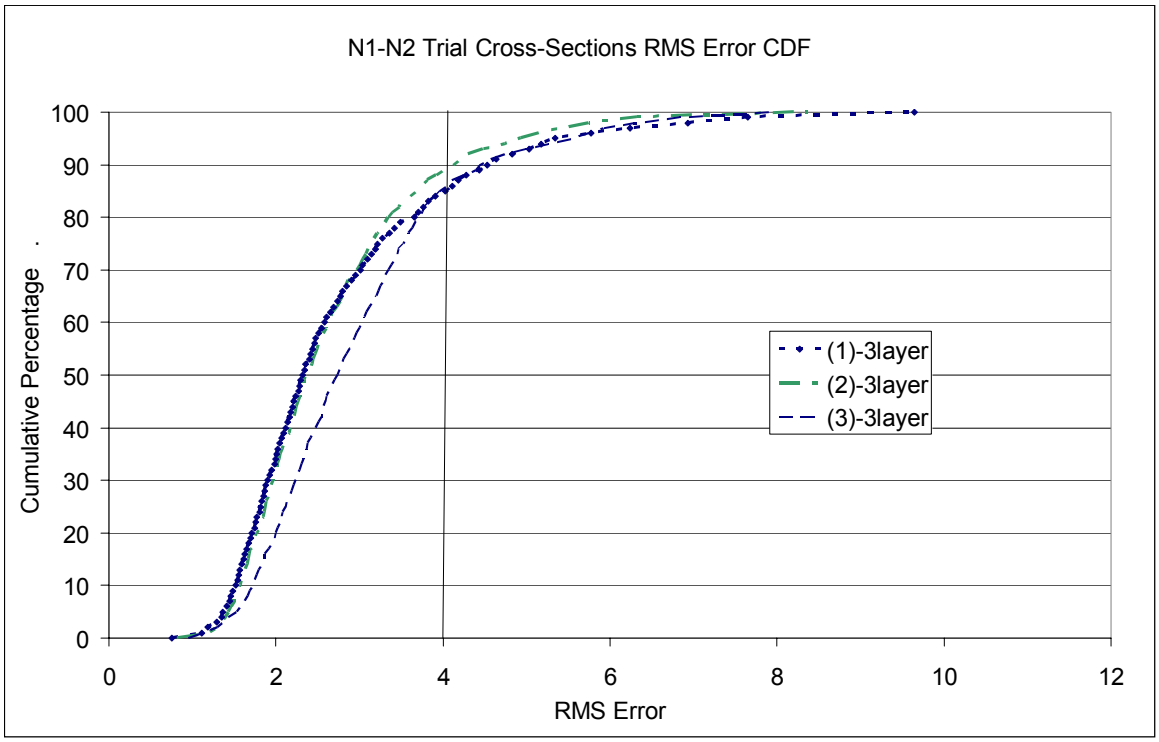


**Figure 5.6 RMS Error Cumulative Distribution Functions (CDF) for the 3-Layer Trial Backcalculation Cross-Sections in Sections N1 and N2.**

Since the (3)-3layer cross-section showed the weakest RMS error behavior, it was then eliminated from consideration (provided the other two cross-sections generated reasonable modulus solutions). Therefore, the final trial cross-sections to evaluate were the (1)-3layer and the (2)-3layer cross-section. The (1)-3layer cross-section would be preferable for final selection due to it isolating the limerock base layer. This would allow for an independent characterization of the resilient modulus stress-sensitivity behavior of that material. The next phase of the investigative process involved analyzing the modulus behavior of each cross-section and comparing the measured versus predicted strain responses calculated using each trial cross-section.

For Section N1, Figures 5.7 and 5.8 show the average and standard deviations of the backcalculated base layer moduli for cross-sections (1)-3layer and (2)-3layer, respectively. The moduli shown are calculated from the 9,000 lb FWD loadings for each testing station on each testing date. Only the 9,000 lb loadings are shown so that the stability of the solution at a constant drop height can be assessed. Figures 5.9 and 5.10 show the same data for Section N2 and cross-sections (1)-3layer and (2)-3layer, respectively.

First, each trial cross-section generates a reasonably stable solution due to the consistency of the modulus values at each testing location. It is evident that the standard deviation values are relatively small at each drop location when compared to the average backcalculated modulus at that location. Secondly, the average backcalculated moduli vary somewhat from station to station, but do not show dramatic variation within a given

day's testing (such as was shown in Figure 5.5). The variations in backcalculated moduli between testing locations is most likely a function of spatial variability. Section N2 seems to show considerably more modulus variation than Section N1. However, the same variation exists regardless of backcalculation cross-section utilized. For example, both backcalculation cross-sections show a dramatic increase in modulus between stations N2-3 and N2-5 on all the testing dates. Were this variation a function of the backcalculation cross-section rather than spatial construction variability, this difference would not be notable in both Figures 5.9 and 5.10.

Finally, it is evident comparing backcalculated data from the same testing location using different cross-sections that average backcalculated base layer moduli using the (2)-3layer cross-section are higher than those generated using the (1)-3layer cross-section. This is most likely because the second layer has been bolstered with the Track fill material. Since this subgrade is a relatively stiff material, it is not surprising that combining the limerock base with this material increases the backcalculated base stiffness.

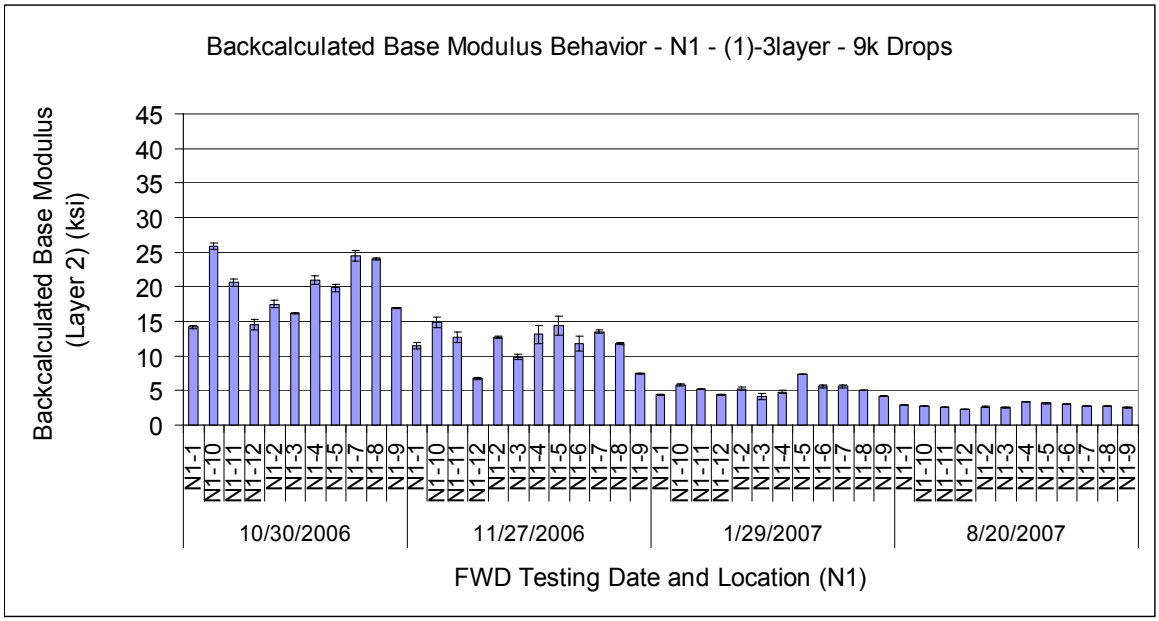


**Figure 5.7 Base Layer Modulus Behavior (Layer 2) (Section N1, (1)-3layer, All Testing Stations and Dates, 9 kip drops).**

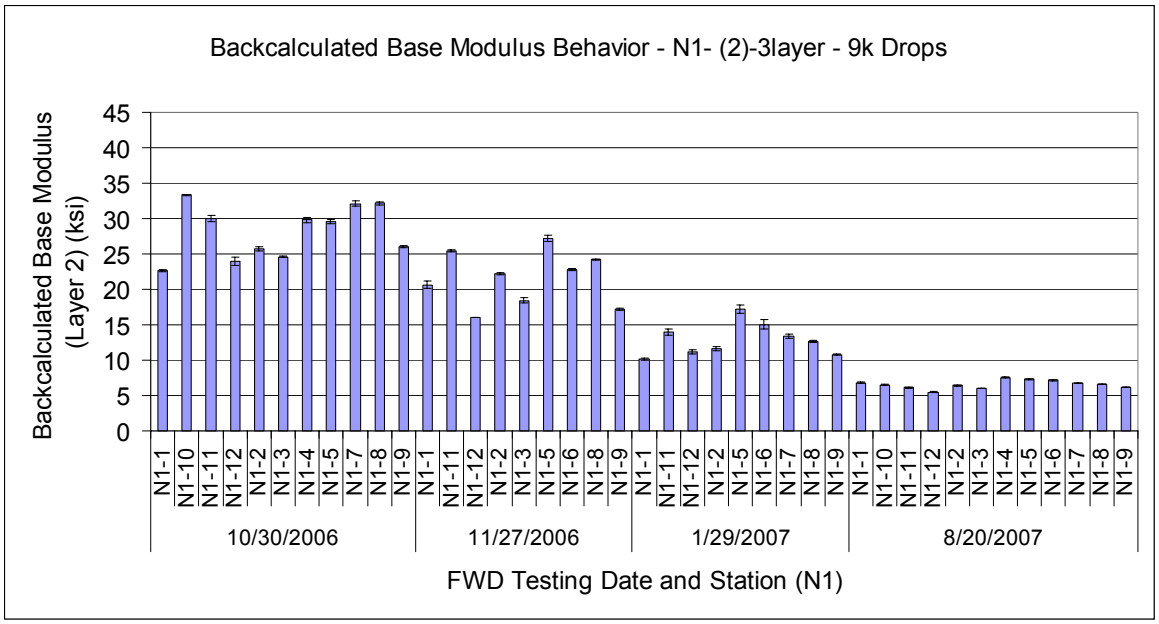


**Figure 5.8 Base Layer Modulus Behavior (Layer 2) (Section N1, (2)-3layer, All Testing Stations and Dates, 9 kip drops).**

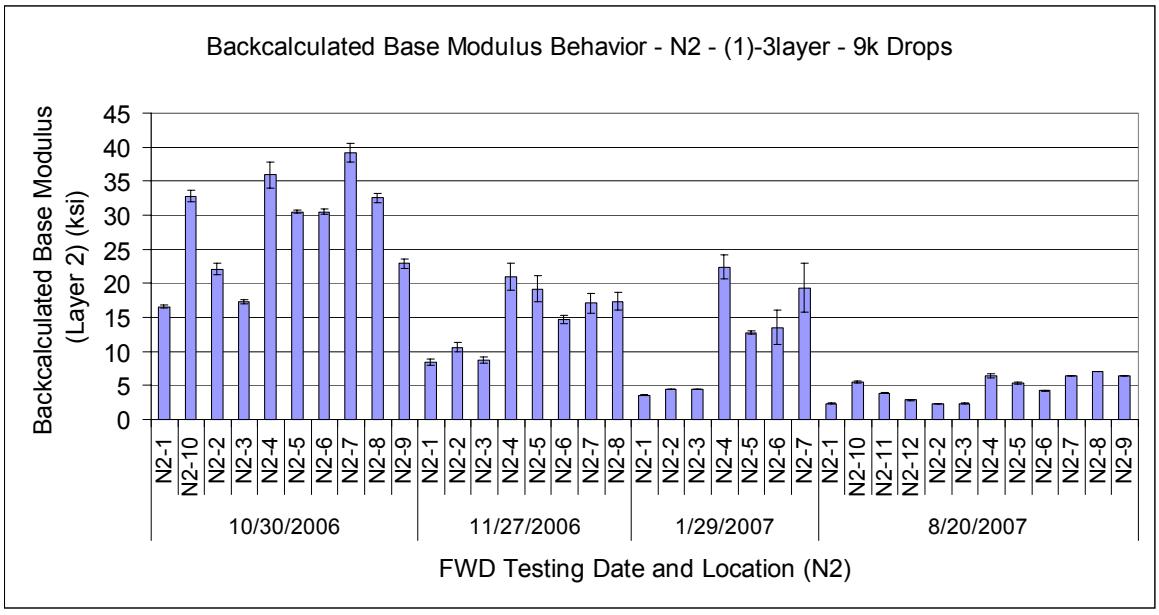


**Figure 5.9 Base Layer Modulus Behavior (Layer 2) (Section N2, (1)-3layer, All Testing Stations and Dates, 9 kip drops).**

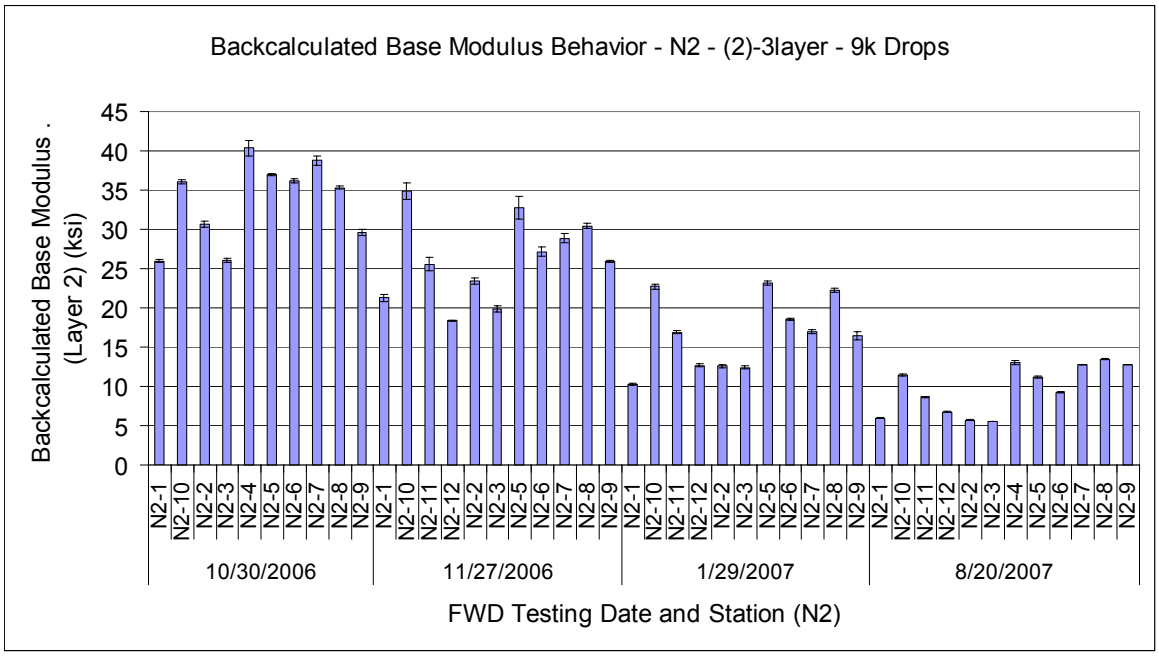


**Figure 5.10 Base Layer Modulus Behavior (Layer 2) (Section N2, (2)-3layer, All Testing Stations and Dates, 9 kip drops).**

For Section N1, Figures 5.11 and 5.12 show the average and standard deviations of the backcalculated subgrade layer moduli for cross-sections (1)-3layer and (2)-3layer, respectively. The moduli shown are calculated from the 9,000 lb FWD loadings for each testing station on each testing date. Figures 5.13 and 5.14 show the same data for Section N2 and cross-sections (1)-3layer and (2)-3layer, respectively. The purpose in analyzing this data is to ascertain whether or not the trial cross-section generates a stable solution with reasonable modulus values for the subgrade layer.

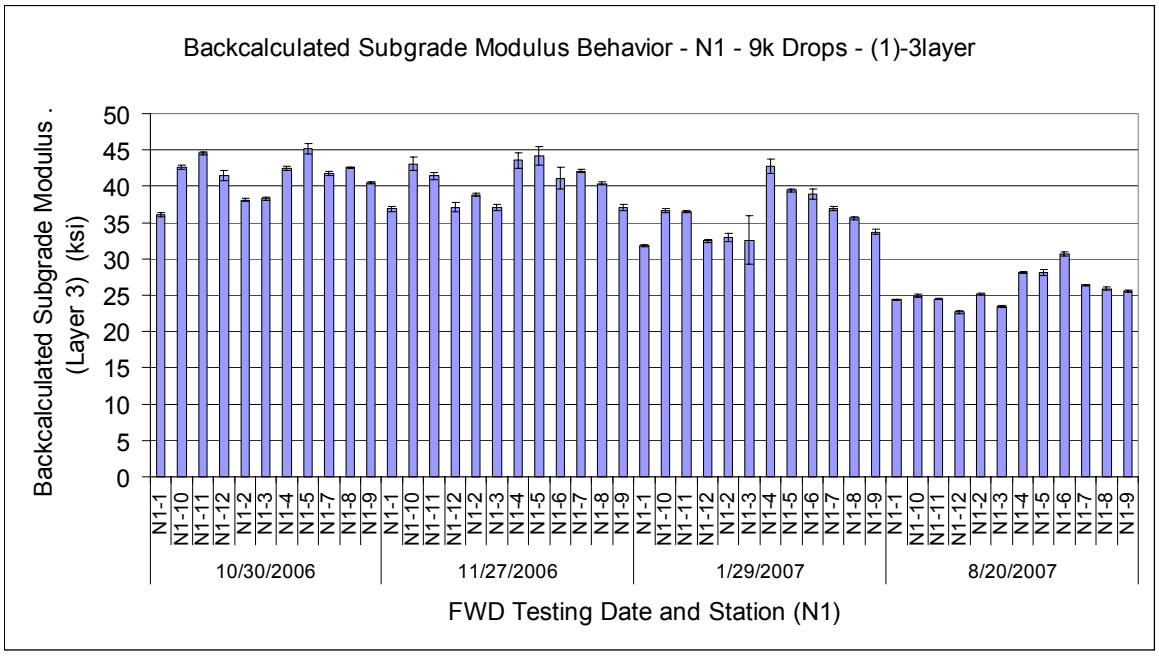


**Figure 5.11 Subgrade Layer Modulus Behavior (Layer 3) (Section N1, (1)-3layer, All Testing Stations and Dates, 9 kip drops).**

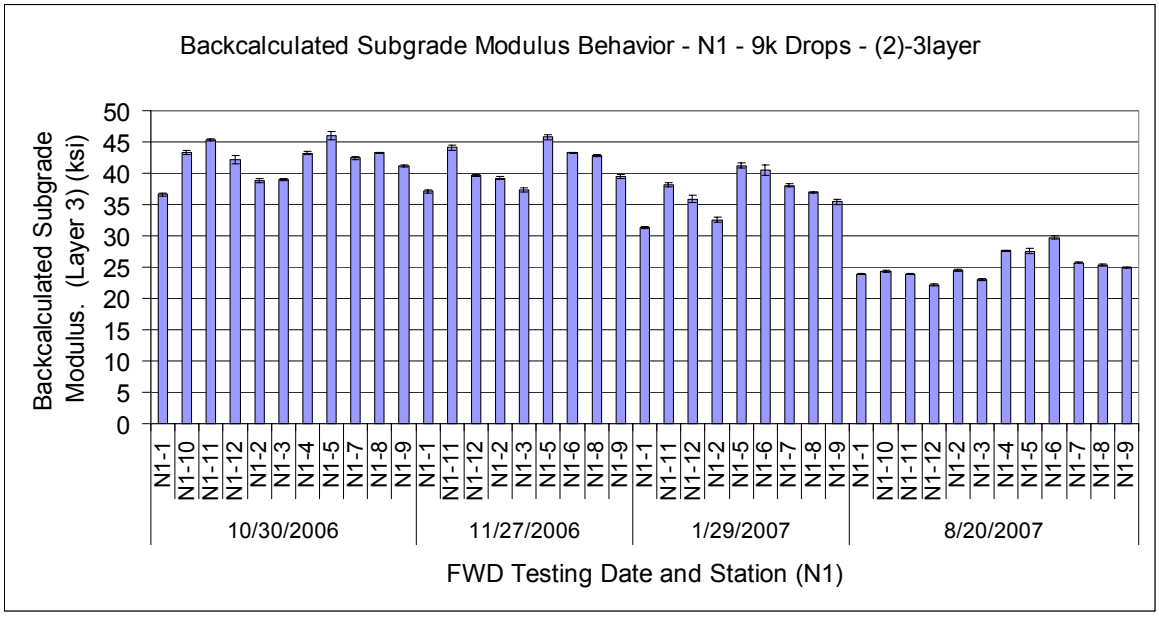


**Figure 5.12 Subgrade Layer Modulus Behavior (Layer 3) (Section N1, (2)-3layer, All Testing Stations and Dates, 9 kip drops).**

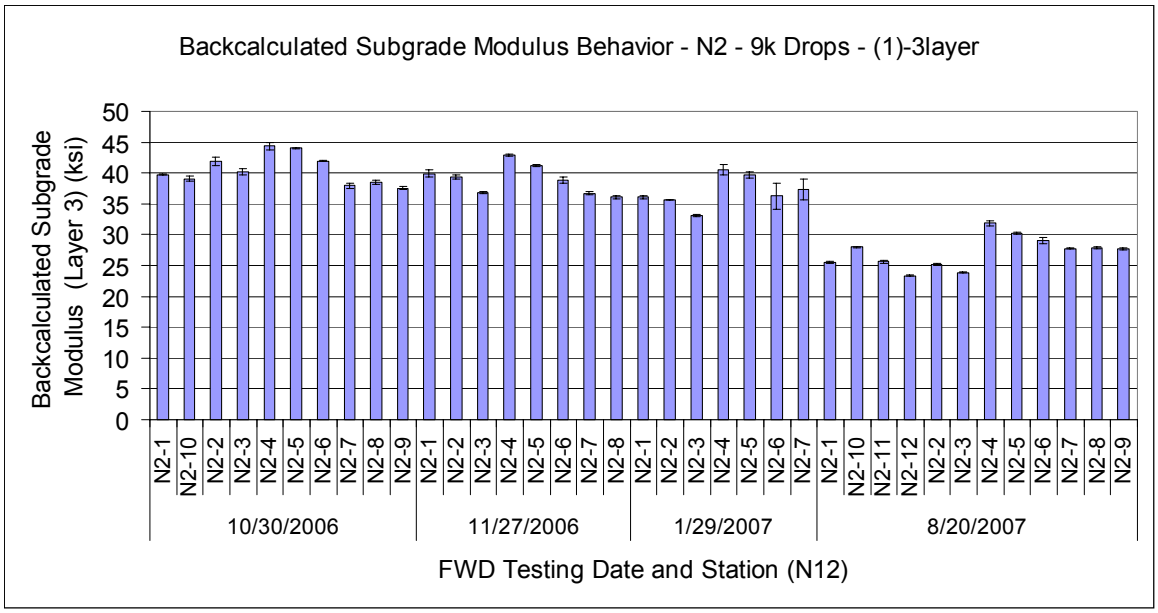


**Figure 5.13 Subgrade Layer Modulus Behavior (Layer 3) (Section N2, (1)-3layer, All Testing Stations and Dates, 9 kip drops).**

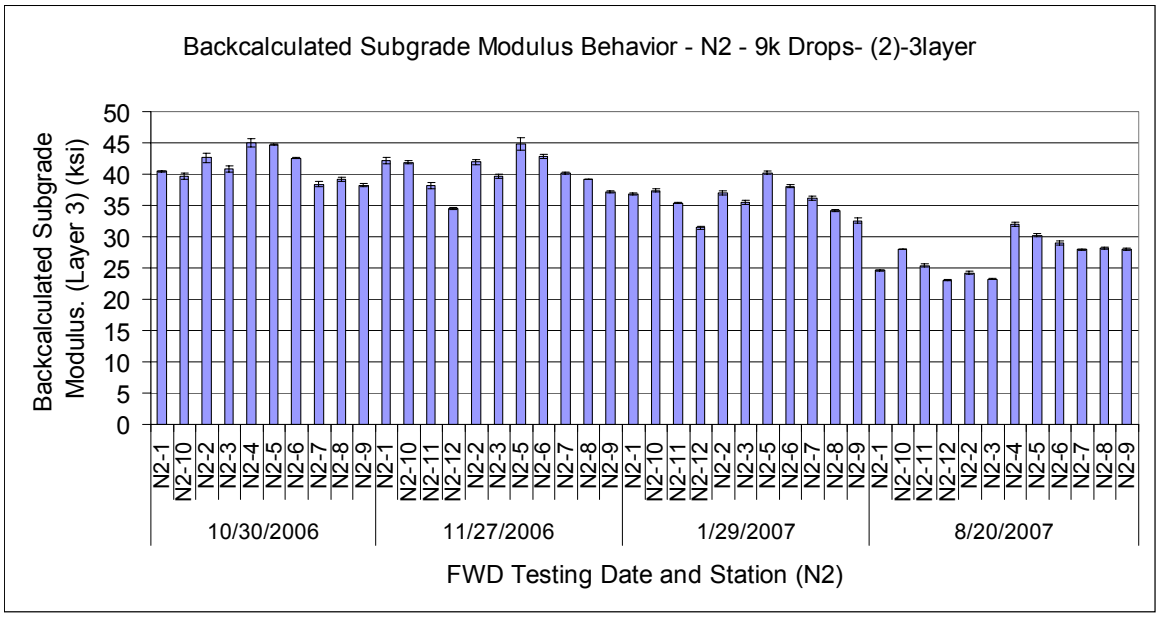


**Figure 5.14 Subgrade Layer Modulus Behavior (Layer 3) (Section N2, (2)-3layer, All Testing Stations and Dates, 9 kip drops).**

Figures 5.11 through 5.14 show stable subgrade modulus behavior at each of the testing locations throughout sections N1 and N2. Again, there does not appear to be any serious modulus fluctuation between testing stations that cannot be attributed to spatial variability. Additionally, there do not appear to be any significant differences between the backcalculated subgrade moduli at the given testing locations regardless of which backcalculation cross-section was utilized. For example, the backcalculated modulus for station N2-1 is approximately 40 ksi regardless of which cross-section was used.

Figure 5.15 is a summary plot used to compare the backcalculated modulus values in sections N1 and N2 using the trial cross-sections (1)-3layer and (2)-3layer. Each data point on this plot represents a comparison between the backcalculated modulus for a given pavement layer at a specific testing location using the two different cross-sections. Again, only the 9,000 lb drops were utilized to eliminate loading variability.

This plot shows that the backcalculated base moduli were significantly higher using the (2)-3layer cross-section than with the (1)-3layer cross-section. As noted previously, this is likely due to increasing the stiffness of the base layer by combining it with the Track fill for the purposes of backcalculation. Another notable feature of this plot is that the difference in backcalculation cross-section does not appear to have a major effect on the modulus results for the subgrade and HMA layers. The comparison points for the subgrade layer fall on the line of unity shown in the figure, indicating that this modulus is unaffected by the composition of the base layer in the cross-section. Additionally, the comparison points for the HMA layer seem to be slightly higher for the (1)-3layer cross-section due to these points falling slightly below the line of unity. However, the offset of these data from the line of unity is not very great, indicating backcalculation cross-section does not have a tremendous effect on HMA modulus. The primary effect of altering the backcalculation cross-section seems to be the effect on the base modulus.

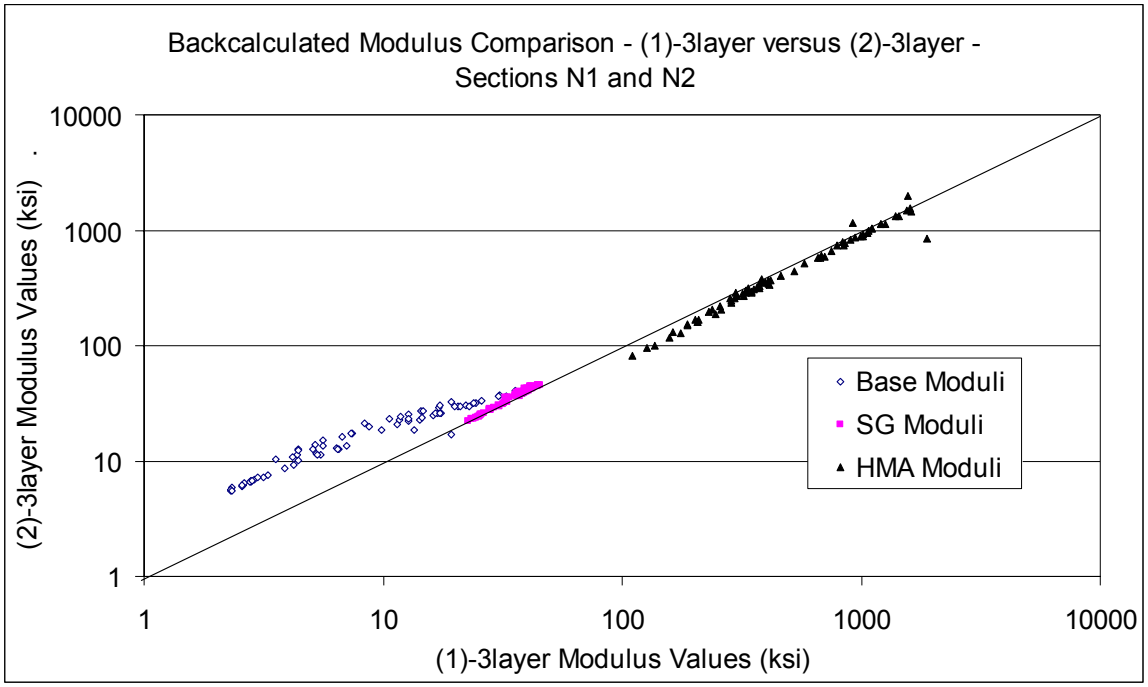


**Figure 5.15 Backcalculated Modulus Comparison between Trial Cross-Sections (1)-3layer and (2)-3layer – Sections N1 and N2 – All Layers.**

At this point in the investigation, it seems that both the (1)-3layer and (2)-3layer cross-sections give a reasonable backcalculation solution. Both exhibit good RMS error values and show stable and reasonable backcalculated modulus values. The only major difference between the two cross-sections is that the (2)-3layer cross-section generates

higher base modulus values due to the limerock base being combined with the Track fill for the purposes of backcalculation. Another means of comparing the two sections is to utilize the FWD on gauge data to compare the measured pavement strains to the predicted (theoretical) pavement strains using the two different cross-sections.

Figures 5.16 and 5.17 show the measured versus predicted pavement strains in sections N1 and N2 for the (1)-3layer and (2)-3layer cross-sections, respectively. Each strain represents one FWD loading above a pavement strain gauge which plots the measured strain from the instrumentation versus the theoretical pavement strain at that location in the pavement structure calculated by the backcalculation software. This testing occurred on one day, so no temperature variability is present. However, these plots show the FWD drops from each of the different load levels, giving a wide range of loading data.

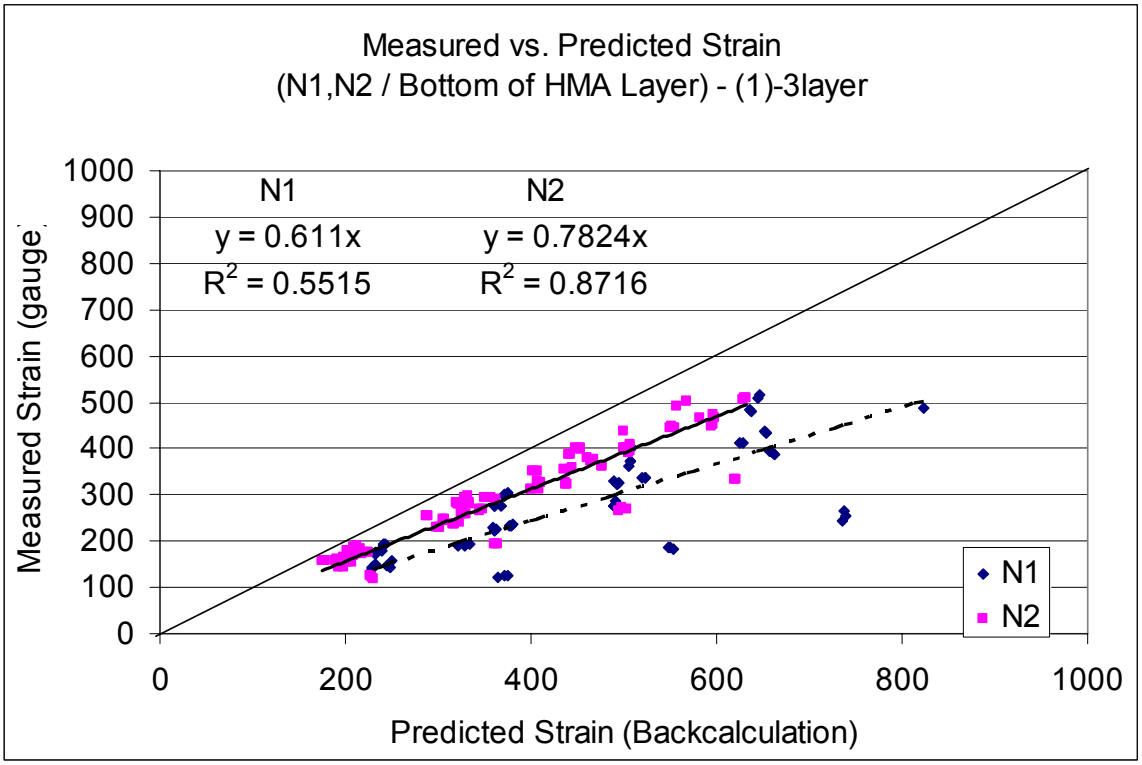


**Figure 5.16 Measured versus Predicted Strains for Sections N1 and N2 – (1)-3layer.**

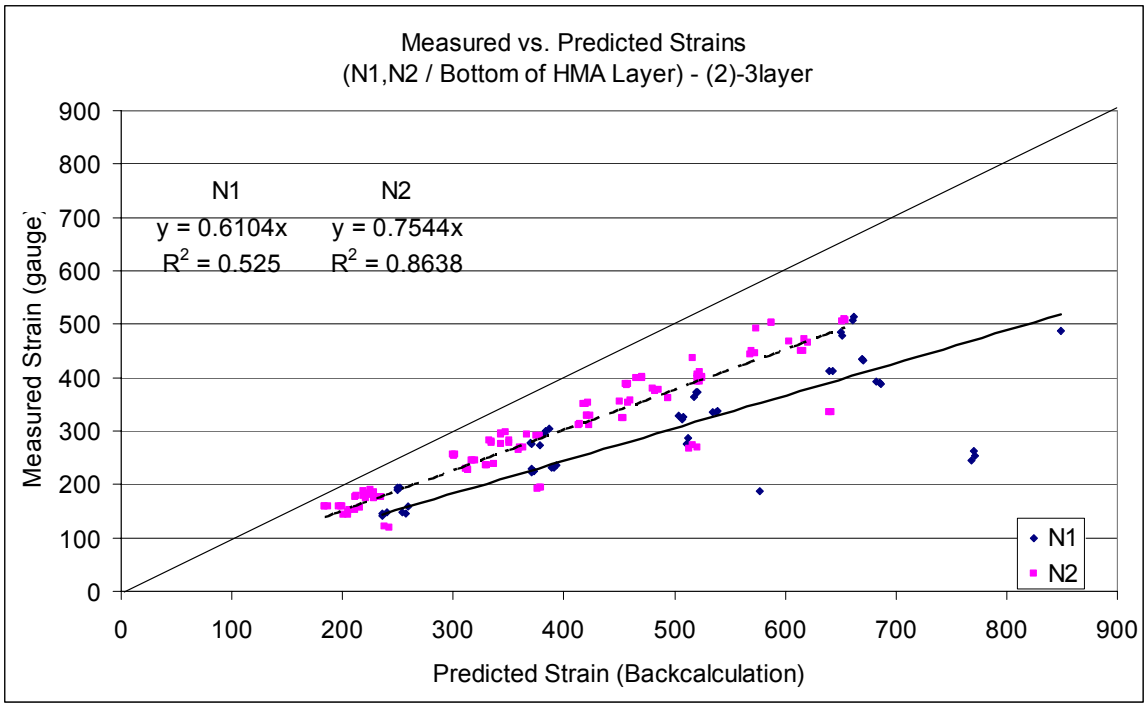


**Figure 5.17 Measured versus Predicted Strains for Sections N1 and N2 – (2)-3layer.**

Each of these plots show a reasonable correlation between measured and predicted strain behavior, regardless of which cross-section is utilized. The data sets for each section are both within 40% of the line of unity (representing equality between measured and predicted response). The data set from section N1 is farther from the line of unity than section N2. This is not surprising since section N1 had seen a large amount of top-down cracking at this stage in its life while N2 showed no visible signs of distress. These values are similar to those produced in a similar study for the 2003 research cycle (Timm and Priest, "Material Properties", 2006). The slopes and $R^2$ values for each of the data sets are very similar regardless of cross-section utilized. However, the values for the (1)-3layer cross-sections track slightly closer to the line of unity with less scatter (higher $R^2$). Therefore, it can be said that the (1)-3layer cross-section performs slightly better than the (2)-3layer cross-section with respect to measured versus predicted behavior.

In summary, the (1)-3layer and (2)-3layer cross-sections were shown to be very comparable to one another. The (2)-3layer cross-section solution had slightly higher RMS error than the (1)-3layer solution. However, the (1)-3layer solution had slightly better performance in the measured versus predicted strain investigation. Both solutions produced stable, reasonable modulus values. The advantage to selecting the (1)-3layer cross-section would be isolating the base layer for the purposes of materials characterization. Since the (2)-3layer cross-section was not determined to yield an appreciably better solution, the (1)-3layer cross-section was deemed most appropriate for backcalculation analyses on sections N1 and N2.

The final step in the investigative process was to analyze the behavior of the measured versus predicted pressures at the surface of the base and fill layers for the (1)-3layer cross-section. This was done with the final cross-section to ensure that there was reasonable agreement between the measured and predicted responses for the pressure as well as the strain responses. Figure 5.18 shows the measured versus predicted base pressure responses and Figure 5.19 shows the measured versus predicted fill pressure responses. The data from section N1 did not pass the RMS filter of having data less than or equal to 4%, so the only data shown is from section N2. The data shows the slope of each data set is within approximately 50% of the line of unity (with base pressure being above the line of unity and subgrade pressure being below) with very good model fit. While not ideal, the data appear to behave reasonably and are in agreement with previous studies (Timm and Priest, "Material Properties", 2006). Therefore, no reason could be found to invalidate the use of (1)-3layer as the final backcalculation cross-section for sections N1 and N2.

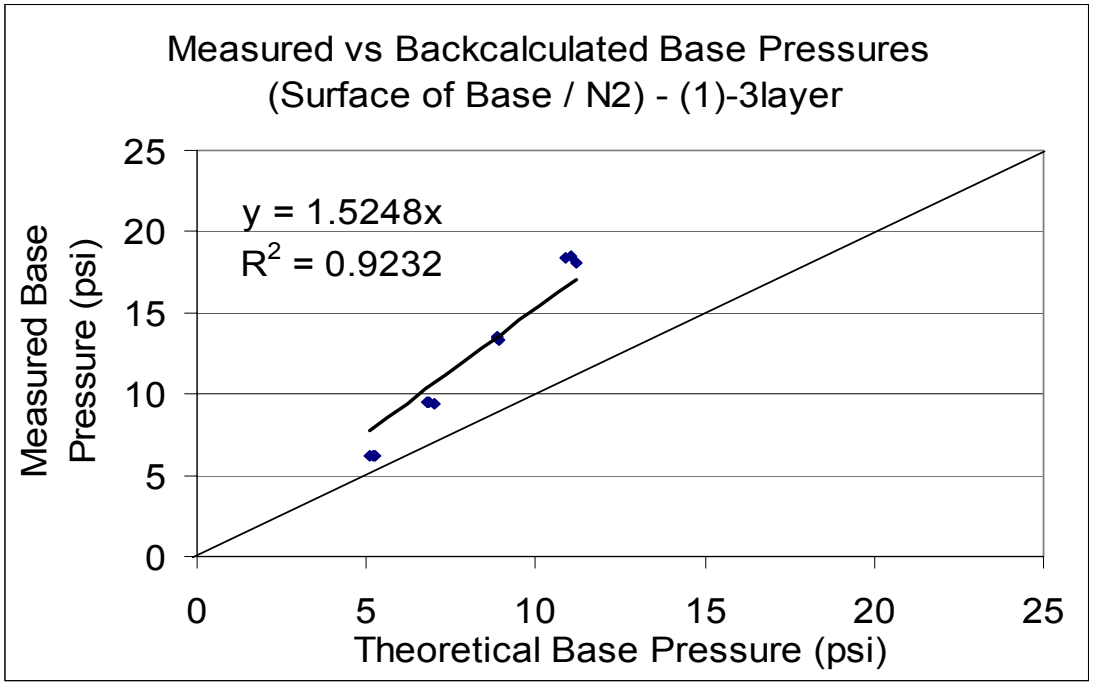


**Figure 5.18 Measured versus Predicted Base Pressures (N1/N2, (1)-3layer).**

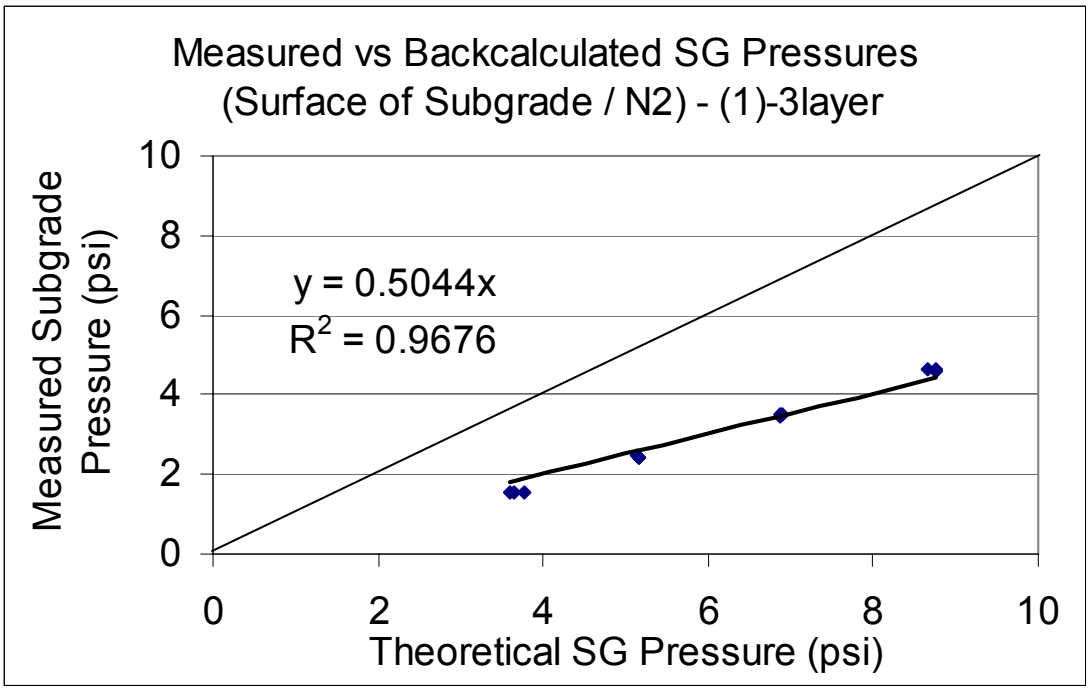


**Figure 5.19 Measured versus Predicted Subgrade Pressures (N1/N2, (1)-3layer).**

**N3-N7 CROSS-SECTION INVESTIGATION**

Sections N3, N4, N5, N6, and N7 were analyzed together for the purposes of determining their optimum backcalculation cross-section. All of these sections were constructed in a similar fashion (as shown in Figure 5.1). Each section was constructed for the 2003 research cycle and were left in-place for the 2006 research cycle. All these sections were milled to a depth of 30 inches prior to construction, and were constructed with between 7 and 9 inches of HMA over 6 inches of the granite base over Track fill. As shown in Figure 5.1, section S11 was also constructed in a similar manner. However, S11 was constructed for the 2006 research cycle and was analyzed separately due to it not having yet undergone three years of age and traffic like the other sections with the granite base. The variance in these sections is mostly due to the composition of the HMA lifts. However, since all the HMA lifts for a given section were typically combined for the purposes of backcalculation (backcalculation software often cannot distinguish differences in similar layers that border each other), it was deemed suitable for the 2003 structural sections to be analyzed together.

Again, through the analysis of the construction information plus layer and material composition of these sections (see Chapter 3 for further details) a set of trial backcalculation cross-sections were generated for sections N3-N7. These cross-sections are shown in Figure 5.20. The same naming scheme is utilized for these cross-sections as was utilized for the N1-N2 trial cross-sections. There is some slight variation in the representative layer names, however. HMA represents all the combined lifts of Hot Mix Asphalt. GB represents the compacted granular base layer (in this case, the granite base).

New Fill represents the Track fill compacted for the 2003 research cycle (between 15 and 17 inches). Old Fill represents the 12 inches of Track fill compacted for the 2000 research cycle. Finally, Subgrade represents the infinitely deep Track soil embankment and Bedrock represents the trial rigid layer entered into the backcalculation software.

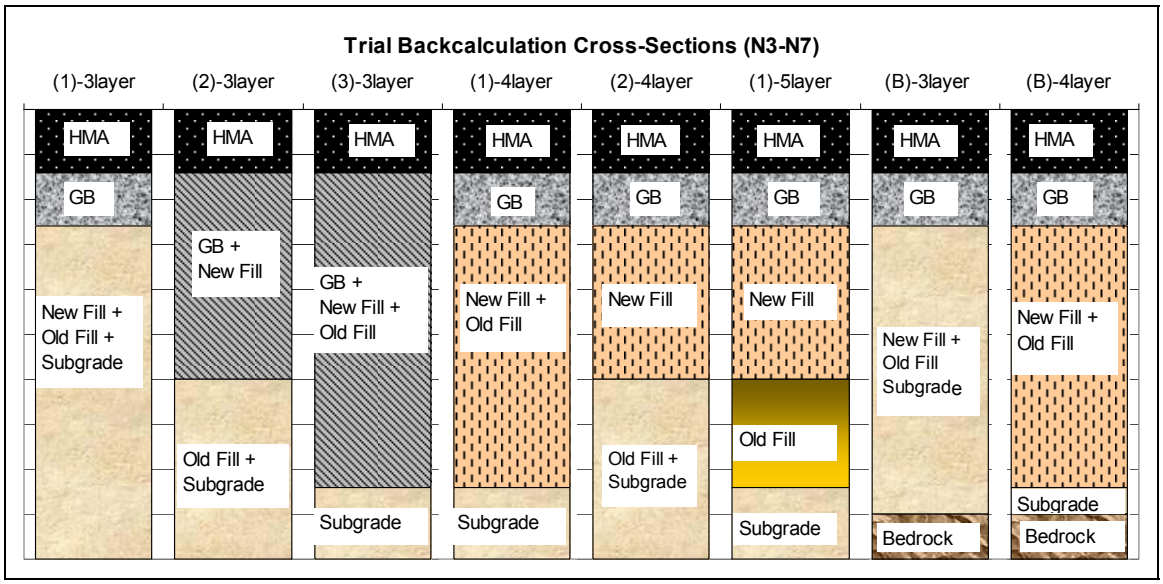


**Figure 5.20 Trial Backcalculation Cross-Sections for Sections N3-N7.**

The first step in the investigative process was to analyze the RMS error CDFs generated by running the four dates worth of data through the backcalculation software for each of the trial cross-sections. Figure 5.21 shows the RMS error CDFs for each of the trial backcalculation cross-sections for sections N3-N7. Two of the cross-sections exhibit a very high percentage of high RMS error FWD loadings. These cross-sections are the (B)-3layer and (B)-4layer cross-section. Again, there does not appear to be any bedrock or stiff layer present to affect the backcalculation. As a result, these cross-sections were eliminated from further analysis. The cross-sections that did not include a stiff layer for analysis all seem to exhibit relatively similar RMS error behavior.

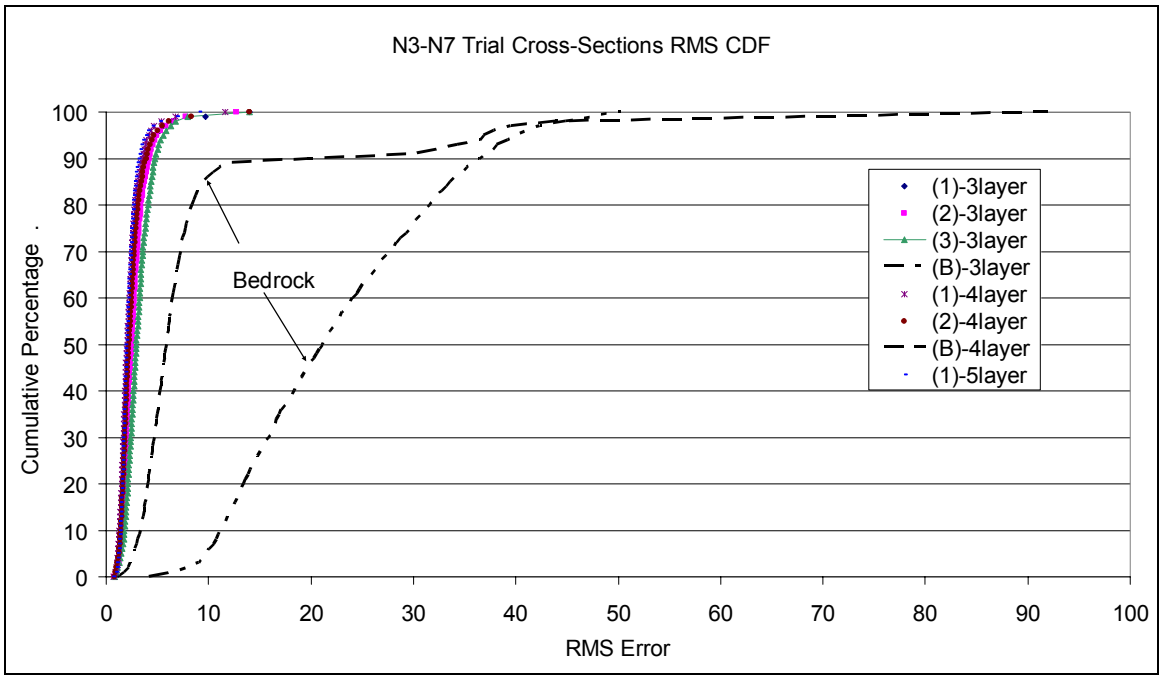


**Figure 5.21 RMS Error Cumulative Distribution Functions (CDF) for the Trial Backcalculation Cross-Sections in Sections N3-N7.**

The next step was to analyze the 4-layer and 5-layer cross-sections to see if any exhibited stable solutions with reasonable modulus behavior. It was determined to begin the analysis with these sections since neither the 4-layer or 5-layer solutions were able to produce a reasonable backcalculation solution for sections N1 and N2. Table 5.3 shows an example of an output summary file from the backcalculation software for the FWD testing at one station on one day using the (1)-5layer cross-section. This figure shows that the solution generated by the 5-layer cross-section is unreasonable. Table 5.3 shows how the 5-layer solution is unable to distinguish the fill layer (layers 3 and 4) from the subgrade layer since the moduli of these layers (E3 and E4) consistently spike on the upper iteration boundary of 80 ksi. Therefore, the 5-layer cross-section was eliminated from consideration.

**Table 5.3 (1)-5layer Cross-Section Modulus Behavior (Station N4-12, 08/20/07)**

| LOAD (LB) | E1(KSI) | E2(KSI) | E3(KSI) | E4(KSI) | E5(KSI) | Error (%) |
|---|---|---|---|---|---|---|
| 5489 | 172.3 | 2.1 | 80 | 46.2 | 27.1 | 2.76 |
| 5537 | 177 | 2.1 | 80 | 26.9 | 28.6 | 2.52 |
| 5553 | 177.6 | 1.9 | 80 | 69.3 | 27.7 | 2.53 |
| 8412 | 187.7 | 1.5 | 80 | 80 | 26.7 | 2.51 |
| 8433 | 189.3 | 1.5 | 80 | 80 | 26.1 | 2.47 |
| 8444 | 189.1 | 1.5 | 80 | 80 | 25.8 | 2.35 |
| 11860 | 192.3 | 1.4 | 80 | 80 | 23.9 | 2.44 |
| 11860 | 197 | 1.3 | 80 | 80 | 24.5 | 2.22 |
| 11900 | 195.7 | 1.4 | 80 | 80 | 24.2 | 2.33 |
| 15797 | 211.6 | 1.3 | 80 | 80 | 23.4 | 2.05 |
| 15816 | 211.9 | 1.3 | 80 | 80 | 23.5 | 2.07 |
| 15829 | 212.1 | 1.3 | 80 | 68.5 | 23.5 | 2.11 |

Figure 5.22 shows the modulus behavior of the fill layer (layer 3) for the (2)-4layer cross-section for the drop locations on the inside wheelpath (IWP) for sections N3-N7. This figure only summarizes the data from the 9,000 lb FWD loadings to eliminate load variability. The data from the inside wheelpath are shown to eliminate spatial variability between the wheelpaths and to pare down the data set. This figure illustrates the unstable and unreasonable solution generated by the (2)-4layer cross-section. There are several drop locations that spike on the upper iteration limit of 80 ksi. There are also several drops which have very large standard deviations, indicating solution instability between subsequent drops at the same location and same load level. The average moduli values also vary greatly between subsequent testing locations. Similar behavior was witnessed for the (1)-4layer cross-section. Given the erratic solution behavior, the 4-layer trial cross-sections were eliminated from consideration.

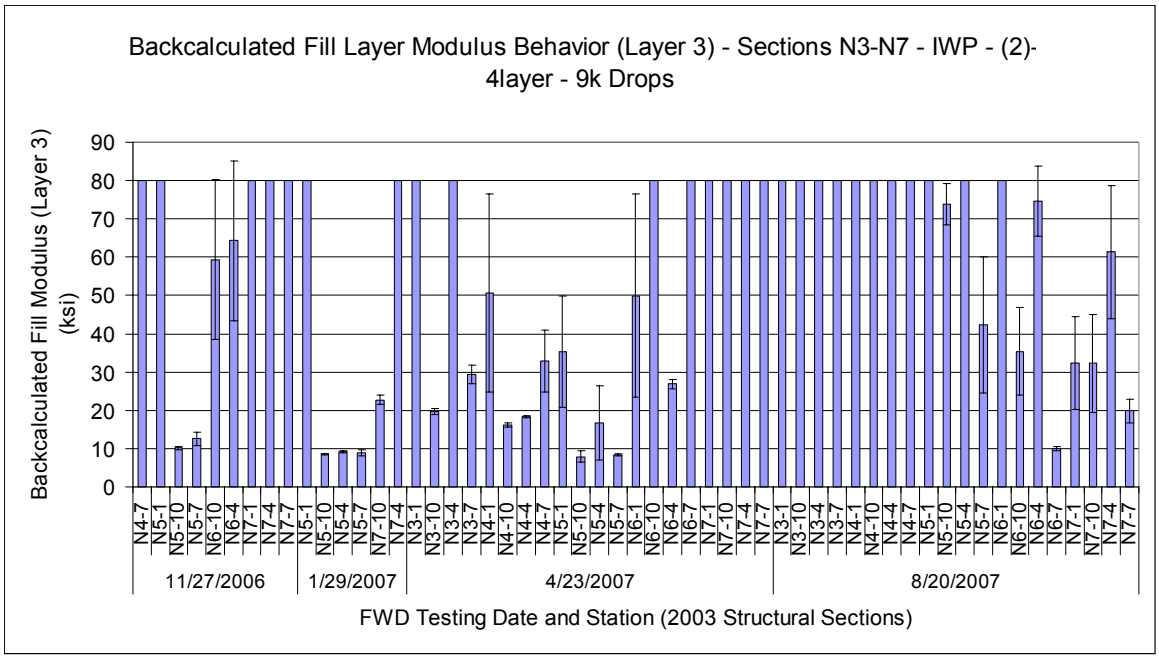


**Figure 5.22 Fill Layer Modulus Behavior (Layer 3) (Section N3-N7, IWP Testing Stations, All Dates, 9 kip drops, (2)-4layer).**

With the 4-layer, 5-layer, and bedrock cross-sections eliminated from consideration, the next task was to better analyze the 3-layer cross-sections. Figure 5.23 shows a CDF of the RMS error values generated from the summary files of each of the 3-layer trial cross-sections for sections N3-N7. From this figure, the (1)-3layer cross-section appears to have the most optimal RMS error distribution. This distribution is to the left of the distribution generated by the other two cross-sections, and has the highest percentage of drops (90%) with an RMS error lower than the cut-off value of 4%. The (2)-3layer cross-section also performs well, with approximately 89% of drops with an RMS error below 4%. The (3)-3layer cross-section appears to have a higher RMS error than the other two sections, with its CDF being to the right of the other two and with a lower percentage of drops (79%) below the RMS error cut-off.

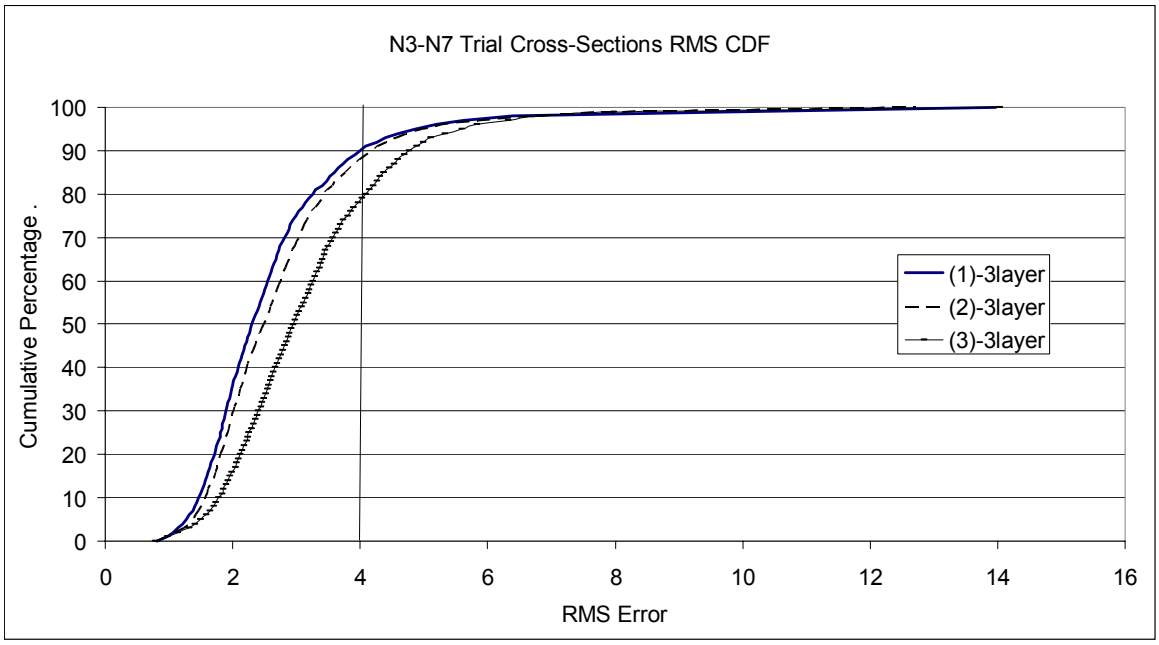


**Figure 5.23 RMS Error Cumulative Distribution Functions (CDF) for the 3-Layer Trial Backcalculation Cross-Sections in Sections N3-N7.**

With the (3)-3layer cross-sections showing the highest RMS error, it was eliminated from consideration (provided the other two cross-sections generated reasonable backcalculation solutions). Therefore, the decision process was reduced to deciding between the (1)-3layer cross-section and the (2)-3layer cross-section. Again, the (1)-3layer cross-section would be preferable since it allows for the independent characterization of the granite base. The (2)-3layer cross-section combines this granite base with the Track fill compacted for the 2003 research cycle. For a more in-depth comparison of the cross-sections, their modulus values and measured versus predicted strain responses were then analyzed.

Next, the modulus behavior of the unbound layers from the backcalculation solutions using the two different cross-sections was analyzed to determine whether they behaved in a stable and reasonable manner. For Sections N3 through N7, Figures 5.24 and 5.25 show the average and standard deviations of the backcalculated base layer moduli for cross-sections (1)-3layer and (2)-3layer, respectively. The moduli shown are calculated from the 9,000 lb FWD loadings for each testing station located in the inside wheelpath (IWP) on each testing date.

Several things are evident from analyzing the base layer behavior from the two different cross-sections. First the backcalculated moduli from the (2)-3layer cross-section are significantly higher than those from the (1)-3layer cross-section. Again, this is expected since the base layer composition of the (2)-3layer cross-section contains the Track fill material as well as the granite base. Secondly, there appears to be a large amount of variation between testing stations on each date. This variability could potentially be indicative of a poor backcalculation solution. For example, there is a large jump between

the backcalculated moduli for stations N6-4 and N7-1 on 11/27/2006. However, these stations are in different test sections, owing to the possibility of construction or trafficking variability causing a differential in the stiffness of the material. Also, this jump is evident regardless of cross-section utilized, meaning that this variability is inherent to the material rather than an artifact of the backcalculation solution. Finally, since the standard deviations at each drop location are relatively small for each solution, there does not appear to be significant modulus variability within each testing location. This is further evidence that the base moduli for each solution behave in a stable manner.

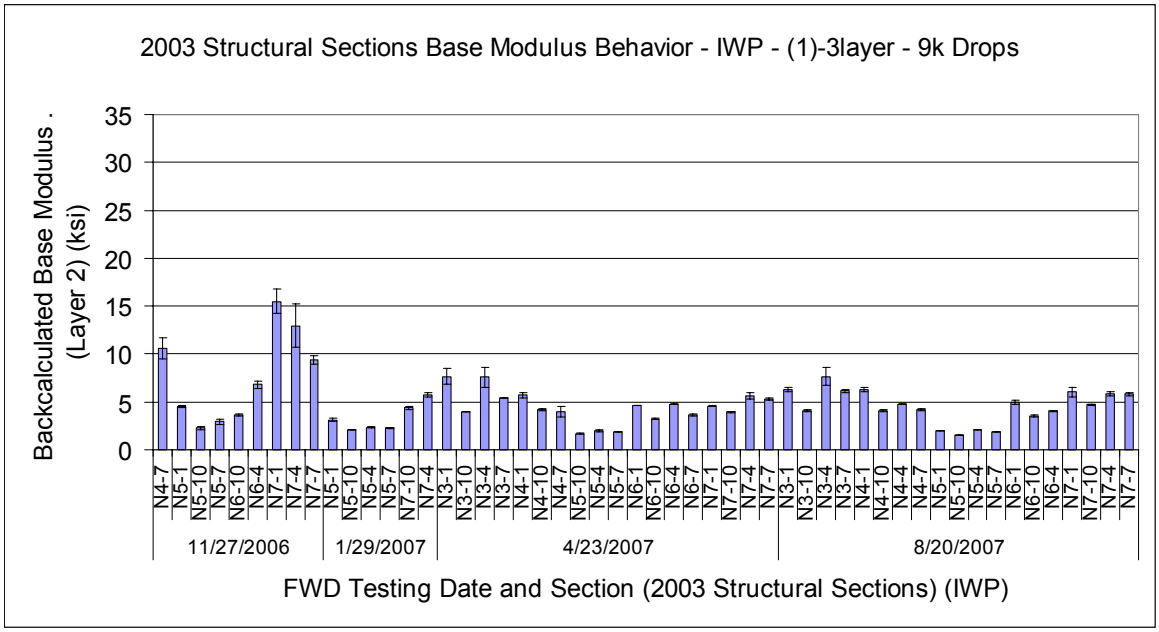


**Figure 5.24 Base Layer Modulus Behavior (Layer 2) (Sections N3-N7, (1)-3layer, All Testing Dates, All IWP Testing Locations, 9 kip drops).**

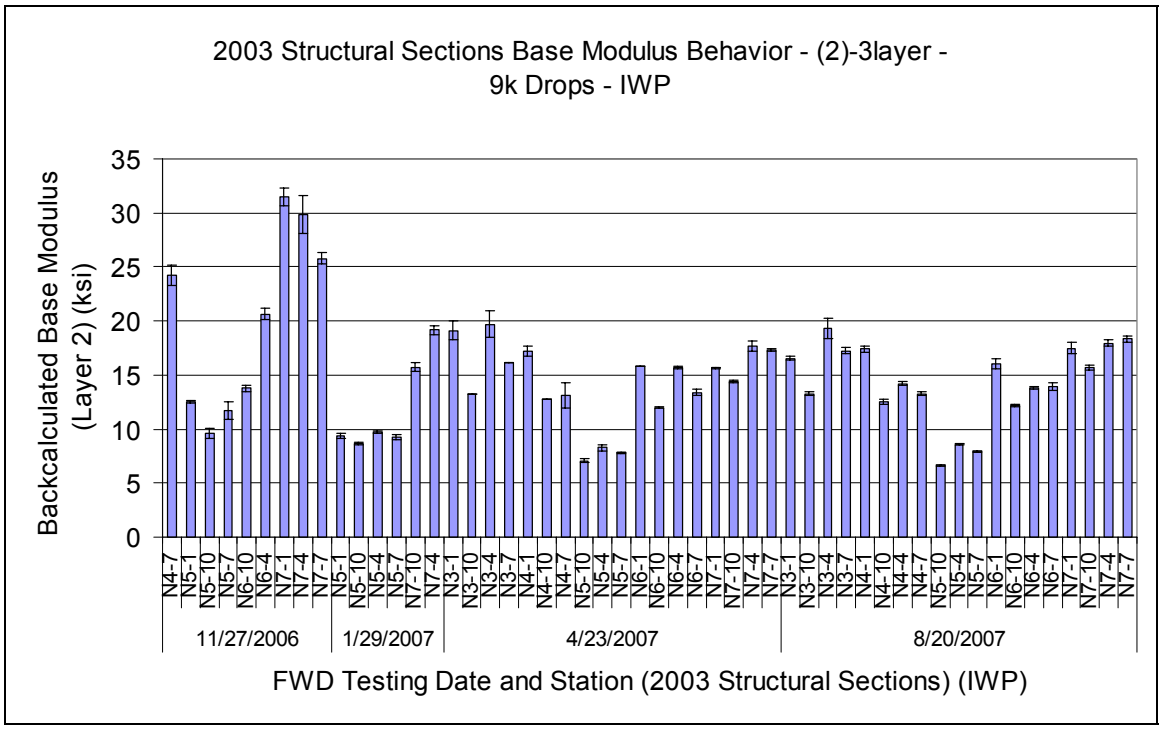


**Figure 5.25 Base Layer Modulus Behavior (Layer 2) (Sections N3-N7, (2)-3layer, All Testing Dates, All IWP Testing Locations, 9 kip drops).**

For Sections N3 through N7, Figures 5.26 and 5.27 show the average and standard deviations of the backcalculated subgrade layer moduli for cross-sections (1)-3layer and (2)-3layer, respectively. The moduli shown are calculated from the 9,000 lb FWD loadings for each testing station located in the inside wheelpath (IWP) on each testing date. The data from these figures seem to indicate a stable and reasonable backcalculation solution regardless of cross-section utilized. Both figures show minimal variation in the backcalculated moduli at each testing station. These figures also show the backcalculated moduli to be very similar at each testing station regardless of cross-section used.

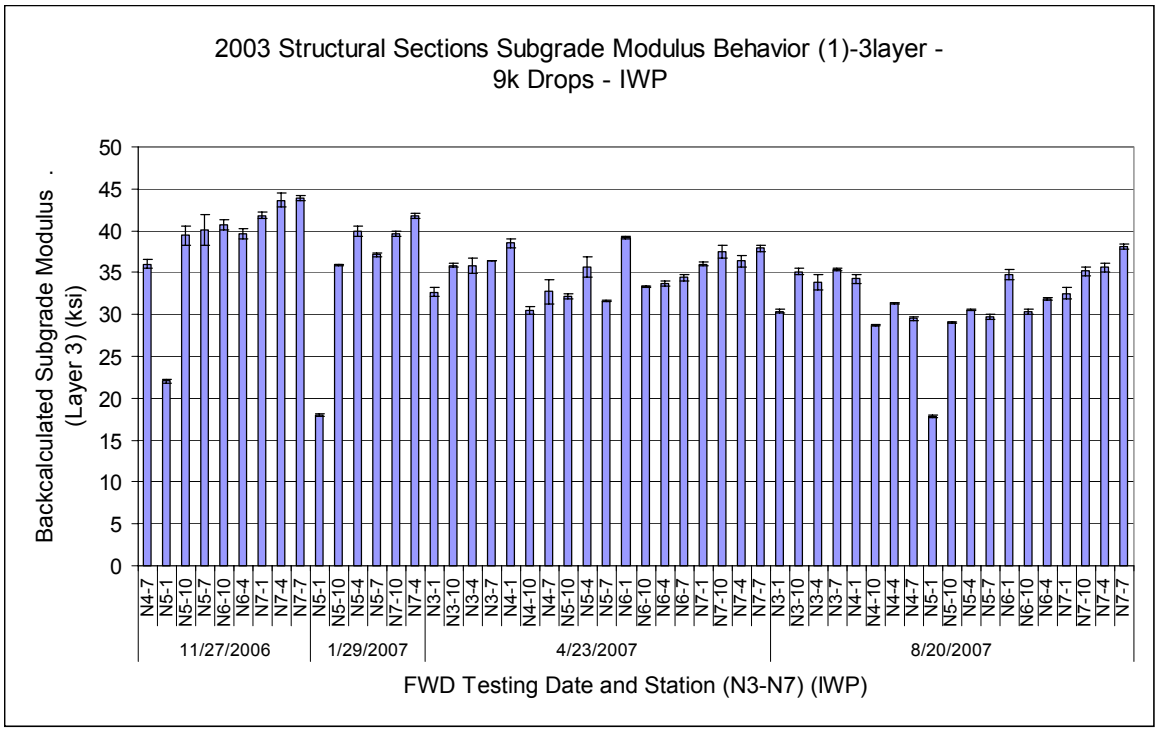


**Figure 5.26 Subgrade Layer Modulus Behavior (Layer 3) (Sections N3-N7, (1)-3layer, All Testing Dates, All IWP Testing Locations, 9 kip drops).**

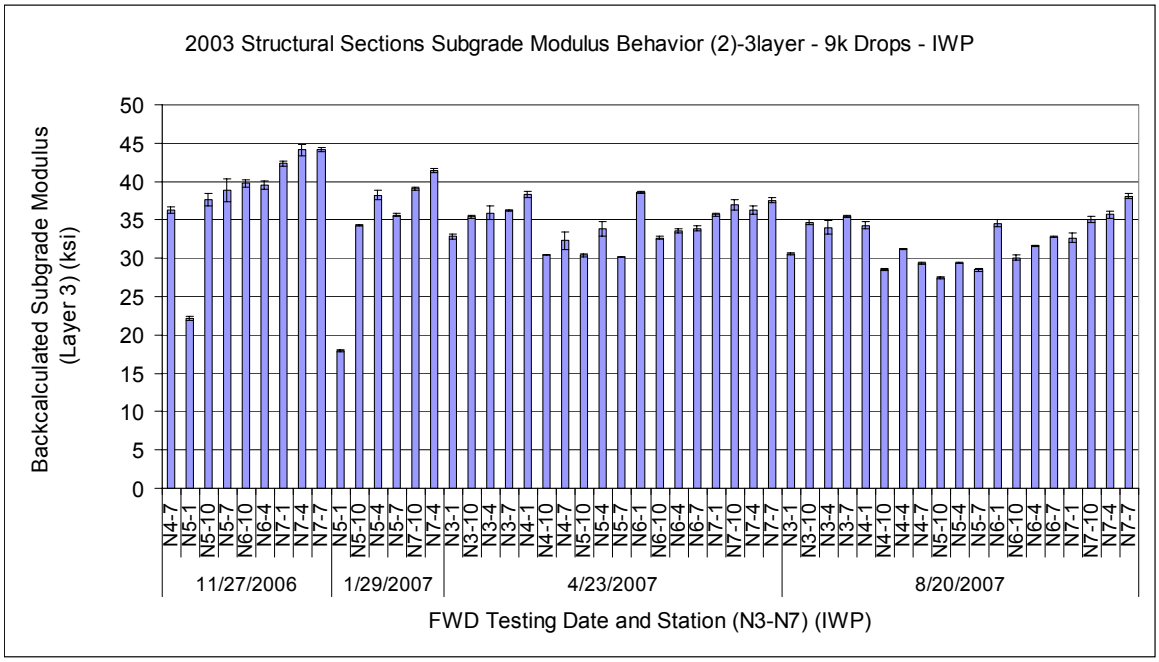


**Figure 5.27 Subgrade Layer Modulus Behavior (Layer 3) (Sections N3-N7, (2)-3layer, All Testing Dates, All IWP Testing Locations, 9 kip drops).**

Figure 5.28 is a summary plot used to compare the backcalculated modulus values in sections N3 through N7 using the trial cross-sections (1)-3layer and (2)-3layer. Each data

point on this plot represents a comparison between the backcalculated modulus for a given pavement layer at a specific testing location using the two different cross-sections. Only the 9,000 lb drops were utilized to eliminate loading variability, but the plot includes data points from each testing station within sections N3 through N7. The results of this analysis show that the difference in cross-section has the most significant impact on the backcalculated base moduli. The base moduli for the (2)-3layer cross-section are significantly higher than those for the (1)-3layer cross-section. However, the difference in cross-section has virtually no impact on the backcalculated HMA and subgrade moduli, as each of these data sets fall on the line of unity in Figure 5.28. This is not surprising since the HMA constitutes one continuous layer in each of the cross-sections, and each structural section has both fill and deep subgrade constructed with the Track material.

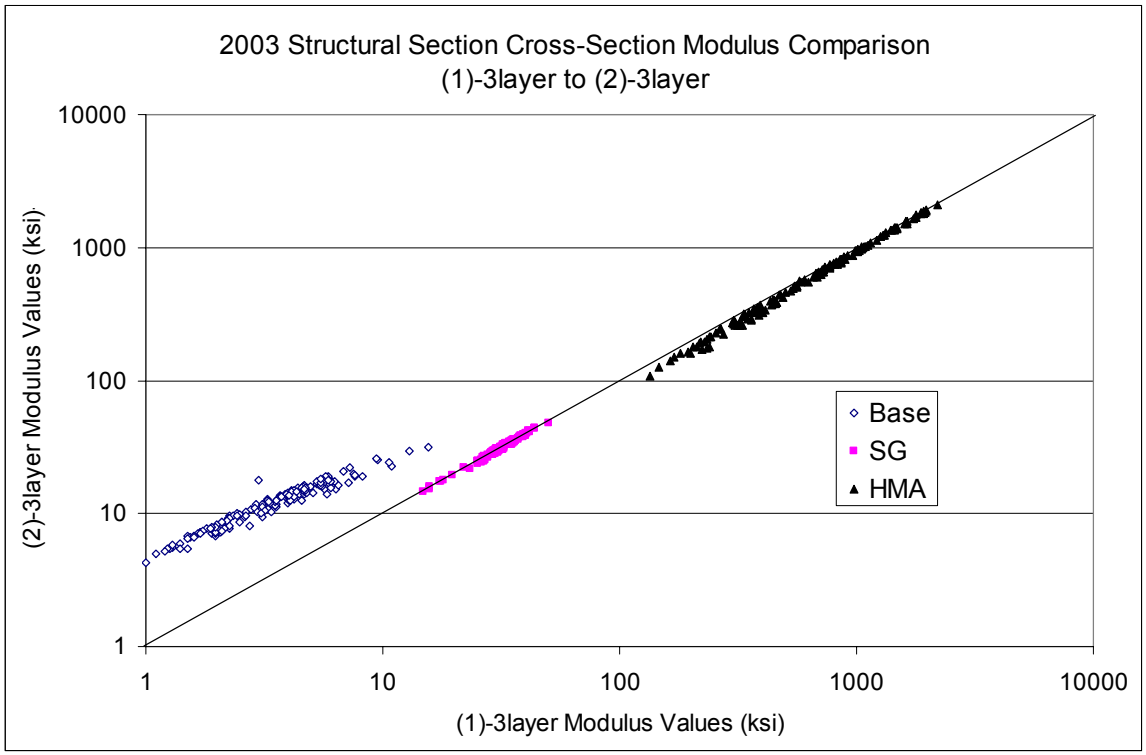


**Figure 5.28 Backcalculated Modulus Comparison between Trial Cross-Sections (1)-3layer and (2)-3layer – Sections N3 through N7 – All Layers.**

The next means of comparing these trial backcalculation cross-sections was to compare the measured pavement strains and predicted (theoretical) pavement strains generated during the FWD on gauge testing. Figures 5.29 and 5.30 show the measured versus predicted pavement strains in sections N3 through N7 for the (1)-3layer and (2)-3layer cross-sections, respectively. Each data series in these plots represent a sequence of FWD loadings on the strain gauges within each of the structural sections. This analysis shows the data from sections N3 and N4 fell closer to the line of unity than the data from sections N6 and N7. This was expected since sections N3 and N4 are thicker pavement sections that have not experienced the levels of pavement distress witnessed by sections

N6 and N7. Additionally, the results of this analysis show that there is little appreciable difference between the data sets for the different structural sections regardless of cross-section utilized. For example, the slope and $R^2$ of the data set for section N3 are 0.8191 and 0.9931, respectively, using the (1)-3layer cross-section. The slope and $R^2$ of the data set change to 0.8247 and 0.9915, respectively, when the (2)-3layer cross-section is utilized. Therefore, these cross-sections exhibit almost identical behavior in comparing measured versus predicted strains.

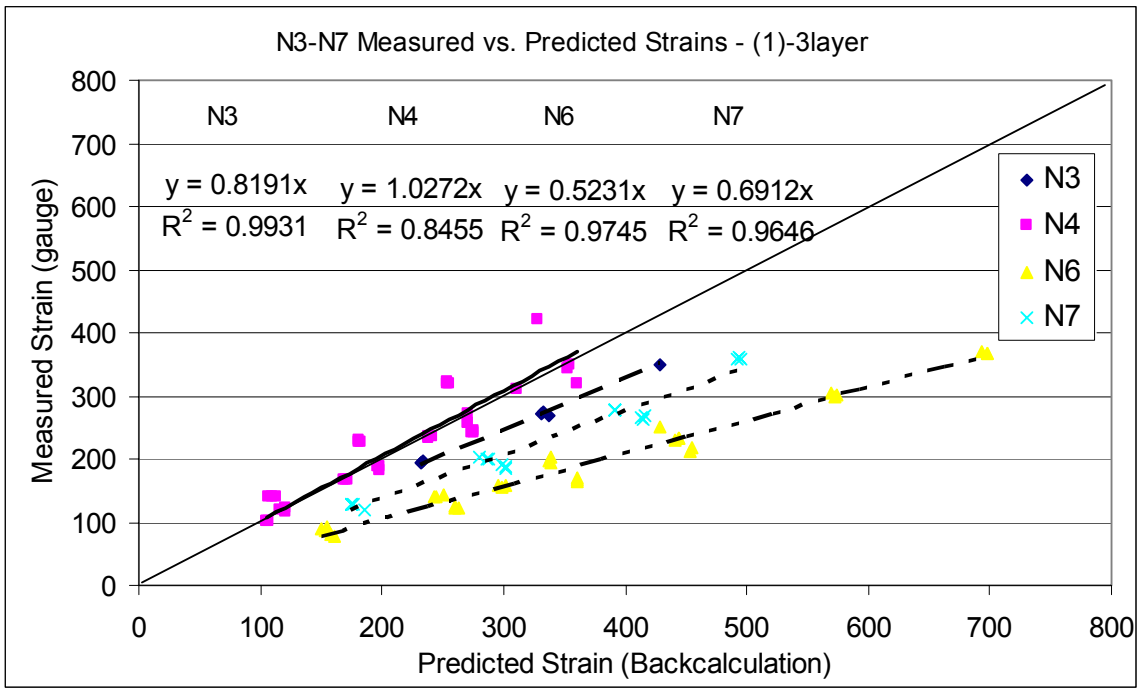


**Figure 5.29 Measured versus Predicted Strains for Sections N3-N7 – (1)-3layer.**

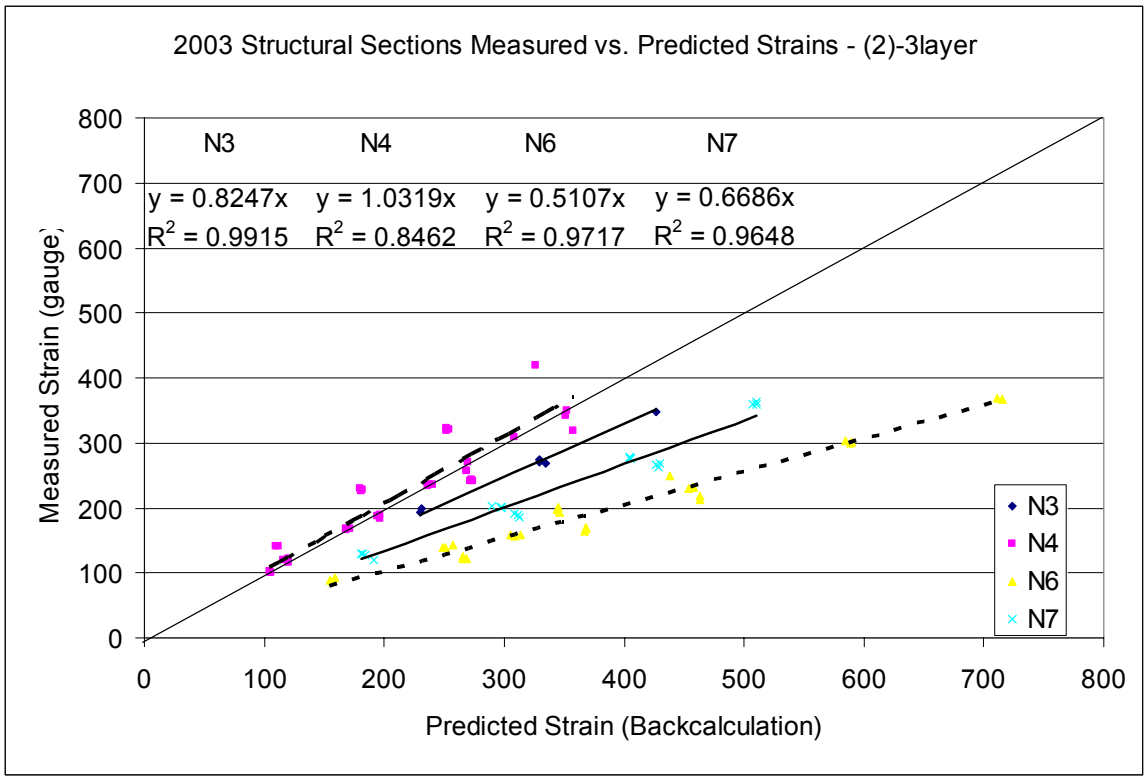


**Figure 5.30 Measured versus Predicted Strains for Sections N3-N7 – (2)-3layer.**

In comparing the trial cross-sections (1)-3layer and (2)-3layer for use in backcalculation of the deflection data from the 2003 structural sections (N3-N7), it was determined that the (1)-3layer cross-section exhibits slightly better RMS error performance than the (2)-3layer cross-section. Both cross-sections exhibit stable backcalculation solutions and reasonable measured versus theoretical strain responses. No appreciable differences could be determined in the measured versus theoretical strain responses by using the two different cross-sections. Therefore, since the (1)-3layer cross-section exhibited the best RMS error behavior and allowed for the isolation of the granite base for characterization, the (1)-3layer cross-section was selected for analysis.

Finally, the measured versus predicted pressures at the surface of the base and fill layers were analyzed for the (1)-3layer cross-section as a final validation check. Figure 5.31 shows the measured versus predicted base pressure responses and Figure 5.32 shows the measured versus predicted fill pressure responses. Much of these data were unavailable due to many of the pressure plates in these sections being off-line. The remainder of the unavailable data points are due to the data not passing the RMS filtering criteria. Figure 5.31 show that slope of the data set is approximately 50% above the line of unity (with measured pressures being higher than the theoretical pressures). Figure 5.32 shows good agreement between measured and theoretical fill pressures, with the slope of both data sets from N3 and N4 falling within 10% of the line of unity (with theoretical pressures being higher than the measured pressures). These results are favorable and consistent with the data from N1 and N2 plus the data from the 2003 research cycle. Thus, the

backcalculation solution from the 2003 structural sections using the (1)-3layer cross-section appear to behave reasonably and this cross-section was deemed suitable for analyses concerning these structural sections.

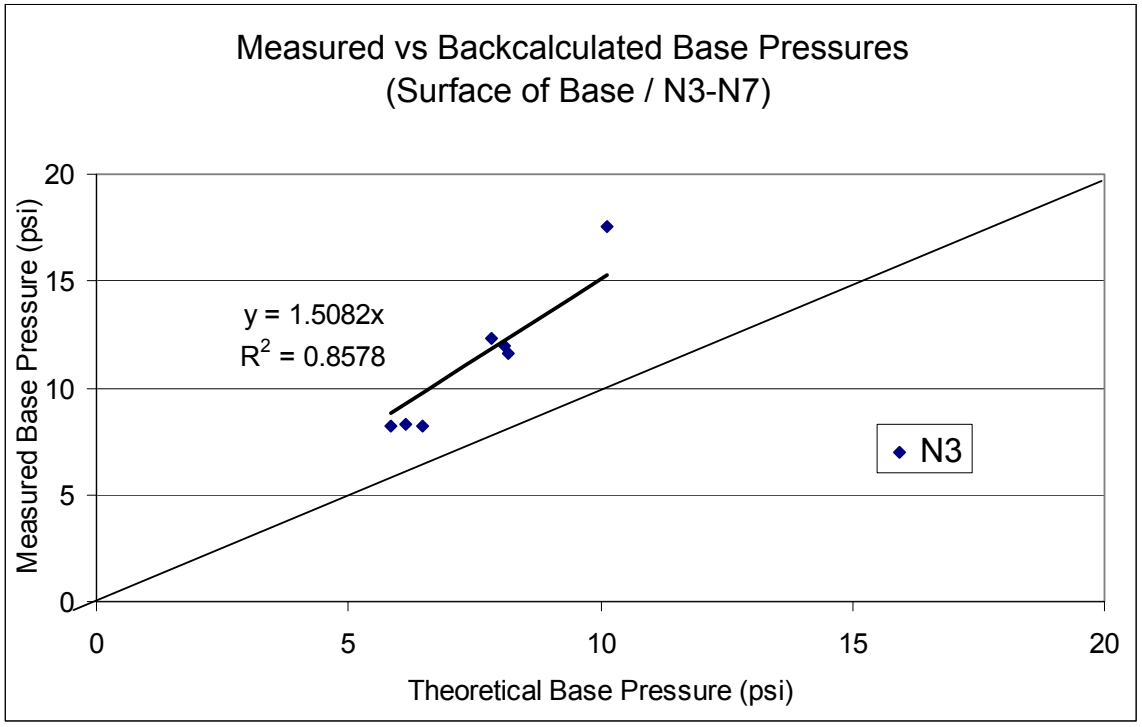


**Figure 5.31 Measured versus Predicted Base Pressures for Sections N3-N7 – (1)-3layer.**

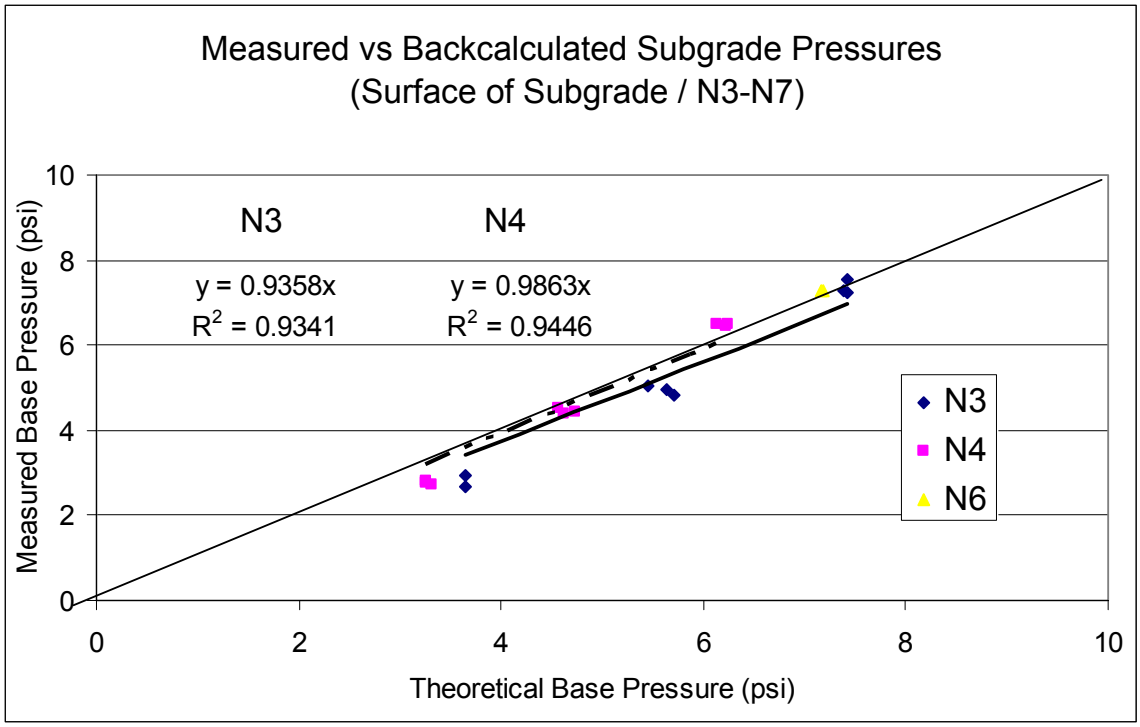


**Figure 5.32 Measured versus Predicted Fill Pressures for Sections N3-N7 – (1)-3layer.**

**N8-N9 CROSS-SECTION INVESTIGATION**

Sections N8 and N9 are the thickest pavement sections, in terms of HMA, available for the 2006 structural experiment and were constructed in a very similar manner. Each section consists of HMA (between 10 and 14 inches) constructed atop 6 to 8 inches of Track soil material compacted as a base layer. Below the Track soil base is approximately 40 inches of a soft subgrade material (Seale clay) above a deep subgrade embankment of the Track soil material. The only appreciable difference in the sections is that N9 has an additional 4 inches of HMA and 2 inches of Track soil base. Given these similarities, sections N8 and N9 were combined for the purpose of analyses determining the optimal backcalculation cross-section for each section.

Through analysis of layer composition and construction information (See Figure 5.3 and Chapter 3), a set of trial backcalculation cross-sections was developed for N8 and N9. These cross-sections are shown in Figure 5.33. Trial cross-sections were developed with between 3 and 5 different layers for backcalculation in addition to two sections including a stiff layer for analysis. The cross-section that most closely approximates the field conditions is the (1)-4layer cross-section, showing the Track soil base and Seale subgrade as separate layers. The (1)-5layer cross-section divides the thick Seale subgrade layer in half for the purposes of backcalculation. The 3-layer sections combine the Seale subgrade with the Track soil base and the Track subgrade. The investigations from the other structural sections to this point indicate that one of the 3-layer systems is most likely the best solution. However, the 4-layer cross-section would be optimal for

selection since it allows independent characterization of both Track soil layers and the Seale subgrade. The numbering and naming scheme remains consistent with what has been explained for the investigations regarding the other structural sections.

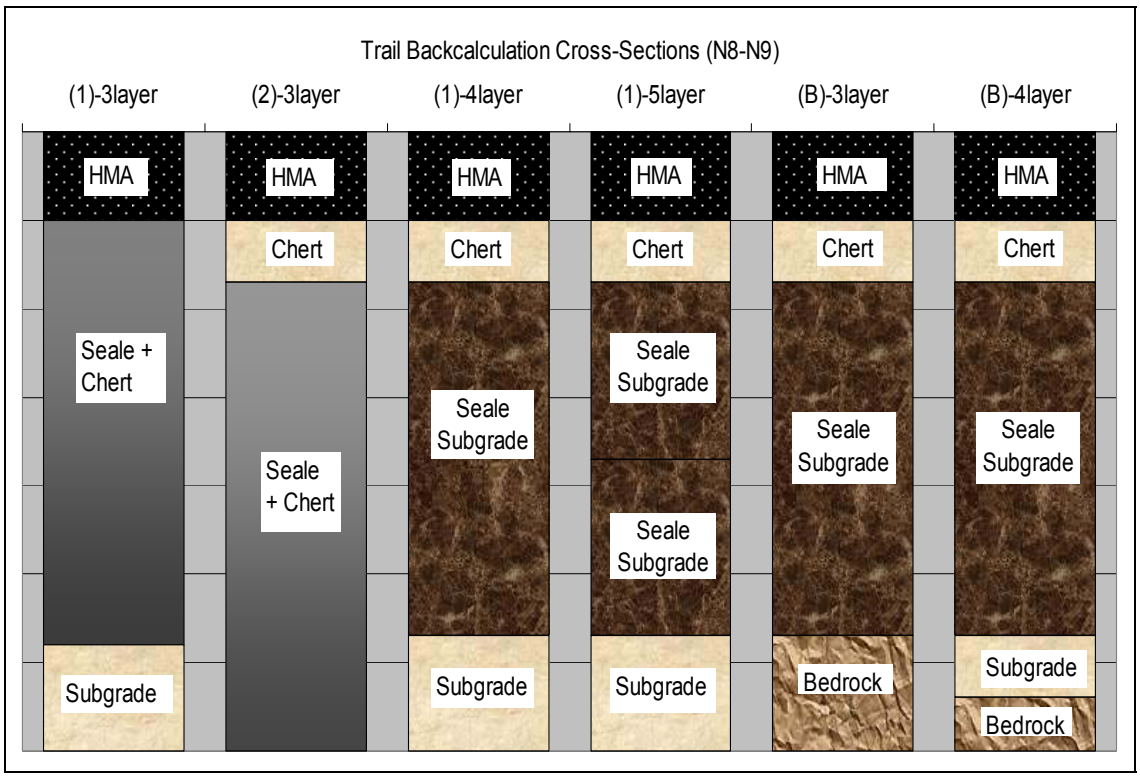


**Figure 5.33 Trial Backcalculation Cross-Sections for Sections N8 and N9.**

The first step in the investigation was to analyze the RMS error values generated by using each of the individual cross-sections. Figure 5.34 shows the various RMS Error CDFs for each of the trial backcalculation cross-sections. The results of this analysis are consistent with the investigations conducted for the previous sections in that the two cross-sections with bedrock generate solutions with very high RMS error values. There do not appear to be any stiff layer effects on the backcalculation for this section of the track. As such, the bedrock cross-sections were eliminated from consideration. The remainder of the cross-sections seem to have very similar RMS error CDFs, with the exception of the (1)-3layer cross-section (which is further to the right than the other non-bedrock CDFs).

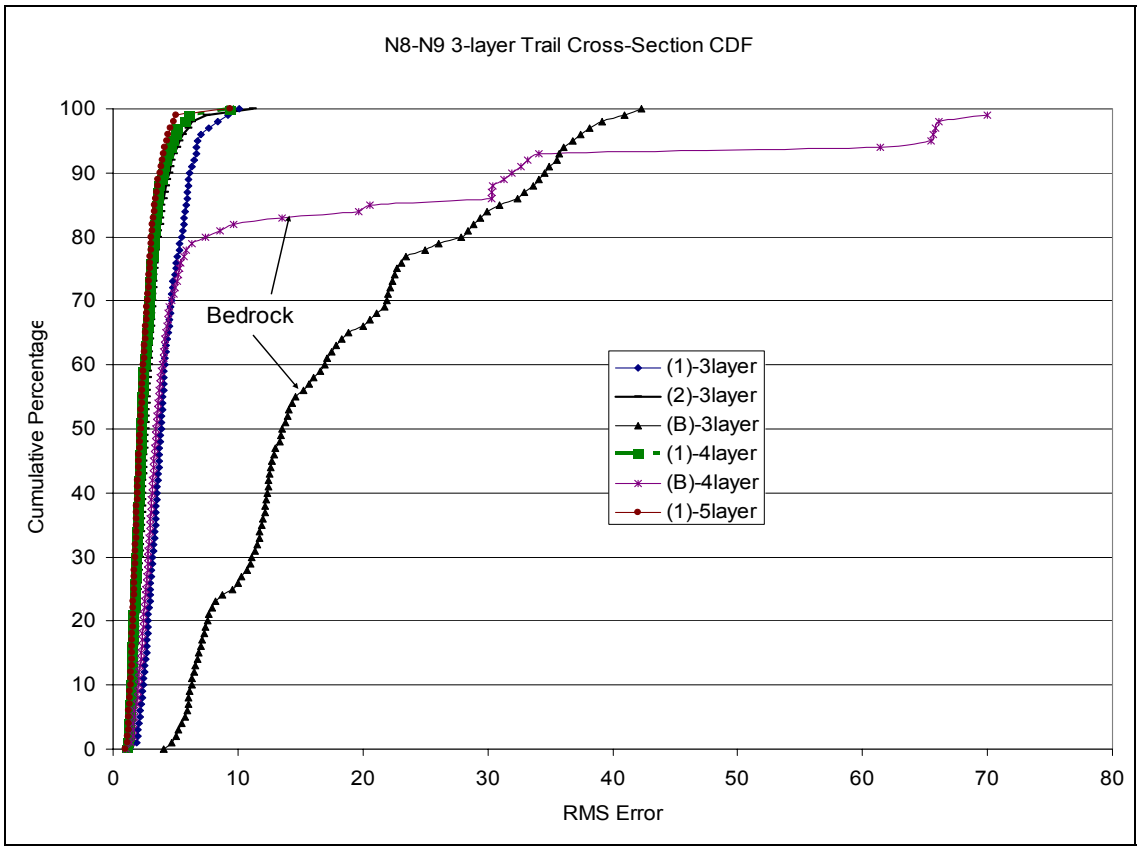


**Figure 5.34 RMS Error Cumulative Distribution Functions (CDF) for the Trial Backcalculation Cross-Sections in Sections N8-N9.**

The results of the previous section investigations showed instabilities and unreasonable modulus values when 4-layer and 5-layer backcalculation cross-sections were utilized. This was most likely due to the software being unable to distinguish the fill layer from the deep subgrade since they consisted of the same material. Upon analyzing the (1)-5layer summary data, it seemed evident this effect was also occurring having two Seale layers bordering each other. Table 5.4 shows the modulus behavior from one testing location (Station N8-8) on 4/23/07. These data show that while the solution has excellent error with reasonable HMA, base layer, and deep subgrade moduli, it appears that the moduli of the third and fourth layers (the divided Seale subgrade) are again compensating for one another. For the same material, the modulus of the third layer is consistently at the upper iteration limit of 80 ksi while the modulus of the fourth layer fluctuates greatly. Therefore, the (1)-5layer cross-section was eliminated from consideration due to it providing an unreasonable solution.

**Table 5.4 (1)-5layer Cross-Section Modulus Behavior (Station N8-8, 04/23/07)**

| LOAD (LB) | E1 (KSI) | E2 (KSI) | E3 (KSI) | E4 (KSI) | E5 (KSI) | Error (%) |
|---|---|---|---|---|---|---|
| 5494 | 417.4 | 2.5 | 80 | 70.5 | 33.9 | 2.2 |
| 5513 | 361.1 | 3.4 | 80 | 31.5 | 34.2 | 2.5 |
| 5542 | 421.6 | 2.6 | 80 | 50.8 | 34.8 | 2.21 |
| 8512 | 380.9 | 2.3 | 80 | 80 | 31.6 | 1.58 |
| 8520 | 387.9 | 2.3 | 80 | 80 | 31.5 | 1.68 |
| 8520 | 365.3 | 2.7 | 80 | 42 | 31.9 | 1.68 |
| 12027 | 371.1 | 2.2 | 80 | 80 | 30 | 1.35 |
| 12055 | 360.8 | 2.5 | 80 | 43 | 30.6 | 1.36 |
| 12066 | 343.1 | 2.8 | 80 | 33.3 | 30.5 | 1.41 |
| 16075 | 352.8 | 2.6 | 80 | 37.7 | 29.6 | 1.22 |
| 16086 | 355.7 | 2.5 | 80 | 40.3 | 29 | 1.12 |
| 16091 | 350 | 2.7 | 80 | 33.3 | 29.3 | 1.15 |

The (1)-4layer trial cross-section for N8 and N9 was the cross-section that most closely approximated the actual material composition of these structural sections. However, upon analyzing the behavior of the backcalculated Seale subgrade modulus values, the solution generated by this cross-section was deemed to be unreasonable. Figure 5.35 illustrates the average backcalculated Seale subgrade moduli for the different testing stations and dates using the (1)-4layer cross-section. These moduli represent only those backcalculated from the 9,000 lb drops to eliminate loading variability in the modulus values. This figure clearly shows highly erratic behavior of the Seale subgrade moduli, with several of the moduli reaching the upper iteration limit of 80 ksi. Though this cross-section would have been ideal from a materials characterization standpoint, it failed to generate a reasonable solution and was subsequently eliminated from consideration.

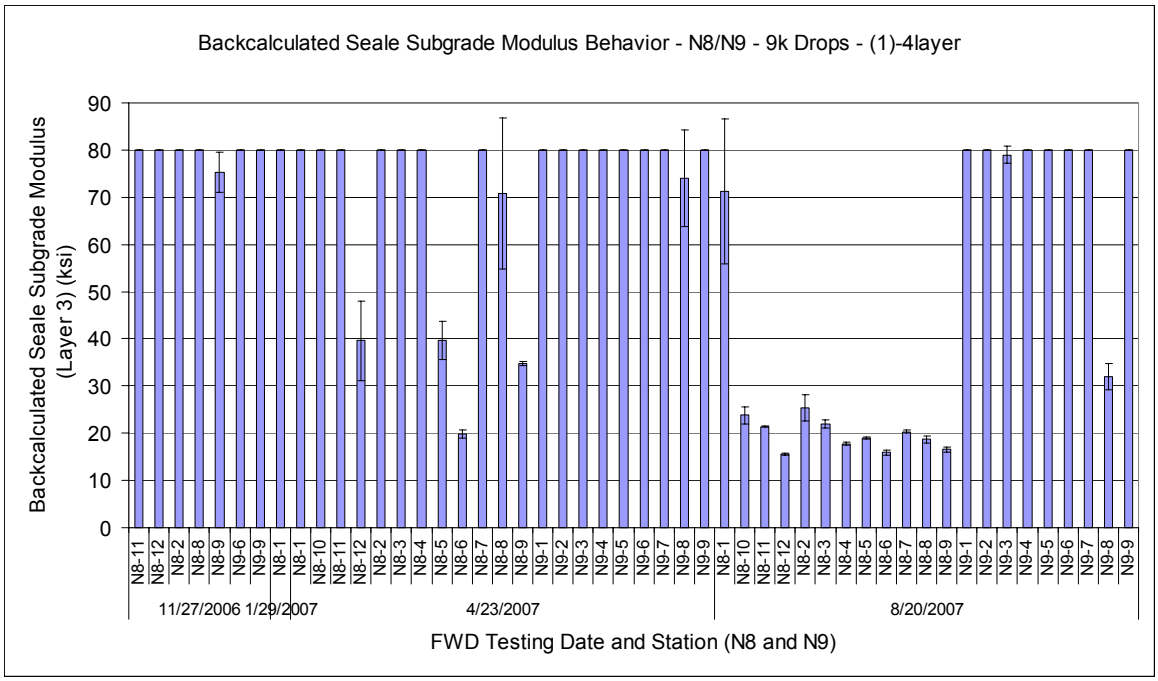


**Figure 5.35 Seale Layer Modulus Behavior (Layer 3) (Sections N8-N9, All FWD Testing Stations and Dates, 9 kip drops, (1)-4layer).**

The next step was to analyze the results generated by the 3-layer cross-sections and determine if either of them were viable for analysis. Figure 5.36 shows the RMS error CDFs for both of the 3-layer cross-sections. This diagram shows a clear separation between the cross-sections. The (2)-3layer cross-section RMS error CDF is significantly to the left of that of the (1)-3layer cross-section. The (2)-3layer cross-section also has a much larger percentage of drops falling under the RMS error cut-off of 4% (85 percent for the (2)-3layer cross-section versus 55 percent for the (1)-3layer cross-section). Given the large differential between the two RMS error CDFs, the (2)-3layer cross-section (combining the Seale subgrade and Track soil subgrade) has a significant advantage over the (1)-3layer cross-section (combining the Track soil base and Seale subgrade).

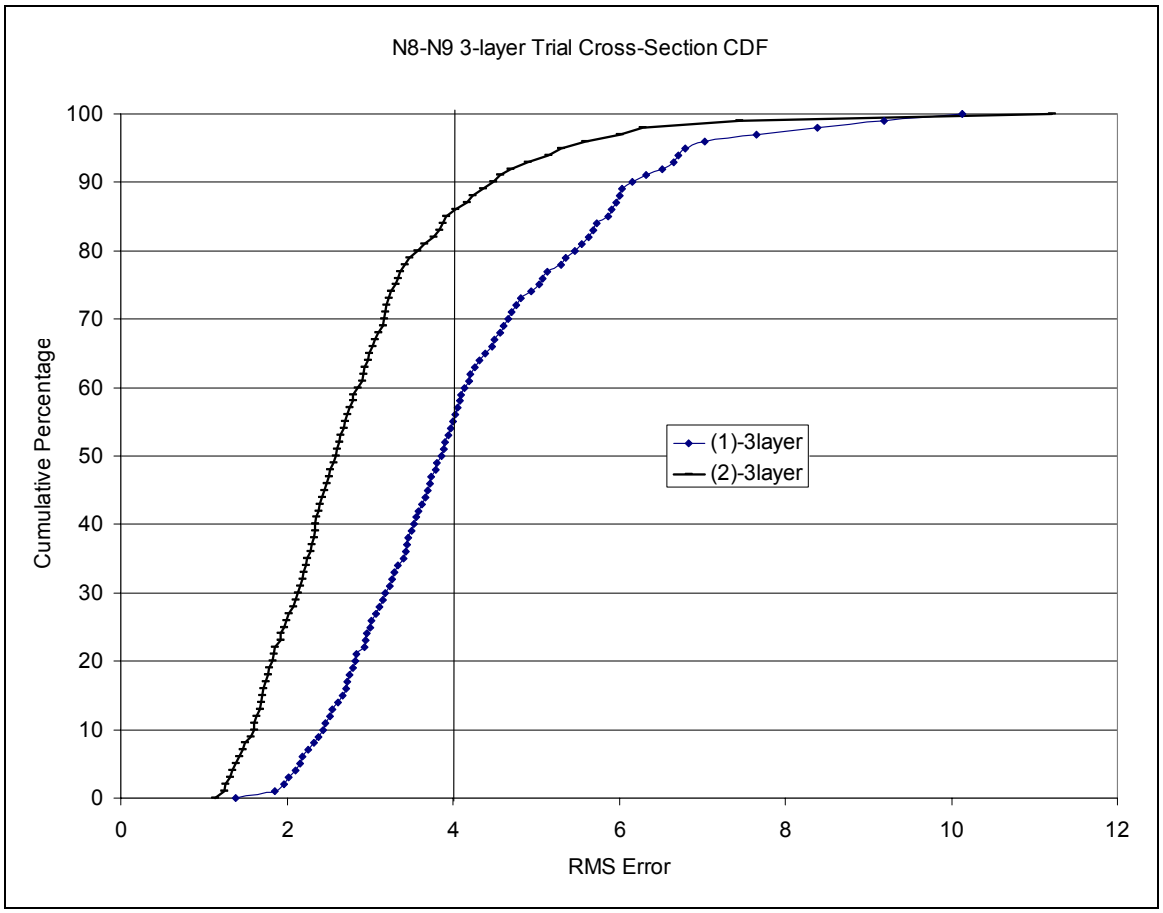


**Figure 5.36 RMS Error Cumulative Distribution Functions (CDF) for the 3-Layer Trial Backcalculation Cross-Sections in Sections N8 and N9.**

The next phase of the investigation involved analyzing the backcalculated moduli generated by the 3-layer solutions to determine whether they were stable and reasonable. For Sections N8 and N9, Figures 5.37 and 5.38 show the average and standard deviations of the backcalculated base layer moduli for cross-sections (2)-3layer and (1)-3layer, respectively. The moduli shown are calculated from the 9,000 lb FWD loadings for every testing station on each testing date. Comparing Figures 5.37 and 5.38 shows that whether the base layer contains the Seale material has a major impact on the backcalculated moduli. For the Track soil base, the majority of modulus values fall between 3 and 5 ksi. When this base is combined with the Seale material, the majority moduli increase to between 15 and 20 ksi. A reasonable amount of spatial variability can be seen in both solutions, but the effect is more noticeable in the (1)-3layer cross-section since the magnitude of the modulus values is much greater. Both cross-sections seem to exhibit reasonable base layer moduli with relatively stable average moduli station to station and minimal standard deviations in the moduli within each testing station.

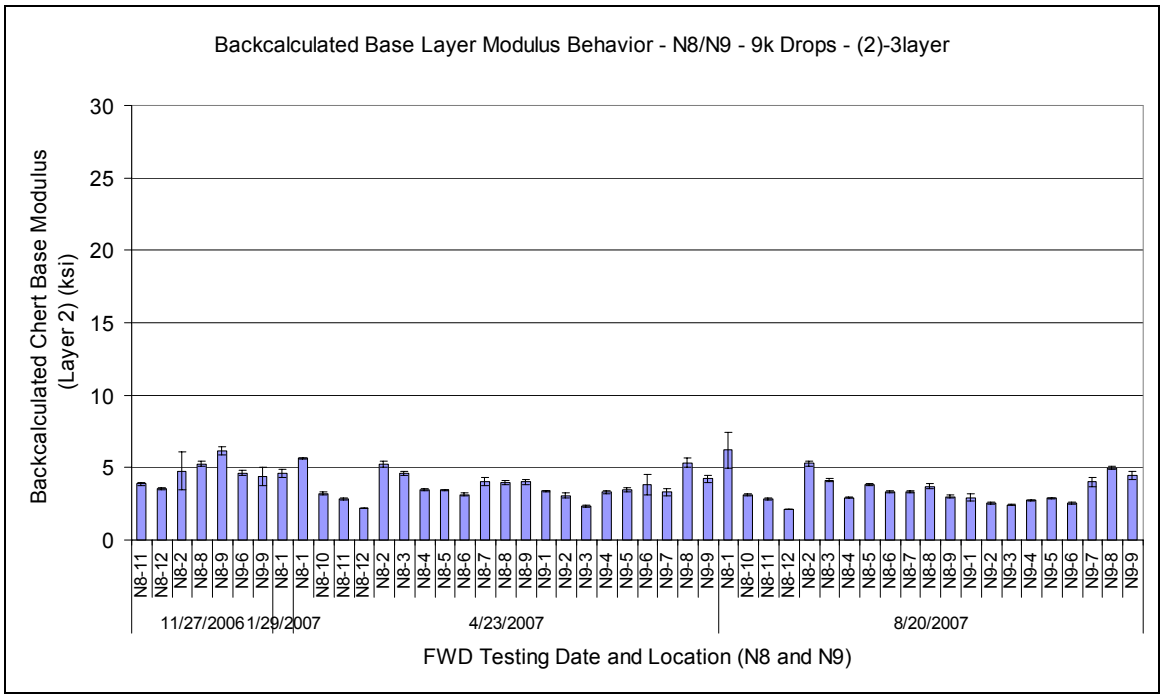


**Figure 5.37 Base Layer Modulus Behavior (Layer 2) (Sections N8 and N9, (2)-3layer, All Testing Dates, All Testing Locations, 9 kip drops).**

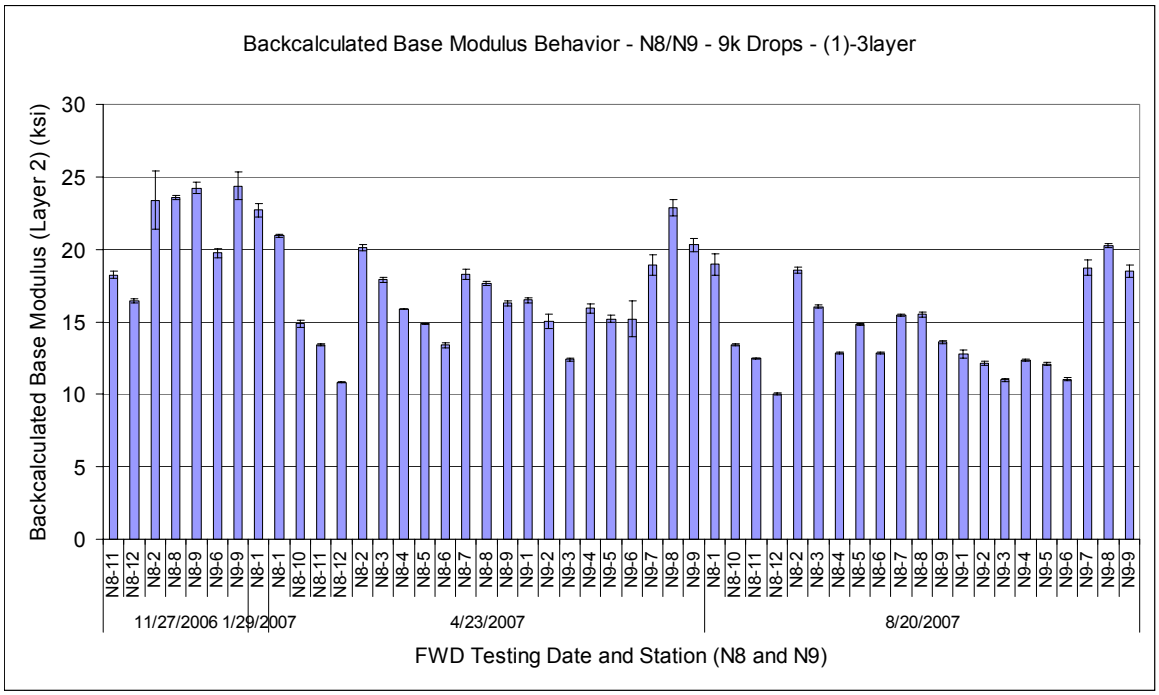


**Figure 5.38 Base Layer Modulus Behavior (Layer 2) (Sections N8 and N9, (1)-3layer, All Testing Dates, All Testing Locations, 9 kip drops).**

For Sections N8 and N9, Figures 5.39 and 5.40 show the average and standard deviations of the backcalculated subgrade layer moduli for cross-sections (2)-3layer and (1)-3layer,

respectively. The moduli shown are calculated from the 9,000 lb FWD loadings for each testing station on each testing date. The subgrade modulus values again appear to be very similar regardless of cross-section utilized. Also, there appears to be a slight disconnect between the modulus values in sections N8 and N9, with the moduli in N9 being slightly higher. This could be due to the differences in the pavement structure causing a difference in the stress-states within the deep subgrade layer for N8 and N9. This variance in the stress-state could lead to a significant difference in backcalculated modulus values. However, the modulus values at each station are very consistent (small standard deviations) and both cross-sections appear to generate reasonable subgrade modulus data.

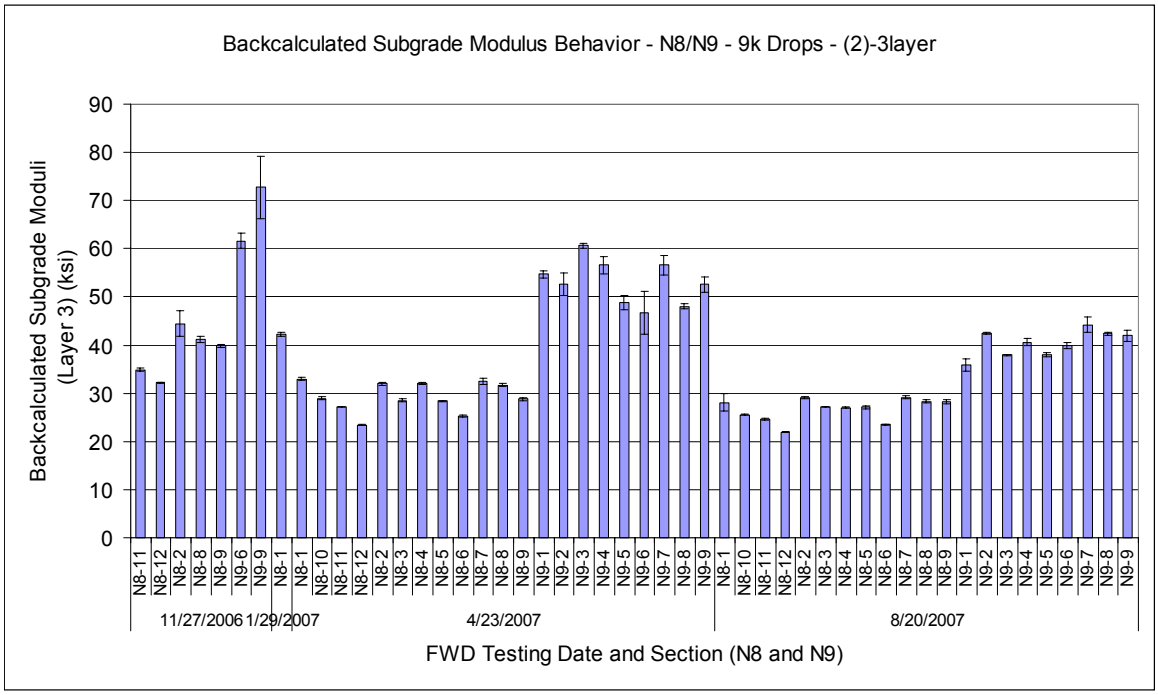


**Figure 5.39 Subgrade Layer Modulus Behavior (Layer 3) (Sections N8 and N9, (2)-3layer, All Testing Dates, All Testing Locations, 9 kip drops).**

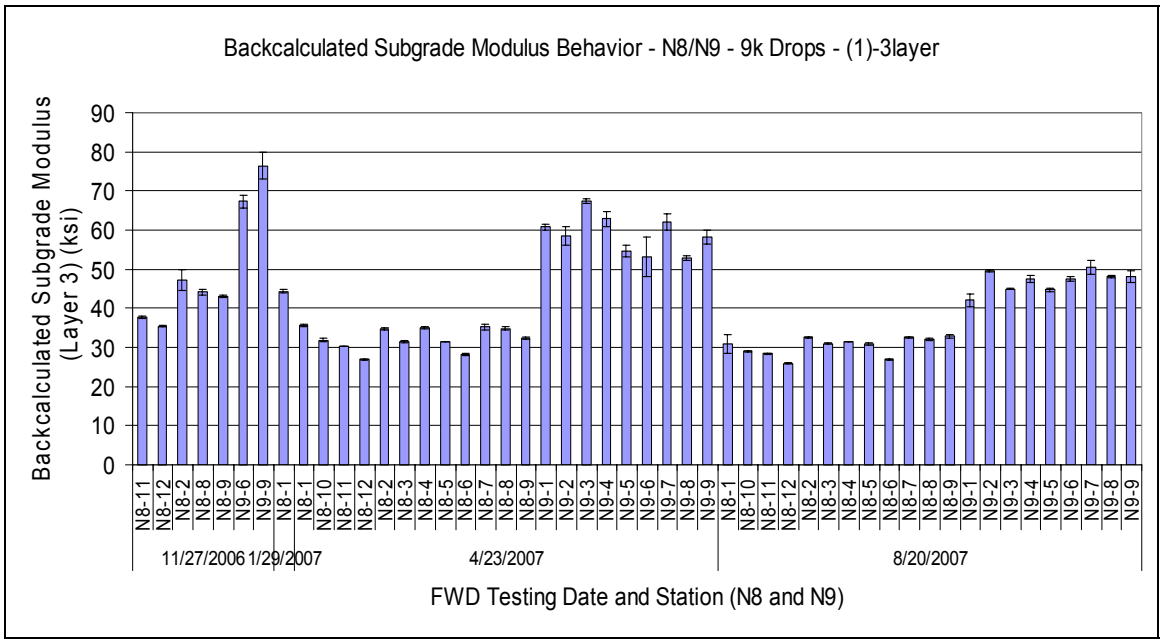


**Figure 5.40 Subgrade Layer Modulus Behavior (Layer 3) (Sections N8 and N9, (1)-3layer, All Testing Dates, All Testing Locations, 9 kip drops).**

Figure 5.41 shows a comparison between the modulus values generated using the two 3-layer cross-sections. Each data point represents a layer modulus from one testing location on one testing date that was backcalculated using both cross-sections. The figure shows that the (1)-3layer base layer modulus values are significantly higher than those from the (2)-3layer cross-section. No appreciable difference can be seen in the modulus values for the other pavement layers that is dependant on backcalculation cross-section.

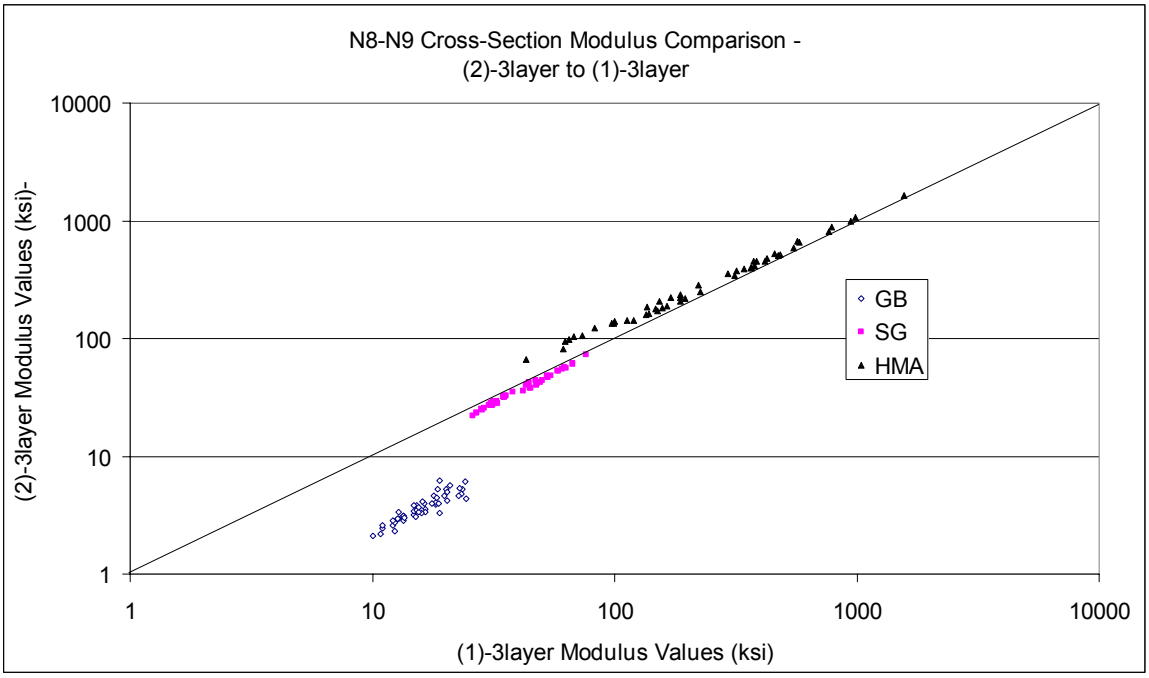


**Figure 5.41 Sections N8 and N9 – Cross-Section Modulus Comparison.**

Figures 5.42 and 5.43 show the measured versus theoretical strain response for the (2)-3layer and (1)-3layer cross-section, respectively. For both sections, the smaller strains measured for section N9 are more accurately predicted than the strain data for section N8. The measured versus predicted strain values for N8 do not appear to vary greatly regardless of cross-section utilized. However, the measured versus predicted strain values fall approximately 7% closer to the line of unity when the (2)-3layer cross-section is used. It should also be noted that the data shown for the (1)-3layer cross-section does not use the RMS error filter of eliminating data points with an RMS above 4%. This would have eliminated too much data from the data set to draw an effective comparison. Given the better RMS error values and more accurate predicted strains in N9, the (2)-3layer cross-section has a distinct advantage over the (1)-3layer cross-section.

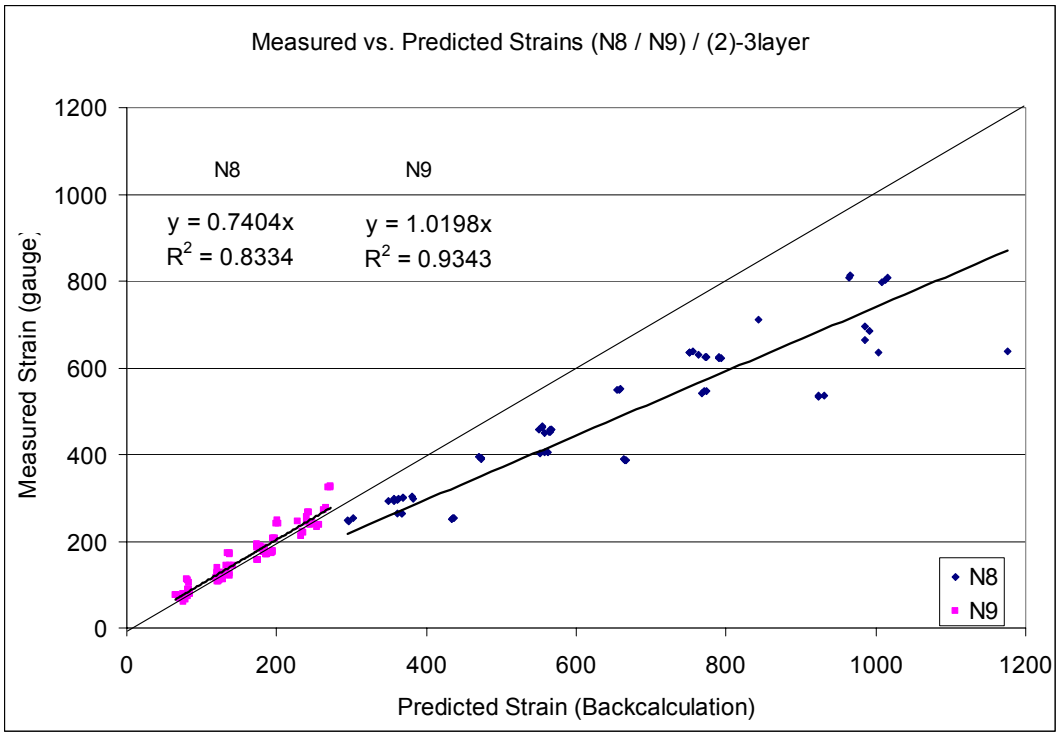


**Figure 5.42 Measured versus Predicted Strains – N8/N9 – (2)-3layer.**

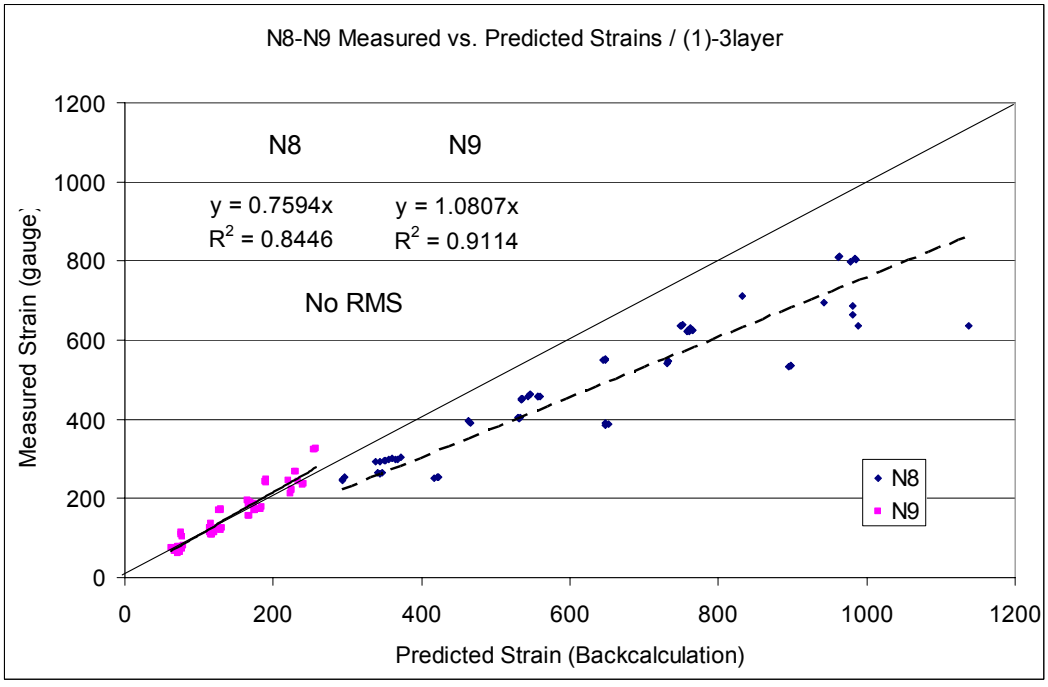


**Figure 5.43 Measured versus Predicted Strains – N8/N9 – (1)-3layer.**

Given the significantly lower RMS error values generated by the (2)-3layer cross-section in addition to better measured versus predicted strain behavior, the (2)-3layer cross-section was selected for use in backcalculation of the deflection data for sections N8 and N9. While the (1)-3layer cross-section generates significantly higher base modulus

values than the (2)-3layer cross-section, the error generated by the (1)-3layer cross-section is too high to be considered usable.

The final validation check for the (2)-3layer cross-section was analyzing the measured versus predicted pressures at the surface of the base layer and Seale subgrade. Figure 5.44 shows the measured versus predicted base pressure responses and Figure 5.45 shows the measured versus predicted pressure responses at the surface of the Seale subgrade. Figure 5.44 shows that the slope of the measured versus predicted base pressures data set falls approximately 56% above the line of unity for N8 and 38% above the line of unity for N9 (with measured pressures being larger than predicted pressures). Figure 5.45 show the slope of the measured versus predicted Seale pressures data set falls within approximately 16% of the line of unity for N8 and 20% for N9 (with predicted pressures being larger than measured pressures). The results of the measured versus predicted response data are in agreement with data collected for the previously investigated structural sections and previous studies. In conclusion, the (2)-3layer cross-section appears to be a valid backcalculation cross-section for sections N8 and N9 and was utilized for backcalculation of the deflection data for these sections.

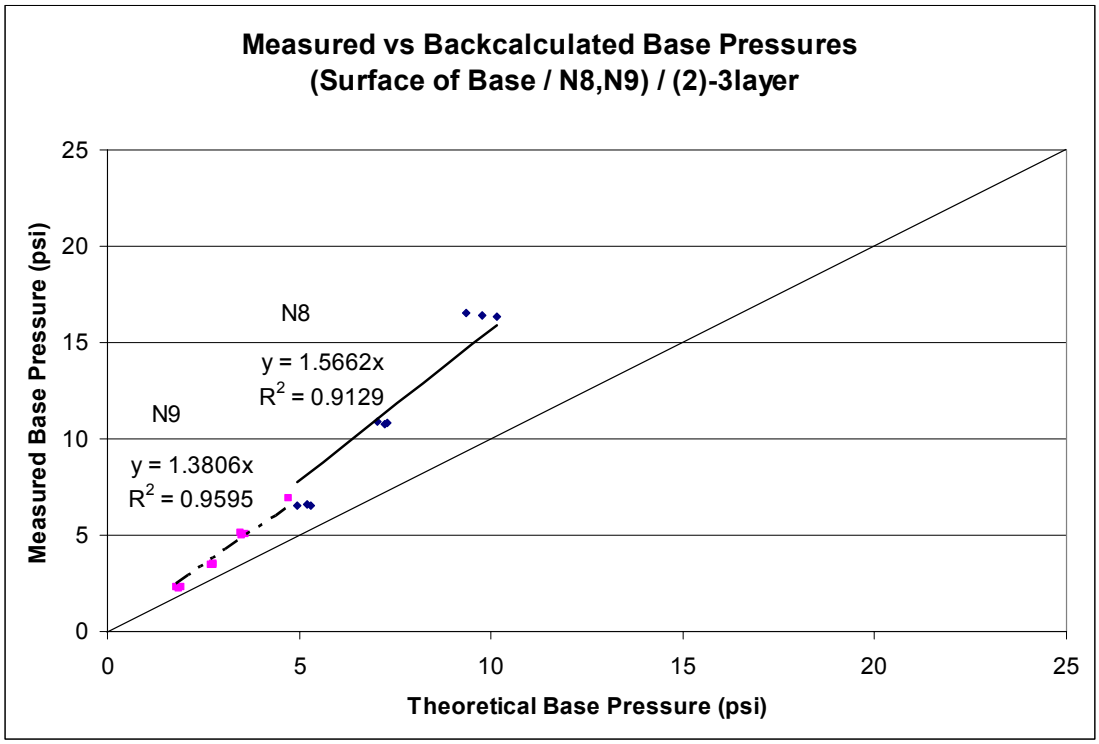


**Figure 5.44 Measured versus Predicted Base Pressures – Sections N8 and N9 – (2)-3layer.**

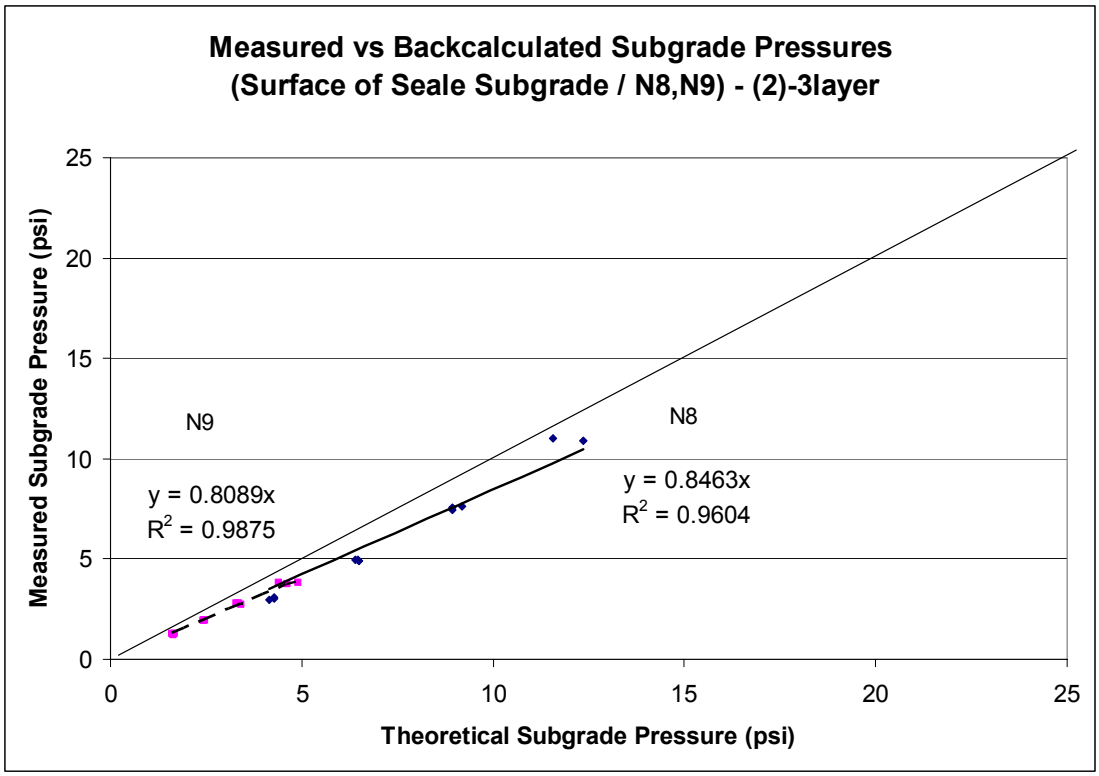


**Figure 5.45 Measured versus Predicted Subgrade Pressures (Seale) – Sections N8 and N9 – (2)-3layer.**

## SECTION N10 CROSS-SECTION INVESTIGATION

Section N10 was analyzed by itself to determine the optimal backcalculation cross-section for analyzing its deflection data. Section N10 was constructed with approximately 8 inches of HMA above 4 inches of Missouri Type 5 base. This base material was not used in any of the other structural sections, so this section warranted an independent cross-section investigation. The HMA and base are constructed atop 6 inches of Track fill compacted to 100% of lab density. This fill is compacted atop approximately 16 inches of Track fill (above the milled depth of 34 inches) compacted to 95% of lab density. Below this fill is 8 inches of Track fill added in the 2000 research cycle above the deep Track subgrade.

Based on the section construction (summarized in Table 5.1 and detailed in Chapter 3), a set of trial backcalculation cross-sections was developed for section N10. These cross-sections are shown in Figure 5.46 below. Given the multiple layers of unbound materials and varying densities of these materials, a greater number of trial cross-sections were developed for N10 than for the previously-investigated structural sections. The numbering scheme for the cross-sections remains consistent with that used for the previous sections (trial cross-section number in parentheses followed by number of layers). However, the naming scheme for the pavement layers has been altered somewhat. HMA represents the combined hot mix asphalt lifts and GB represents the four inches of Type 5 Base. New Fill (1) represents the six inches of higher density

(100% of lab density) Track fill compacted for the 2006 research cycle. New Fill (2) represents the approximately 16 inches of lower density (95% of lab density) Track fill compacted for the 2006 research cycle. Old Fill represents the 8 inches of Track fill compacted for the 2000 research cycle. SG represents the deep Track soil embankment and BR represents the stiff layer induced into the backcalculation program for certain sections.

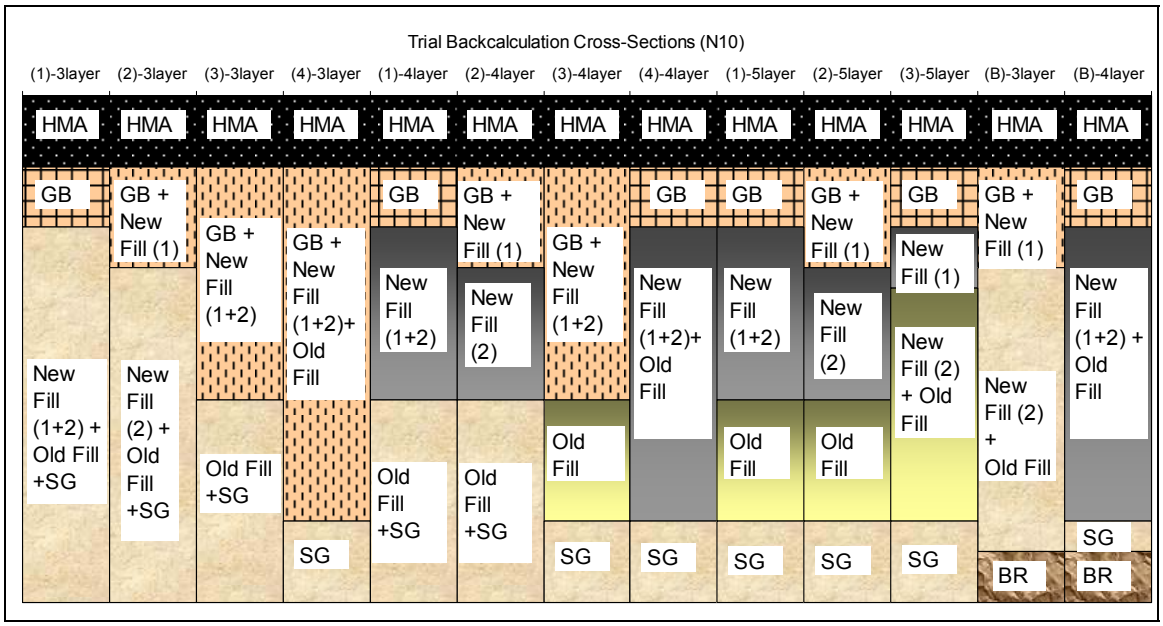


**Figure 5.46 Trial Backcalculation Cross-Sections for Section N10.**

The first phase of the investigation involved analyzing the RMS error cumulative distribution functions generated by running the backcalculation with each of the trial cross-sections. Figure 5.47 shows the RMS error CDFs for the 3-layer solution while figure 5.48 shows the RMS error CDFs for the 4-layer and 5-layer solutions. These figures show relatively consistent RMS error behavior for most of the cross-sections that did not include a stiff layer (bedrock) for backcalculation. The (B)-3layer and (B)-4layer cross-sections exhibited unreasonably high RMS error solutions. Given the poor match between measured and predicted deflections, it seemed apparent that there was no stiff layer beneath this section that was influencing the deflection basin. This finding was consistent with the findings from the previous structural section investigations. Therefore, the (B)-3layer and (B)-4layer cross-sections were eliminated from consideration.

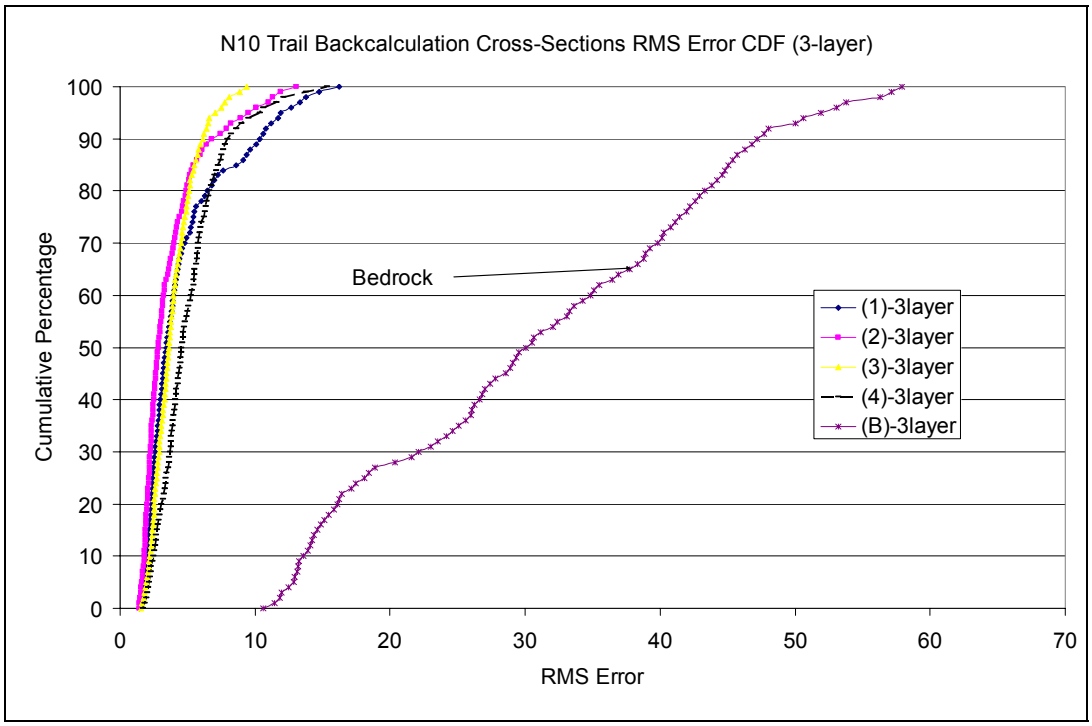


**Figure 5.47 RMS Error Cumulative Distribution Functions (CDF) for the Trial Backcalculation Cross-Sections in Section N10 (3-layer only).**

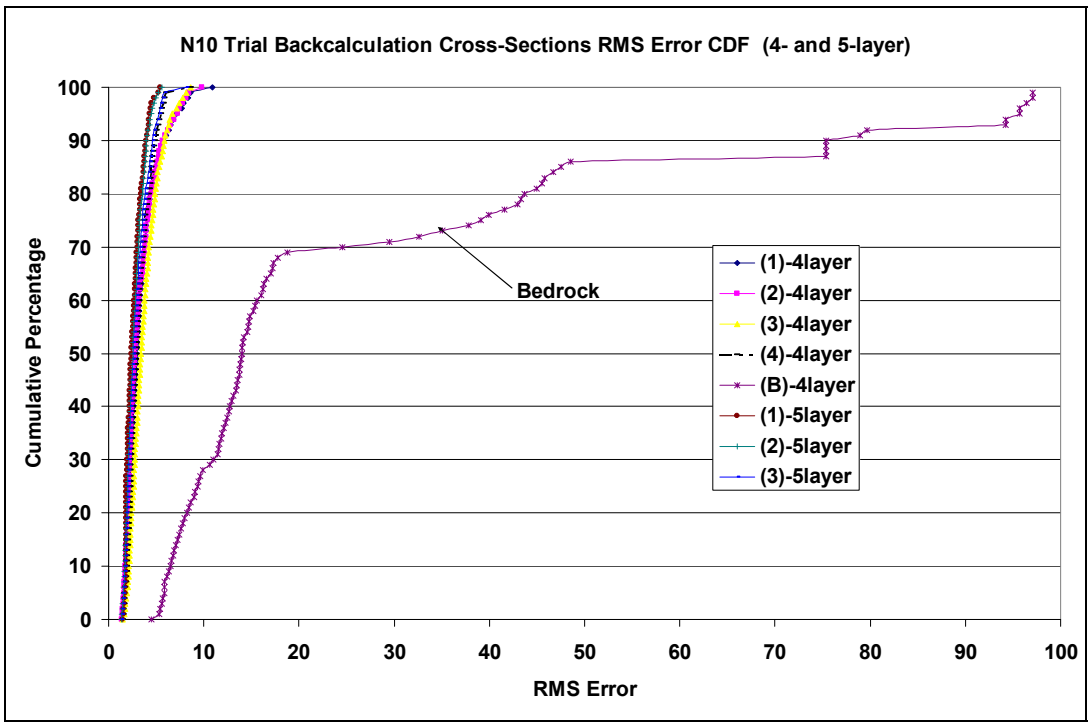


**Figure 5.48 RMS Error Cumulative Distribution Functions (CDF) for the Trial Backcalculation Cross-Sections in Section N10 (4-layer and 5-layer only).**

The results of the cross-section investigations from the other structural sections indicated that while the cross-sections with 4 or more layers provided reasonable RMS error values, they tended to generate unreasonable and unstable modulus data. This performance was also expected in section N10, given the multiple layers of Track fill located within the pavement structure. The results from analyzing the modulus behavior for the 4-layer and 5-layer systems were consistent with this expectation. Table 5.5 shows the modulus behavior at one testing location for one date with the (1)-5layer cross-section. Table 5.6 shows the same information for the (2)-4layer cross-section. Table 5.5 shows very erratic modulus values for the third layer (Track fill compacted in 2006). The modulus values for the fourth layer (Track fill compacted in 2000) all spike on the upper iteration boundary of 80 ksi. Table 5.6 shows that the modulus values for the third layer (lower density Track fill compacted in 2006) predominantly spike on the upper limit of 80 ksi. Similar behavior was observed in all of the 4-layer and 5-layer solutions. Consequently, the modulus behavior from these solutions was determined to be unreasonable and these cross-sections were eliminated from consideration.

**Table 5.5 (1)-5layer Cross-Section Modulus Behavior (Station N10-5, 01/29/07)**

| LOAD (LB) | E1(KSI) | E2(KSI) | E3(KSI) | E4(KSI) | E5(KSI) | Error (%) |
|---|---|---|---|---|---|---|
| 5775 | 1019.5 | 5.9 | 11 | 80 | 48.6 | 3.3 |
| 5791 | 1034.3 | 2.6 | 17 | 80 | 51.7 | 3.34 |
| 5804 | 1034.3 | 2.1 | 20.6 | 80 | 52.7 | 4.2 |
| 9072 | 1004.9 | 1.1 | 80 | 80 | 50.7 | 2.58 |
| 9084 | 999.1 | 1.1 | 80 | 80 | 50.2 | 2.36 |
| 9092 | 989.3 | 1.1 | 80 | 80 | 50.3 | 2.2 |
| 12413 | 1006.3 | 1 | 80 | 80 | 47.1 | 2.16 |
| 12416 | 1006.3 | 1 | 76.8 | 80 | 48 | 2.23 |
| 12421 | 1022 | 1 | 66.9 | 80 | 48 | 2.09 |
| 16571 | 1028.3 | 1.1 | 34.2 | 80 | 43.5 | 1.85 |
| 16575 | 1032.8 | 1.6 | 13.1 | 80 | 40.7 | 1.7 |
| 16591 | 1029.8 | 2 | 10.4 | 80 | 39.7 | 1.79 |

**Table 5.6 (2)-4layer Cross-Section Modulus Behavior (Station N10-11, 04/23/07)**

| LOAD (LB) | E1(KSI) | E2(KSI) | E3(KSI) | E4(KSI) | Error (%) |
|---|---|---|---|---|---|
| 5597 | 212.8 | 2.4 | 80 | 41.2 | 3.76 |
| 5621 | 212.6 | 2.3 | 80 | 44.5 | 3.45 |
| 5629 | 221.9 | 2.3 | 80 | 44.9 | 6.23 |
| 8520 | 217.6 | 2 | 80 | 39.5 | 2.16 |
| 8524 | 219.5 | 1.9 | 80 | 39.9 | 3.1 |
| 8552 | 219.4 | 2 | 80 | 39.1 | 3.25 |
| 12011 | 220.5 | 1.9 | 80 | 34.5 | 1.88 |
| 12027 | 225.3 | 1.8 | 80 | 34.9 | 2.17 |
| 12039 | 225.8 | 1.9 | 80 | 34.7 | 2.22 |
| 15983 | 233.5 | 1.8 | 80 | 32.8 | 1.69 |
| 15988 | 234.2 | 1.9 | 61.9 | 32.4 | 1.99 |
| 16038 | 234.3 | 1.9 | 80 | 32.3 | 1.83 |

Figure 5.49 shows the RMS Error cumulative distribution functions for the trial 3-layer cross-sections in N10 (excluding the bedrock cross-section). The results show that none of the cross-sections exhibited truly good RMS error behavior. The (2)-3layer cross-section (which combines the Type 5 base with 6" of higher density Track fill) shows the greatest percentage of drops (approximately 71%) falling below the RMS error cut-off of 4%. The CDF for this cross-section is also to the left of the CDFs generated by the other cross-sections below the RMS error cutoff. However, this cross-section also appears to generate some high RMS error values as well, with the 95$^{th}$ percentile value falling in the range of about 9% RMS error.

Both the (1)-3layer cross-section (Type 5 base modeled by itself) and the (3)-3layer cross-section (Type 5 base combined with all Track fill compacted for the 2006 research cycle) have about 61% of drops below the RMS error cut-off. In spite of the CDF intersection at 4% RMS error, the two distributions behave very differently. The (3)-3layer cross-section exhibits a much lower 95$^{th}$ percentile RMS error (about 7%) than the (1)-3layer cross-section (about 13%). Thus, the (3)-3layer cross-section generates a much more reasonable RMS error distribution than the (1)-3layer cross-section. This is not surprising since it was thought that modeling a relatively thin 4 inch base layer by itself could be problematic. Therefore, the results indicate that the (2)-3layer and (3)-3layer cross-sections generate the best (though certainly not optimal) RMS error distributions.

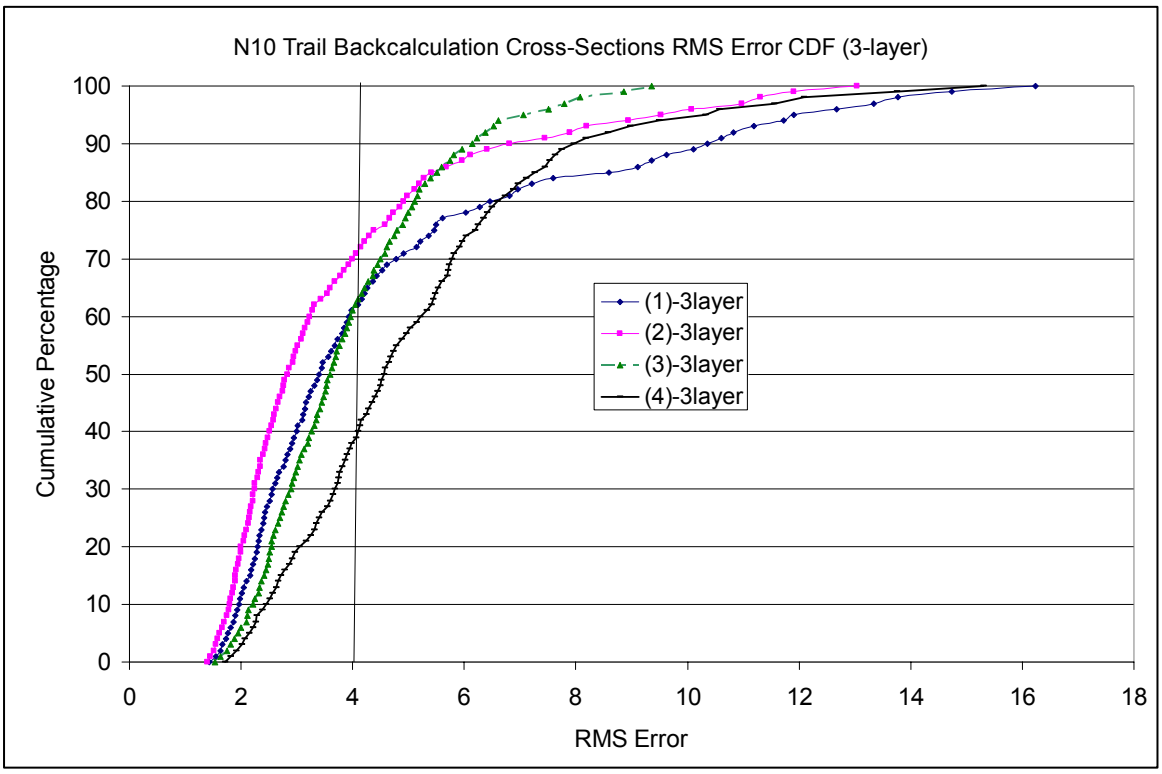


**Figure 5.49 RMS Error Cumulative Distribution Functions (CDF) for the 3-Layer Trial Backcalculation Cross-Sections in Section N10.**

Next, the modulus behavior for the unbound materials layers for the two remaining cross-sections were examined to determine whether they behaved reasonably. For Section N10, Figures 5.50 and 5.51 show the average and standard deviations of the backcalculated base layer moduli for cross-sections (2)-3layer and (3)-3layer, respectively. The moduli shown are calculated from the 9,000 lb FWD loadings for each testing station on each testing date. The results of this analysis show that both solutions seem to generate reasonable backcalculated moduli. There is an obvious increase in modulus values for the base layer when the additional lower density Track fill is included with the base layer for the (3)-3layer cross-section. Both solutions show reasonably consistent modulus values station to station (with mild spatial variability being evident in both solutions) and small standard deviations at each testing location, both being indicators of a reasonable solution.

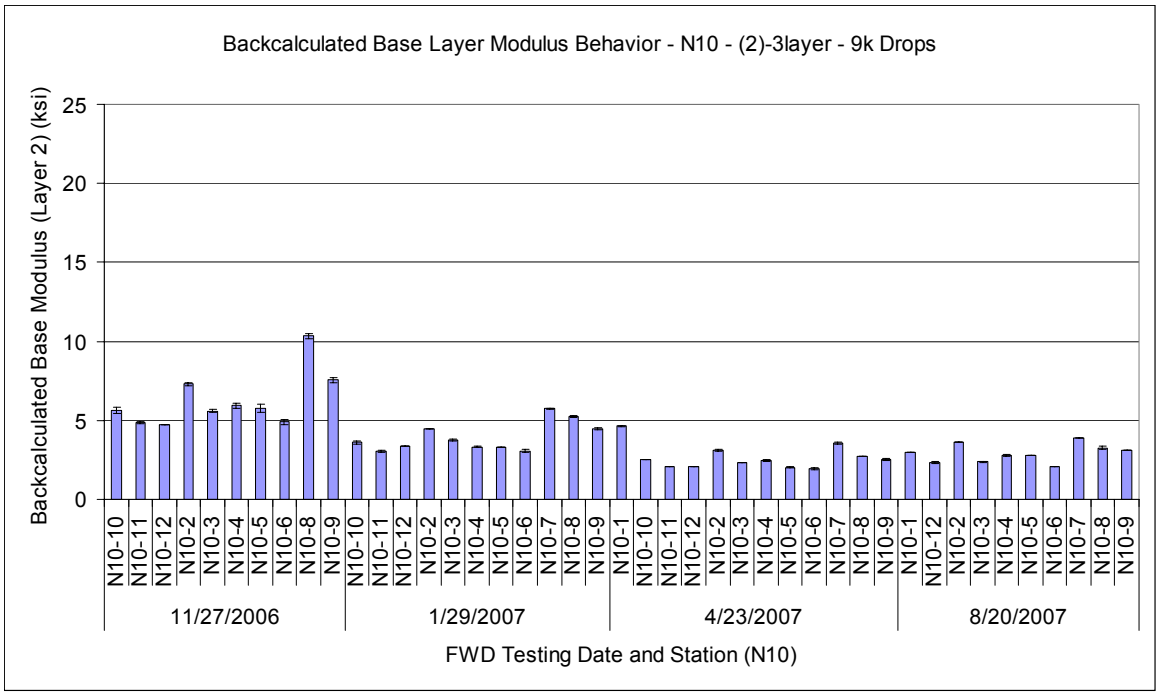


**Figure 5.50 Base Layer Modulus Behavior (Layer 2) (Section N10, (2)-3layer, All Testing Dates, All Testing Locations, 9 kip drops).**

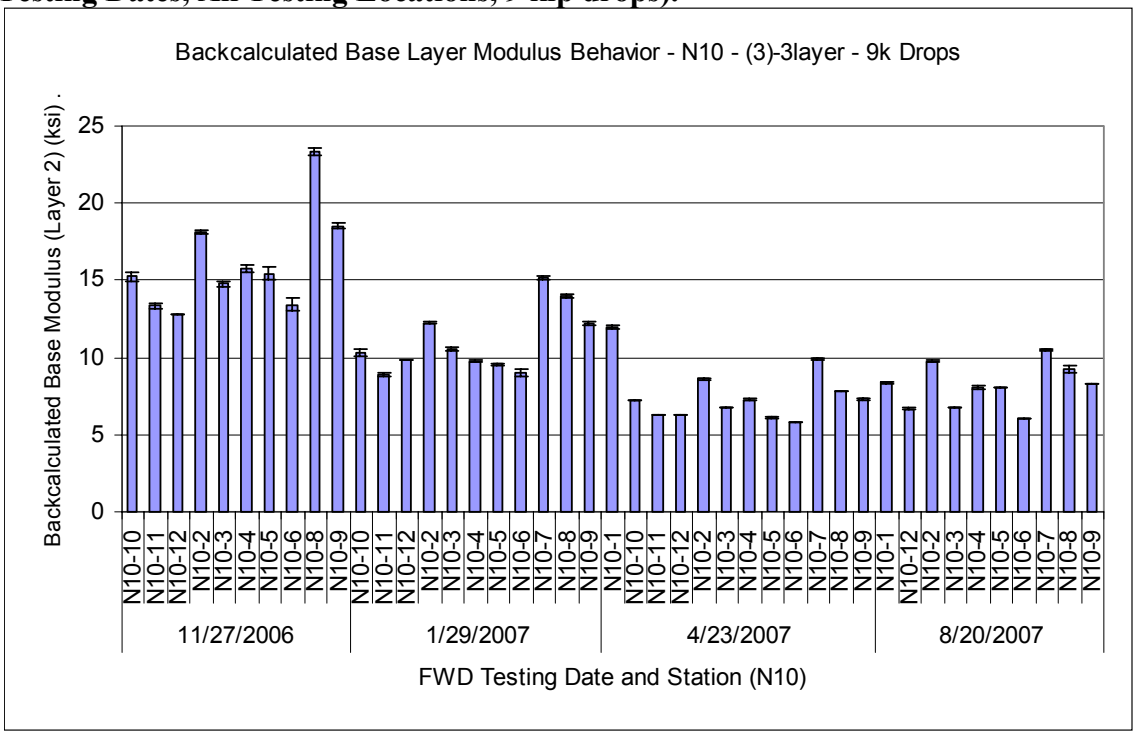


**Figure 5.51 Base Layer Modulus Behavior (Layer 2) (Section N10, (3)-3layer, All Testing Dates, All Testing Locations, 9 kip drops).**

For section N10, Figures 5.52 and 5.53 show the average and standard deviations of the backcalculated subgrade layer moduli for cross-sections (2)-3layer and (3)-3layer,

respectively. The moduli shown are calculated from the 9,000 lb FWD loadings for each testing station on each testing date. Again, the subgrade moduli for the comparison cross-sections appear to be very similar and the composition of the base layer for backcalculation does not seem to greatly impact the backcalculated subgrade moduli. The average modulus values for each solution are very consistent within each testing date and small standard deviations at each drop locations are further evidence of solution stability.

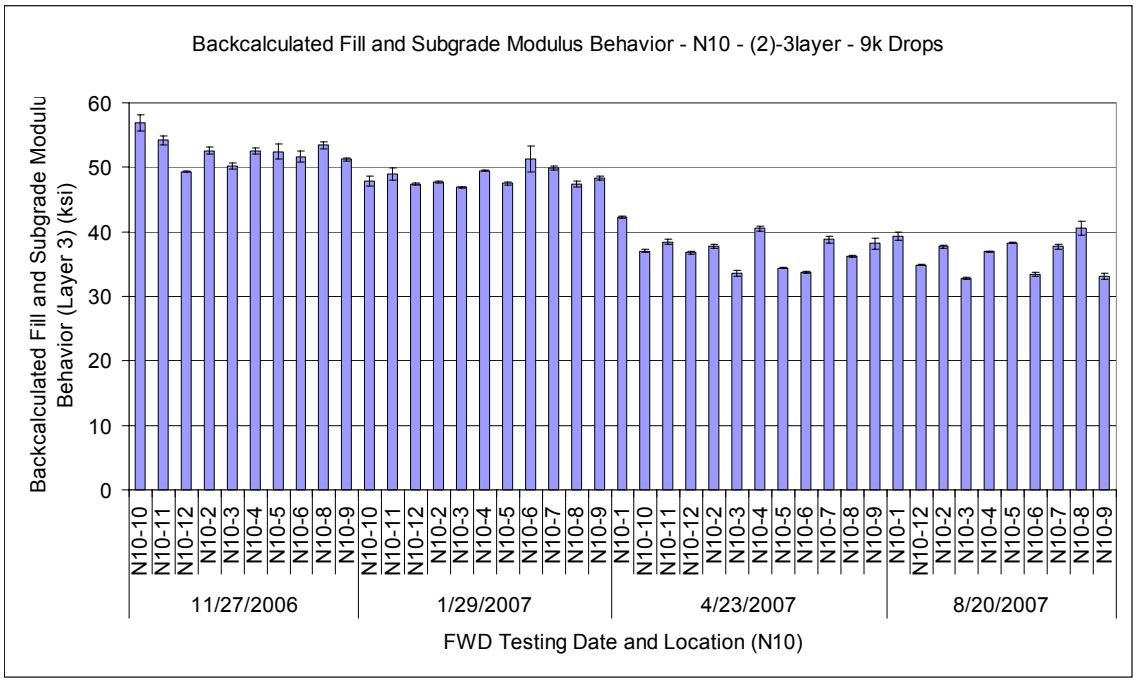


**Figure 5.52 Fill and Subgrade Layer Modulus Behavior (Layer 3) (Section N10, (2)-3layer, All Testing Dates, All Testing Locations, 9 kip drops).**

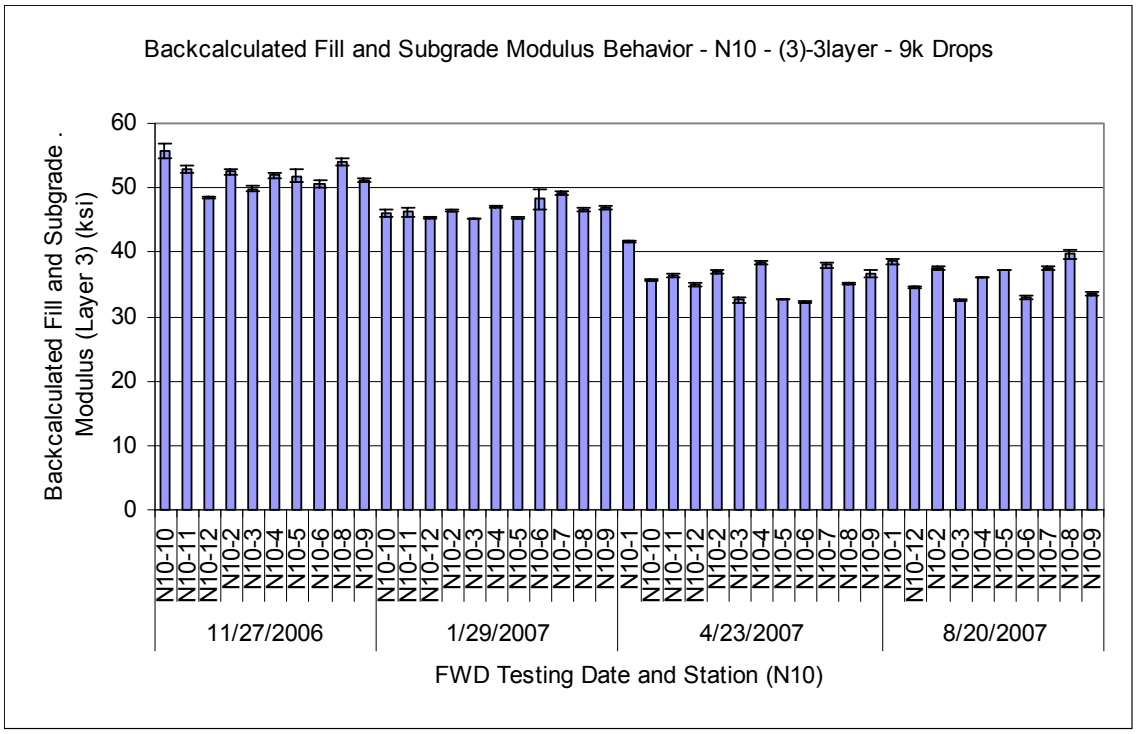


**Figure 5.53 Fill and Subgrade Layer Modulus Behavior (Layer 3) (Section N10, (3)-3layer, All Testing Dates, All Testing Locations, 9 kip drops).**

Figure 5.54 compares the backcalculated modulus values from the (2)-3layer and (3)-3layer cross-section for Section N10. Each data point represents a pavement layer modulus at a specific test site that was backcalculated using both trial cross-sections. The comparison results from this section are very consistent with the results from the other structural sections. The altered base composition only seems to seriously impact the backcalculated moduli of the base layer. It appears the HMA moduli for the (2)-3layer cross-section are slightly higher than those from the (3)-3layer cross-section. However, the base moduli from the (3)-3layer cross-section are significantly higher than those calculated using the (2)-3layer cross-section due to the additional Track fill included in the base layer for that cross-section.

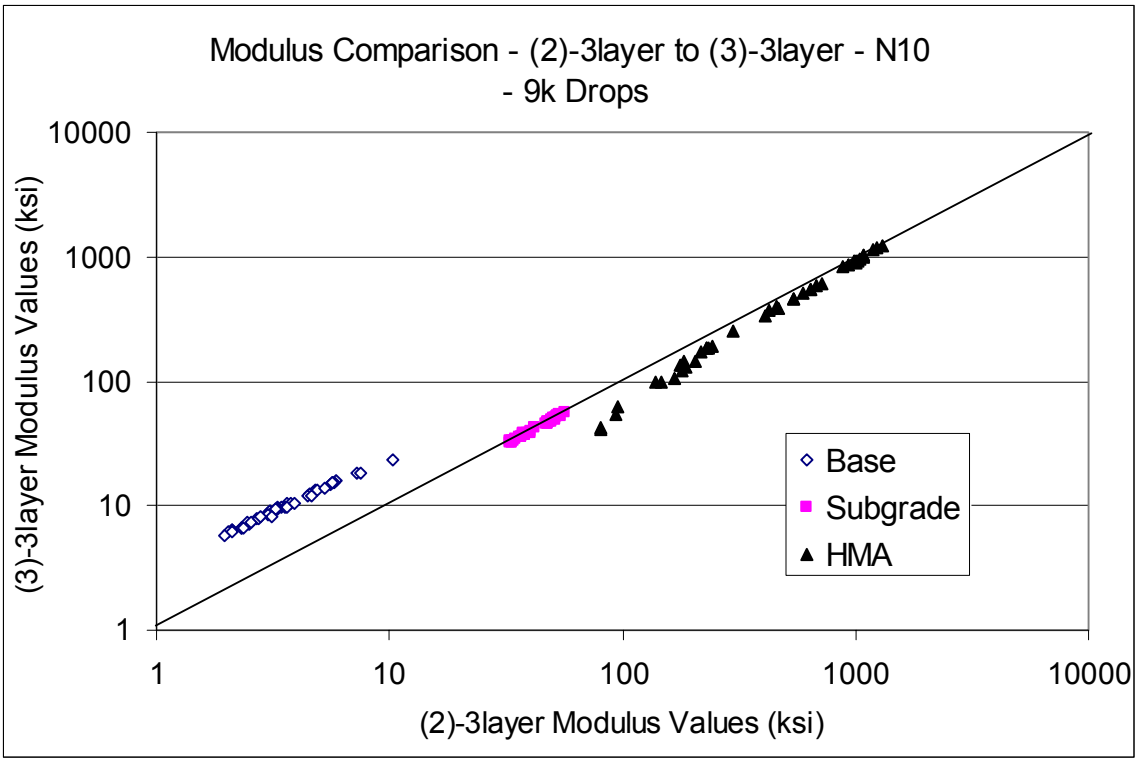


**Figure 5.54 Section N10 – Cross-Section Modulus Comparison.**

The final comparison to be made between the (2)-3layer and (3)-3layer cross-section is between their measured versus predicted pavement strain behavior. The backcalculation data from the FWD on gauge testing yielded results in which the majority of the RMS error values were above the cut-off value of 4%. This was not surprising since the FWD on Gauge testing was performed in mid-July, and N10 was one of the structural sections to exhibit higher levels of rutting. Figure 5.55 shows the measured rut depths taken from each of the structural sections on 7/16/07, immediately before the FWD on Gauge testing. This figure clearly shows that section N10 had experienced the highest amount of rutting of any of the structural sections at that point in time. Therefore, it could be reasonably expected that section N10 would exhibit poor deflection matching for its set of backcalculation data. Therefore, the RMS filter was not used due to the need to have a reasonable data set for comparison.

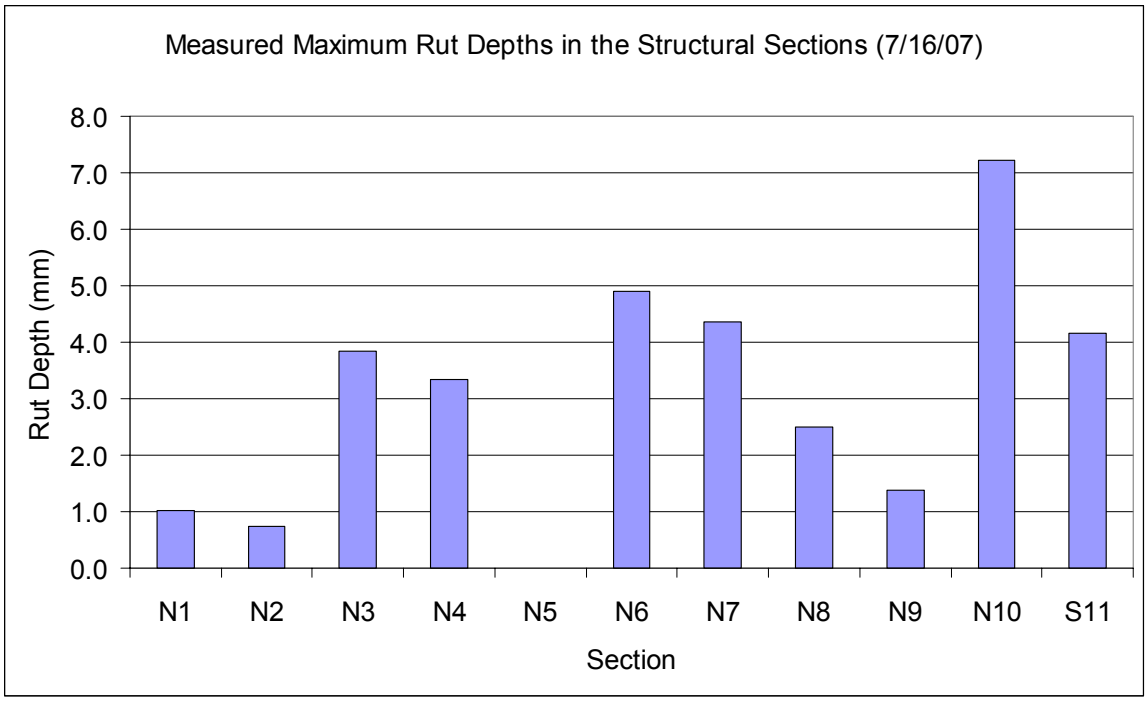


**Figure 5.55 Structural Section Rut Depths (7/16/07).**

Figure 5.56 shows the measured versus predicted strains at the bottom of the HMA layer for the (2)-3layer cross-section. Figure 5.57 shows the same data for the (3)-3layer cross-section. Both datasets seem to exhibit poor agreement between measured and predicted strains and a large scatter within the dataset. The predicted strains for the (2)-3layer cross-section are approximately 52% higher than the measured strains and the predicted strains are approximately 58% higher than the measured strains for the (3)-3layer cross-section. The $R^2$ values for both datasets are relatively low (about 0.45). Therefore, neither dataset exhibits high quality measured versus predicted strain behavior. While not optimal, the (2)-3layer cross-section exhibits slightly better agreement between measured and predicted strains than the (3)-3layer cross-section.

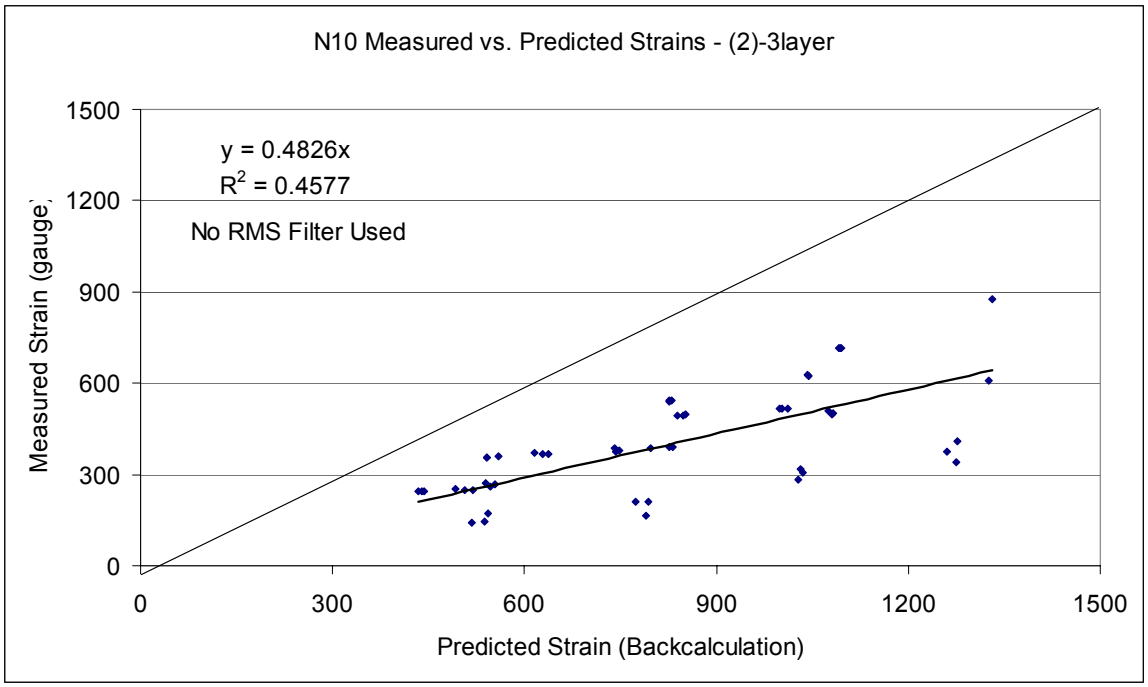


**Figure 5.56 Measured versus Predicted Strains – N10 – (2)-3layer.**

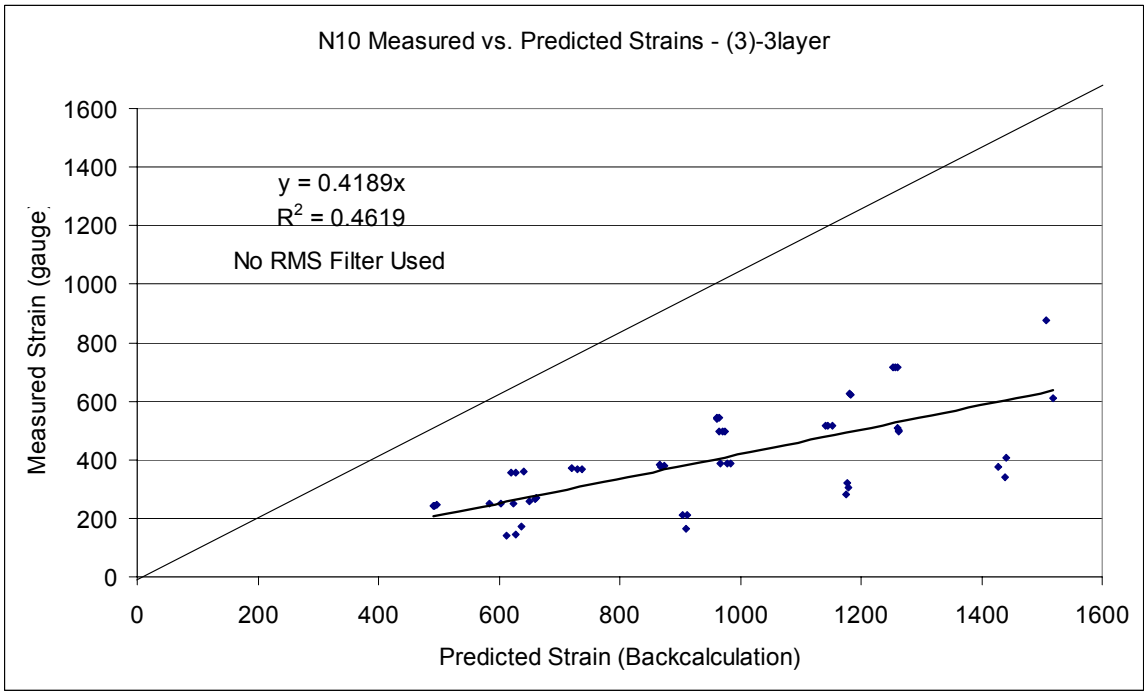


**Figure 5.57 Measured versus Predicted Strains – N10 – (3)-3layer.**

The results of the cross-section investigation from section N10 yielded no truly optimal cross-section for backcalculation. The solutions containing bedrock and more than 3 layers did not yield reasonable modulus results for backcalculation. However, the solutions generated with the 3-layer cross-sections did not have one solution that

exhibited optimal RMS error or measured versus predicted strain behavior. The (2)-3layer cross-section (combining the Type 5 base material with the higher density Track fill compacted in 2006) appears to be yield the best results of the multiple cross-sections tried. This cross-section has the highest percentage of FWD loadings falling below the RMS error cut-off of 4%. Also, this cross-section exhibits slightly better (though not optimal) measured versus strain behavior than the (3)-3layer cross-section. Thus, the (2)-3layer cross-section was selected for analysis of deflection data in section N10.

Finally, the measured versus predicted pressure behavior at the surface of the Type 5 base and Track fill layers were analyzed to ensure reasonable behavior using the (2)-3layer cross-section. Figure 5.58 shows the measured versus predicted base pressure responses and Figure 5.59 shows the measured versus predicted pressure responses at the surface of the Track fill. Since the second layer for the (2)-3layer cross-section contains both the base and high density Track fill layers, the program could not calculate the output stress state at the exact location of the fill pressure plate. Therefore, it was necessary to use WESLEA layered-elastic analysis software to simulate the predicted pressures at the surface of the high density Track fill for the various FWD loadings.

Figure 5.58 shows that the slope of the measured versus predicted base pressures data set falls approximately 57% above the line of unity for N10 (with measured pressures being larger than predicted pressures). Figure 5.59 show the slope of the measured versus predicted fill pressures data set falls within approximately 3% of the line of unity (with predicted pressures being larger than measured pressures). The results of the measured versus predicted response data are reasonable given comparisons with data collected for the previously investigated structural sections and previous studies. In conclusion, the (2)-3layer cross-section is the best backcalculation cross-section available for use with section N10 and was utilized for backcalculation of the deflection data for this section.

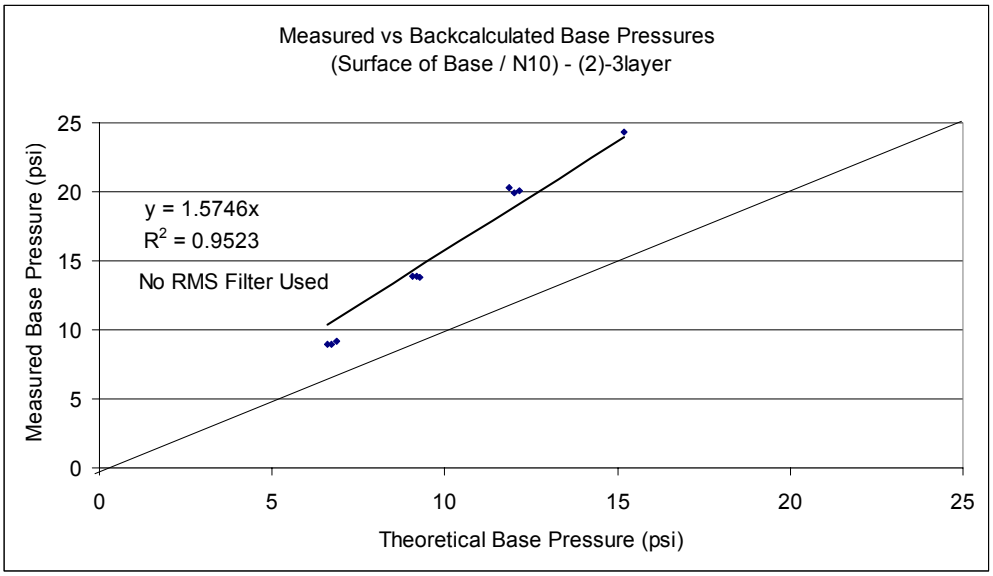


**Figure 5.58 Measured versus Predicted Base Pressures (Surface of Base Layer)-N10 – (2)-3layer.**

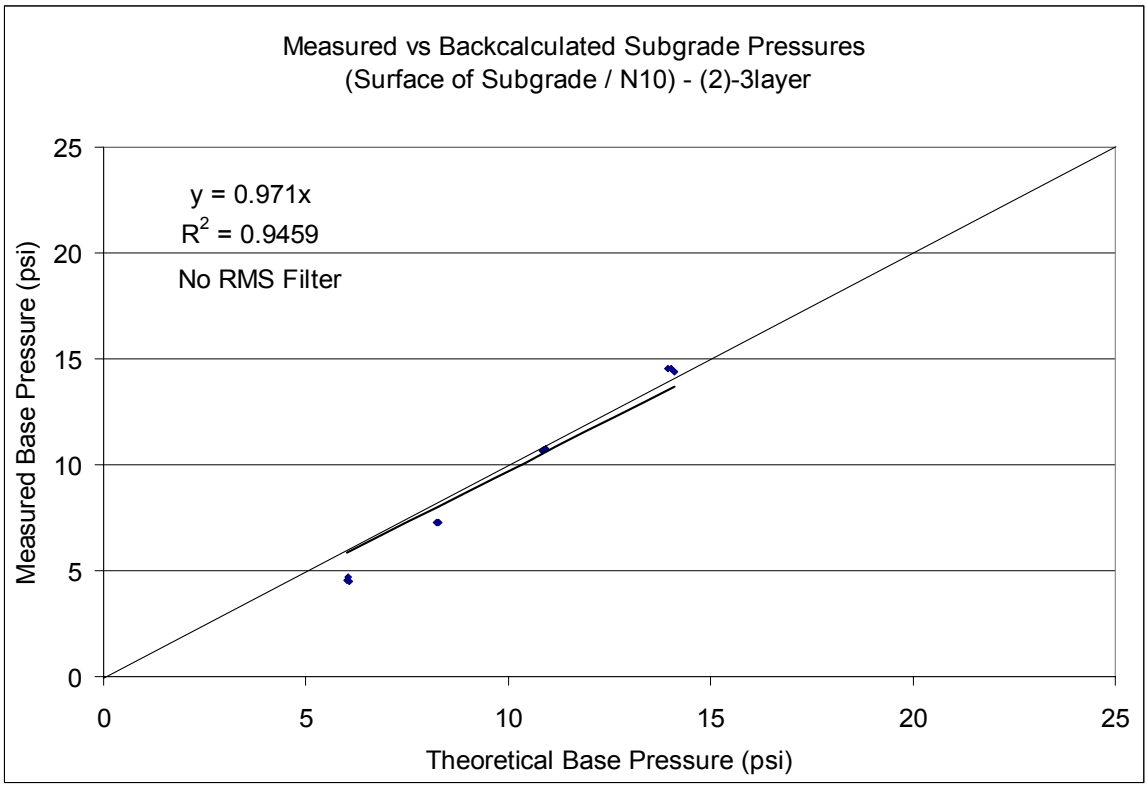


**Figure 5.59 Measured versus Predicted Fill Pressures (Surface of Fill Layer) – N10 – (2)-3layer.**

**S11 CROSS-SECTION INVESTIGATION**

Section S11 was analyzed by itself to determine the optimal cross-section for backcalculation. This section was constructed in a similar manner to sections N3-N7, the structural sections left in-place from the 2003 research cycle. The section was constructed with approximately 7 inches of HMA over 6 inches of the granite base used in the 2003 structural sections. The section was milled to a depth of 30 inches. Above the milled depth, 6 inches of high density (compacted to 100% of lab density) Track fill was placed atop approximately 11 inches of lower density (compacted to 95% of lab density) Track fill. Below the milled depth lies approximately 12 inches of Track fill that was compacted for the 2000 research cycle above the deep Track subgrade material. Though section S11 was constructed very similarly to sections N3-N7, it was isolated for analysis because aging effects of time and traffic could make sections N3-N7 behave very differently under loading than a newly constructed section.

Figure 5.60 shows the different trial cross-sections for backcalculation utilized in section S11. The numbering scheme for the cross-sections remains consistent with that used for the previous sections (trial cross-section number in parenthesis followed by number of layers). In Figure 5.60, HMA represents the combined hot mix asphalt lifts within the section and GB represents the granite base. New Fill (1) represents the 6 inches of Track fill compacted in 2006 to the higher density values (100% of lab density). New Fill (2)

represents the fill compacted in 2006 to the lower density values (95% of lab density). Old Fill represents the 12 inches of Track fill compacted for the 2000 research cycle. Subgrade represents the deep Track subgrade and Bedrock represents a trial stiff layer used with the backcalculation software. Given the results from the previous sections, it seemed likely that the best cross-section would be a 3-layer cross-section without the use of a stiff layer.

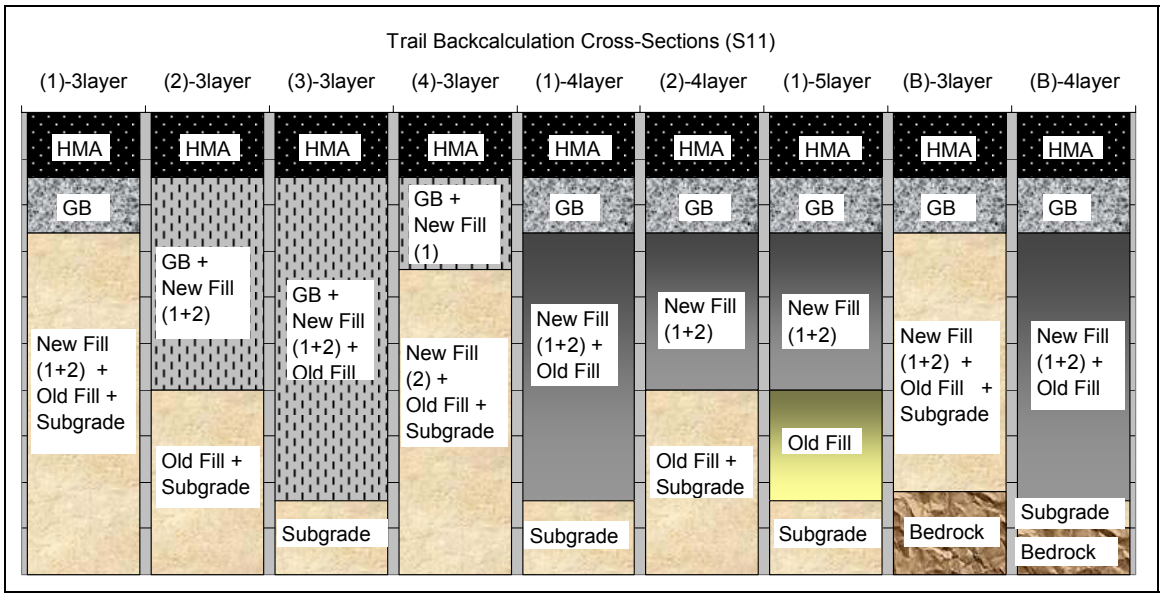


**Figure 5.60 S11 Trial Backcalculation Cross-Sections.**

The first phase of the analysis was to analyze the RMS error behavior for the backcalculated data from each of the trial cross-sections. Cumulative distribution functions of the RMS error values for the four dates' backcalculated data with each cross-section are shown in Figure 5.61. As with the investigations for the other structural sections, the RMS error values seem relatively consistent for the cross-sections not including a stiff layer for backcalculation. However, the (B)-3layer and (B)-4layer cross-sections exhibit exceptionally high RMS error values. Given the results in Figure 5.61, it appears there is no stiff layer influencing the backcalculation for the lone structural section on the south tangent (S11). Therefore, the (B)-3layer and (B)-4layer cross-sections were eliminated from consideration.

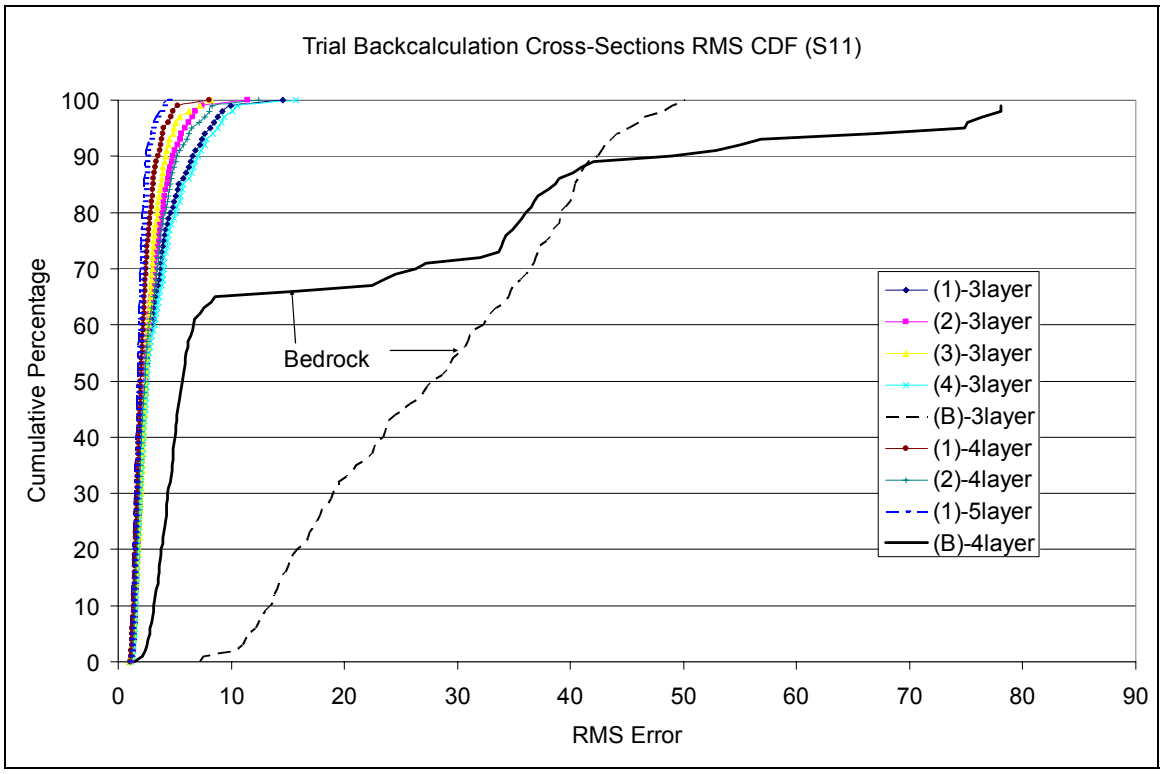


**Figure 5.61 RMS Error Cumulative Distribution Functions (CDF) for the Trial Backcalculation Cross-Sections in Section S11.**

The next phase of the investigation involved looking more closely at the backcalculated modulus values generated by the individual cross-sections. Since the 4-layer and 5-layer cross-sections each have adjoining Track soil layers and have performed poorly in the previous structural sections, they were analyzed first. Table 5.7 shows the modulus behavior from one testing location (Station S11-3) on 11/27/06 for the (1)-5layer cross-section. The modulus behavior was as expected for the two fill layers (layers four and five). The moduli for layer 3 are forced to the upper iteration limit of 80 ksi while the moduli for layer four seem to behave erratically between loadings. This result was expected given the previous results of backcalculation with bordering Track fill layers.

**Table 5.7 (1)-5layer Cross-Section Modulus Behavior (Station S11-3, 11/27/06)**

| LOAD(LB) | E1(KSI) | E2(KSI) | E3(KSI) | E4(KSI) | E5(KSI) | Error (%) |
|---|---|---|---|---|---|---|
| 5489 | 362.6 | 2.9 | 80 | 27.3 | 36.8 | 2.39 |
| 5494 | 372.5 | 2.8 | 80 | 36.8 | 37 | 2.39 |
| 5534 | 358.4 | 2.9 | 80 | 30.1 | 36.3 | 2.29 |
| 8960 | 373.1 | 2.1 | 80 | 53.2 | 34.3 | 1.83 |
| 8968 | 369.6 | 2.2 | 80 | 42.6 | 34.4 | 2.02 |
| 8968 | 378.6 | 2 | 80 | 79.3 | 34.7 | 1.84 |
| 12074 | 361.5 | 1.9 | 80 | 35.9 | 32.1 | 1.57 |
| 12082 | 365.8 | 1.9 | 80 | 35.2 | 32.1 | 1.71 |
| 12087 | 366.3 | 1.8 | 80 | 47.7 | 32 | 1.63 |
| 16308 | 379.1 | 1.8 | 80 | 36.7 | 31.1 | 1.64 |
| 16313 | 380.1 | 1.7 | 80 | 49.6 | 31.1 | 1.55 |
| 16313 | 377.3 | 1.8 | 80 | 34.3 | 31 | 1.62 |

Figure 5.62 illustrates the backcalculated Track fill modulus behavior for the (1)-4layer cross-section in section S11. This graph summarizes only the 9,000 lb FWD loadings and shows the backcalculated moduli for all the FWD testing locations within S11 for the four different testing dates. The results of Figure 5.62 show a fairly unstable backcalculation solution. There are several stations where the modulus values are forced to the upper iteration boundary of 80 ksi. Additionally, multiple stations show relatively large standard deviations indicating an inconsistent solution between loadings. Results of analysis were similar for the (1)-4layer cross-section as well. Therefore, it appears that the 4-layer and 5-layer cross-sections were incapable of producing a reasonable solution and were subsequently eliminated from consideration.

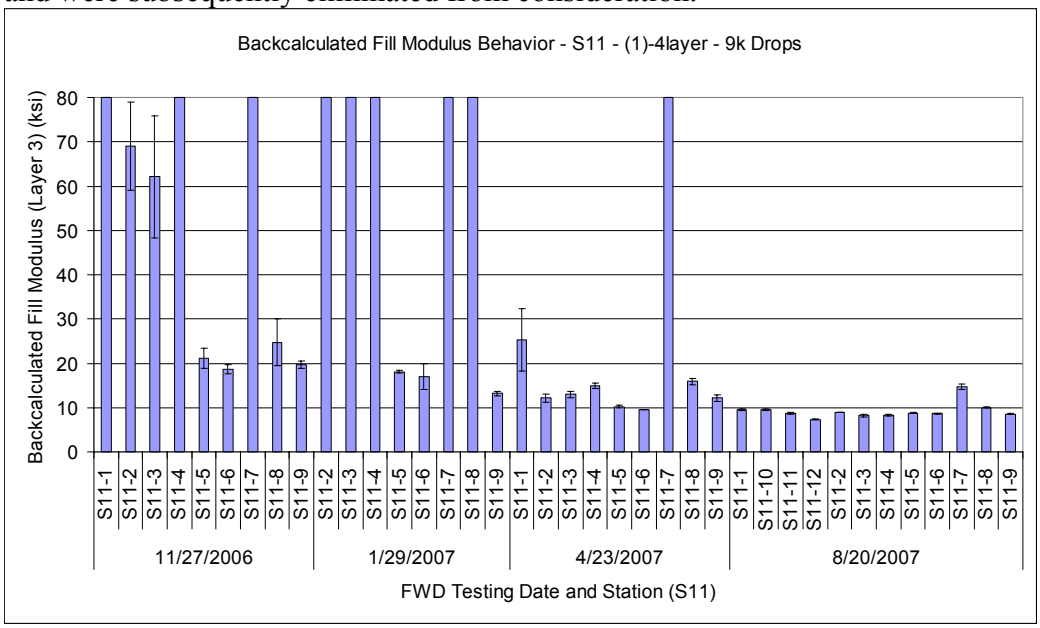


**Figure 5.62 Fill Layer Modulus Behavior (Layer 3) (Section S11, All Testing Stations and Dates, 9 kip drops).**

With the elimination of the trial cross-sections using more than 3 layers for backcalculation and the cross-sections using a stiff layer, only the 3-layer cross-sections remained for consideration. The next phase of the investigation involved a closer inspection of the RMS error cumulative distribution functions for the 3-layer cross-sections. These data are shown in Figure 5.63. The figure shows that the CDFs for the various cross-sections are almost identical below an RMS error of approximately 2.5%. Above this RMS error value, the CDFs seem to diverge. The cross-section with the largest percentage of drops (approximately 90%) below the cut-off value of 4% was the (3)-3layer cross-section (granite base combined with all Track fill for backcalculation). The cross-section with the next highest percentage of drops (approximately 83%) below the RMS error cut-off was the (2)-3layer cross-section (granite base combined with all Track fill compacted in 2006). Given their superior performance, these two cross-sections were further analyzed to isolate the optimal backcalculation cross-section.

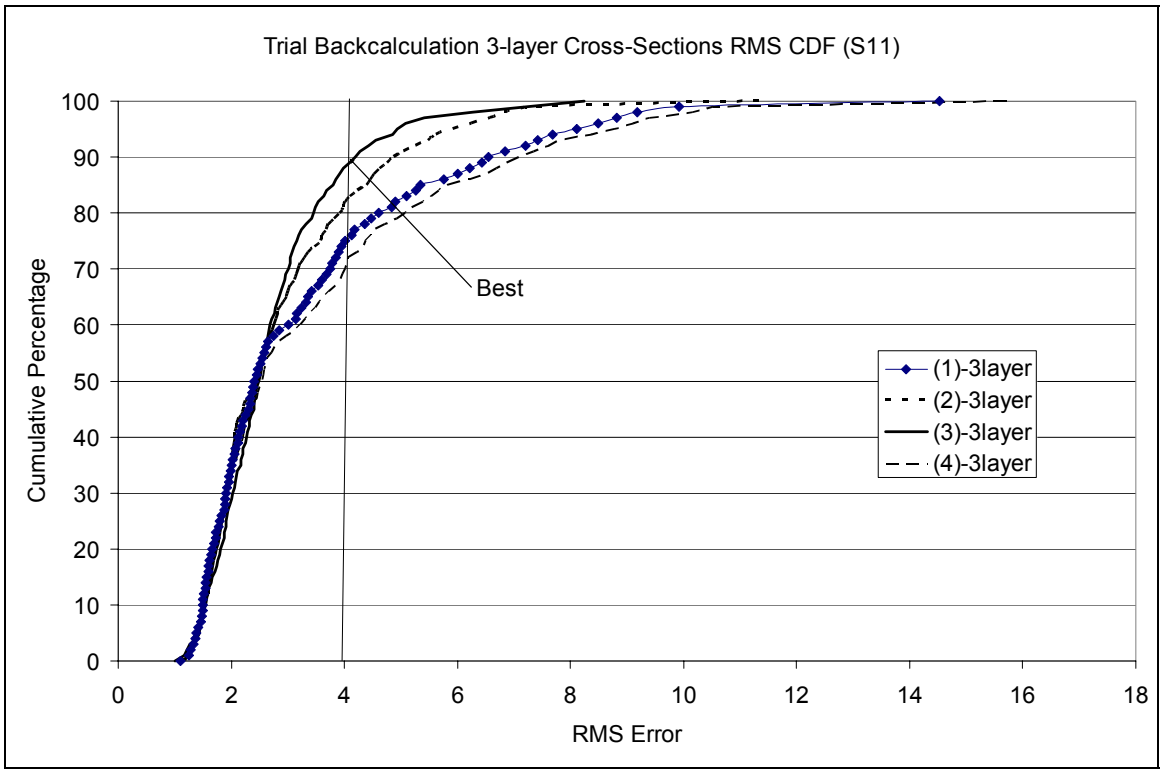


**Figure 5.63 RMS Error Cumulative Distribution Functions (CDF) for the 3-Layer Trial Backcalculation Cross-Sections in Section S11.**

Next, the backcalculated modulus behavior for the unbound materials in section S11 was analyzed for each cross-section to determine whether the modulus values were stable and reasonable. For section S11, Figures 5.64 and 5.65 show the average and standard deviations of the backcalculated base layer moduli for cross-sections (3)-3layer and (2)-3layer, respectively. The moduli shown are calculated from the 9,000 lb FWD loadings for each testing station on each testing date. The results of this analysis show that both solutions seem to generate reasonable backcalculated moduli. The modulus values for

each cross-section are relatively consistent on a given testing date, aside from some minor spatial variability. Similar average modulus fluctuation is witnessed in using both cross-sections, meaning the fluctuation is most likely more a function of spatial variability than backcalculation procedure. Both cross-sections exhibit small standard deviations for the individual testing locations under the same loading, indicating solution stability. There does not appear to be a large differential between the base moduli using the (3)-3layer and (2)-3layer cross-section, though the (3)-3layer moduli are slightly higher. Thus, the base layer moduli for both cross-sections seem to generate a stable solution.

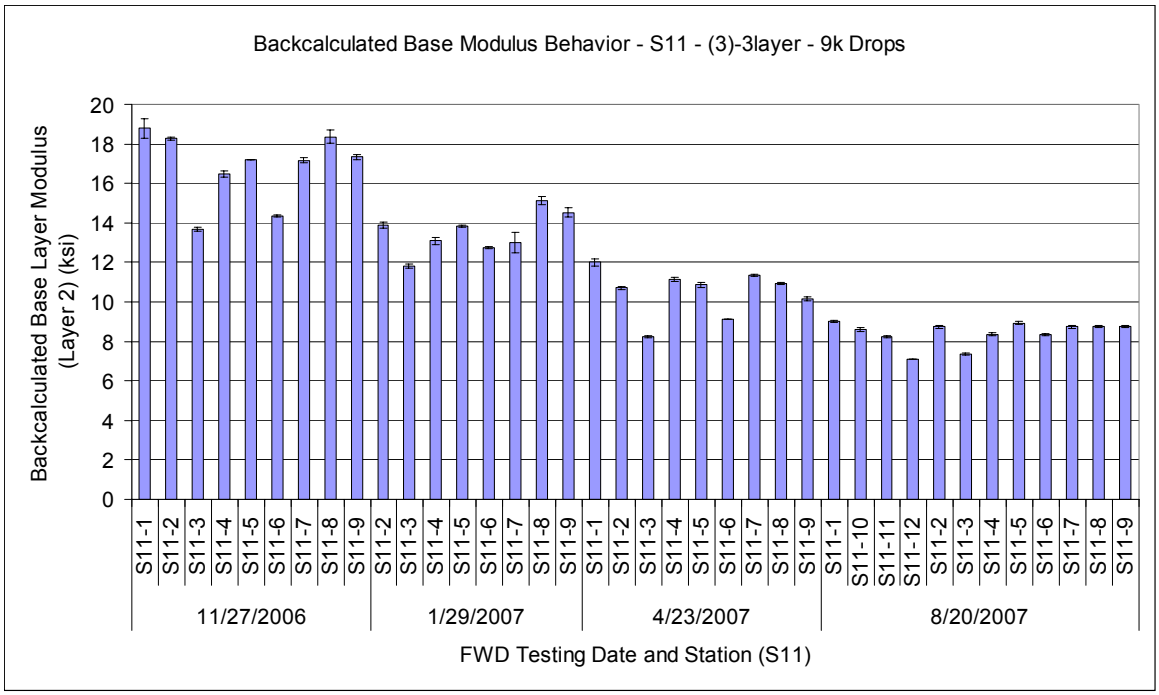


**Figure 5.64 Base Layer Modulus Behavior (Layer 2) (Section S11, (3)-3layer, All Testing Dates, All Testing Locations, 9 kip drops).**

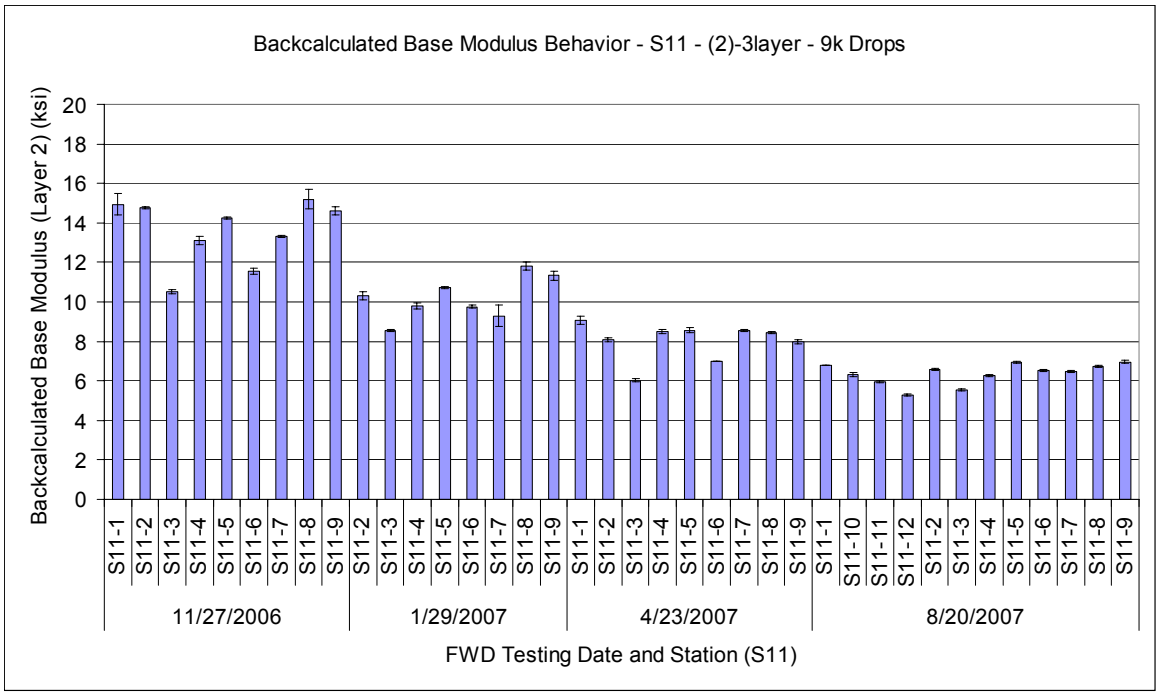


**Figure 5.65 Base Layer Modulus Behavior (Layer 2) (Section S11, (2)-3layer, All Testing Dates, All Testing Locations, 9 kip drops).**

For section S11, Figures 5.66 and 5.67 show the average and standard deviations of the backcalculated subgrade layer moduli for cross-sections (3)-3layer and (2)-3layer, respectively. The moduli shown are calculated from the 9,000 lb FWD loadings for each testing station on each testing date. The analysis for the deep layer moduli is consistent with the findings from the previously investigated structural sections. There does not appear to be a great difference between the calculated subgrade moduli between the two cross-sections. This provides further evidence of the minimal impact of base layer composition on backcalculated subgrade moduli. Also, the average modulus values are very consistent for both cross-sections, and both solutions appear to be stable.

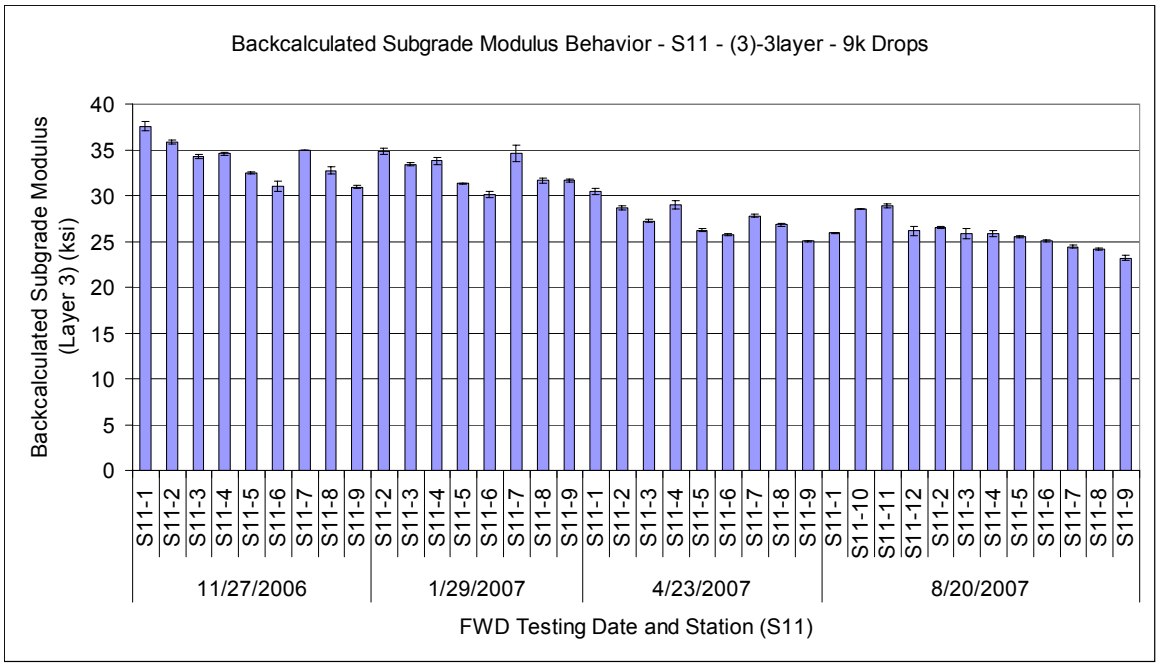


**Figure 5.66 Subgrade Layer Modulus Behavior (Layer 3) (Section S11, (3)-3layer, All Testing Dates, All Testing Locations, 9 kip drops).**

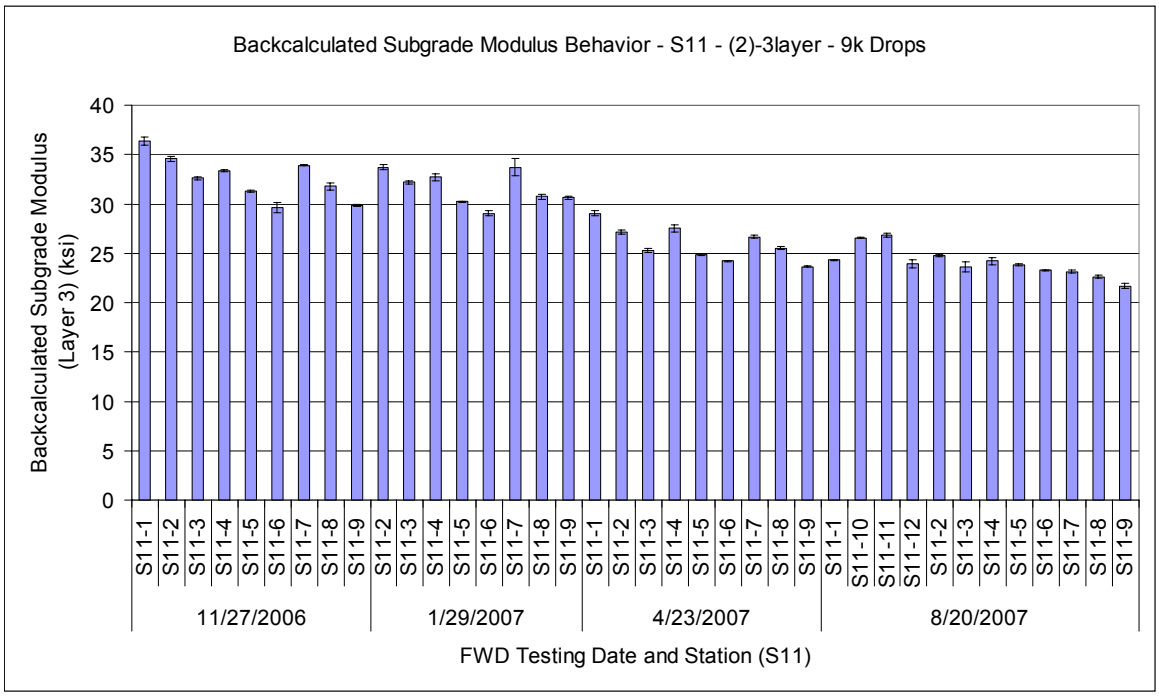


**Figure 5.67 Fill and Subgrade Layer Modulus Behavior (Layer 3) (Section S11, (2)-3layer, All Testing Dates, All Testing Locations, 9 kip drops).**

Figure 5.68 compares the backcalculated modulus values for the different pavement layers backcalculated by both the (2)-3layer and (3)-3layer cross-section. Each data point represents the average modulus for a pavement layer from a given testing station that was

backcalculated using both trial backcalculation cross-sections. The results of this analysis show that the choice of the (2)-3layer or (3)-3layer cross-section does not have a dramatic impact on the backcalculated modulus values. The base layer moduli for the (3)-3layer cross-section are slightly higher than for the (2)-3layer cross-section. The HMA moduli appear slightly higher for the (2)-3layer cross-section than for the (3)-3layer cross-section. The subgrade moduli appear relatively consistent regardless of backcalculation cross-section utilized.

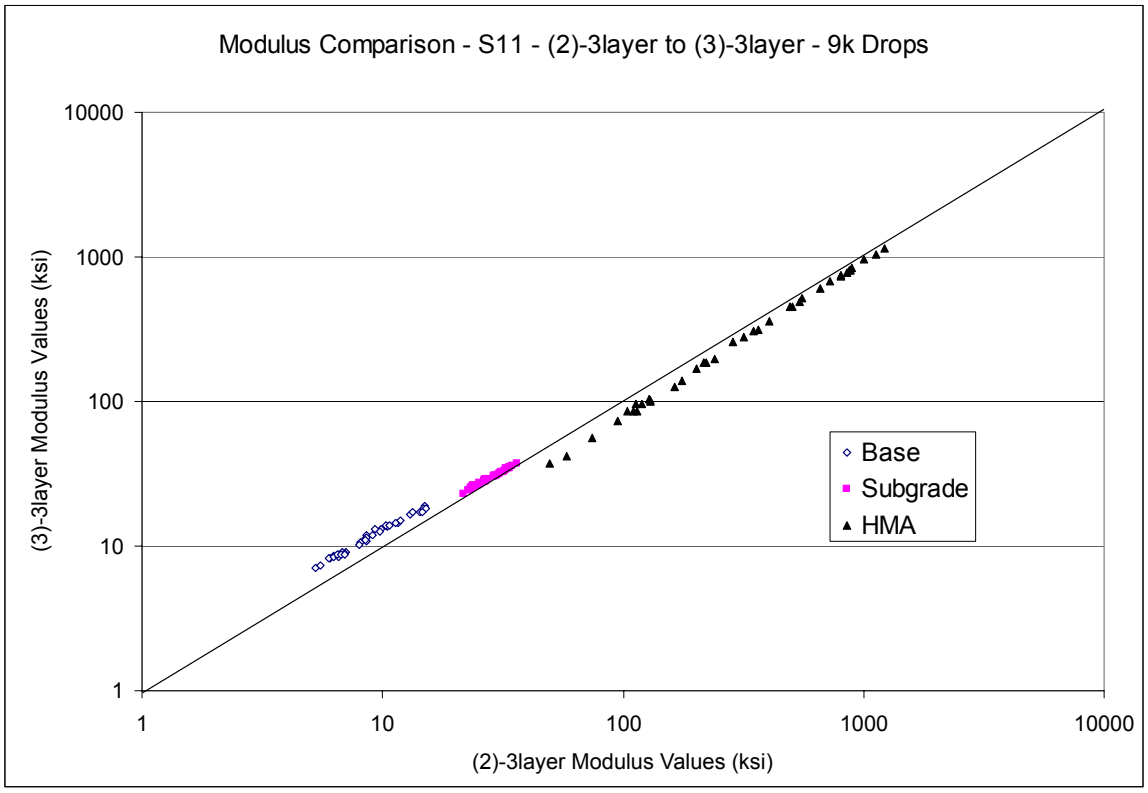


**Figure 5.68 Section S11 – Cross-Section Modulus Comparison.**

The final comparison made between the (2)-3layer and (3)-3layer cross-sections was between their measured versus predicted strain performance. Figures 5.69 and 5.70 show the measured versus predicted strain behavior for the (3)-3layer and (2)-3layer cross-sections, respectively. The data set for the (3)-3layer cross-section showed a slope that was approximately 36% below the line of unity (with predicted strains being higher than measured strains). Additionally, this data set shows a reasonable model fit for a linear trendline ($R^2$ of 0.7485). This result is in agreement with the data from the previously investigated structural sections as well as previous research conducted at the test track. The data set from the (2)-3layer cross-section has far fewer data points that are below the RMS error cut-off of 4%. Therefore, the (3)-3layer data set exhibits higher quality deflection matching than the (2)-3layer data set. Additionally, the scatter of the quality (2)-3layer data makes it such that a reasonable regression model could not be generated. Therefore, the (3)-3layer cross-section exhibits far greater measured versus predicted strain behavior than the (2)-3layer cross-section.

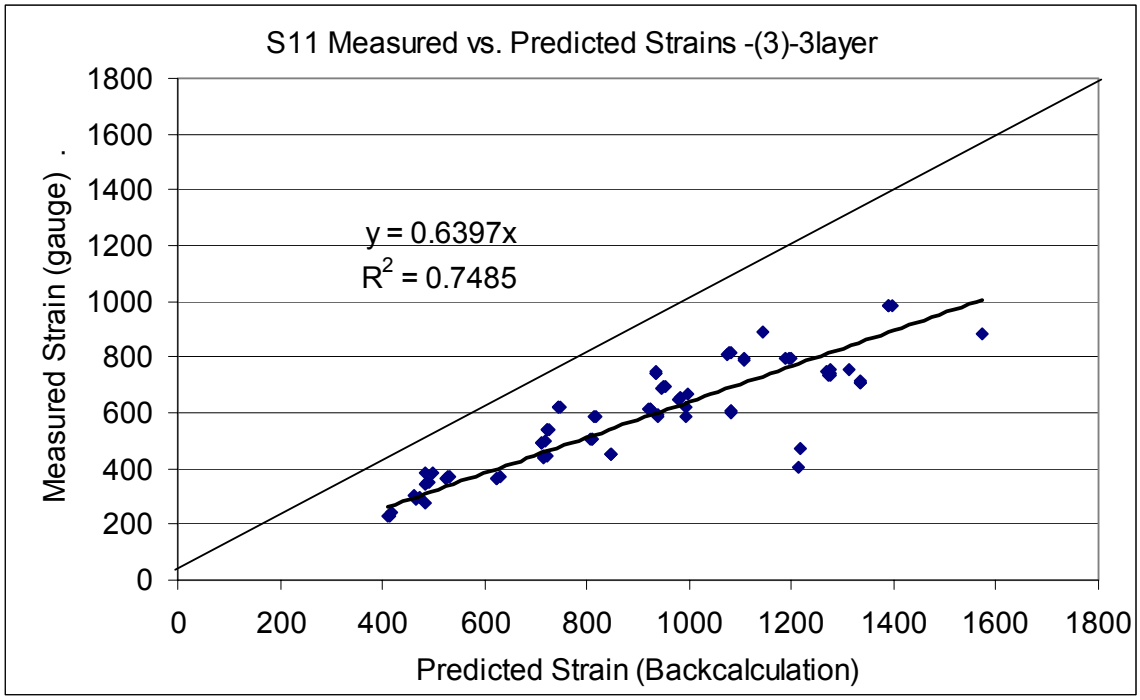


**Figure 5.69 Measured versus Predicted Strain Behavior – (3)-3layer – Section S11.**

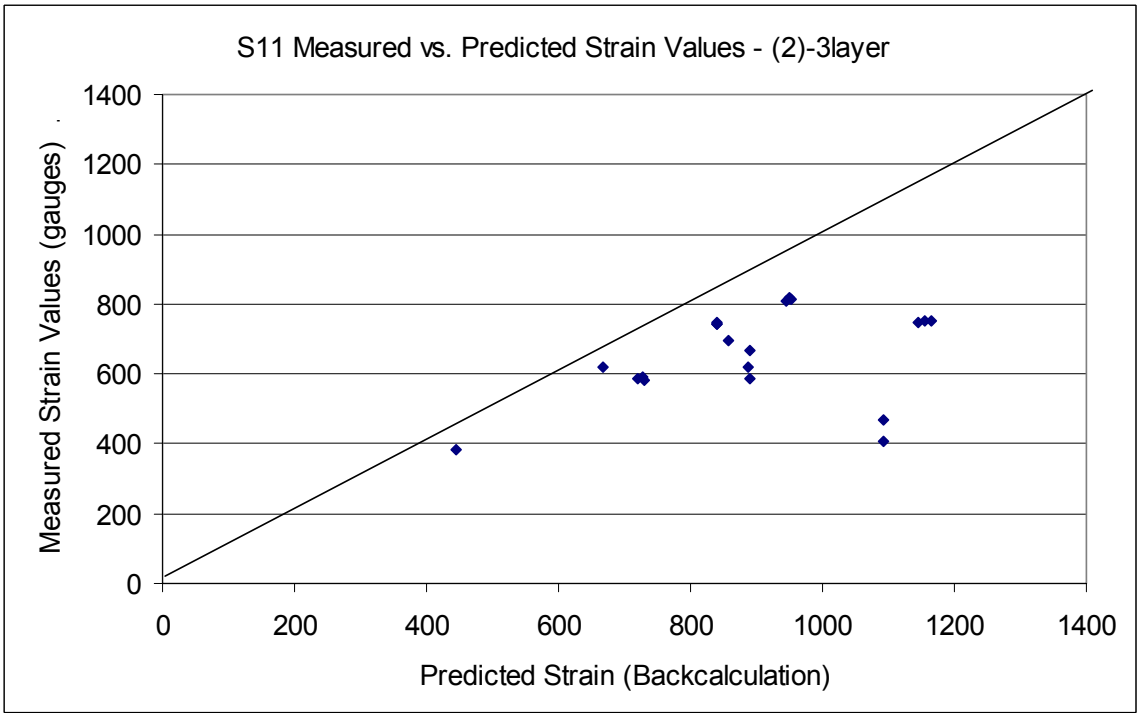


**Figure 5.70 Measured versus Predicted Strain Behavior – (2)-3layer – Section S11.**

In summary, the results of the comparisons between the (3)-3layer and (2)-3layer cross-sections show that the (3)-3layer cross-section is the preferable cross-section for backcalculation of deflection data from section S11. The (3)-3layer cross-section has

preferable RMS error behavior to the (2)-3layer cross-section, exhibiting a larger percentage of drops below the RMS error cut-off of 4%. Additionally, the (3)-3layer cross-section exhibited substantially preferable measured versus predicted strain behavior, making it the clear alternative.

The final validation of the (3)-3layer trial cross-section for section S11 was ensuring that the measured versus predicted base and fill pressures behaved reasonably. Figure 5.71 shows the measured versus predicted base pressures and Figure 5.72 shows the measured versus predicted pressures at the surface of the Track fill for section S11. For the measured versus predicted base pressure, no data was calculated that were below the RMS error cut-off of 4%. The data points in Figure 5.71 do not pass the RMS error filter, but still are within 10% of the line of unity (with predicted pressures being higher than measured pressures). This data set is different from the other structural sections, since the backcalculation seems to over-predict base pressures rather than under-predict them. However, the data still show good general agreement between measured and predicted response.

The data in Figure 5.72 show the comparison between measured and predicted pressures at the surface of the fill layer. Since the base layer for the (3)-3layer cross-section contains both the base and fill layer, the program could not calculate the output stress state at the location of the fill pressure plate. Therefore, it was necessary to use WESLEA layered-elastic analysis software to simulate the predicted pressures at the fill surface for the various FWD loadings. The results show good general agreement between measured and predicted fill pressures, with the data set being approximately 40% above the line of unity (with measured pressures being higher than predicted pressures). This result is different from those witnessed previously in the other structural sections, since the backcalculation typically over-predicts subgrade pressure and the layered-elastic analysis under-predicts the pressures for this section. However, the data set still provide a reasonable prediction of pressures at the surface of the fill. As a result, the (3)-3layer cross-section was deemed viable for backcalculation the deflection data for section S11.

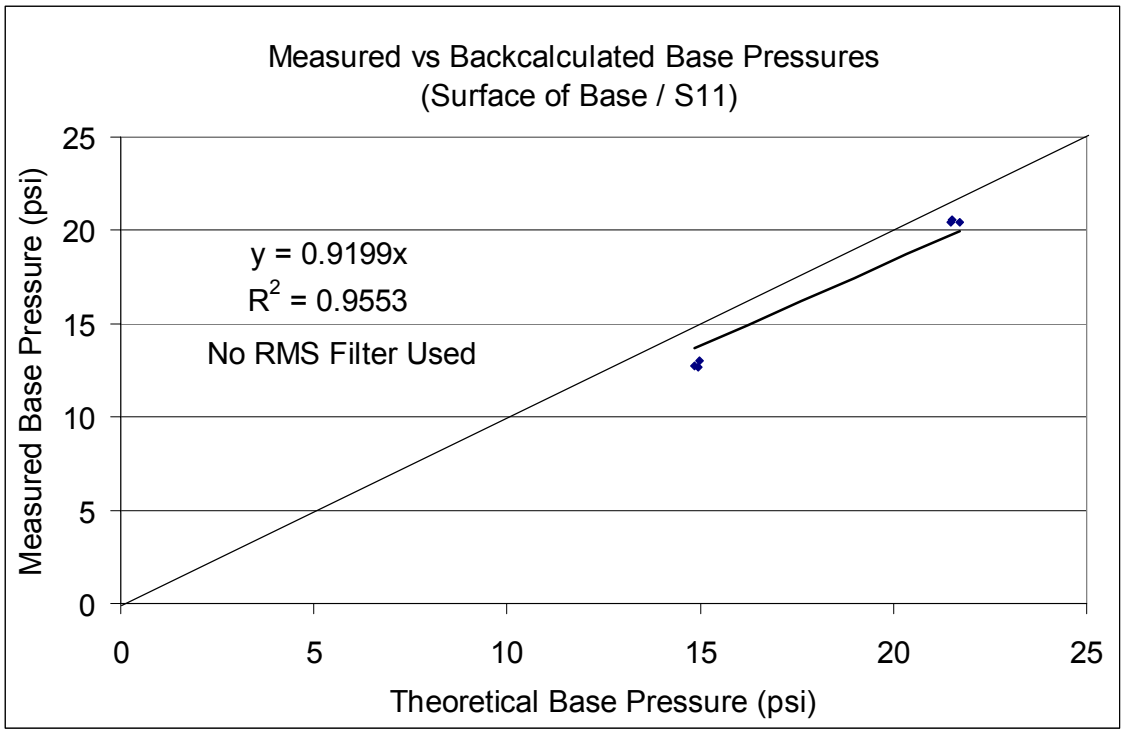


**Figure 5.71 Measured versus Predicted Base Pressure Behavior – (3)-3layer – Section S11.**

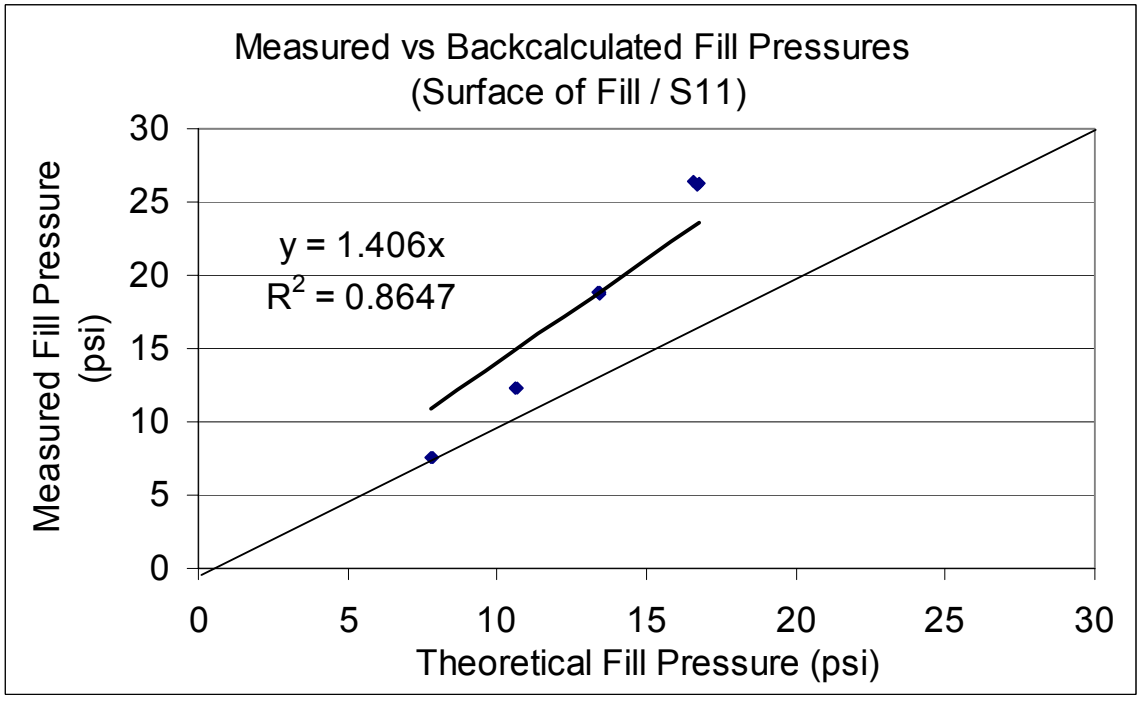


**Figure 5.72 Measured versus Predicted Fill Pressure Behavior – (3)-3layer – Section S11.**

## CONCLUDING REMARKS ON BACKCALCULATION CROSS-SECTION DETERMINATION

To generate the most accurate backcalculated pavement layer moduli, each of the eleven structural sections at the Test Track were examined to determine the optimal cross-section for backcalculation. For each structural section, four dates of FWD data were backcalculated with multiple trial backcalculation cross-sections. These results were analyzed to determine which cross-sections produced the best results in terms of: RMS error values (deflection matching), reasonable and stable backcalculated modulus values, and measured versus predicted pavement response data from FWD on gauge testing. Through this investigation, it was shown that bedrock or stiff layer effects do not seem to influence the deflection data at the Test Track. It was also shown that 3-layer pavement systems perform much better than 4-layer or 5-layer systems (possibly due to material similarities between base and fill layers). Figure 5.73 is a summary diagram of the final cross-sections selected for each of the structural sections. Given these cross-sections, backcalculation of the deflection data at the test track could then be performed with the aim of characterizing the various unbound material moduli.

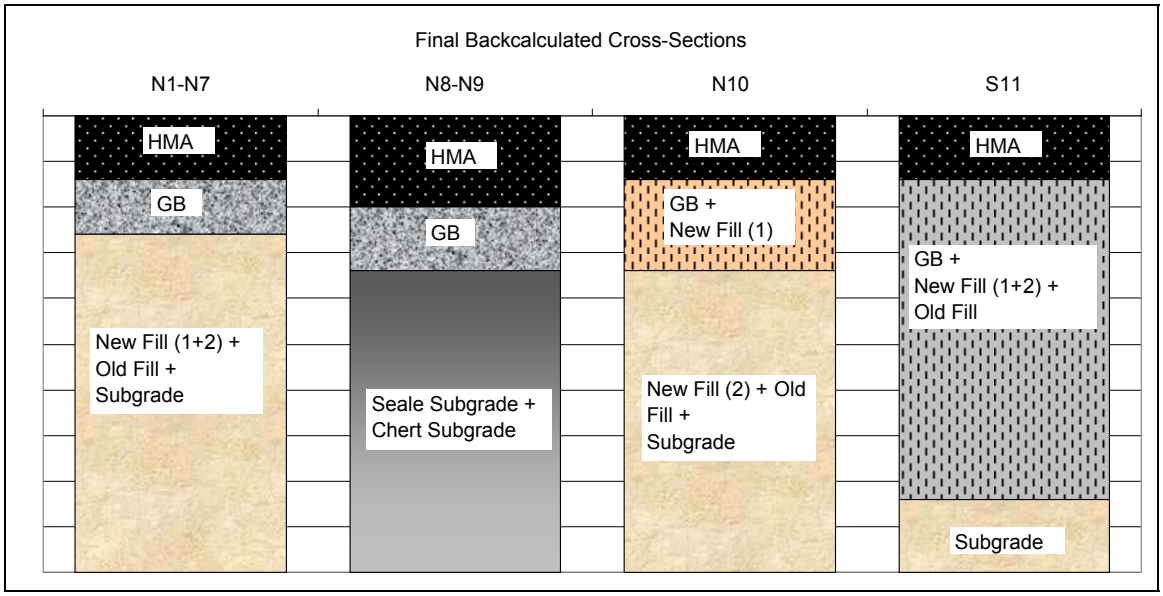


**Figure 5.73 Final Selected Backcalculation Cross-Sections.**

# CHAPTER 6 -
# FIELD CHARACTERIZATION OF UNBOUND MATERIALS

## INTRODUCTION

The structural study at the NCAT Test Track provides an excellent testing facility for in-situ characterization of unbound materials. For this study, eleven full-depth instrumented pavement test sections with a variety of structural cross-sections and construction materials were tested at regular intervals with a falling weight deflectometer (see Chapter 3 for more details regarding the FWD testing program). The FWD testing program at the Test Track was designed to capture the spatial and seasonal variability inherent to these materials. Additionally, the variable loadings employed in the FWD testing allowed for the in-situ characterization of the stress-sensitivity of the unbound materials.

For this study, deflection data collected from each of the structural sections at the Test Track were used to evaluate the stress-sensitivity of the unbound materials within those sections. The deflection data used for this study were collected over multiple dates in which a wide range of pavement temperatures was observed to capture the seasonal variability of these materials. Backcalculation was performed on the deflection data for each section using the optimal backcalculation cross-section generated for that section (see Chapter 5). For each FWD test, this process yielded both a backcalculated modulus value for each of the pavement layers as well as a comprehensive stress-state at a pre-defined location within each of the pavement layers. These layered-elastic generated stresses were then adjusted for overburden so that the true stress-state within the pavement cross-section was represented. Given this information, four commonly used stress-sensitivity models were generated and evaluated for the various unbound materials.

These stress-sensitivity models were calibrated based on data from four testing dates that encompassed a wide range of pavement temperatures and consequently wide ranging stress-states. These calibrated models were evaluated based on model-fit, the statistical significance of the regression coefficients, and on backcalculated versus predicted modulus behavior. If the selected models for each material were deemed viable, they next underwent the process of validation. This process utilized data from four other FWD testing dates (over a similar wide pavement temperature range) to generate a second database of representative pavement layer stresses and material moduli. These data were then used to determine how well the calibrated models could predict the unbound material moduli from a different data set. Additionally, the behavior of the HMA layer moduli with changing temperatures was evaluated to ensure that the backcalculated solutions were reasonable for each of the test sections.

## MODEL CALIBRATION METHODOLOGY

To generate field-calibrated non-linear stress-sensitivity models for the unbound material resilient moduli, accurate deflection data that covered multiple forms of variability (spatial, seasonal, and loading) were generated. Four dates worth of data were used for these models to generate a sufficiently large database for model calibration, and to provide stress-states and moduli in the database generated from various seasonal

conditions. The surface pavement temperatures on these dates ranged from approximately 45°F to over 130°F. These dates were also utilized in the investigation to determine the optimal backcalculation cross-section (see Chapter 5). Table 6.1 shows the testing dates utilized for this investigation as well as the structural sections in which the testing was performed. For quality control purposes, deflection basins that yielded an RMS error above 4 percent and basins that showed increasing pavement deflection with distance from the load were not analyzed.

**Table 6.1 FWD Testing Dates Used in Stress-Sensitivity Model Calibration**

| FWD Testing Date | Sections N1 and N2 | Sections N3-N10 and S11 |
|---|---|---|
| 10/30/2006 | X | |
| 11/27/2006 | X | X |
| 1/29/2007 | X | X |
| 4/23/2007 | | X |
| 8/20/2007 | X | X |

For each structural section, a database was generated containing the backcalculated pavement layer moduli and layered-elastic simulated stress-states at specified points within the different pavement layers. EVERCALC contains layered-elastic analysis software that simulates the state of stress at specified points in the pavement layers for each FWD loading. The critical location selected within EVERCALC for the different pavement layers was always the bottom of the HMA layer, the mid-depth of the granular base or base/fill layer, and the surface of the deep subgrade layer. These simulated stresses were then adjusted for overburden to represent the true state of stress within the pavement materials (adjusting these pressures for overburden will be discussed in the following section). Given this database of stresses and moduli, DATAFIT non-linear regression modeling software was utilized to fit four different stress-sensitivity models to the data set for the eleven structural sections and five unbound materials. The stress-sensitivity models utilized are shown as Equations 6-1 through 6-4 where: Equation 6-1 is referred to as the 'bulk' model, Equation 6-2 is referred to as the 'deviatoric' model, Equation 6-3 is referred to as the 'MEPDG' model, and Equation 6-4 is referred to as the 'universal' model. These models have been widely used in modeling non-linear stress-sensitivity of unbound material moduli and were described in greater detail in Chapter 2.

$$M_r = k_1 * \left( \frac{\theta}{p_a} \right)^{k_2} \tag{6-1}$$

$$M_r = k_1 * \left( \frac{\sigma_d}{p_a} \right)^{k_2} \tag{6-2}$$

$$M_r = k_1 p_a * \left( \frac{\theta}{p_a} \right)^{k_2} * \left[ \left( \frac{\tau_{oct}}{p_a} \right) + 1 \right]^{k_3} \tag{6-3}$$

$$M_r = k_1 p_a * \left(\frac{\theta}{p_a}\right)^{k_2} * \left(\frac{\sigma_d}{p_a}\right)^{k_3} \quad (6\text{-}4)$$

where: $M_r$ = Resilient Modulus
$P_a$ = Atmospheric Pressure (14.7 psi)
$\theta$ = Bulk Stress
$\sigma_d$ = Deviatoric Stress
$\tau_{oct}$ = Octahedral Shear Stress
$k_1$, $k_2$, $k_3$ = Regression Coefficients

**ADJUSTING STRESSES FOR OVERBURDEN**

To accurately quantify the state of stress at various points throughout the pavement structure, the calculated stresses must include both the effects of the loading and the stresses caused by the weight of the pavement structure above that critical point (or overburden). The simplest way to adjust these stresses for overburden is to first calculate the horizontal and vertical principal stresses caused by overburden. Then, the total horizontal principal stress was calculated by adding the horizontal principal stress induced by loading to the horizontal stress generated by overburden. The same procedure was then followed for the vertical principal stresses.

Figure 6.1 illustrates conceptually how the horizontal and vertical principal stresses were adjusted for overburden. The theory that the horizontal principal stress was related to the vertical principal stress by the multiple of an at-rest lateral earth pressure coefficient ($k_o$) was utilized (McCarthy, 2002). This coefficient is a function of the angle of internal friction ($\varphi$) for granular materials, as shown in the Equation in Step 1 of Figure 6.1. The angle of internal friction typically ranges between 30° and 50°+ for crushed stone materials (Buchanan, 2007). An angle of internal friction of 40° was assumed for this study.

The second step was to calculate a representative unit weight ($\gamma_p$) of the paving materials above the critical location. This was done by taking a weighted average (based on layer thickness) of the unit weights of the materials above the critical location (Buchanan 2007). The equation for calculating $\gamma_p$ for a critical location located at the surface of the subgrade is shown in Step 2 of Figure 6.1. Similar analysis is performed when the critical location is at the mid-depth of the base layer or there are additional unbound layers included in the pavement structure above the critical location. Next, the horizontal principal stress due to overburden ($\sigma_{3p}$) was calculated using the equation in Step 3 of Figure 6.1. Given the at-rest lateral earth pressure coefficient and the horizontal principal stress, the vertical principal stress could then be calculated given their relationship. This relationship is shown as Step 4 of Figure 6.1. Lastly, the adjusted principal stresses were calculated for each FWD loading by adding the principal stresses due to both loading and overburden in both the horizontal and vertical directions (Step 5 of Figure 6.1).

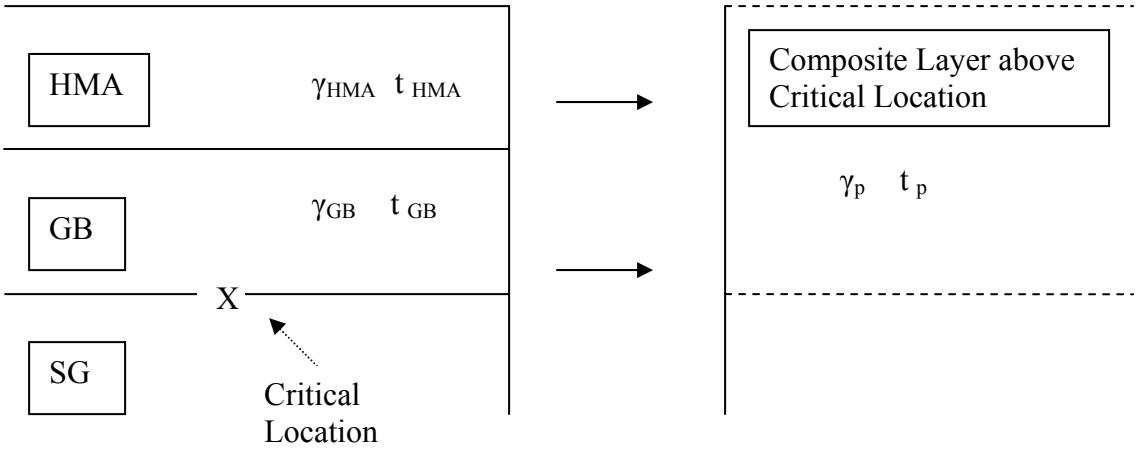


Step 1: Calculate At-Rest Earth Pressure Coefficient ($k_o$)

$$k_o = 1 - \sin\phi$$

Step 2: Calculate Representative Density of All Paving Materials above the Critical Location ($\gamma_p$)

$$\gamma_p = \frac{\gamma_{HMA}(t_{HMA}) + \gamma_{GB}(t_{GB})}{t_{HMA} + t_{GB}}$$

Step 3: Calculate At-Rest Lateral Stress at the Critical Location ($\sigma_{3p}$)

$$\sigma_{3p} = k_o[\gamma_p(t_{HMA} + t_{GB})]$$

Step 4: Calculate At-Rest Vertical Stress at the Critical Location ($\sigma_{1p}$)

$$\sigma_{1p} = \left(\frac{\sigma_{3p}}{k_o}\right)$$

Step 5: Calculate Total Principal Stresses ($\sigma_{1T}$, $\sigma_{3T}$) by Summing Loading Stresses ($\sigma_{1L}$, $\sigma_{3L}$) and Overburden Stresses ($\sigma_{1p}$, $\sigma_{3p}$)

$$\sigma_{1T} = \sigma_{1L} + \sigma_{1p}$$
$$\sigma_{3T} = \sigma_{3L} + \sigma_{3p}$$

**Figure 6.1 Methodology for Adjusting Principal Stresses to Include Overburden under Loading.**

With the horizontal and vertical principal stresses adjusted for overburden, the bulk stress, deviatoric stress, and octahedral shear stress were then calculated using Equations 6-5, 6-6, and 6-7, respectively. It should be noted that the layered-elastic analysis software within EVERCALC assumes the confining pressures in each direction to be equal (i.e. $\sigma_2 = \sigma_3$). These terms were calculated for each FWD loading using the adjusted principal stresses. These stress terms, along with the backcalculated pavement layer moduli from each FWD loading, were consolidated into a database that contained the suitable data to generate the four stress-sensitivity models for the various unbound materials at the Test Track.

$$\theta = \sigma_1 + 2(\sigma_3) \tag{6-5}$$

$$\sigma_d = \sigma_1 - \sigma_3 \tag{6-6}$$

$$\tau_{oct} = \frac{1}{3}\sqrt{(\sigma_1 - \sigma_2)^2 + (\sigma_2 - \sigma_3)^2 + (\sigma_3 - \sigma_1)^2} \tag{6-7}$$

**FIELD-CALIBRATED STRESS-SENSITIVITY MODELS**

Given a database of stress states and backcalculated moduli for each of the unbound material layers, the four stress-sensitivity models (bulk, deviatoric, MEPDG, and universal) were then generated for each structural section and each unbound material type. The first set of data evaluated was the base layer moduli. This layer is defined as the supporting unbound material layer directly below the HMA layer. The materials contained in the base layers for each section can be seen in Figure 5-73 (optimal backcalculation cross-sections) in Chapter 5.

Table 6.2 shows the field-calibrated bulk models for the base layer materials in each of the structural sections. The data sets for the structural sections with similar base materials and construction were then combined to generate field-calibrated models for similar material types. The field-calibrated bulk models for the base layer unbound materials are shown in Table 6.3. The results of this analysis clearly show a very poor model fit for the majority of the structural sections ($R^2$ below 0.25). Only one of the structural sections (S11) has an $R^2$ slightly above 0.5. This model shows a negative $k_2$ regression coefficient, indicating stress-softening behavior of the granular materials. Therefore, it can be said that the unbound materials at the Test Track do not exhibit a strong resilient modulus dependence on bulk stress alone.

It should be noted that a model was fitted to the granite base material in the 2003 structural sections that both included and excluded sections N5, N6, and N7. This was done because these sections have shown significant surface distress, and it was believed that this might negatively impact the backcalculated data from these sections. Evidence of the effect of pavement distress on the stability of the backcalculated moduli for these sections will be presented later in this chapter when the characterization of the HMA layers is discussed.

**Table 6.2 Field-Calibrated Bulk Models (Base Layer, by Section)**

| Section | $k_1$ | p-value ($k_1$) | $k_2$ | p-value ($k_2$) | $R^2$ |
|---|---|---|---|---|---|
| N1 | 10849.93 | 0 | -0.1295 | 0.1769 | 0.0046 |
| N2 | 14092.46 | 0 | -0.0859 | 0.3612 | 0.0017 |
| N3 | 5014.43 | 0 | -0.2694 | 0.0000 | 0.0542 |
| N4 | 3981.19 | 0 | -0.1977 | 0.0058 | 0.0245 |
| N5 | 1895.99 | 0 | -0.3594 | 0.0000 | 0.129 |
| N6 | 3945.88 | 0 | -0.3844 | 0.0000 | 0.1812 |
| N7 | 4784.58 | 0 | -0.3826 | 0.0000 | 0.0741 |
| N8 | 4148.11 | 0 | -0.1458 | 0.0001 | 0.0553 |
| N9 | 3332.32 | 0 | -0.1867 | 0.0000 | 0.0304 |
| N10 | 3818.78 | 0 | -0.3001 | 0.0000 | 0.0511 |
| S11 | 13955.05 | 0 | -0.5555 | 0.0000 | 0.51 |

**Table 6.3 Field-Calibrated Bulk Models (Base Layer, by Material)**

| Base Material | $k_1$ | p-value ($k_1$) | $k_2$ | p-value ($k_2$) | $R^2$ |
|---|---|---|---|---|---|
| Limerock (N1-N2) | 12602.32 | 0 | -0.0830 | 0.2335 | 0.0016 |
| Granite Base (N3-N4) | 4501.93 | 0 | -0.2080 | 0.0000 | 0.0279 |
| Granite Base (N3-N7) | 3738.83 | 0 | -0.2453 | 0.0000 | 0.0272 |
| Track Soil (N8-N9) | 3915.71 | 0 | -0.0320 | 0.2749 | 0.0023 |
| Type 5 Base + High Density Track Fill (N10) | 3818.78 | 0 | -0.3001 | 0.0000 | 0.0511 |
| Granite Base + All Track Fill (S11) | 13955.05 | 0 | -0.5555 | 0.0000 | 0.51 |

Table 6.4 shows the field-calibrated deviatoric models for the base layer materials in each of the structural sections, while Table 6.5 shows the field-calibrated deviatoric models for the different base material types. The use of this model as opposed to the bulk model does not appear to create a significant improvement in model fit. Again, the model $R^2$ are very low (below 0.25) for every structural section except S11. The model fit for S11 was improved slightly by using the deviatoric model as opposed to the bulk model. The results of this analysis seem to indicate that the single-variable stress-sensitivity models are not well-suited to model the non-linear resilient modulus behavior of the base materials at the Test Track.

**Table 6.4 Field-Calibrated Deviatoric Models (Base Layer, by Section)**

| Section | $k_1$ | p-value ($k_1$) | $k_2$ | p-value ($k_2$) | $R^2$ |
|---|---|---|---|---|---|
| N1 | 18801.00 | 0 | 0.6635 | 0.0000 | 0.1871 |
| N2 | 23955.66 | 0 | 0.7591 | 0.0000 | 0.251 |
| N3 | 5247.11 | 0 | 0.0272 | 0.6619 | 0.0006 |
| N4 | 4330.93 | 0 | 0.0446 | 0.5264 | 0.0014 |
| N5 | 1415.24 | 0 | -0.2148 | 0.0000 | 0.0474 |
| N6 | 2842.05 | 0 | -0.2408 | 0.0000 | 0.0738 |
| N7 | 4010.17 | 0 | -0.1246 | 0.0714 | 0.0086 |
| N8 | 3588.56 | 0 | -0.1165 | 0.0004 | 0.0417 |
| N9 | 2802.15 | 0 | -0.1519 | 0.0546 | 0.0178 |
| N10 | 3153.77 | 0 | -0.1761 | 0.0000 | 0.0194 |
| S11 | 10416.45 | 0 | -0.4488 | 0.0000 | 0.5222 |

**Table 6.5 Field-Calibrated Deviatoric Models (Base Layer, by Material)**

| Base Material | $k_1$ | p-value ($k_1$) | $k_2$ | p-value ($k_2$) | $R^2$ |
|---|---|---|---|---|---|
| Limerock (N1-N2) | 22529.61 | 0 | 0.7718 | 0.0000 | 0.2397 |
| Granite Base (N3-N4) | 5099.15 | 0 | 0.0815 | 0.0859 | 0.0049 |
| Granite Base (N3-N7) | 4082.50 | 0 | 0.0596 | 0.0697 | 0.0018 |
| Track Soil (N8-N9) | 3848.15 | 0 | -0.0165 | 0.5572 | 0.0007 |
| Type 5 Base + High Density Track Fill (N10) | 3153.77 | 0 | -0.1761 | 0.0000 | 0.0194 |
| Granite Base + All Track Fill (S11) | 10416.45 | 0 | -0.4488 | 0.0000 | 0.5222 |

Table 6.6 shows the field-calibrated MEPDG models for the base layer materials in the individual structural sections while Table 6.7 shows the field-calibrated MEPDG models for the various base layer material types. The model $R^2$ for this model show a significant improvement over those generated using the single-variable stress-sensitivity models for the majority of the structural sections. However, sections N8, N9, and N10 still exhibit very poor model $R^2$, even with the more complex stress-sensitivity model. For section S11, the use of the MEPDG model does not show a significant increase in model fit over the single-variable stress-sensitivity models.

It should be noted that the regression analysis using this model type yielded a negative $k_2$ coefficient and a positive $k_3$ coefficient. These are the opposite sign coefficients that were seen in literature for materials tested in the laboratory with stress-sensitivity modeled using the MEPDG model. This indicates the materials in the field are exhibiting a stress-softening behavior under increased loading in the field. A more detailed comparison of the laboratory and field data is provided in Chapter 7.

**Table 6.6 Field-Calibrated MEPDG Models (Base Layer, by Section)**

| Section | $k_1$ | p-value ($k_1$) | $k_2$ | p-value ($k_2$) | $k_3$ | p-value ($k_3$) | $R^2$ |
|---|---|---|---|---|---|---|---|
| N1 | 59.46 | 0 | -2.6368 | 0 | 13.7026 | 0 | 0.8105 |
| N2 | 177.05 | 0 | -2.0015 | 0 | 8.5716 | 0 | 0.7123 |
| N3 | 38.70 | 0 | -2.1936 | 0 | 16.1940 | 0 | 0.4803 |
| N4 | 28.97 | 0 | -2.0812 | 0 | 17.8533 | 0 | 0.3132 |
| N5 | 38.88 | 0 | -1.4136 | 0 | 10.3392 | 0 | 0.3367 |
| N6 | 72.30 | 0 | -1.5950 | 0 | 10.7520 | 0 | 0.4147 |
| N7 | 56.25 | 0 | -2.0166 | 0 | 14.1733 | 0 | 0.2642 |
| N8 | 242.57 | 0 | -0.2830 | 0.01895 | 1.1042 | 0.22919 | 0.0599 |
| N9 | 133.25 | 0.0296 | -0.5125 | 0.07541 | 4.5461 | 0.24367 | 0.0365 |
| N10 | 34.55 | 0.00107 | -1.8687 | 0 | 14.8570 | 0 | 0.1583 |
| S11 | 1416.18 | 0 | -0.0254 | 0.78748 | -1.7371 | 0 | 0.5487 |

**Table 6.7 Field-Calibrated MEPDG Models (Base Layer, by Material)**

| Base Material | $k_1$ | p-value ($k_1$) | $k_2$ | p-value ($k_2$) | $k_3$ | p-value ($k_3$) | $R^2$ |
|---|---|---|---|---|---|---|---|
| Limerock (N1-N2) | 151.07 | 0 | -2.0306 | 0 | 9.1537 | 0 | 0.7109 |
| Granite Base (N3-N4) | 34.29 | 0 | -2.1330 | 0 | 16.7861 | 0 | 0.4079 |
| Granite Base (N3-N7) | 34.82 | 0 | -2.0703 | 0 | 15.9938 | 0 | 0.2894 |
| Track Soil (N8-N9) | 229.46 | 0 | -0.1557 | 0 | 1.0890 | 0 | 0.0058 |
| Type 5 Base + High Density Track Fill (N10) | 34.55 | 0.0011 | -1.8687 | 0 | 14.8570 | 0 | 0.1583 |
| Granite Base + All Track Fill (S11) | 1416.2 | 0 | -0.0254 | 0.7875 | -1.7371 | 0 | 0.5487 |

Table 6.8 shows the field-calibrated universal models for the base layer materials in the individual structural sections while Table 6.9 shows the field-calibrated universal models for the various base layer material types. Again, the multi-variable constitutive models show considerably higher model $R^2$ values than those of the single-variable models. This model provides a much higher model $R^2$ for the Granite base material, raising the $R^2$

values for the material from sections N3 and N4 from approximately 0.41 (for the MEPDG model) to 0.67. It is also evident that the materials in sections N8, N9, and N10 appear to exhibit low $R^2$ values regardless of the model used. These sections either had the Track soil material utilized as the base layer material (as in N8 and N9) or combined with base layer material for the purposes of backcalculation (as in N10). Given the laboratory data that suggest the relative lack of stress-sensitivity for this material, it was expected that the Track soil material in the field should exhibit poor stress-sensitivity as well. Also, section S11 exhibits an $R^2$ value that is roughly equivalent to that generated by all the other models.

**Table 6.8 Field-Calibrated Universal Models (Base Layer, by Section)**

| Section | $k_1$ | p-value ($k_1$) | $k_2$ | p-value ($k_2$) | $k_3$ | p-value ($k_3$) | $R^2$ |
|---|---|---|---|---|---|---|---|
| N1 | 6072.58 | 0 | -2.4302 | 0 | 2.2810 | 0 | 0.8946 |
| N2 | 4362.92 | 0 | -1.9681 | 0 | 1.7683 | 0 | 0.8056 |
| N3 | 8073.68 | 0 | -2.8735 | 0 | 2.5307 | 0 | 0.7294 |
| N4 | 17453.77 | 0 | -3.3873 | 0 | 3.1751 | 0 | 0.5782 |
| N5 | 3225.82 | 0 | -2.6639 | 0 | 2.2766 | 0 | 0.4937 |
| N6 | 6030.31 | 0 | -2.6951 | 0 | 2.3001 | 0 | 0.6002 |
| N7 | 19564.05 | 0 | -3.4962 | 0 | 3.0770 | 0 | 0.5383 |
| N8 | 634.20 | 0.00004 | -0.8430 | 0.00007 | 0.6495 | 0.0008 | 0.0875 |
| N9 | 1022.34 | 0.04136 | -1.2621 | 0.00037 | 1.1681 | 0.00215 | 0.0694 |
| N10 | 8243.90 | 0.00251 | -3.1639 | 0 | 2.8650 | 0 | 0.2542 |
| S11 | 769.73 | 0 | -0.1598 | 0.17916 | -0.3246 | 0.0008 | 0.5244 |

**Table 6.9 Field-Calibrated Universal Models (Base Layer, by Material)**

| Base Material | $k_1$ | p-value ($k_1$) | $k_2$ | p-value ($k_2$) | $k_3$ | p-value ($k_3$) | $R^2$ |
|---|---|---|---|---|---|---|---|
| Limerock (N1-N2) | 4621.71 | 0 | -2.0788 | 0 | 1.8908 | 0 | 0.8266 |
| Granite Base (N3-N4) | 10465.42 | 0 | -3.0449 | 0 | 2.7613 | 0 | 0.6742 |
| Granite Base (N3-N7) | 14380.51 | 0 | -3.3340 | 0 | 3.0202 | 0 | 0.5603 |
| Track Soil (N8-N9) | 576.16 | 0.00001 | -0.6687 | 0.00026 | 0.6202 | 0.0004 | 0.0237 |
| Type 5 Base + High Density Track Fill (N10) | 8243.90 | 0.00251 | -3.1639 | 0 | 2.8650 | 0 | 0.2542 |
| Granite Base + All Track Fill (S11) | 769.73 | 0 | -0.1598 | 0.17916 | -0.3246 | 0.0008 | 0.5244 |

Figure 6.2 shows a summary of the model $R^2$ values for the four constitutive models for the base layer materials used in the eleven structural sections. Figure 6.3 shows the model $R^2$ summary for the various base material types. In evaluating the goodness-of-fit for the various models, both figures indicate that the universal model provides the highest model $R^2$ for the field stress and modulus data. Also, these figures illustrate the superiority of the multiple-variable models versus the single-variable models in terms of model fit for the base layer materials.

The universal model seems to provide the best fit for both the limerock and the granite base materials. This model generates $R^2$ values of 0.83 and 0.67, respectively, for the two material types. These models were deemed high quality considering the vast amount of data generated across four days of testing in addition to the large amount of spatial and seasonal variability generated within the data set. Figure 6.3 also illustrates the poor model fit exhibited by all four models for the Track soil base and combined Type 5 base and Track fill materials. This was expected given the relative stress-insensitivity of the Track soil material in laboratory testing. The combined granite and Track fill in section S11 seems to generate approximately the same model $R^2$ regardless of model used.

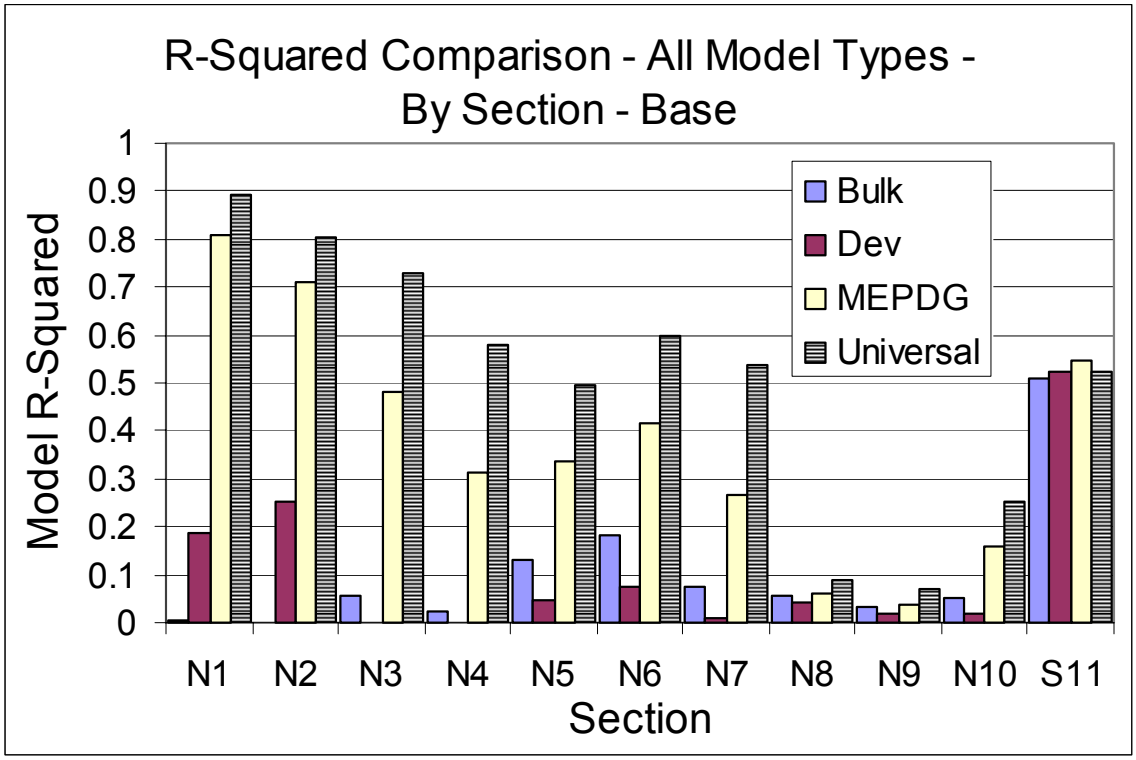


**Figure 6.2 Model R-Squared Summary (Base Layer, by Section).**

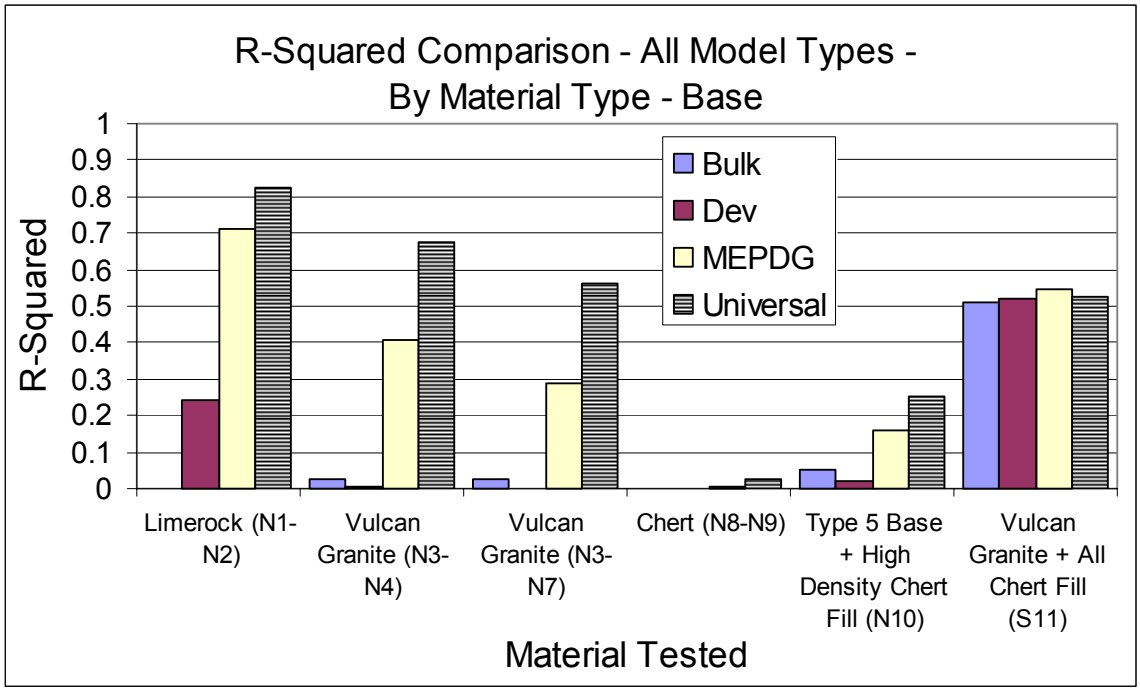


**Figure 6.3 Model R-Squared Summary (Base Layer, by Material).**

The next step in the process was to evaluate the measured versus predicted resilient modulus values for each base material type using the most appropriate constitutive model. The models that exhibited reasonable $R^2$ values, statistically significant regression coefficients, and good agreement between measured and predicted resilient moduli were deemed acceptable. The materials with models that did not meet the criteria of acceptability were deemed non stress-sensitive. An average and standard deviation of the field-calculated moduli for these materials were reported in lieu of a stress-sensitivity model.

For the limerock base material (sections N1 and N2), Figure 6.3 shows that the universal constitutive model provided the highest model $R^2$ for this data set. Table 6.9 shows that each of the regression coefficients for this model were statistically significant (p-values less than 0.05). Next, the actual backcalculated moduli from this data set were plotted against the modulus values predicted using the field-calibrated model as illustrated in Figure 6.4. This figure shows that the data points for this model seem to track closely to the line of unity (representing the condition where the measured moduli equal the model predicted moduli). As a result, the universal model was deemed suitable for modeling the stress-sensitivity of the limerock base material in the field. This model will be further validated later in this chapter.

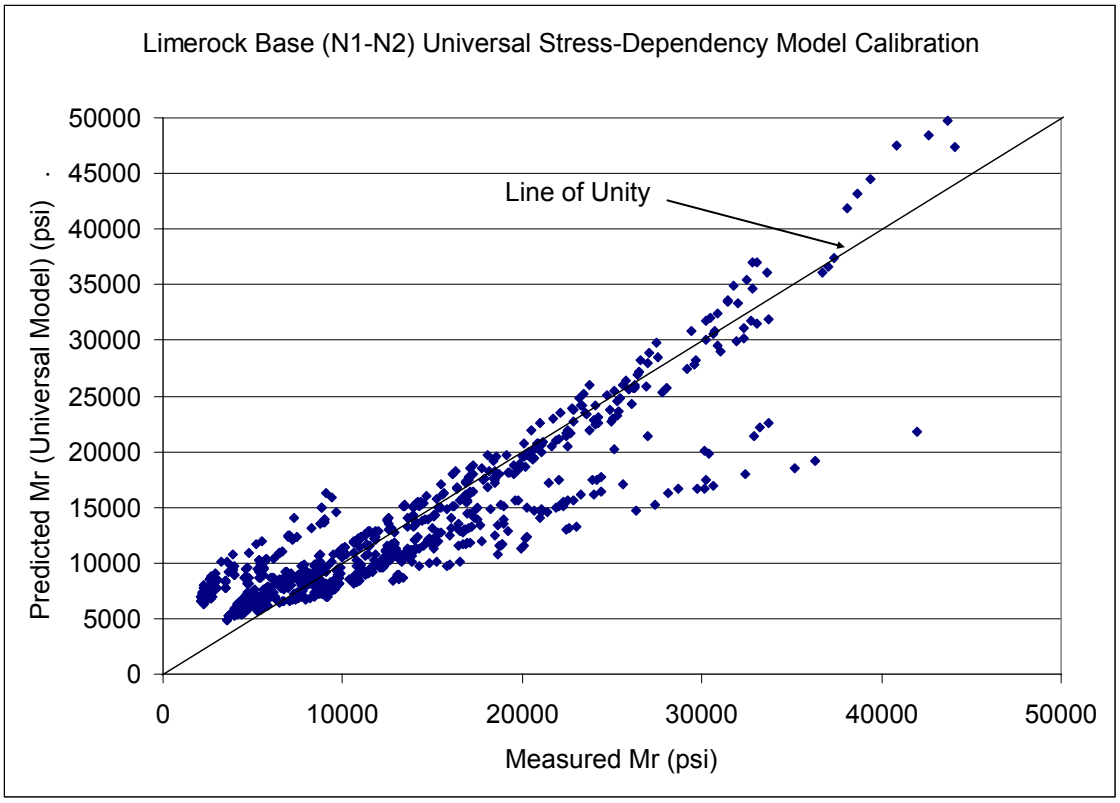


**Figure 6.4 Limerock Base Material Universal Model Calibration Data.**

For the granite base material (sections N3 and N4), Figure 6.3 shows that the universal constitutive model provided the highest model $R^2$ for this data set. Table 6.9 shows that each of the regression coefficients for this model were statistically significant (p-values less than 0.05). Figure 6.3 also shows that the $R^2$ value for the model generated from sections N3 and N4 was higher than that of a model containing all the data from sections N3 through N7. Given the large amounts of surface distresses present in sections N5, N6, and N7, there was much greater confidence in the backcalculated data from sections N3 and N4, which have exhibited no significant distresses. Figure 6.5 shows the plot of the backcalculated moduli versus the moduli generated using the predictive equation. The data in this figure seem to track along the line of unity reasonably well, indicating the suitability of the universal model for predicting the moduli of the granite base in the field given accurate knowledge of the material stress-state. This model will be further validated later in this chapter.

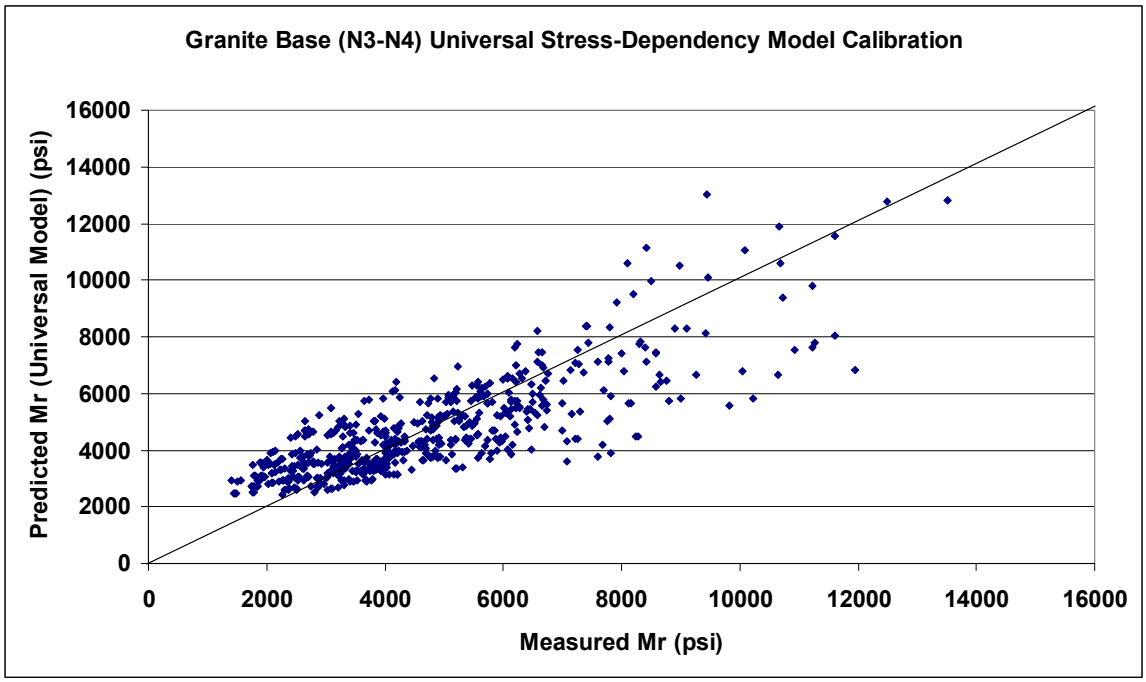


**Figure 6.5 Granite Base Material Universal Model Calibration Data.**

The results of the model generation process indicated that no 'good' model existed to model the stress-sensitivity of the Track soil base material for sections N8 and N9 in the field. Figure 6.3 indicated that the universal model gave the highest $R^2$ value of any of the model types (approximately 0.02). Figure 6.6 illustrates the measured versus predicted moduli for the Track soil base data using this model. As expected, the model does not appear to be viable, as the measured and predicted moduli only appear to cross the line of unity at approximately 4,000 psi. Therefore, this material was deemed insensitive to changing stress-state. An average modulus of 3,942 psi and standard deviation of 1,109 psi were generated in the field for the entirety of the Track soil base data set.

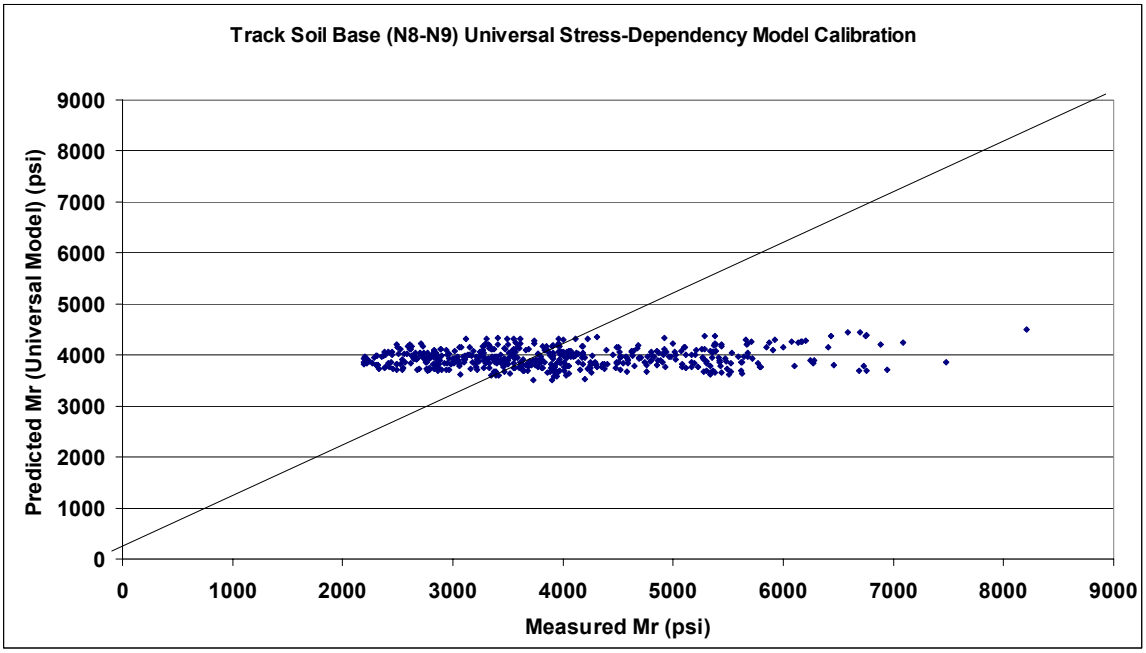


**Figure 6.6 Track Soil Base Material Universal Model Calibration Data.**

For section N10, the combination of the Type 5 base and Track fill as a composite base layer did not show strong stress-sensitivity with any of the generated models. Figure 6.3 indicated that the universal model gave the highest $R^2$ value of any of the model types (approximately 0.25). Figure 6.7 illustrates the measured versus predicted moduli for the Track soil base data using this model. This figure shows a large amount of scatter in the data set, with poor agreement between the measured and predicted moduli using the field-calibrated universal model. Hence, no substantial stress-sensitivity was witnessed for the composite base layer in section N10. This was expected given the inclusion of the Track fill material in this base layer. An average modulus of 4,022 psi and standard deviation of 1,746 psi were calculated from the base modulus data generated in section N10.

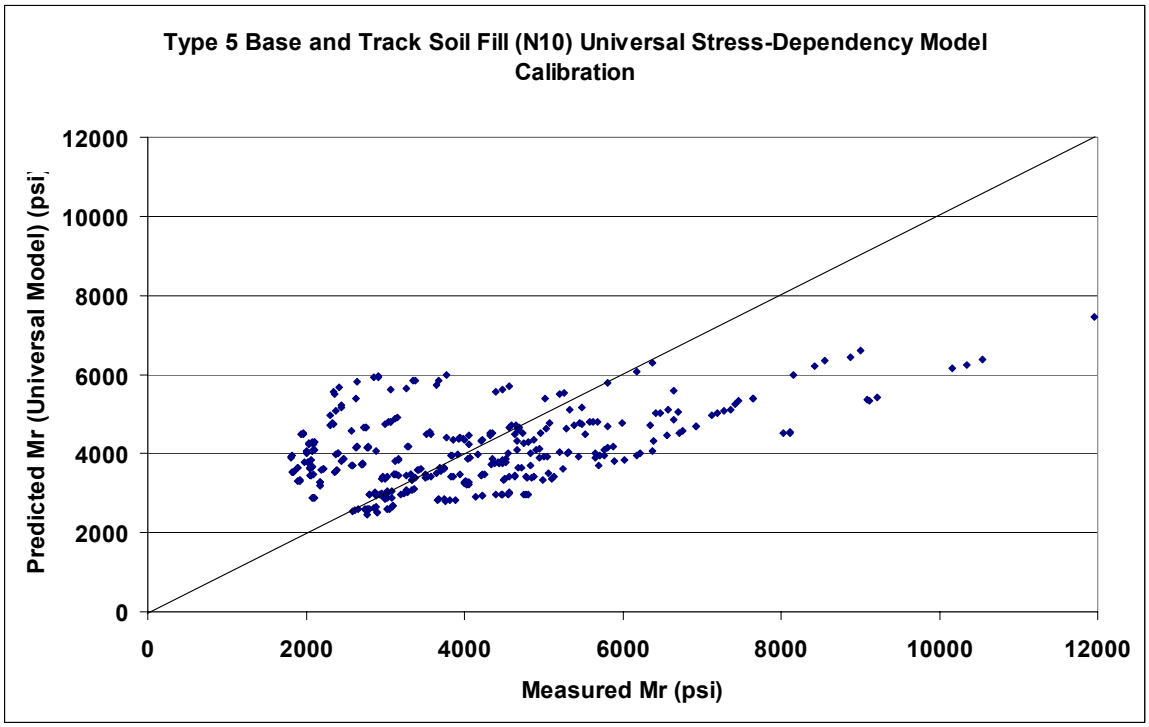


**Figure 6.7 Type 5 Base and Track Fill Material Universal Model Calibration Data.**

In section S11, the four stress-sensitivity models exhibited relatively similar model $R^2$ values (see Figure 6.3). However, analysis of Table 6.9 shows that the two multi-variable stress-sensitivity models exhibited statistically insignificant $k_2$ coefficients (effects of bulk stress). Therefore, the deviatoric model was selected because it had the highest $R^2$ value of the single-variable constitutive models (approximately 0.52). Figure 6.8 shows the measured versus predicted moduli for the S11 data set. The figure shows that the data set tends to follow the line of unity, albeit with considerable scatter. Thus, given the $R^2$ value above 0.5, statistically significant regression coefficients, and practical measured versus predicted modulus behavior using the deviatoric model, this model was deemed suitable to predict the backcalculated moduli in S11 and will be validated later in this chapter.

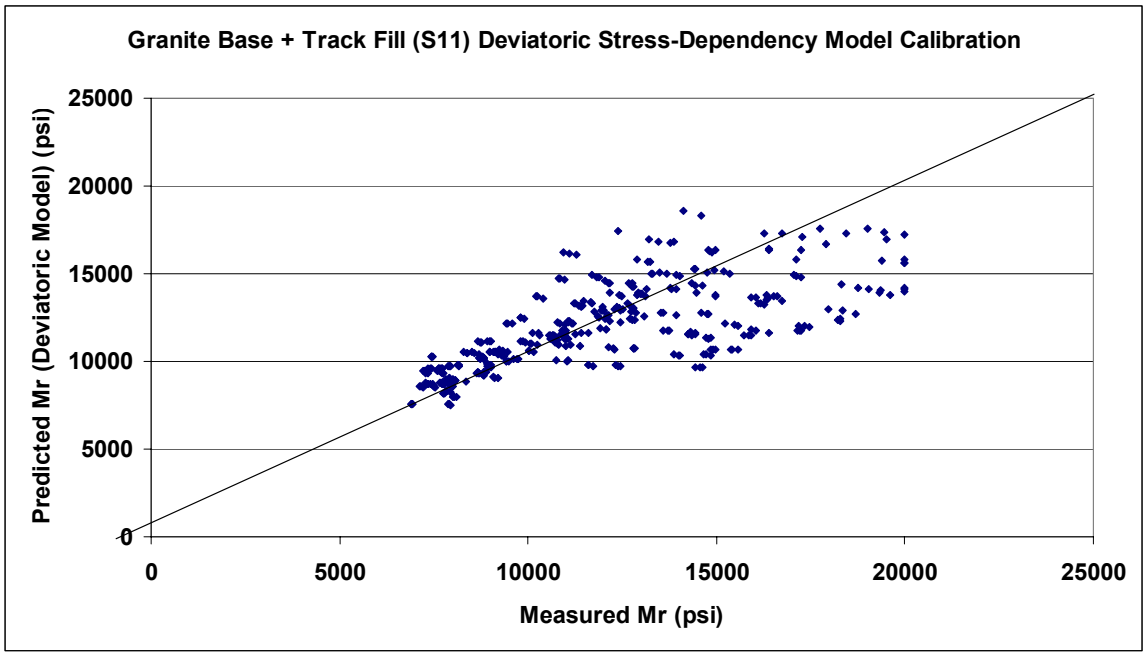


**Figure 6.8 Granite Base and Track Fill Material Deviatoric Model Calibration Data.**

The next task was the calibration of stress-sensitivity models for the deep subgrade moduli. This layer is defined as semi-infinite unbound material layer directly below the granular base layer. This layer consists of the Track soil material for sections N1 through N7, N10, and S11. The subgrade layer in sections N8 and N9 is a composite layer of the Seale subgrade and the Track subgrade material.

Table 6.10 shows the field-calibrated bulk models for the subgrade layer materials in each of the structural sections. Table 6.11 shows the field-calibrated bulk models that are delineated by material type and test section. To generate a material-specific model for the Track soil base material, several combinations of the data sets were utilized to generate the best model fit. This was done because the different cross-sections at the Test Track have this material at various depths. For example, in section S11 the Track soil material was approximately 42 inches below the surface of the pavement while in N1 and N2 this material was only 17 inches below the surface of the pavement. Additionally, this material was used as a fill layer and deep subgrade in several of the backcalculation cross-sections (i.e. sections N1 and N2), but only as a deep subgrade in others (i.e., section S11). Therefore, multiple combinations of structural section data were utilized to determine the best data set for use with the Track soil material. Sections N8 and N9 were combined for analysis due to them having the same combination of Track soil and Seale subgrade material.

**Table 6.10 Field-Calibrated Bulk Models (Subgrade Layer, by Section)**

| Section | $k_1$ | p-value ($k_1$) | $k_2$ | p-value ($k_2$) | $R^2$ |
|---|---|---|---|---|---|
| N1 | 35851.03 | 0 | -0.1733 | 0 | 0.1053 |
| N2 | 34234.47 | 0 | -0.1774 | 0 | 0.1303 |
| N3 | 31331.23 | 0 | -0.2729 | 0 | 0.4194 |
| N4 | 29456.53 | 0 | -0.2277 | 0 | 0.286 |
| N5 | 26134.22 | 0 | -0.3686 | 0 | 0.2424 |
| N6 | 32842.07 | 0 | -0.2923 | 0 | 0.6117 |
| N7 | 34879.85 | 0 | -0.1988 | 0 | 0.2785 |
| N8 | 28763.22 | 0 | -0.3682 | 0 | 0.4676 |
| N9 | 38621.45 | 0 | -0.3937 | 0 | 0.2483 |
| N10 | 40929.37 | 0 | -0.3338 | 0 | 0.3395 |
| S11 | 18101.98 | 0 | -0.5998 | 0 | 0.4412 |

**Table 6.11 Field-Calibrated Bulk Models (Subgrade Layer, by Material)**

| Subgrade Material | Sections | $k_1$ | p-value ($k_1$) | $k_2$ | p-value ($k_2$) | $R^2$ |
|---|---|---|---|---|---|---|
| Track Soil | N1-N7, N10, S11 | 32655.5826 | 0 | -0.132881 | 0 | 0.0563 |
| Track Soil | N1-N7, N10 | 32940.1429 | 0 | -0.283376 | 0 | 0.1922 |
| Track Soil | N1-N7 | 31956.2866 | 0 | -0.242144 | 0 | 0.1791 |
| Track Soil | N1-N4 | 33024.4311 | 0 | -0.208355 | 0 | 0.1576 |
| Track Soil | N1-N2 | 34972.2782 | 0 | -0.1746 | 0 | 0.1147 |
| Seale/Track Soil | N8-N9 | 31329.3174 | 0 | -0.5759 | 0 | 0.489 |

The results in Table 6.10 show that the bulk stress model does not have very good model $R^2$ values for any of the structural sections. The only section with a model $R^2$ above 0.5 is section N6. This was to be expected since previous testing has shown little stress-sensitivity with the Track soil material. For sections N8 and N9, where the combination of the Track soil with the Seale subgrade material was thought might increase stress-sensitivity, no significant stress-sensitivity was evident. This is likely due to the Seale subgrade being more dependent on deviatoric stress than bulk stress, given its finer gradation. Table 6.11 shows that no combination of Track soil data sets yields an $R^2$ above 0.2 for the bulk stress model. Additionally, the combined Seale and Track soil material did not yield significant stress-sensitivity with the bulk model.

Table 6.12 shows the field-calibrated deviatoric models for each of the structural sections for the subgrade material. Table 6.13 shows the deviatoric models that were generated based on subgrade material type. Again, the results do not seem to show particularly strong stress-sensitivity among any one of the structural sections, though a handful of sections exhibit an $R^2$ above 0.5. For the material-specific model for the composite Seale and Track soil layer, the deviatoric model offered an improvement in model fit over the

bulk model, raising the $R^2$ from 0.49 to 0.6. This was expected given the applicability of the deviatoric model to more fine-grained soils (such as the Seale material).

**Table 6.12 Field-Calibrated Deviatoric Models (Subgrade Layer, by Section)**

| Section | $k_1$ | p-value ($k_1$) | $k_2$ | p-value ($k_2$) | $R^2$ |
|---|---|---|---|---|---|
| N1 | 37650.43 | 0 | 0.0208 | 0.34577 | 0.0023 |
| N2 | 35150.49 | 0 | -0.0028 | 0.88002 | 0.0001 |
| N3 | 22893.26 | 0 | -0.2671 | 0 | 0.5006 |
| N4 | 23856.33 | 0 | -0.1753 | 0 | 0.1955 |
| N5 | 12615.25 | 0 | -0.4988 | 0 | 0.4819 |
| N6 | 23221.16 | 0 | -0.2665 | 0 | 0.5434 |
| N7 | 29212.45 | 0 | -0.1388 | 0 | 0.151 |
| N8 | 19018.22 | 0 | -0.3605 | 0 | 0.5919 |
| N9 | 17288.28 | 0 | -0.5888 | 0 | 0.5064 |
| N10 | 28344.63 | 0 | -0.3190 | 0 | 0.3252 |
| S11 | 14626.95 | 0 | -0.4818 | 0 | 0.5484 |

**Table 6.13 Field-Calibrated Deviatoric Models (Subgrade Layer, by Material)**

| Subgrade Material | Sections | $k_1$ | p-value ($k_1$) | $k_2$ | p-value ($k_2$) | $R^2$ |
|---|---|---|---|---|---|---|
| Track Soil | N1-N7, N10, S11 | 29357.75 | 0 | -0.1020 | 0 | 0.0307 |
| Track Soil | N1-N7, N10 | 30002.40 | 0 | -0.1001 | 0 | 0.0326 |
| Track Soil | N1-N7 | 30703.65 | 0 | -0.0520 | 0 | 0.0115 |
| Track Soil | N1-N4 | 34096.22 | 0 | 0.0002 | 0.98539 | 0 |
| Track Soil | N1-N2 | 36098.36 | 0 | 0.0036 | 0.80359 | 0.0001 |
| Seale/Track Soil | N8-N9 | 15602.60 | 0 | -0.5890 | 0 | 0.6004 |

Table 6.14 shows the field-calibrated MEPDG models for each of the structural sections for the subgrade material. Table 6.15 shows the MEPDG models that were generated based on subgrade material type. These models tend to show some improvement in terms of model fit over the single-variable models. However, this improvement in $R^2$ is not as noteworthy as it was for the base materials. The material-specific model for the Track subgrade was optimized with the highest $R^2$ value when the data from sections N1 through N4 were included. This was likely due to those sections being constructed similarly with approximately the same depth to the Track fill material (17 inches for N1 and N2, 15 inches for N3 and N4). However, none of the material-specific Track subgrade models showed an $R^2$ above 0.5. The model for the combined Seale and Track soil materials yields a reasonable $R^2$ (0.56), but has a statistically insignificant $k_2$ coefficient. Therefore, this model yields no improvement over the simpler deviatoric model for this material.

**Table 6.14 Field-Calibrated MEPDG Models (Subgrade Layer, by Section)**

| Section | $k_1$ | p-value ($k_1$) | $k_2$ | p-value ($k_2$) | $k_3$ | p-value ($k_3$) | $R^2$ |
|---|---|---|---|---|---|---|---|
| N1 | 1346.02 | 0 | -0.6438 | 0 | 3.2016 | 0 | 0.4767 |
| N2 | 1469.11 | 0 | -0.5405 | 0 | 2.3274 | 0 | 0.4358 |
| N3 | 2537.16 | 0 | -0.1324 | 0.0007 | -1.2242 | 0.00005 | 0.4492 |
| N4 | 1672.46 | 0 | -0.3692 | 0 | 1.3810 | 0.00102 | 0.3101 |
| N5 | 5057.29 | 0 | 0.4679 | 0 | -9.3817 | 0 | 0.5339 |
| N6 | 2174.59 | 0 | -0.3158 | 0 | 0.2130 | 0.40519 | 0.6125 |
| N7 | 1957.89 | 0 | -0.3665 | 0 | 1.4853 | 0 | 0.323 |
| N8 | 3051.55 | 0 | 0.0113 | 0.86547 | -2.9854 | 0 | 0.5236 |
| N9 | 27340.60 | 0 | 1.0117 | 0 | -19.3845 | 0 | 0.6798 |
| N10 | 3027.99 | 0 | -0.2719 | 0.00034 | -0.6045 | 0.38459 | 0.3408 |
| S11 | 20683.83 | 0 | 1.1994 | 0 | -12.7825 | 0 | 0.6239 |

**Table 6.15 Field-Calibrated MEPDG Models (Subgrade Layer, by Material)**

| Subgrade Material (Sections) | $k_1$ | p-value ($k_1$) | $k_2$ | p-value ($k_2$) | $k_3$ | p-value ($k_3$) | $R^2$ |
|---|---|---|---|---|---|---|---|
| Track Soil (N1-N7, N10, S11) | 2124.87 | 0 | -0.1578 | 0 | 0.3051 | 0.002 | 0.0587 |
| Track Soil (N1-N7, N10) | 1758.89 | 0 | -0.4675 | 0 | 1.6582 | 0 | 0.2658 |
| Track Soil (N1-N7) | 1648.40 | 0 | -0.4539 | 0 | 1.8807 | 0 | 0.3136 |
| Track Soil (N1-N4) | 1506.30 | 0 | -0.5228 | 0 | 2.3546 | 0 | 0.4448 |
| Track Soil (N1-N2) | 1482.61 | 0 | -0.5482 | 0 | 2.4597 | 0 | 0.4043 |
| Seale/ Track Soil (N8-N9) | 5176.27 | 0 | 0.0889 | 0.239 | -6.3022 | 0 | 0.5602 |

Table 6.16 shows the field-calibrated universal models for each of the structural sections for the subgrade material. Table 6.17 shows the universal models that were generated based on subgrade material type. The section specific models for the Track soil material exhibit $R^2$ values ranging from a low of 0.3 to a high of 0.675. However, the universal models for sections N3, N6, and N10 contained at least one statistically insignificant regression coefficient. For the material-specific models, the Track soil model with the best model fit contained the data set from sections N1 through N4 ($R^2$ of 0.41). The combined Seale and Track subgrade model exhibited the highest model $R^2$ (0.645) of any of the four model types.

**Table 6.16 Field-Calibrated Universal Models (Subgrade Layer, by Section)**

| Section | $k_1$ | p-value ($k_1$) | $k_2$ | p-value ($k_2$) | $k_3$ | p-value ($k_3$) | $R^2$ |
|---|---|---|---|---|---|---|---|
| N1 | 3735.90 | 0 | -0.6609 | 0 | 0.4798 | 0 | 0.4591 |
| N2 | 3209.57 | 0 | -0.5693 | 0 | 0.3891 | 0 | 0.414 |
| N3 | 1590.78 | 0 | -0.0230 | 0.5522 | -0.2487 | 0 | 0.5012 |
| N4 | 2341.26 | 0 | -0.3495 | 0 | 0.1240 | 0.00963 | 0.3012 |
| N5 | 268.07 | 0 | 0.8952 | 0 | -1.3143 | 0 | 0.6563 |
| N6 | 2239.21 | 0 | -0.2940 | 0 | 0.0017 | 0.96166 | 0.6117 |
| N7 | 3192.53 | 0 | -0.4226 | 0 | 0.2314 | 0 | 0.3427 |
| N8 | 747.37 | 0 | 0.5767 | 0 | -0.8473 | 0 | 0.6586 |
| N9 | 241.09 | 0 | 1.3563 | 0 | -1.9191 | 0 | 0.806 |
| N10 | 2539.74 | 0 | -0.2563 | 0.00325 | -0.0788 | 0.34988 | 0.3411 |
| S11 | 677.51 | 0 | 1.7303 | 0 | -1.7079 | 0 | 0.6751 |

**Table 6.17 Field-Calibrated Universal Models (Subgrade Layer, by Material)**

| Subgrade Material (Sections) | $k_1$ | p-value ($k_1$) | $k_2$ | p-value ($k_2$) | $k_3$ | p-value ($k_3$) | $R^2$ |
|---|---|---|---|---|---|---|---|
| Track Soil (N1-N7, N10, S11) | 2190.86 | 0 | -0.1250 | 0 | -0.0119 | 0.360 | 0.0565 |
| Track Soil (N1-N7, N10) | 2886.41 | 0 | -0.4832 | 0 | 0.2171 | 0 | 0.2583 |
| Track Soil (N1-N7) | 2885.62 | 0 | -0.4648 | 0 | 0.2435 | 0 | 0.2933 |
| Track Soil (N1-N4) | 3144.19 | 0 | -0.5376 | 0 | 0.3356 | 0 | 0.4115 |
| Track Soil (N1-N2) | 3350.83 | 0 | -0.5798 | 0 | 0.4010 | 0 | 0.3923 |
| Seale/ Track Soil (N8-N9) | 514.96 | 0 | 0.7188 | 0 | -1.2255 | 0 | 0.6453 |

Figure 6.9 shows a summary of the model $R^2$ values for the four constitutive models for the subgrade layer materials used in the eleven structural sections. Figure 6.10 shows the model $R^2$ summary for the subgrade material types. These figures show that the sections featuring only the Track soil material in the subgrade do not exhibit very strong stress-sensitivity. Many of these sections exhibit model $R^2$ below 0.5. Additionally, the best $R^2$ for the material-specific Track soil model (containing the data from sections N1 through N4) is only 0.44. The most appropriate model for modeling the combined Seale and Track subgrade in terms of model $R^2$ was the universal stress-sensitivity model.

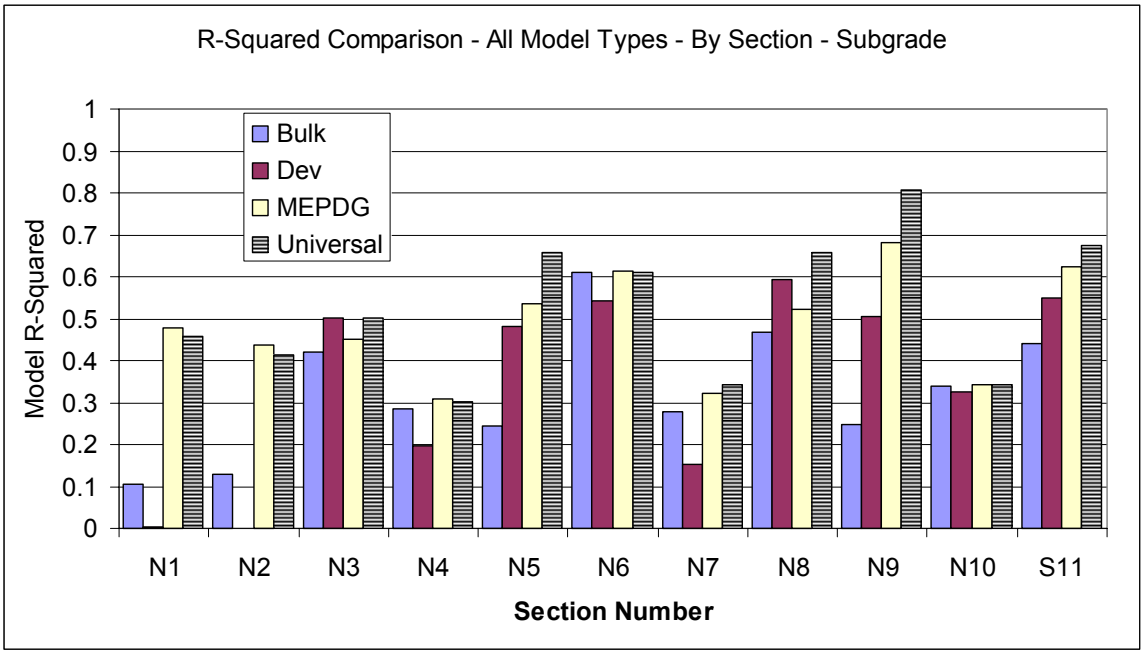


**Figure 6.9 Model R-Squared Summary (Subgrade Layer, by Section).**

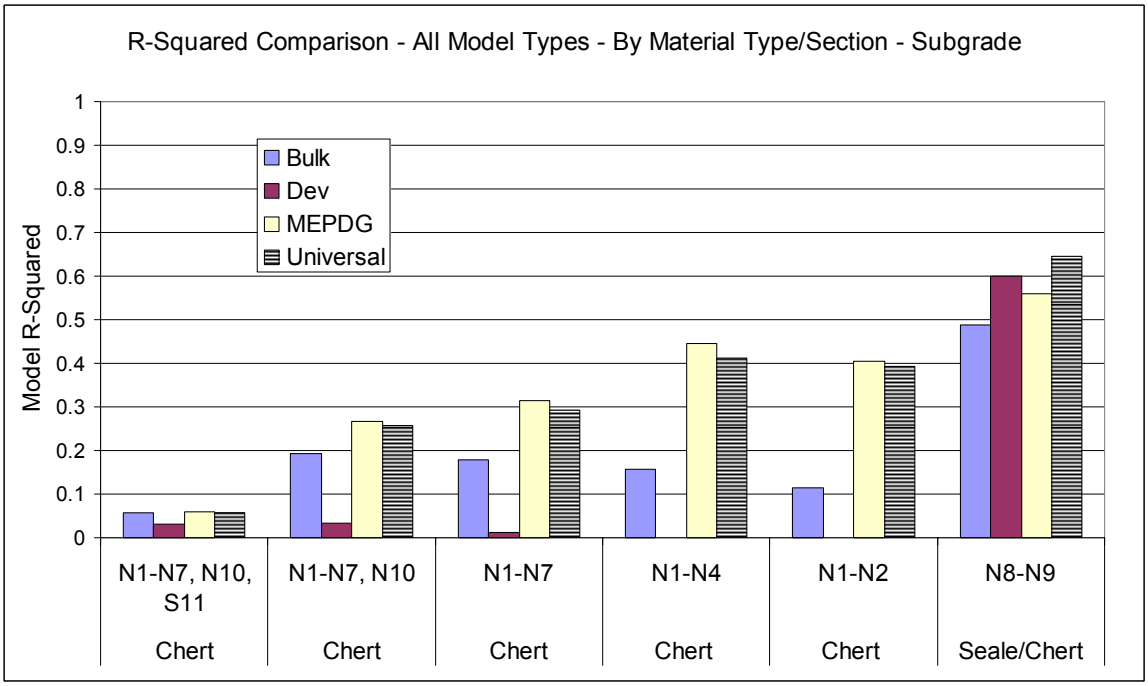


**Figure 6.10 Model R-Squared Summary (Subgrade Layer, by Material).**

The results of the model generation process indicated that no ideal model existed to model the stress-sensitivity of the Track subgrade in the field. Figure 6.10 indicated that the MEPDG model gave the highest $R^2$ value of any of the model types (approximately 0.44). This model was calibrated using only the data from sections N1 through N4 given the construction similarities and generally good condition of these test sections. Figure

6.11 illustrates the measured versus predicted moduli for the Track soil data using this model. Surprisingly, this model exhibits reasonable measured versus predicted behavior despite the relatively low model $R^2$.

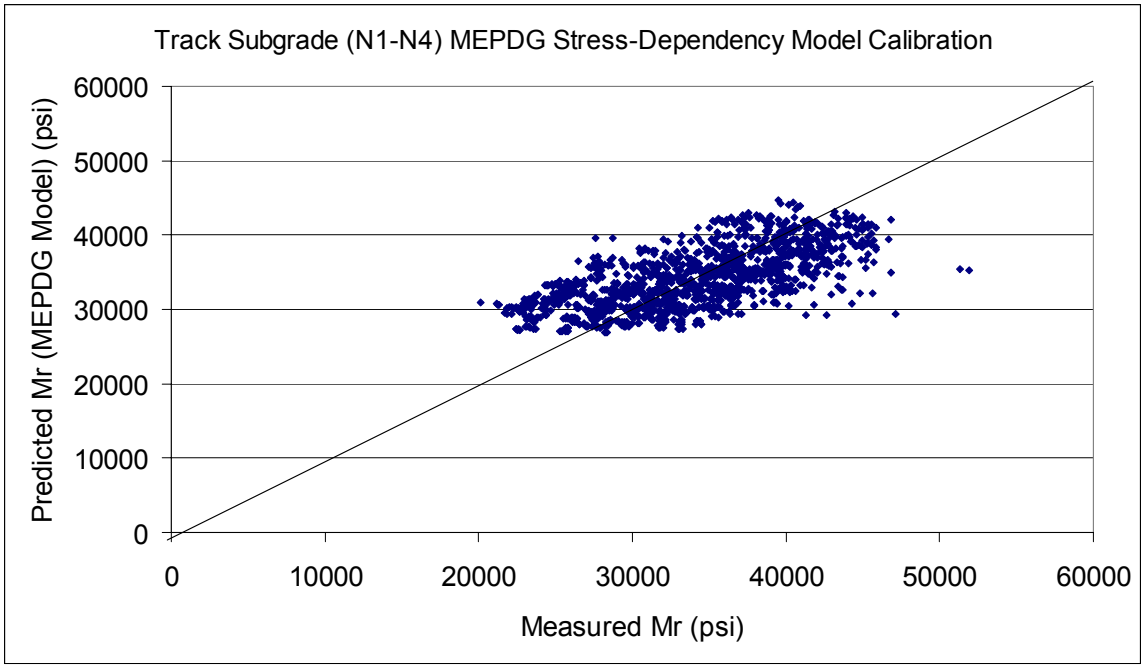


**Figure 6.11 Track Subgrade Material MEPDG Model Calibration Data.**

Given the inability to produce a stress-sensitivity model with a substantial data set with an $R^2$ above 0.5, the Track soil material was not determined to be stress-sensitive as a subgrade material. Therefore, the modulus of this material as a subgrade was quantified by taking the average and the standard deviation of the entire Track soil subgrade data containing data from sections N1-N4, N10, and S11. Sections N5, N6, and N7 were excluded due to lower confidence in the backcalculated moduli due to pavement distresses witnessed in those sections. The average backcalculated modulus for the Track subgrade was 34,755 psi with a standard deviation of 7,525 psi. This average modulus agrees well with the average Track subgrade modulus of 32,000 psi calculated from FWD tested conducted for the 2003 research cycle at the Test Track (Timm and Priest, "Material Properties" 2006).

For the combined Seale and Track subgrade material (sections N8 and N9), Figure 6.10 shows that the universal constitutive model provided the highest model $R^2$ for this data set (approximately 0.645). Table 6.17 shows that each of the regression coefficients for this model were statistically significant (p-values less than 0.05). Figure 6.12 shows the measured (or backcalculated) moduli plotted against the model predicted subgrade moduli at identical stress-states. The figure shows that the data appear to follow the line of unity, albeit with some degree of scatter, across a wide range of measured modulus values. Given the model fit and measured versus predicted behavior, the universal stress-

sensitivity model was deemed suitable for predicting the modulus values of the combined Seale and Track subgrade in the field. This model will be validated later in this chapter.

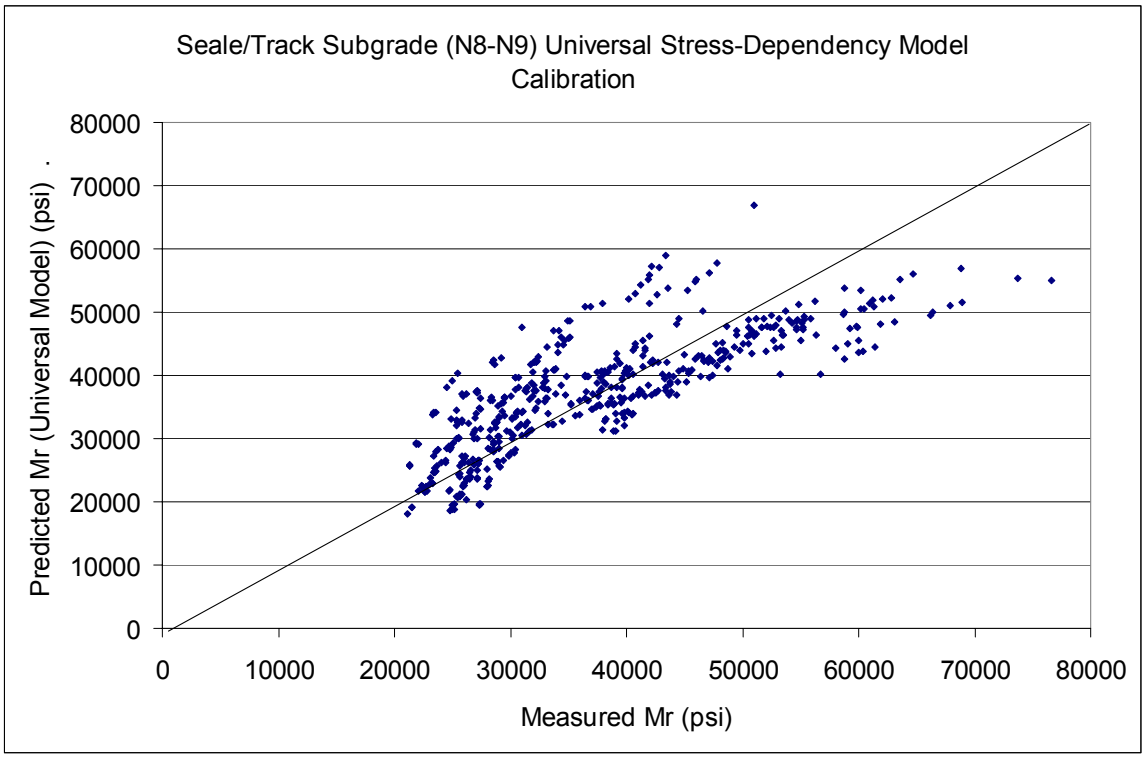


**Figure 6.12 Seale/Track Subgrade Material Universal Model Calibration Data.**

## SPATIAL VARIABILITY IN DEFLECTION DATA

One of the primary issues in generating a field-calibrated stress-sensitivity model for backcalculated resilient moduli is the considerable variability in the data set. A prime source of this variability is generated when testing a pavement structure at multiple locations due to the large amounts of spatial variability inherent to pavement construction. As such, the models calibrated from these data will vary depending on the size of the data set and which data is included in the data set. To illustrate this point, Table 6.18 shows the calibrated models for the limerock base material with various sample sizes included in the calibration data. Models for the entire limerock data base (sections N1 and N2), section N1 alone, and drop locations N1-7, N1-8, and N1-9 are shown. Drop locations N1-7, N1-8, and N1-9 are located in the inside wheelpath, between the wheelpaths, and in the outside wheelpath of the trucking lane, respectively.

**Table 6.18 Spatial Variability in Field-Calibrated Universal Stress-Sensitivity Models for the Limerock Base Material**

| Data Set | $k_1$ | p-value ($k_1$) | $k_2$ | p-value ($k_2$) | $k_3$ | p-value ($k_3$) | $R^2$ |
|---|---|---|---|---|---|---|---|
| All Limerock (N1 and N2) | 4621.709 | 0 | -2.0788 | 0 | 1.8908 | 0 | 0.8266 |
| N1 | 6072.583 | 0 | -2.43019 | 0 | 2.2810 | 0 | 0.8946 |
| N1-7 | 7210.493 | 0 | -2.62613 | 0 | 2.5730 | 0 | 0.9566 |
| N1-8 | 6302.366 | 0 | -2.3178 | 0 | 2.3285 | 0 | 0.9165 |
| N1-9 | 7158.827 | 0 | -2.67956 | 0 | 2.5375 | 0 | 0.9605 |

Table 6.18 shows there is a definite improvement in model fit as less data is included in the data set. The entire limerock database generates a calibrated model with an $R^2$ value of 0.83 while the single drop locations in the wheelpaths (N1-7 and N1-9) generate models with $R^2$ values of 0.96. It can also be seen that the individual drop locations each yield very good $R^2$ values of 0.9 or higher due to the elimination of spatial variability from the data set. Also, the models generated from the testing locations in the wheelpaths generate models with almost identical regression coefficients. The model for the testing location between the wheelpaths (N1-8) yields somewhat different model coefficients, but also exhibits a very high $R^2$.

It can be seen that the calibrated model coefficients and goodness-of-fit of the field-calibrated models can significantly vary based upon which data is included for model calibration. Therefore, it should come as no surprise that the $R^2$ values generated for most in-situ unbound materials are significantly lower than those generated in the laboratory given the large amount of variability inherent to pavement construction and field testing. However, the inclusion of section-wide data in the model calibration and validation data helps to capture the wide array of variability typical of pavement construction, and should be included in the field-calibrated stress-sensitivity models to improve ability of the model to predict moduli in the field.

## MODEL VALIDATION

The next phase in assessing the quality of the field-calibrated stress-sensitivity models was to evaluate the ability of the model at predicting the backcalculated moduli from a different set of deflection data. This process of model validation was performed by first compiling a database containing backcalculated layer moduli and representative stress-states (layered-elastic stresses due to load plus overburden) from four different dates of FWD testing at the Test Track. This testing was performed on all eleven structural sections over a similar wide range of pavement temperatures that were experienced during the dates of calibration testing (45 to 130°F). To validate the generated models, the appropriate stress-states generated within the various unbound materials under a given FWD load were entered into the calibrated constitutive equation for that material to generate a predicted layer modulus under that loading. This predicted modulus was then

compared to the measured (or backcalculated) modulus to assess how well the calibrated equation could predict the backcalculated moduli for a different data set. The four dates of FWD testing used in the model validation process are shown in Table 6.19.

**Table 6.19 FWD Testing Dates used for Model Validation**

| |
|---|
| 12/11/2006 |
| 2/12/2007 |
| 4/9/2007 |
| 9/10/2007 |

Figure 6.13 shows the validation data set for the universal stress-sensitivity model calibrated for the limerock base material (shown in Table 6.9). This data set shows a plot of measured versus model predicted backcalculated moduli using a new set of backcalculation data. The figure shows that the equation tends to over-predict modulus values that fall below approximately 5,000 to 7,000 psi. Also, the model tends to under-predict the moduli that fall above approximately 13,000 to 15,000 psi. This trend can also be seen when the residual values (the difference in measured and predicted moduli) are plotted against the measured moduli. This analysis is shown in Figure 6.14. Even though the equation over-predicts at low modulus values and over-predicts at the higher ones, it appears that the vast majority of the data set fall within 3,000 psi of the measured value. Also, the measured moduli are on the same order of magnitude as the predicted moduli. In summary, the field-calibrated universal model for the limerock material offers reasonable, though not ideal, predicted field modulus values. For future work, perhaps a larger data set for model calibration and validation would yield a more robust model.

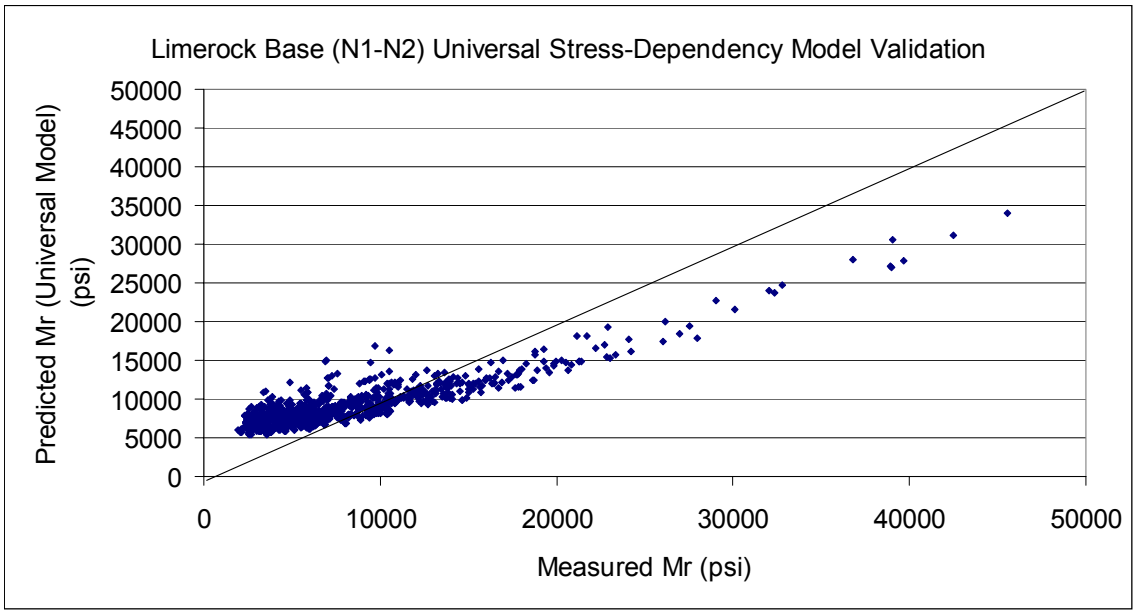


**Figure 6.13 Limerock Base Universal Stress-Sensitivity Model Validation.**

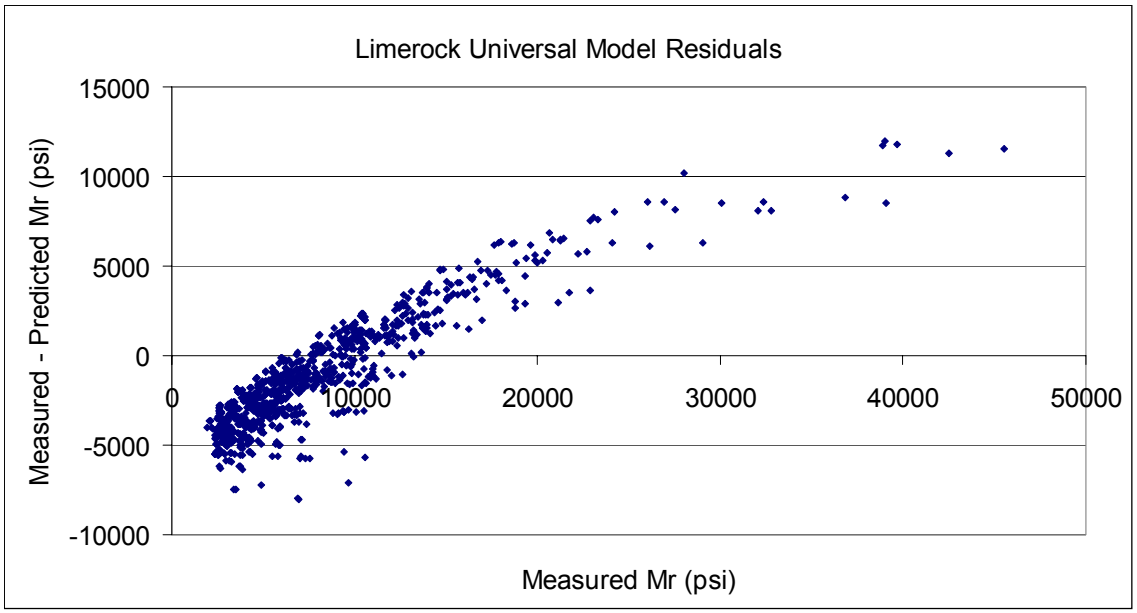


**Figure 6.14 Limerock Base Universal Stress-Sensitivity Model Residuals.**

Figure 6.15 shows the validation data for the field-calibrated universal model for the granite base. This model appears to have reasonable measured versus predicted behavior, with the data set following closely along the line of unity. Figure 6.16 shows the same data set, but looks more closely at the bulk of the data set by eliminating the outlier moduli above 14,000 psi. This figure shows similar behavior to the limerock validation data, with over-predicted moduli and under-predicted moduli outside a certain range. For these data, the range of best prediction appears to be between 3,000 and 5,000 psi. This range is also where the majority of the backcalculated moduli fall within the data set. Therefore, this model offers a reasonable prediction of the backcalculated layer moduli, though it could potentially be improved by adding data to the calibration and validation data sets.

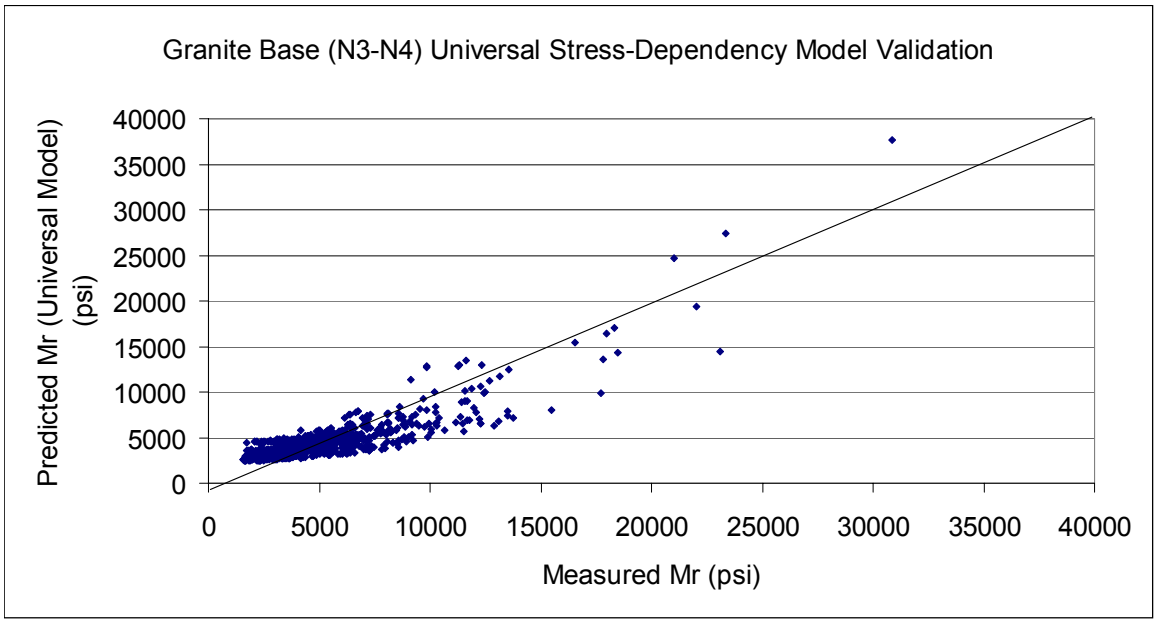


**Figure 6.15 Granite Base Universal Stress-Sensitivity Model Validation.**

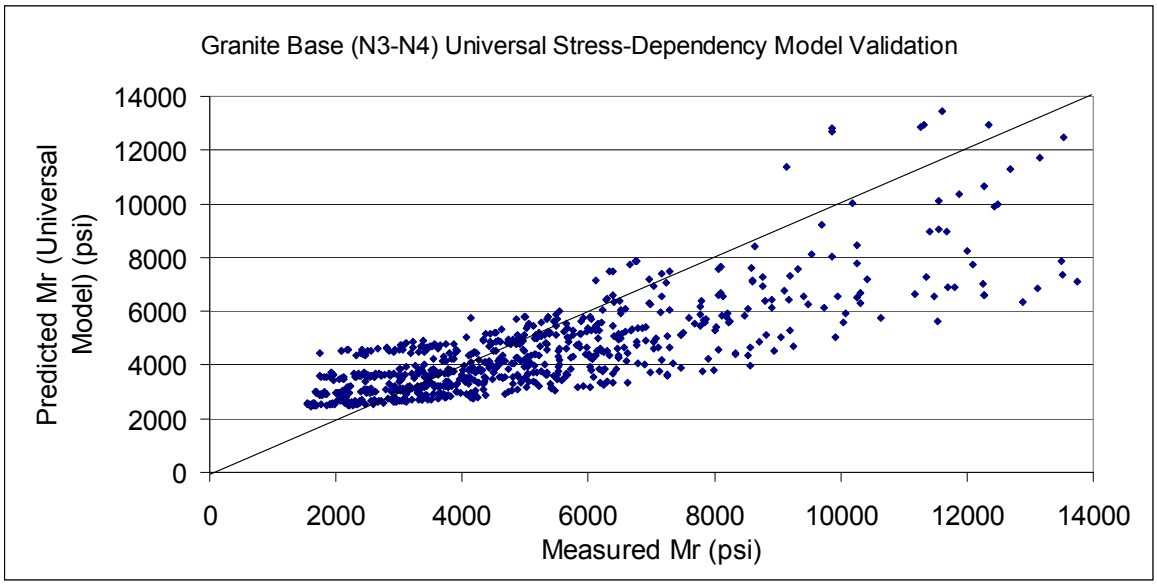


**Figure 6.16 Granite Base Universal Stress-Sensitivity Model Validation (up to 14,000 psi).**

Figure 6.17 shows the validation data set for the deviatoric model calibrated for the combined granite base and Track fill material used in section S11. The results of this validation show that the deviatoric model consistently over-predicts the backcalculated moduli from a different data set. As shown in Figure 6.3, the four stress-sensitivity models all exhibited similar model $R^2$ values for the calibration data for this section. As such, the other three models were evaluated with respect to the validation data as well. The results for the other models were very similar and offered no improvement over the behavior shown in Figure 6.17. The difficulties in model validation may be due in part to

the large amount of the less stress-sensitive Track soil material being included in the base layer. As such, this model does not provide a reasonable predictor of backcalculated moduli in the field and should not be used as such.

From the calibration data set, an average modulus of 11,835 psi with a standard deviation of 3,384 psi was calculated. For the validation data, an average of 12,153 psi with a standard deviation of 3,059 psi was calculated. Additionally, for the FWD testing at the 2003 Test Track, an average value of 11,000 psi was calculated when the granite base and Track fill materials were combined for the purposes of backcalculation (Timm and Priest, "Material Properties" 2006). Given the agreement in the average moduli and modulus variability for the two data sets and previous studies, it is recommended that an average backcalculated modulus is the best representation of the combined granite base and Track fill material in the field.

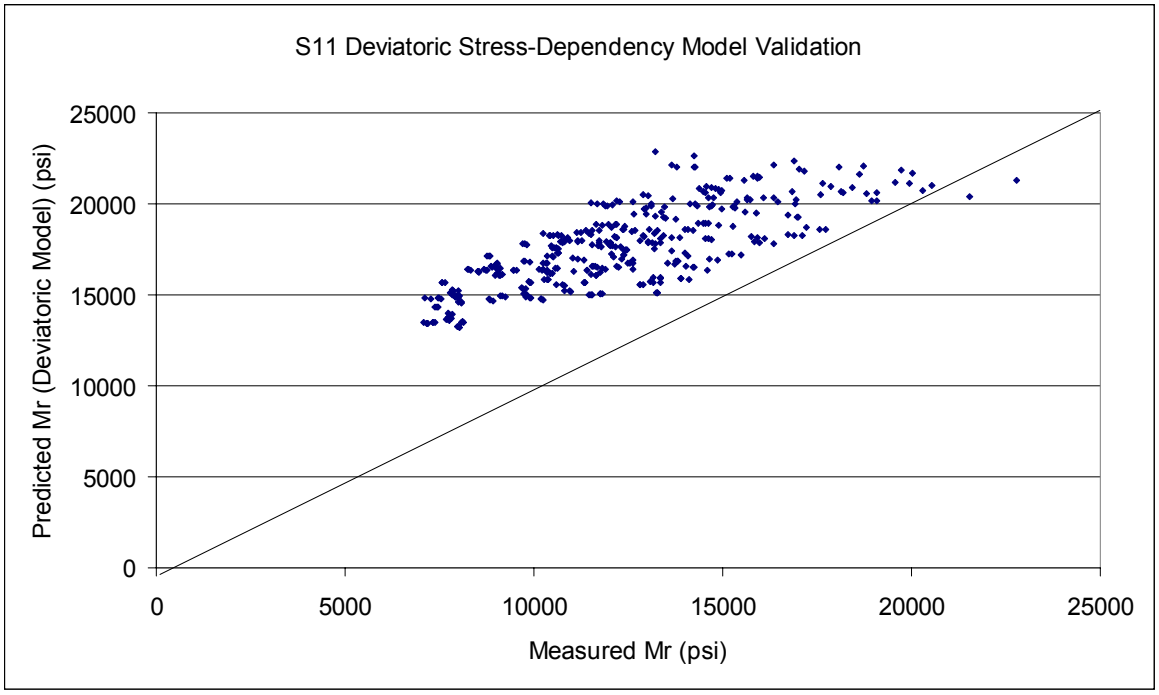


**Figure 6.17 Granite Base and Track Fill Deviatoric Stress-Sensitivity Model Validation.**

Figure 6.18 shows the validation data for the field-calibrated universal model for the combined Seale and Track subgrade layer for sections N8 and N9. This figure shows that the calibrated universal model seems to offer a reasonable prediction of the backcalculated moduli for the validation data set. The validation data points seem to track closely to the line of unity, indicating reasonable modulus prediction for this material using the universal model. Therefore, this model is recommended for use of modeling this composite subgrade material in the field at the Test Track.

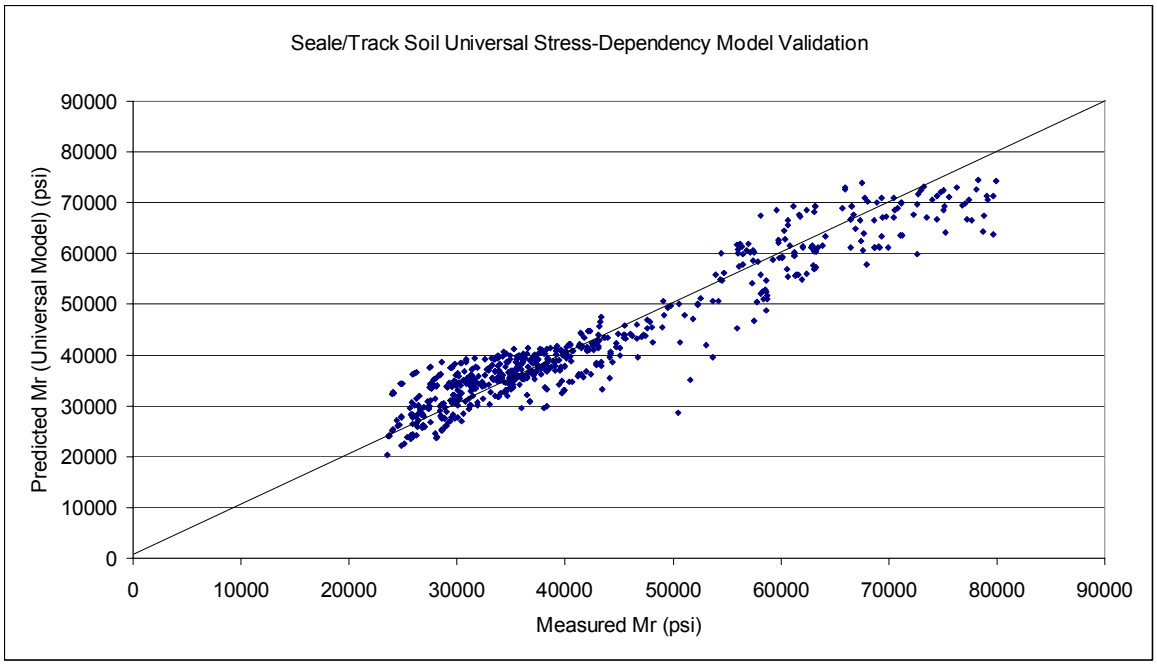


**Figure 6.18 Seale and Track Subgrade Universal Stress-Sensitivity Model Validation.**

**HMA CHARACTERIZATION**

Another means of assessing the quality of the various backcalculated solutions was to assess the temperature-stiffness behavior of the backcalculated HMA moduli. It is well known that the stiffness of HMA materials is temperature dependent. Priest and Timm ("Fatigue" 2006) correlated the HMA layer moduli ($E_{HMA}$) to the mid-depth HMA temperature (T, $^{o}$F) via an exponential function. This function is shown as Equation 6-8, where $\alpha_1$ and $\alpha_2$ are regression coefficients. A strong relationship between the backcalculated moduli and measured mid-depth pavement temperature for each structural section would give good confidence in the validity of the backcalculated solution.

$$E_{HMA} = \alpha_1 e^{\alpha_2 * T} \tag{6-8}$$

For each of the eleven structural sections, the backcalculated HMA moduli from eight days of deflection data were compiled. These data included the days of testing used for both the calibration and validation of the unbound material stress-sensitivity models. Next, the individual backcalculated moduli were paired with the mid-depth pavement temperature measured at the time of FWD testing. For the sections constructed in 2006, the mid-depth temperature was registered directly from a probe at that depth. For the sections constructed in 2003, this temperature had to be interpolated from the temperature data from surrounding probes. A model following the form of Equation 6-5 was then generated for each structural section. These models are listed in Table 6.20, along with the model generated for the 2003 structural study at the Test Track (Priest and Timm "Fatigue" 2006).

**Table 6.20 Results of HMA Characterization for Structural Sections**

| Section | $\alpha_1$ | $\alpha_2$ | $R^2$ |
|---|---|---|---|
| N1 | 6999477 | -0.0355 | 0.9345 |
| N2 | 7459014 | -0.0324 | 0.9086 |
| N3 | 10269355 | -0.037 | 0.9558 |
| N4 | 9968812 | -0.0346 | 0.9502 |
| N5 | 5713817 | -0.0312 | 0.6742 |
| N6 | 7699036 | -0.0288 | 0.7963 |
| N7 | 7651894 | -0.0299 | 0.8748 |
| N8 | 11121090 | -0.042 | 0.942 |
| N9 | 10164654 | -0.0393 | 0.9225 |
| N10 | 10943001 | -0.0435 | 0.9486 |
| S11 | 8996073 | -0.0424 | 0.9499 |
| 2003 Track (N1-N8) | 8187876 | -0.034 | 0.85 |

The results of the regression analyses show that the majority of the $\alpha_1$ coefficients fall between 7,000 and 11,000 ksi (where $\alpha_1$ represents the pavement temperature at 0°F). The $\alpha_2$ coefficients largely fall between -0.029 and -0.044. The model coefficients generated from FWD testing on the 2003 structural study fall between these values. Therefore, the model coefficients for the various structural sections appear reasonable. Figure 6.19 shows the temperature-stiffness model for the HMA in section N3 plotted against the model generated for section N3 during the 2003 research cycle (Priest and Timm, "Fatigue" 2003). The decrease in HMA stiffness with increasing mid-depth pavement temperature is evident. Also, the effects of aging can be seen where the model trendline for the 2006 data lies above the trendline for the 2003 model. This was to be expected since HMA tends to stiffen over time.

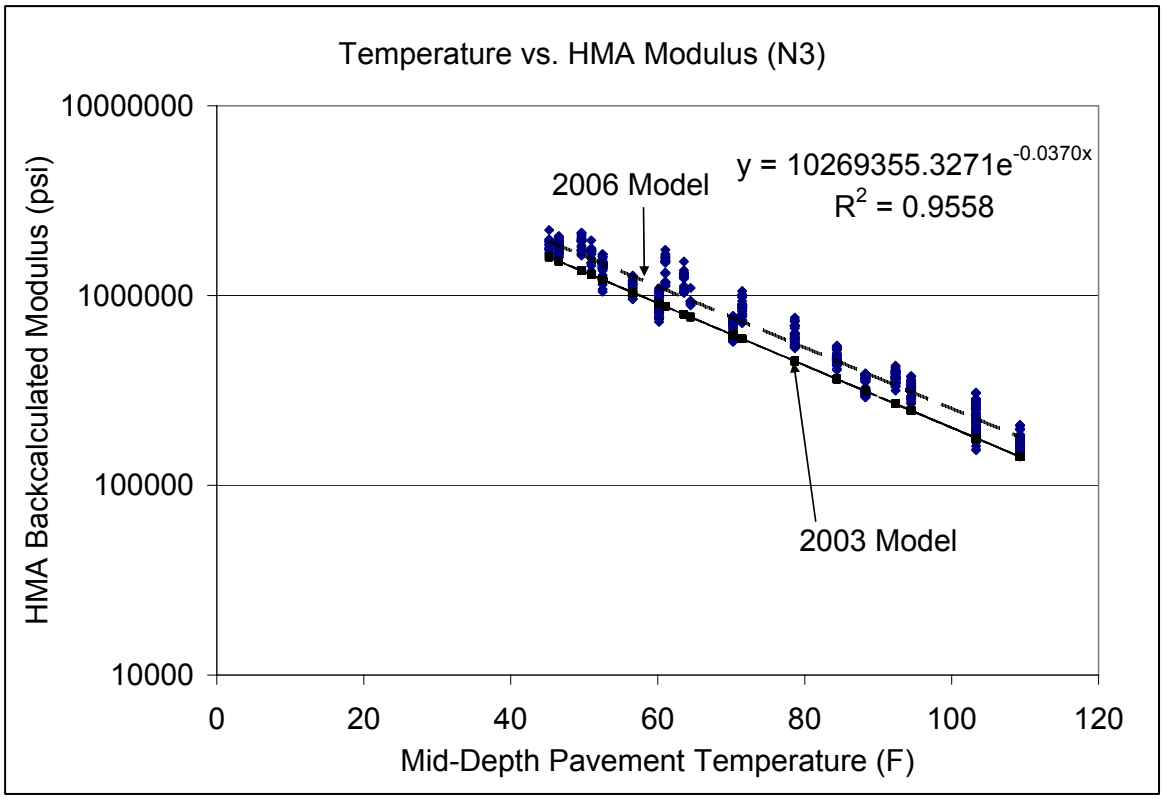


**Figure 6.19 Temperature-Stiffness Model Behavior for Section N3.**

It is also notable that the only model $R^2$ values that fall below 0.9 for the eleven structural sections are those from sections N5, N6, and N7. These backcalculated data were largely excluded from the unbound material stress-sensitivity model generation data due to large amounts of pavement distress seen in those sections. The relatively low temperature-stiffness model fit of sections N5, N6, and N7 compared to the other structural sections provides justification for excluding those data from the unbound material stress-sensitivity model calibration.

## SUMMARY OF RECOMMENDED MODELS AND BACKCALCULATED MODULI

For sections N1 and N2, the universal stress-sensitivity model shown as Equation 6-7 was calibrated to model the resilient modulus behavior of the limerock base material under changing stress-conditions. This model exhibited a very high $R^2$ (0.83) given its calibration with deflection data taken over a wide range of testing locations and seasonal conditions. The validation of this model with a different data set yielded mixed results. While the model seemed to offer a reasonable modulus prediction for the vast majority of the data set, it would tend to over-predict modulus values below 7,000 psi and over-predict modulus values above 13,000 psi. Therefore, Equation 6-9 is reasonable for moduli in this range, but is not ideal. A more robust model would likely require a larger data set for calibration and validation.

$$M_r = 4621.71 * 14.7 * \left(\frac{\theta}{14.7}\right)^{-2.0788} * \left(\frac{\sigma_d}{14.7}\right)^{1.8908} \quad (6\text{-}9)$$

For sections N3 and N4, the universal stress-sensitivity model shown as Equation 6-9 was calibrated to model the resilient modulus behavior of the granite base under changing stress-conditions. Data from sections N5, N6, and N7 containing this material were not included in the calibration data set given low confidence in this backcalculated data due to large amounts of pavement surface distress in those sections. Equation 6-9 showed a reasonable model fit ($R^2$ slightly below 0.7) to the calibration data set. This model showed a reasonable ability to predict the backcalculated moduli from a different data set during the model validation process. However, this model exhibited similar behavior to the universal model used for the limerock material in that it tended to over-predict lower modulus values (below 3,000 psi) and under-predict higher modulus values (above 5,000 psi). Despite this, the vast majority of the data set yielded a reasonable predicted resilient modulus for this material. Again, a larger data set for model calibration and validation might generate a more robust model.

$$M_r = 10465.42 * 14.7 * \left(\frac{\theta}{14.7}\right)^{-3.0449} * \left(\frac{\sigma_d}{14.7}\right)^{2.7613} \quad (6\text{-}10)$$

The base layers that contained the Track soil material for the purposes of backcalculation did not exhibit strong stress-sensitivity with respect to resilient modulus. As such, no stress-sensitivity model could be calibrated to predict the resilient modulus of these materials in the field. For the Track soil base in sections N8 and N9, the average backcalculated modulus was 3,942 psi with a standard deviation of 1,109 psi. For the combined Type 5 base and Track fill used as the composite base layer in section N10, the average backcalculated modulus was 4,022 psi with a standard deviation of 1,745 psi. For the combined granite base and Track fill in section S11, the average backcalculated modulus was 11,835 psi with a standard deviation of 3,384 psi.

The deep Track subgrade behaved similarly to the Track soil material tested in the laboratory and in the field as a base layer in that it did not exhibit any tangible stress-sensitivity. The average backcalculated modulus for the Track soil material in sections N1 through N4, N10, and S11 was 34,755 psi with a standard deviation of 7,525 psi. This value compared well to the average Track subgrade modulus of 32,000 generated via FWD testing during the 2003 research cycle at the Test Track (Timm and Priest "Material Properties" 2006).

In sections N8 and N9, the combined Seale and Track subgrade material exhibited tangible stress-sensitivity in the field. The universal stress-sensitivity model shown in Equation 6-11 was calibrated to predict the moduli of this layer in the field. This model was validated with another data set and offers a reasonable estimate of backcalculated moduli for this composite subgrade layer. This stress-sensitivity is likely due to this layer containing approximately 40 inches of the Seale material, which was shown to be very stress-sensitive in laboratory testing.

$$M_r = 514.96 * 14.7 * \left(\frac{\theta}{14.7}\right)^{0.7188} * \left(\frac{\sigma_d}{14.7}\right)^{-1.2255} \quad (6\text{-}11)$$

**KEY FINDINGS FROM FIELD MODULUS CHARACTERIZATION**

The use of FWD testing, combined with backcalculation software capable of using layered-elastic analysis to predict the pavement material stress-states under loading, can be an excellent tool for modeling the stress-sensitivity of unbound pavement materials in the field. Given the large amounts of spatial and seasonal variability in the data used to calibrate and validate these models, the models generated in the field typically have much lower $R^2$ values than the models generated for the same materials in the laboratory. An $R^2$ value of 0.5 was selected as the cut-off value below which the material was considered insensitive to changing stresses. Despite reasonable model $R^2$ values and good measured versus predicted moduli calculated with a calibration set of deflection data, most of the field-calibrated stress-sensitivity models were not ideal predictors of the backcalculated moduli for another set of deflection data used for model validation. For future work of this nature, a larger database of deflection data for both calibration and validation is recommended to generate a more robust field-calibrated stress-sensitivity model. These data are readily available having been collected on a nearly weekly frequency during the 2006 Test Track research cycle.

# CHAPTER 7 - COMPARISON OF LABORATORY AND FIELD-DETERMINED RESILIENT MODULI

## INTRODUCTION

For this project, resilient modulus testing was performed on the unbound materials used in the construction of the eleven structural sections at the NCAT Test Track. This testing was performed in the field using non-destructive FWD testing and in the laboratory using triaxial testing (following the specification set forth by NCHRP 1-28A). Both forms of testing generate a resilient modulus value or a constitutive equation relating resilient modulus to material stress-state, but the two forms of testing are very different in many respects. Namely, laboratory testing is done on smaller samples that are usually re-compacted to simulate field conditions. These samples typically aren't completely representative of in-situ conditions due to differences in: sample disturbance, aggregate orientation, water content, and level of compaction (Seeds et al., 2000; Nazarian et al., 1998). Also, the laboratory sample is much smaller than the mass of materials within the pavement structure that respond to a moving wheel load (Seeds et al., 2000). As such, it is not surprising that multiple studies have documented poor agreement between the laboratory and field-measured resilient moduli for various unbound materials (see Chapter 2). This chapter will highlight the agreement and disagreement between the laboratory and field-determined resilient moduli for the unbound materials used in the structural study at the NCAT Test Track.

## METHODOLOGY

For this project, the five unbound materials were characterized in the laboratory and in the field under various stress-states and load levels. The result of the laboratory resilient modulus testing was a constitutive relationship relating resilient modulus to stress-state for each of the unbound materials (see Chapter 4). The results of the field resilient modulus testing with the FWD were constitutive equations for stress-sensitive materials and average modulus values for non stress-sensitive materials (see Chapter 6). To compare the laboratory and field-determined resilient moduli to each other, they must be compared at equivalent stress-states.

First, the stress-states (bulk, deviatoric, octahedral shear) tested in the field at the four FWD drop heights (6k, 9k, 12k, and 16k) were averaged to determine a representative field stress for that particular loading. These representative stresses were entered into both the laboratory-calibrated and field-calibrated constitutive equations to draw comparisons between the two values. For this comparison, the universal stress-sensitivity models were used due to their superior $R^2$ values generated during field calibration. Additionally, these values were plotted against the average and standard deviation of the backcalculated moduli from the various load levels. This was done to show the range of backcalculated moduli that were generated due to spatial and construction variability in the field. For this analysis, dates of FWD testing were analyzed separately. This was done to eliminate the effects of stress-sensitivity in the modulus variability at the different load levels, since different pavement temperatures will change the modulus of

the asphalt and consequently alter the stress-states that are experienced by the unbound layers.

For this analysis, comparisons of the results of the laboratory and field testing were only performed for the materials in which a direct comparison could be made. Several sections required combining materials for the purposes of generating a viable backcalculation cross-section (see Chapter 5). As a result, no direct comparison could be made between the laboratory and field-determined resilient moduli for those combined layers. This was true for the combined Seale and Track subgrade layer in sections N8 and N9, the combined Type 5 and Track soil base layer for section N10, and the combined granite and Track soil base layer in section S11.

**LIMEROCK BASE (SECTIONS N1 AND N2)**

Figures 7.1 through 7.4 show the laboratory versus field-determined moduli for the four FWD testing dates used to generate the backcalculated data for the limerock base material. Figure 7.1 corresponds to the testing date on 10/30/06, Figure 7.2 corresponds to the testing on 11/27/06, Figure 7.3 corresponds to the testing on 1/29/07, and Figure 7.4 corresponds to the testing on 8/20/07. As stated earlier, the analysis was subdivided by date to more accurately quantify the stress-states under the various load levels without the addition of seasonal variability as an additional variable.

Figure 7.1 shows that the laboratory and backcalculated resilient moduli are almost identical at the stress-state induced by the 12 kip FWD loading. At lower load levels (6 kip and 9 kip), the backcalculated moduli are higher than the laboratory determined moduli at equivalent stress-states. At the larger load level (16 kip), the laboratory predicted modulus is higher than that measured in the field. This also shows that the laboratory and field-measured moduli exhibit different behavior with respect to stress-sensitivity. The laboratory constitutive equation suggests the material to be stress-hardening while the field-calibrated constitutive equation and backcalculated moduli suggest the material is stress-softening. This is opposite of what was expected, since studies have shown unbound materials usually show the same stress-sensitivity behavior in the lab and in the field but with very different resilient moduli (see Chapter 2). Potential reasons for this divergence in behavior will be discussed later in this chapter. Figure 7.1 also shows that the field-calibrated constitutive equation predicts the average backcalculated moduli well for this day's deflection data.

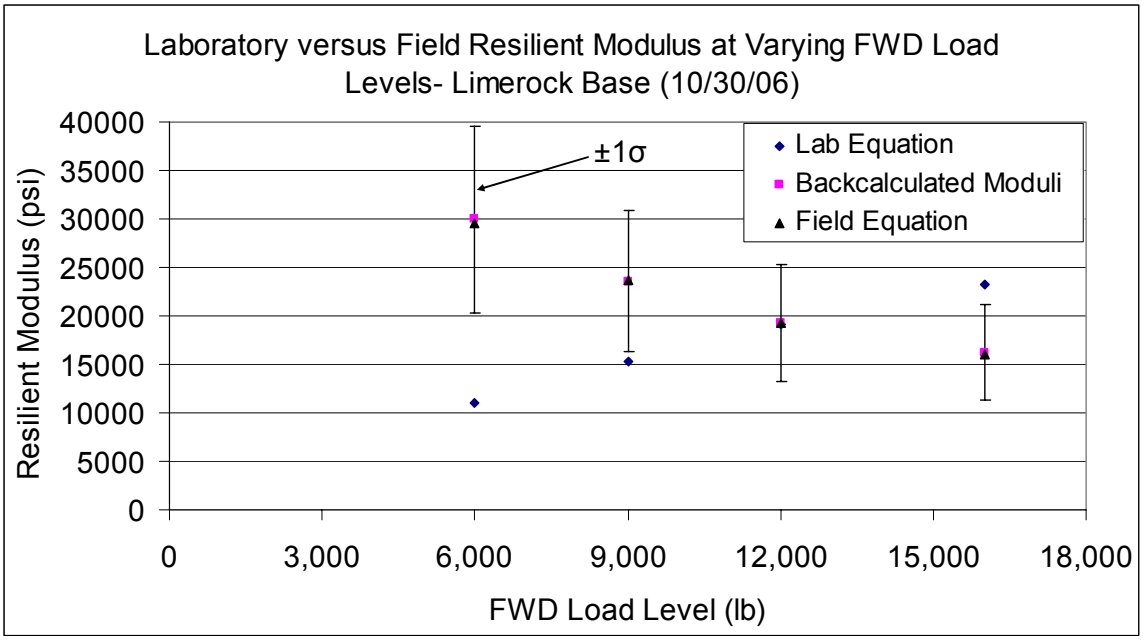


**Figure 7.1 Laboratory versus Field Resilient Moduli Comparison (Limerock Base Material, FWD Testing on 10/30/06).**

Figure 7.2 shows that laboratory and field measured data seem to agree well at the lower levels for the deflection testing on 11/27/06. The laboratory predicted resilient moduli fall within one standard deviation of the average backcalculated moduli at the 6 kip and 9 kip FWD load levels. The trend of opposite stress-sensitivity behavior with the lab and field data sets is witnessed here as well. This plot shows reasonable agreement between the field-calibrated constitutive equation and average backcalculated moduli at the different load levels as well. It should be noted that the standard deviations of the average backcalculated moduli are smaller for this data set than for the data collected on 10/30/06. This could be a function of two factors: additional compaction of the base layer materials under traffic, and cooler pavement temperatures reducing the stresses imparted on the base layer by FWD loading.

Figure 7.3 shows good agreement between the laboratory predicted and field-calculated resilient moduli under the stresses generated by the lowest FWD load level (6 kip). Above this load level, the laboratory predicted modulus is between 2 and 4 times larger than the field-calculated value at equivalent stress-states. The opposite stress-sensitivity behavior is still apparent between the two data sets. Again, less modulus variability in the backcalculated data is evident than the earlier data collected under warmer conditions and less trafficking. Also, reasonable agreement is seen between the field-calibrated constitutive equation and the average backcalculated moduli.

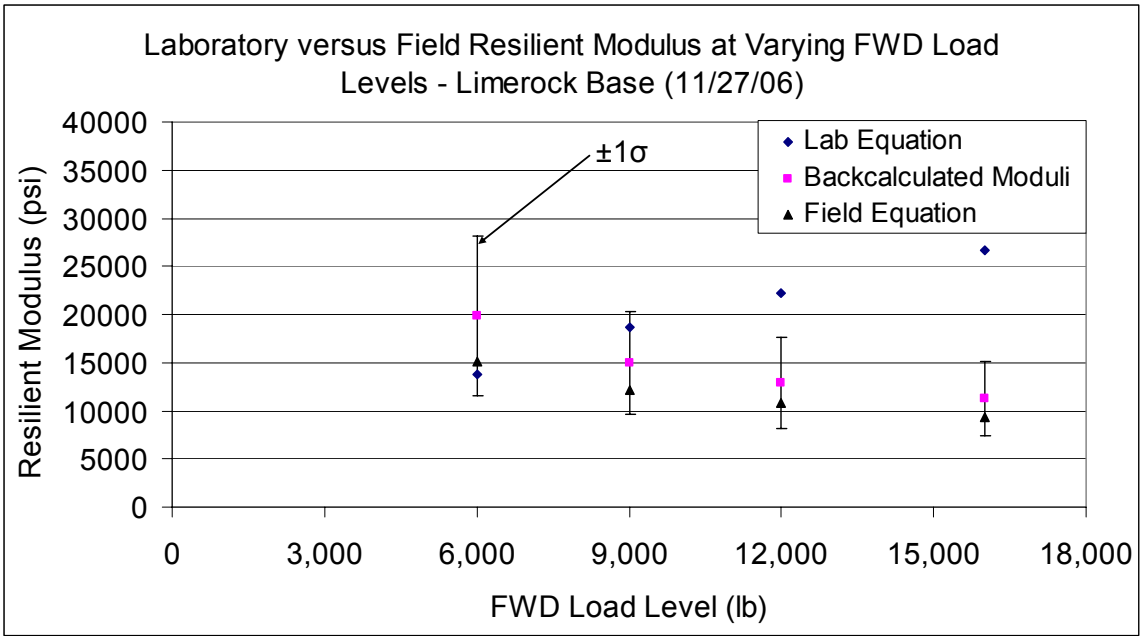


**Figure 7.2 Laboratory versus Field Resilient Moduli Comparison (Limerock Base Material, FWD Testing on 11/27/06).**

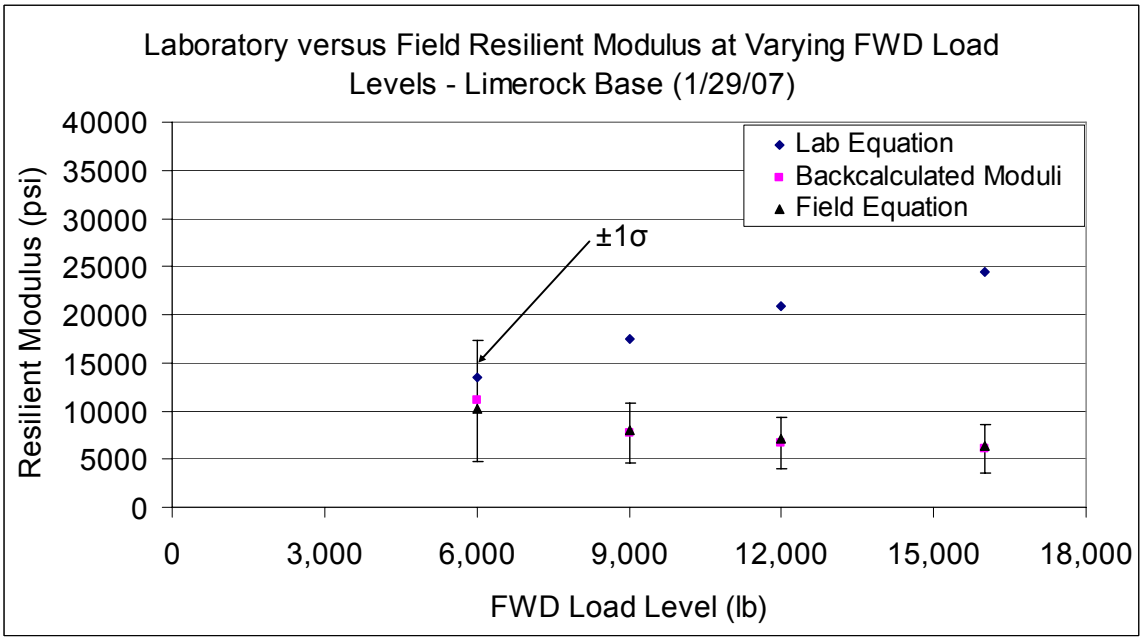


**Figure 7.3 Laboratory versus Field Resilient Moduli Comparison (Limerock Base Material, FWD Testing on 1/29/07).**

Figure 7.4 shows generally poor agreement between the behavior of both constitutive equations and the average backcalculated moduli at the various load levels on the warmest day of FWD testing (pavement temperatures ranging between 100°F and 130°F). At the 6 kip load level, the laboratory predicted resilient modulus is 2.3 times

larger than the average backcalculated modulus. This factor increases to approximately 7.7 times at the 16 kip load level. Again, the laboratory and field modulus values exhibit opposite stress-sensitivity behavior. The field-calibrated constitutive equation also appears to over-predict the average backcalculated modulus values for this date of testing. The backcalculated moduli at the various load levels also have lower average modulus values and smaller standard deviations than the other data sets. These modulus values would be smaller than on a warm day for a truly stress-softening material, since hotter pavement temperatures yield a reduction in stiffness of the HMA layer. This HMA reduction in stiffness imposes larger stresses to be placed on the unbound material labors due to loading.

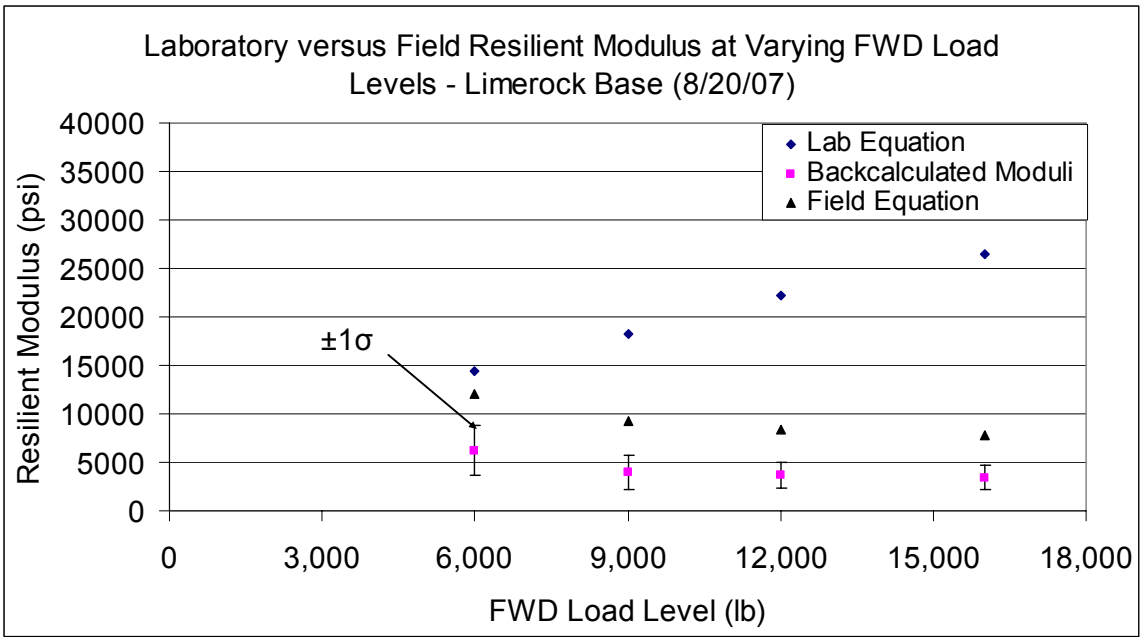


**Figure 7.4 Laboratory versus Field Resilient Moduli Comparison (Limerock Base Material, FWD Testing on 8/20/07).**

**GRANITE BASE (SECTIONS N3 AND N4)**

Figures 7.5 through 7.8 show the laboratory versus field-determined moduli for the four FWD testing dates used to generate the backcalculated data for the granite base material. Figure 7.5 corresponds to the testing date on 11/27/06, Figure 7.6 corresponds to the testing on 1/29/07, Figure 7.7 corresponds to the testing on 4/23/07, and Figure 7.8 corresponds to the testing on 8/20/07.

Figure 7.5 shows generally poor agreement between the predicted moduli using both the laboratory and field-calibrated stress-sensitivity models to the average backcalculated moduli at the various FWD load levels. The best agreement between the laboratory constitutive equation and the backcalculated moduli is at the stress-state corresponding to a 12 kip FWD loading (where the lab modulus is predicted to be 20 percent higher than the backcalculated modulus at equivalent stress-states). At the lower load levels (6 kip and 9 kip) the field moduli are larger than the laboratory predicted moduli by 62 percent at the 6 kip load level and 27 percent at the 9 kip load level. At the highest load level (16

kip), the lab predicted modulus is approximately 60 percent higher than the average backcalculated modulus. Again, the material appears to be stress-hardening in the laboratory and stress-softening in the field. The field backcalculated moduli are significantly larger than the moduli calculated by the field-calibrated predictive equation at equivalent stress-states. Also, very little variability is seen in the backcalculated moduli for this data set at varying load levels.

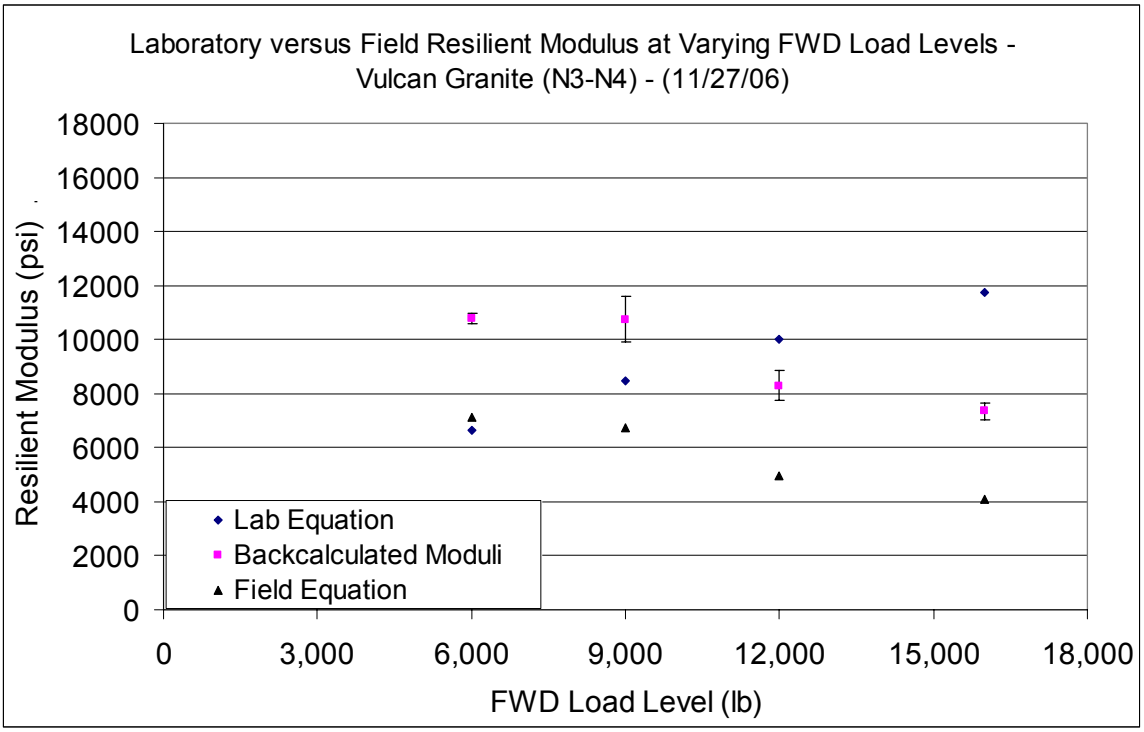


**Figure 7.5 Laboratory versus Field Resilient Moduli Comparison (Granite Base Material, FWD Testing on 11/27/06).**

Figure 7.6 shows that the laboratory predicted moduli and average backcalculated moduli agree very well at the 6 kip load level for testing performed on 1/29/07. However, the laboratory and field data sets exhibit opposite stress-sensitivity, and the laboratory predicted moduli is approximately 4 times larger than the average backcalculated modulus at the 16 kip load level. This date of FWD testing also exhibits larger variability in the backcalculated moduli than did the testing date shown in Figure 7.5. Additionally, the field-calibrated constitutive equation appears to accurately predict the average backcalculated moduli at the different load levels.

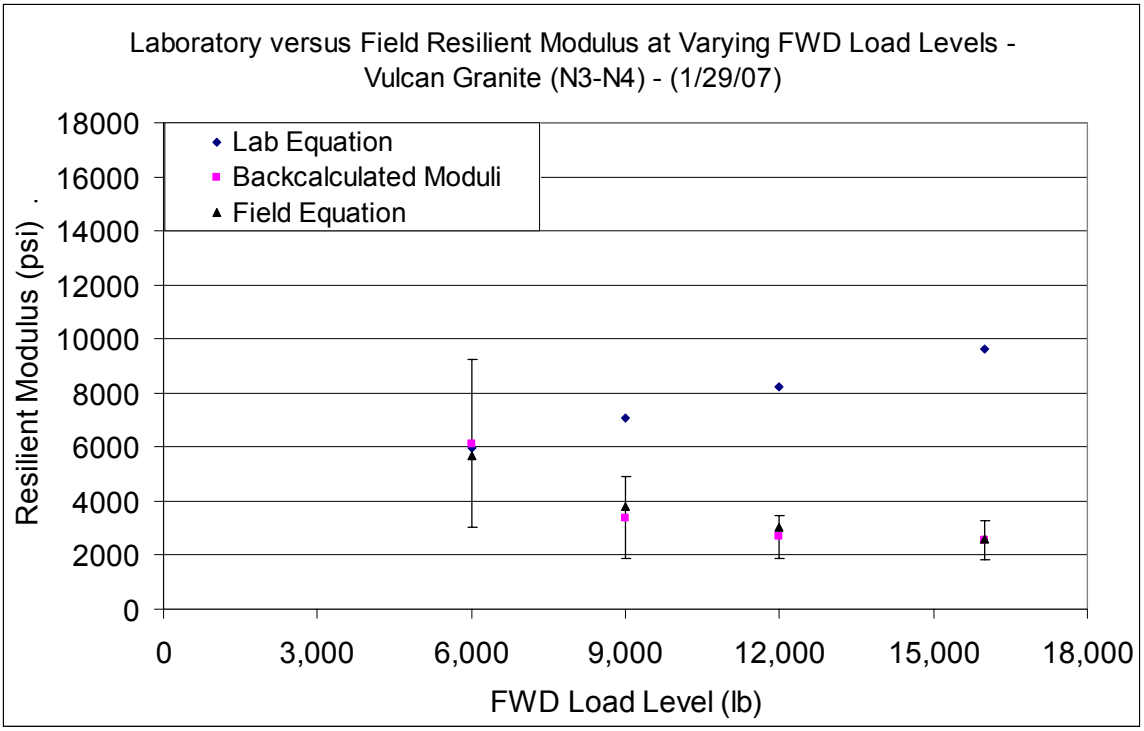


**Figure 7.6 Laboratory versus Field Resilient Moduli Comparison (Granite Base Material, FWD Testing on 1/29/07).**

Figure 7.7 shows that the laboratory predicted moduli over-predict the backcalculated moduli for the granite base for FWD testing on 4/23/07. Again, the lab and field data sets exhibit opposite stress-sensitivity. The laboratory modulus is larger than the backcalculated modulus by approximately 50 percent at the 6 kip load level, and is almost 4 times as larger than the backcalculated modulus at the 16 kip load level. The backcalculated moduli seem to exhibit moderate variability at each load level (standard deviations between approximately 1,200 and 1,700 psi). The field-calibrated constitutive equation also accurately predicts the average backcalculated moduli for this data set.

Figure 7.8 shows that the data set corresponding to FWD testing on 8/20/07 exhibit similar trends in terms of laboratory and field comparisons to the other testing dates. First, the laboratory predicted moduli exhibit stress-hardening behavior while the backcalculated moduli exhibit stress-softening behavior. Once more, the best agreement between the laboratory and backcalculated moduli occurs at the 6 kip load level. The field-calibrated constitutive equation generates a good prediction of the average backcalculated modulus for this day of FWD testing as well.

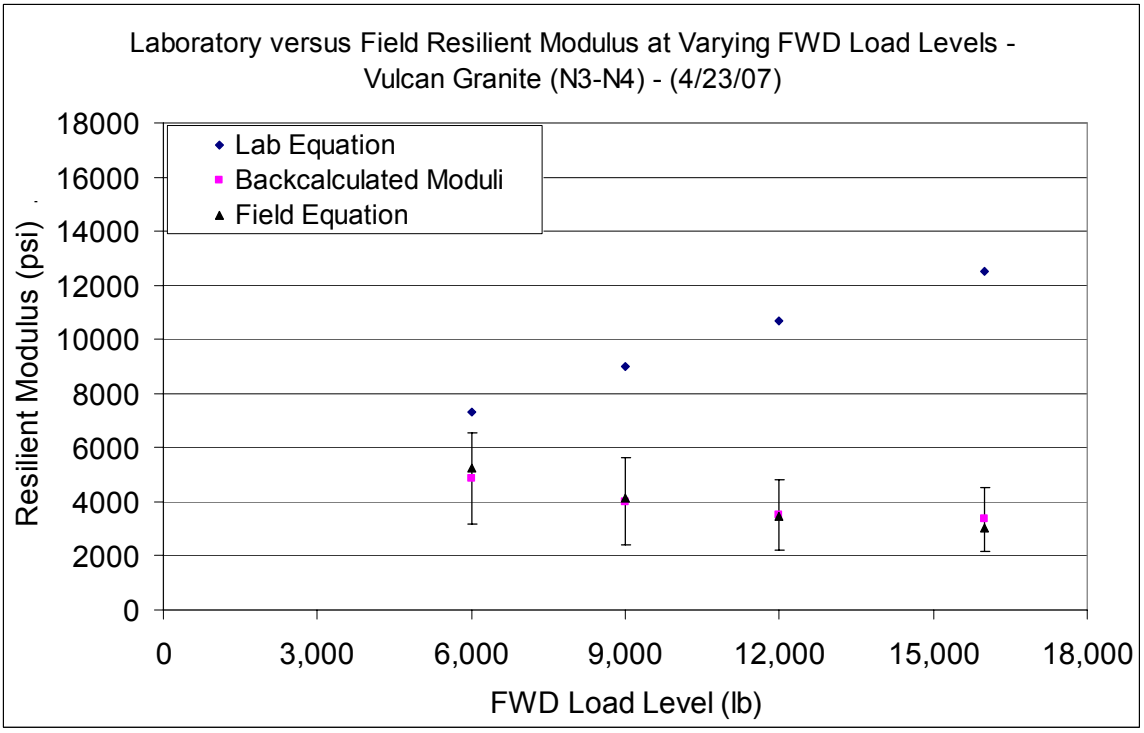


**Figure 7.7 Laboratory versus Field Resilient Moduli Comparison (Granite Base Material, FWD Testing on 4/23/07).**

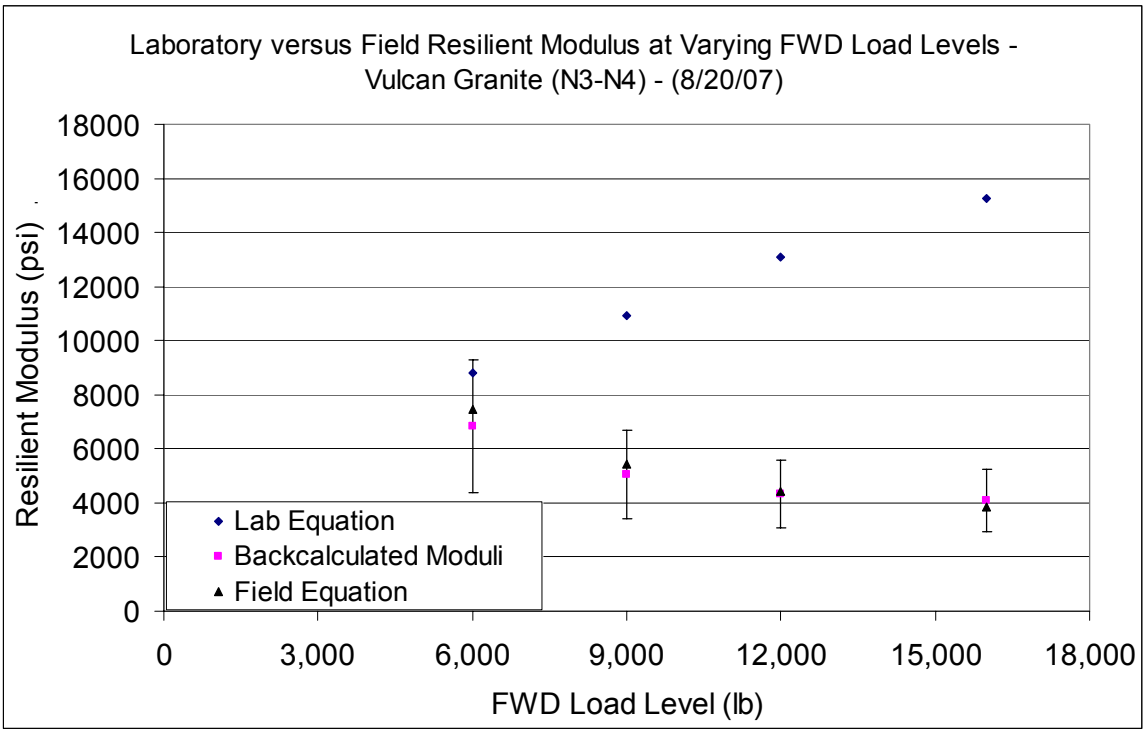


**Figure 7.8 Laboratory versus Field Resilient Moduli Comparison (Granite Base Material, FWD Testing on 8/20/07).**

**TRACK SOIL BASE (SECTIONS N8 AND N9)**

For sections N8 and N9, the Track soil material was utilized as the base material between the HMA layer and the Seale subgrade layer. No tangible stress-sensitivity was exhibited for this material in the field. The average backcalculated modulus for this material in the field was 3,942 psi with a standard deviation of 1,109 psi. This was considerably lower than the average modulus of 28,335 psi (standard deviation of 6,650 psi) for this material measured in the laboratory. It was also considerably lower than the average value of 32,000 psi calculated for this material from FWD testing during the 2003 research cycle (Timm and Priest, "Material Properties" 2006). The average values themselves indicate very poor agreement between the lab and field data for the Track soil material compacted as a base layer.

This disagreement could potentially be an artifact of the backcalculation solution. Literature indicates that backcalculation is not ideal for determining the modulus of a relatively thin layer between two thicker layers (Von Quintus and Killingsworth, 1998). In this case, both of these sections have a relatively thin Track soil layer (between 6 to 8 inches thick) sandwiched between a very thick HMA layer (10 to 14 inches thick) and a deep subgrade layer. Additionally, this material may not compare well to the compacted Track subgrade values due to its compaction over the relatively soft Seale subgrade material. Without the benefit of a strong supporting embankment, this material should exhibit somewhat lower modulus values.

**TRACK SOIL SUBGRADE**

The Track soil material was utilized as the deep subgrade material throughout the structural study at the Test Track. This material was deemed to be non stress-sensitive through both laboratory and field testing (Chapters 4 and 6). The average laboratory modulus for this material was calculated as 28,335 psi with a standard deviation of 6,650 psi. In the field, the average modulus was calculated as 34,755 psi with a standard deviation of 7,525 psi. The average field modulus was taken from the FWD data calculated in sections N1 through N4, N10, and S11. The data from sections N5, N6, and N7 were excluded from this data given the larger amounts of pavement distress in those sections leading to lower confidence in the accuracy of the deflection data. Sections N8 and N9 were excluded from this data set because the deep subgrade contained both the Seale and Track soil materials in this section.

A one-way ANOVA test between the two data sets showed that there was a statistical difference between the means of the two data sets (F-statistic = 58.03). Comparing the averages of the means yielded a ratio of field moduli to lab moduli of 1.23. This ratio shows good general agreement between the laboratory and field-measured behavior of the Track soil material when used as a subgrade. This was expected, since literature indicated that agreement between lab and field data tends to improve when unbound materials deeper in the pavement structure are compared (see Chapter 2).

## POTENTIAL CAUSES OF DISAGREEMENT BETWEEN LAB AND FIELD DATA

There are several potential reasons why good agreement was not achieved between the laboratory and backcalculated resilient moduli for the unbound materials used for this study. First is the disagreement between the samples tested by each testing method. The triaxial resilient modulus test only tests a small sample of material that is not equivalent to the mass of unbound material that responds to a moving wheel load over a pavement. The FWD tests the materials in their in-situ condition, allowing a much larger mass of the unbound materials to be subjected to the test loading.

Secondly, laboratory samples are often reconstituted to simulate the in-situ unbound material conditions at the construction site. Changing seasonal conditions in the field and the compaction effects of continuous trafficking could potentially have altered the unbound material properties in the field (density and moisture content) so that the laboratory tested samples were no longer representative of these materials at the time of FWD testing. Additionally, any variation in sample preparation in the laboratory that causes these samples to be non-representative of the field conditions can significantly alter the measured resilient moduli.

Literature has shown that sampling technique has a significant impact on laboratory resilient modulus values and many studies recommend excavating within the pavement structure to gather samples for laboratory testing (Yau and Von Quintus, 2002; Nazarian et al., 1998)). For this project, the unbound materials for laboratory testing were sampled from the compacted base or fill layer prior to HMA construction. This material had not yet been conditioned under traffic loading. Therefore, the material tested in the lab would not have experienced the same degree of compaction and conditioning as the materials that were tested in-situ with the FWD after considerable trafficking. However, the only way to gather unbound material that had experienced consolidation under trafficking would be to excavate material from within the trucking lane. This was not a practical option given the nature of the project, making the sampling technique used the best available.

Also, the opposite stress-sensitivity seen for the laboratory and field moduli for the limerock and granite base materials could be in-part due to the method of backcalculation. Given the better agreement between lab and field data at the lower load levels, it is possible that the increasing disparity between lab and field moduli with increasing load was due to a computational artifact of the backcalculation software which reduced the accuracy of the backcalculated moduli at larger load levels.

Finally, the Test Track subgrade is unique in that it exhibits strength far higher than that of most highway subgrade materials as well as some base layers (average resilient modulus of nearly 35 ksi in the field). This supporting platform is present in the field but not for laboratory testing and the effects of surrounding or supporting pavement layers are not accounted for in laboratory resilient modulus testing. The presence of this

condition could lead to a distinct difference in laboratory predicted and backcalculated unbound material behavior.

## KEY FINDINGS FROM COMPARISON OF LABORATORY AND FIELD RESILIENT MODULI

For the unbound granular base materials for which comparisons could be drawn (the limerock base and granite base), poor agreement was seen between the moduli backcalculated in the field and a modulus predicted from a laboratory-calibrated constitutive equation over various representative stress-states. For these materials, the laboratory predicted moduli exhibited stress-hardening behavior and the backcalculated moduli exhibited stress-softening behavior. This reversal in stress-sensitivity between the two data sets was opposite of what was seen in literature. Potential reasons for this disagreement include: laboratory samples that were non-representative of the in-situ conditions (compaction, density, moisture content, etc.), inherent disagreement between the nature of the two test methods, reduced accuracy of the backcalculation software at higher load levels, and the existence of a very stiff subgrade at the Test Track supporting and altering the stress-sensitivity behavior of these materials in the field.

Despite the opposing trends, generally good agreement was seen between the lab and field data at the stresses representative of the lower FWD loading level (6 kip) on multiple testing dates for both the limerock and the granite base. Given the opposite stress-sensitivity, the laboratory moduli were often larger than the field moduli at the larger FWD load levels (12 kip and 16 kip). Also, the field-calibrated constitutive equation was shown to be a good predictor of the unbound material moduli for these two materials at the Test Track.

For the Track soil material, poor agreement was seen between the moduli of the field-tested base material and the laboratory tested material. The average laboratory modulus was approximately 7.2 times larger than the average backcalculated base modulus for this material. This was expected since the Track soil material for this layer was sandwiched between two much larger layers for the purposes of backcalculation and was supported by the softer Seale subgrade material. The Track subgrade compared well with the laboratory values, however. The average backcalculated Track subgrade modulus was only 23 percent larger than the average laboratory Track soil modulus. This was expected since literature indicates that agreement between laboratory and field-measured resilient moduli show better agreement in the deeper pavement layers (Seeds et al., 2000; Parker and Elton, 1990).

Based on the results of this comparison, it is recommended that the laboratory constitutive equation be utilized to characterize the unbound materials at the Test Track for Level 1 MEPDG design. The poor agreement between the laboratory and field resilient moduli is not necessarily an indicator of low quality lab or field data, but of inherent disagreement between the testing method and conditions. The field-generated resilient moduli and stress-sensitivity models were shown to accurately characterize the unbound materials in-situ. However, the backcalculation data and field-generated stress-

sensitivity models are site-specific to the NCAT Test Track. Additional testing at other locations containing the various unbound materials is advised to further validate the field-calibrated stress-sensitivity models.

# CHAPTER 8 - CONCLUSIONS AND RECOMMENDATIONS

## SUMMARY OF KEY FINDINGS

The NCAT Test Track testing facility provided an ideal testing ground for characterizing the resilient moduli of multiple unbound materials. For this study, five different unbound materials were utilized in the construction of eleven instrumented pavement test sections at the Test Track. These materials were tested both in the laboratory (through triaxial resilient modulus testing) and in the field with the falling weight deflectometer (FWD). These respective data sets provided an excellent tool for characterizing the unbound material resilient modulus behavior. For this project, several common non-linear stress-sensitivity models were calibrated to both the laboratory and field-measured resilient modulus values for each material type. Based on the results of this analysis, recommendations regarding the most appropriate stress-sensitivity model and mode of testing (lab or field) could be recommended for each material type.

### Key Findings from Laboratory Testing

- The multi-variable stress-sensitivity models (the MEPDG and universal models) exhibited much higher model $R^2$ values (typically above 0.9) than the single-variable stress-sensitivity models (the bulk and deviatoric models) for the different unbound materials. Both the MEPDG and universal models were adequate for modeling the stress-sensitive resilient modulus behavior of the laboratory data.
- The granular base materials from the Test Track (Florida limerock, granite base, Type 5 base) exhibited stress-hardening behavior in the laboratory under increasing load while the Seale subgrade material exhibited stress-softening behavior. The Track soil material showed no significant stress-sensitivity in the laboratory (MEPDG and universal model $R^2$ of 0.42 and 0.66, respectively).
- In comparing the materials at equivalent stress-states, the Track soil material exhibited the highest modulus in the lowest and middle representative stress-states. The limerock base material was the stiffest material at the highest representative stress-states.

### Key Findings from Backcalculation Cross-Section Determination

- Variation in section construction and material composition warranted independent optimal cross-section investigations for the different structural sections. Multiple trial cross-sections were tried for each structural section, and the optimal cross-section was evaluated based on several criteria: RMS error values (deflection matching), reasonable and stable backcalculated modulus values, and measured versus predicted pavement response data from FWD on gauge testing.
- No bedrock or stiff layer effects are present that have an effect on the deflection data collected at the Test Track. The trial cross-sections using a stiff-layer for analysis exhibited RMS error values that were too high to be considered viable.
- A three-layer cross-section was used for the different structural sections at the Test Track. The four-layer and five-layer trial cross-sections usually generated reasonable deflection matching (i.e., low RMS), but generated unreasonable modulus values in one or more of the unbound layers. The three-layer cross-sections exhibited the best

combination of low RMS error values and reasonable backcalculated moduli. To generate the three-layer cross-section, it was necessary to combine one or more of the unbound layers that exhibited similar properties.

**Key Findings from FWD Unbound Material Characterization**

- The field-calibrated stress-sensitivity models generated much lower model $R^2$ values than did the laboratory-calibrated constitutive models. Given the large amounts of seasonal and spatial variability contained within the calibration deflection data, an $R^2$ value of 0.5 was used to differentiate stress-sensitive materials from non stress-sensitive materials.
- The multi-variable stress-sensitivity models generated better model fit (per $R^2$ values) for the base layer materials (Florida limerock, granite base, Type 5 base) than the single-variable stress-sensitivity models.
- The universal stress-sensitivity model gave the best prediction of backcalculated moduli for the limerock base, the granite base base, and the combined Seale and Track subgrade. The majority of the pavement layers containing the Track soil material for backcalculation did not show tangible stress-sensitivity.
- The model validation process indicated that the field-calibrated constitutive models had the tendency of over-predicting the backcalculated moduli below a certain modulus value and under-predicting the backcalculated moduli above a certain modulus values. However, the majority of the validation data set fell within a range of reasonable prediction with a similar order of magnitude to the backcalculated moduli.
- Temperature-stiffness characterization of the HMA layer in each structural section gave strong confidence in the accuracy of the backcalculation solution. Sections N5, N6, and N7 were believed to exhibit lower model $R^2$ with this relationship due to large amounts of pavement surface distress in these sections. These sections were not included for material-specific model unbound stress-sensitivity model development.

**Key Findings from Comparison of Laboratory and Field Resilient Moduli**

- For both the Florida limerock and the granite base material, poor agreement was shown between the backcalculated field moduli and the moduli predicted with the laboratory-calibrated stress-sensitivity model at equivalent stress-states. For each material, the laboratory moduli exhibited stress-hardening behavior under increasing load while the backcalculated moduli exhibited stress-softening behavior. Potential reasons for this disagreement include: laboratory samples that were non-representative of the in-situ conditions (compaction, density, moisture content, etc.), inherent disagreement between the nature of the two test methods, reduced accuracy of the backcalculated solution at higher load levels, and the existence of a very stiff subgrade at the Test Track supporting and altering the stress-sensitivity behavior of these materials in the field.
- Poor agreement was seen between the average moduli of the Track soil base material used in sections N8 and N9 and the average Track soil modulus in the laboratory. The backcalculated modulus of the Track soil base was much lower than the laboratory modulus. Potential reasons for this are the structural composition of the

section being non-conducive to the backcalculation of this layer modulus and this layer being supported by a very soft material (Seale subgrade).
- Good agreement was shown between the laboratory and backcalculated moduli for the Track subgrade material.
- No direct comparison between laboratory and backcalculated resilient moduli could be made for the Seale subgrade material and the Type 5 base material since these materials were combined with other materials for the purposes of backcalculation.

**RECOMMENDATIONS**

This research highlighted the effective use of triaxial testing and FWD testing to give a mechanistic characterization of the different unbound pavement materials utilized at the NCAT Test Track. The laboratory testing gives a quality representation of the stress-sensitivity of the resilient moduli for each of these materials. Characterization of the materials in this manner is sufficient for obtaining a good representation of the unbound material behavior for Level 1 mechanistic pavement design using the new MEPDG.

A quality FWD testing program that encompasses the seasonal and spatial variability of the pavement and tests the pavement at multiple critical load levels can also be used to develop a constitutive relationship for the in-situ unbound material moduli. The equations calibrated for this study are site-specific to the NCAT Test Track, and should be validated through comparison of moduli to additional pavement structures that contain the given unbound materials, but have varying structural compositions and thicknesses. Additionally, the models developed for this study could be made more robust by adding additional deflection data to the calibration and validation data sets.

The results of this study showed that either the MEPDG model or the universal model provide the best fit to laboratory resilient modulus data, and the universal model provided the best model fit to backcalculated resilient moduli. Therefore, the multi-variable constitutive models are recommended over the single-variable models given the results of this study.

## REFERENCES

American Association of State Highway and Transportation Officials. *AASTHO Guide for Design of Pavement Structures.* AASHTO: Washington, D.C., 1993.

American Association of State Highway and Transportation Officials. "Determining the Resilient Modulus of Soils and Aggregate Materials." Specification Number T307-99. *Standard Specifications for Transportation Materials and Methods of Sampling and Testing: Part 2B Tests.* 25th ed. AASHTO: Washington, D.C., 2005.

Andrei, D., M.W. Witczak, C.W. Schwartz, and J. Uzan. "Harmonized Resilient Modulus Test Method for Unbound Pavement Materials." *Transportation Research Record: Journal of the Transportation Research Board No. 1874.* TRB, National Research Council, Washington D.C., 2004. pp. 29-37.

Briggs, R.C. and E. O. Lukanen. "Variations in Backcalculated Pavement Layer Moduli in LTPP Seasonal Monitoring Sites." *Nondestructive Testing of Pavements and Backcalculation of Moduli: Third Volume, ASTM STP 1375*. S.D. Tayabji and E.O. Lukanen, Eds. American Society for Testing and Materials: West Conshohocken, PA, 2000.

Buchanan, S. *Resilient Modulus: What, Why, and How?* Vulcan Materials Company. (in draft) 2007.

Bush, A.J. and D.R. Alexander. "Pavement Evaluation Using Deflection Basin Measurements and Layered Theory." *Transportation Research Record: Journal of the Transportation Research Board No. 1022.* TRB, National Research Council, Washington D.C., 1985. pp. 16-28.

Eres Consultants Division (2004). *Guide For Mechanistic-Empirical Pavement Design of New and Rehabilitated Pavement Structures*. Final Report, NCHRP 1-37A.

Huang, Y.H. *Pavement Analysis and Design.* 2nd ed. New Jersey: Prentice Hall, 2004.

Irwin, L.H. "Backcalculation: An Overview and Perspective." Proceedings of the Pavement Evaluation Conference. Roanoke, VA. 2002.

McCarthy, D.F. *Essentials of Soil Mechanics and Foundations: Basic Geotechnics.* 6th ed. New Jersey: Prentice Hall, 2002.

Monismith, C.L. Analytically Based Asphalt Pavement Design and Rehabilitation: Theory in Practice, 1962-1992. *Transportation Research Record: Journal of the Transportation Research Board, No. 1354*, TRB, National Research Council, Washington, D.C., 1992, pp. 5-26.

National Cooperative Highway Research Program. "Laboratory Determination of Resilient Modulus for Flexible Pavement Design." *Research Results Digest No. 285*. Transportation Research Board, Washington D.C., 2004.

Nazarian, S., J. Rojas, R. Pezo, D. Yuan, I. Abdullah, and T. Scullion. "Relating Laboratory and Field Moduli of Texas Base Materials." *Transportation Research Record: Journal of the Transportation Research Board No. 1639.* TRB, National Research Council, Washington D.C., 1998. pp. 1-11.

Papagiannakis, A.T. and E.A. Masad. *Pavement Design and Materials.* Wiley, 2008.

Parker, F. "Estimation of Paving Materials Design Moduli from Falling Weight Deflectometer Measurements." *Transportation Research Record: Journal of the Transportation Research Board, No. 1293*: TRB, National Research Council, Washington, D.C., 1991, pp. 42-51.

Parker, F. and D.J. Elton. *Methods for Evaluating Resilient Moduli of Paving Materials.* Auburn University Highway Research Center: Auburn, AL. 1990.

Priest, A.L. and D.H. Timm. *Methodology and Calibration of Fatigue Transfer Functions for Mechanistic-Empirical Flexible Pavement Design.* Report No. 06-03, National Center for Asphalt Technology: Auburn University, 2006.

Rwebangira, T., R.G. Hicks and M. Truebe. "Sensitivity Analysis of Selected Backcalculation Procedures." *Transportation Research Record: Journal of the Transportation Research Board No. 1117.* TRB, National Research Council, Washington D.C., 1987. pp. 25-37.

Sebally, P.E., S. Bemanian, and S. Lani. "Nevada's Approach to the Backcalculation Process." *Nondestructive Testing and Backcalculation of Moduli: Third Volume.* ASTM STP 1375. S.D. Tayabji and E.O. Lukanen, Eds., American Society of Testing and Materials, West Conshohocken, PA, 2000.

Seeds, S.B., S.H. Alavi, W.C. Ott, M. Mikhail, and J.A. Mactutis. "Evaluation of Laboratory Determined and Nondestructive Test Based Resilient Modulus Values from the WesTrack Experiment." *Nondestructive Testing and Backcalculation of Moduli: Third Volume.* ASTM STP 1375. S.D. Tayabji and E.O. Lukanen, Eds., American Society of Testing and Materials, West Conshohocken, PA, 2000.

Sivaneswaran, N., L.M. Pierce, and J.P. Mahoney. *EVERCALC Help File*. EVERCALC version 5.0. Washington State Department of Transportation Materials Laboratory: 2001.

Timm, D.H. and A.L. Priest. *Material Properties of the 2003 NCAT Test Track Structural Study.* Report No. 06-01, National Center for Asphalt Technology: Auburn University, 2006.

Uzan, J. "Characterization of a Granular Material." *Transportation Research Record: Journal of the Transportation Research Board, No. 1022.* TRB, National Research Council, Washington, D.C. 1985. pp 52-59.

Von Quintus, H. and B. Killingsworth. *Analyses Relating to Pavement Material Characterizations and Their Effects on Pavement Performance.* Federal Highway Administration. McLean, VA. Publication No. FHWA-RD-97-085. 1998.

Willis, J.R. and D.H. Timm. *Repeatability of Asphalt Strain Measurements Under Full Scale Dynamic Loading.* Presented at the 87th Annual Meeting of the Transportation Research Board: Washington, D.C., 2008.

Yau, A. and H.L. Von Quintus. *Study of Laboratory Resilient Modulus Test Data and Response Characteristics, Final Report.* Federal Highway Administration. McLean, VA. Publication No. FHWA-RD-02-051. 2002.

Zhou, H. "Comparison of Backcalculated and Laboratory Measured Moduli on AC and Granular Base Layer Materials," *Nondestructive Testing and Backcalculation of Moduli: Third Volume.* ASTM STP 1375. S.D. Tayabji and E.O. Lukanen, Eds., American Society of Testing and Materials, West Conshohocken, PA, 2000.